Information Transmission Using the Nonlinear Fourier Transform

by

Mansoor Isvand Yousefi

A thesis submitted in conformity with the requirements
for the degree of Doctor of Philosophy
Graduate Department of Electrical and Computer Enginering
University of Toronto

Abstract

Information Transmission Using the Nonlinear Fourier Transform

Mansoor Isvand Yousefi
Doctor of Philosophy
Graduate Department of Electrical and Computer Enginering
University of Toronto
2013

The central objective of this thesis is to suggest and develop one simple, unified method for communication over optical fiber networks, valid for all values of dispersion and nonlinearity parameters, and for a single-user channel or a multiple-user network. The method is based on the nonlinear Fourier transform (NFT), a powerful tool in soliton theory and exactly solvable models for solving integrable partial differential equations governing wave propagation in certain nonlinear media. The NFT decorrelates signal degrees of freedom in such models, in much the same way that the Fourier transform does for linear systems. In this thesis, this observation is exploited for data transmission over integrable channels such as optical fibers, where pulse propagation is governed by the nonlinear Schrödinger (NLS) equation. In this transmission scheme, which can be viewed as a nonlinear analogue of orthogonal frequency-division multiplexing commonly used in linear channels, information is encoded in the nonlinear spectrum of the signal. Just as the (ordinary) Fourier transform converts a linear convolutional channel into a number of parallel scalar channels, the nonlinear Fourier transform converts a nonlinear dispersive channel described by a *Lax convolution* into a number of parallel scalar channels. Since, in the spectral coordinates the NLS equation is multiplicative, users of a network can operate in independent nonlinear frequency bands with no deterministic inter-channel interference. Unlike most other fiber-optic transmission schemes, this technique deals with both dispersion and nonlinearity directly and unconditionally without the need for dispersion or nonlinearity compensation methods. This thesis lays the foundations of such a nonlinear frequency-division multiplexing system.

Acknowledgements

First I wish to thank my advisor, Professor Frank R. Kschischang, for his excellent academic supervision during the course of my doctoral work. Frank is a superb teacher and a brilliant researcher from whom I learned enormously. He donates countless hours training and educating his students and closely supervising them. His clarity of thought, profound intuition and fundamental attitude toward problems have been a source of inspiration. I am deeply indebted to him for many helpful and stimulating meetings that we have had in the past years. The pleasant ambiance that he has created in his research group and his generous financial support have made my time at the University of Toronto a joyful experience.

I also wish to express my gratitude to the members of my Ph.D. committee, namely, Professors Ashish Khisti, Raymond Kwong, Lacra Pavel, and Wei Yu. I wish to extend my deep appreciation to Professor Andrew C. Singer, from University of Illinois at Urbana-Champaign, both for agreeing to serve as my external examiner, and particularly for his careful reading of the dissertation and his many constructive comments.

I am grateful to the University of Toronto for funding my Ph.D. program. This thesis would not have been possible without financial support from the Government of Canada and private donors of student scholarships. I acknowledge the Qureshi family for their continued commitment to the student scholarships for the Communications Group.

Finally, I thank my friends and colleagues for the fun times, which will leave many fond memories.

Contents

List of Tables

List of Figures

Chapter 1

Introduction

> It can scarcely be denied that the supreme goal of all theory is to make the irreducible basic elements as simple and as few as possible.
>
> Albert Einstein

Optical fiber is a very convenient medium for high data rate information transmission. A large bandwidth, on the order of THz, is available in silica fiber at only a modest cost, allowing transmission of information over distances as long as 6000 km with only 0.2 dB/km loss and exceptionally small probability of error. This makes optical fiber an ideal medium for high data rate communications.

It is a good thing that fibers have a large bandwidth, as demand for bandwidth is also increasing rapidly. It is widely observed that data rate requirements for core networking applications is doubling every 18 months, or every 24 months for I/O servers and storage area networks [2,3]. Many observers predict that to support high bandwidth applications such as video-on-demand, access to high-performance computing clusters, and for information transfer between data centers, tera bits per second (bits/s) per wavelength links will be needed by around 2015 [2, 3]. The conclusion is that, sooner or later, we will exhaust most practical bandwidth available in optical fibers, even if we use the whole 1-1.7 μm wavelength window in a wavelength-division multiplexing (WDM) setup. It is therefore eminently important to study techniques that will improve the spectral efficiency of fiber-optic communication systems.

Today is a promising time for research into increasing spectral efficiencies in optical communication systems. Coherent optical systems are becoming a practical reality and it is now possible to implement highly sophisticated signal processing algorithms involving

tens of giga-operations per second. Sophisticated electronic precompensation methods at the transmitter can potentially be be combined with sophisticated post-processing and channel decoding algorithms.

The mathematical theory of communication systems was laid out by C. E. Shannon in 1948. According to this theory, every communication channel has a capacity, beyond which reliable communications is not possible.

Traditionally communication and information theory has been mostly developed for linear Gaussian channels. While the majority of communication media can be modeled as linear channels under Gaussian perturbations, there are a few important cases where the channel is inherently nonlinear. An important example, and the one that motivates this thesis, is the optical fiber channel, in which signal propagation is modeled by the stochastic nonlinear Schrödinger (NLS) equation.

Although the capacity of many classical communication channels has been established, determining the capacity of fiber-optic channels has remained an open and challenging problem. The capacity of the optical fiber channel is difficult to evaluate because signal propagation in optical fibers is governed by the stochastic nonlinear Schrödinger equation, in which three effects simultaneously interact with one another: chromatic dispersion, Kerr nonlinearity, and additive white Gaussian noise. This gives rise to a complicated dynamic of pulse propagation in long-haul optical fibers.

In particular, what makes the optical fiber difficult to study is the presence of the nonlinear term in the NLS equation. The underlying nonlinear dispersive partial differential equation waveform channel is difficult to analyze compared to, say, the classical additive white Gaussian noise (AWGN) or wireless fading channels. In the NLS equation, signal degrees of freedom couple together through dispersion and nonlinearity in a complicated manner, making it difficult to establish the channel input output relationship, even deterministically.

1.1 Related Work

Current approaches to the design of optical fiber communication systems often assume a linearly-dominated regime of operation [4], consider the nonlinearity as a small perturbation [5], treat the effects of the nonlinearity as unknown or as noise [6] [7, and references therein]. In these studies, the channel capacity $\mathcal{C}(\mathcal{P})$ increases with power $\mathcal{P}$ until a certain power $\mathcal{P}_{\text{op}}$, and decays to zero afterwards [8]. Thus according to these studies, increasing the average input power beyond $\mathcal{P}_{\text{op}}$ deteriorates system performance, in sharp contrast with linear channels.

While using coherent detection and wavelength-division multiplexing (WDM) spectral efficiencies as high as 5 bits/s/Hz are achievable in a simulation experiment [7], the limitation of the spectral efficiency in the prior work may well be due to the fact that the nonlinearity is not treated in these works (see Chapter 3). These methods need to compensate and manage the nonlinearity and dispersion by means of signal processing and equalization. While these approaches have worked for many years now, with the rapidly increasing demand for bandwidth, they may no longer be adequate as the spectral efficiency is pushed. It is the main theme of this work that the nonlinearity needs to be understood and treated properly if higher capacities are desired in the coming years.

Progress in better communication over partial differential equation (PDE) channels is ultimately tied to progress made in nonlinear models in mathematics. Nonlinear dispersive waves are currently the subject of much research in mathematics, as many core equations in various areas of applied mathematics and theoretical physics turn out to be nonlinear (see, for instance, the literature on Yang-Mills equations, Navier-Stokes equations, integrable PDEs, nonlinear waves, Einstein equations, Ricci flow, turbulence problem, etc.). Even for well-structured PDEs such as the NLS equation, so far, it has appeared to the optical fiber community that computing the information theoretic quantities of the stochastic NLS equation, and for that matter all stochastic integrable PDEs, is still challenging and likely to require the introduction of new ideas to our present knowledge of the subject.

1.2 Contributions

The aim of this thesis is to suggest and develop one simple, unified method for communication over optical fiber channels, valid for all values of dispersion and nonlinearity parameters, and for a single user channel or a multiple user network. All deterministic distortions such as dispersion, nonlinearity, inter-symbol interference, inter-channel interference and in some cases polarization mode dispersion are zero for a single user channel or all users of a multiple user channel. The new method has the potential to offer significant improvements in the performance of optical fiber systems.

We adopt a different philosophy with regard to the previous work. Rather than treating nonlinearity and dispersion as nuisances, we seek a transmission scheme that is fundamentally compatible with these effects. We effectively "diagonalize" the nonlinear Schrödinger channel with the help of the nonlinear Fourier transform (NFT), a powerful tool for solving *integrable* nonlinear dispersive partial differential equations [9, 10]. The NFT uncovers linear structure hidden in the one-dimensional cubic nonlinear Schrödinger

equation, and can be viewed as a generalization of the (ordinary) Fourier transform to certain nonlinear systems.

With the help of the nonlinear Fourier transform, we are able to represent a signal by its discrete and continuous nonlinear spectra. While the signal propagates along the fiber based on the complicated NLS equation, the action of the channel on its spectral components is given by simple independent linear equations. Just as the (ordinary) Fourier transform converts a linear convolutional channel $y(t) = x(t) * h(t)$ into a number of parallel scalar channels, the nonlinear Fourier transform converts a nonlinear dispersive channel described by a *Lax convolution* (see Sec. 4.2) into a number of parallel scalar channels. This suggests that information can be encoded (in analogy with orthogonal frequency-division multiplexing) in the nonlinear spectra.

The nonlinear Fourier transform is intertwined with the existence of soliton solutions to the NLS equation. Solitons are pulses that retain their shape (or return periodically to their initial shape) during propagation, and can be viewed as system eigenfunctions, similar to the complex exponentials $e^{j\omega t}$, which are eigenfunctions of linear systems. An arbitrary waveform can be viewed as a combination of solitons, associated with the discrete nonlinear spectrum, and a non-solitonic (radiation) component, associated with the continuous nonlinear spectrum.

Motivated by the severe limitations that the nonlinearity imposes on the performance of the optical fiber networks, this thesis takes the first steps towards a nonlinear frequency-division multiplexing (NFDM) communication system operating based on the NFT. We simplify the NFT to a great degree, highlighting the analogies with the ordinary Fourier transform and orthogonal frequency-division multiplexing (OFDM). Numerical methods for calculating the NFT are provided. We clarify the structure of the receiver, which is able to estimate the nonlinear spectrum of the received signal rather efficiently. Finally, we determine the task of the transmitter and provide illustrative examples of how to use NFT for data transmission.

1.3 Thesis Outline

The subject of this research is inter-disciplinary, lying at the intersection of information and communication theory, applied mathematics, and lightwave and photonic systems. To assist in reading, Chapter 2 is dedicated to readers not familiar with some of these subjects. Information theorists can skip Section 2.1, mathematicians do not need Section 2.2, and Section 2.3 is not new to lightwave system engineers. In Chapter 3, the origin of the capacity limitations when using transmission techniques traditionally suited

for linear systems for communication over fiber-optic communications is explained. We introduce the nonlinear Fourier transform and some of its properties in Chapter 4, and numerical methods to compute the forward NFT in Chapter 5. Examples of using the NFT for communications with performance evaluation can be found in Chapter 6.

1.4 Notation

When possible, we use upper-case letters to denote scalar random variables (RVs) taking values on the real line $\mathbb{R}$ or in the complex plane $\mathbb{C}$, and lower-case letters for their realizations. Real and complex normal distributions are shown as $\mathcal{N}_{\mathbb{R}}$ and $\mathcal{N}_{\mathbb{C}}$. We use the shorthand notation X_k I.I.D. $\sim p_X(x)$ to denote a sequence of independent, identically-distributed random variables with common distribution $p_X(x)$. As customary, the Landua's big O notation $f(n) = \mathcal{O}(g(n))$ is used to say that $f(n)$ does not grow faster than $g(n)$ with n, *i.e.*, $\exists N, M < \infty \ni \forall n > N$, $|f(n)| \leq M|g(n)|$. A sequence of numbers $(x_1, \cdots, x_n)$ is occasionally denoted by x^n. Convergence of random variables almost surely, in probability, and in distribution are shown, respectively, by $\overset{\text{a.s.}}{\to}$, $\overset{\text{p}}{\to}$ and $\overset{\text{d}}{\to}$. We say $p \in \mathbb{R}$ is within $f(\mu \pm \epsilon)$ if $f(x - \epsilon) \leq p \leq f(x + \epsilon)$.

Chapter 2

Preliminaries

> It seems that if one is working from the point of view of getting beauty in one's equations, and if one has really a sound insight, one is on a sure line of progress.
>
> Paul A.M. Dirac

2.1 Origin of Information Theory

There is fundamentally one problem in communications theory: given a source and a destination in relation with one another and a message at the source, to recover, as well as possible, the message at the destination. Or more generally: given a set of messages at a number of sources, to reconstruct these messages at their intended destinations.

The cause and effect relationship between the source and the destination is represented by a communications channel. One can thus think of a communication channel as a black box mapping an input message to an output message. The interesting case, motivated by practice, is when the map has unknown parameters, reflecting disturbance, interference or noise in the communication medium. In this case, the channel is described by a set of transition probabilities between input and output messages.

In communications theory, information is modeled as a stochastic process [11]. The input to a communications channel is therefore a realization of a stochastic process $\{X_t, t \in T\}$, where X_t is a random variable on a sample space Ω_x and T is the index set of time t. The process can be discrete or continuous in time, and discrete or continuous in state. A communication channel is just a conditional probability distribution between

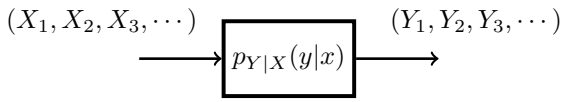

Figure 2.1: Discrete memoryless channel.

an input and an output, as defined more precisely below.

Definition 1 (Communication channel)**.** Let $(\Omega_x, \mathcal{F}_x)$ and $(\Omega_y, \mathcal{F}_y)$ be measurable spaces. A communications channel $\mathcal{C}$ from an input alphabet Ω_x to a set of measurements $\mathcal{F}_y$ performed at the output is a conditional probability measure $p(\mathcal{F}_y|\Omega_x) : \Omega_x \times \mathcal{F}_y \to [0, 1]$ such that:

1. for any $\omega_x \in \Omega_x$, $p(.|\omega_x)$ is a probability measure on $(\Omega_y, \mathcal{F}_y)$,
2. for any $y \in \mathcal{F}_y$, $p(y|.)$ is $\mathcal{F}_x-$ measurable.

The input and output alphabets Ω_x and Ω_y can take several forms. If Ω_x is a set of functions in $L^2(\mathbb{R})$, $\mathcal{C}$ is called a *waveform channel*. Roughly speaking, one can think of a waveform channel as a set of transition probabilities from the sample functions of a stochastic process $\{X_t, t \in T\}$ to the sample functions of another stochastic process $\{Y_t, t \in T\}$. The discrete case where Ω_x is a set of vectors in $\mathbb{R}^n$ is referred to as a *discrete channel (DC)*. A DC is described by a set of transition probabilities $p_{Y^n|X^n}(y^n|x^n)$ from realizations of a random vector X^n to the realizations of another random vector Y^n. A *discrete memoryless channel (DMC)* is a DC where $p_{Y^n|X^n}(y^n|x^n) = \prod_{k=1}^{n} p_{Y|X}(y_k|x_k)$, $\forall n$, and can be described by a conditional probability distribution $p(y|x)$, $x, y \in \mathbb{R}$. DCs and DMCs can be considered as, respectively, n- and one-dimensional special cases of the infinite-dimensional waveform channel. Thus the inputs of a DMC, a discrete channel with memory, and a waveform channel can be considered as, respectively, a real number, a vector, and a function. The actual output Ω_y, corresponding to the "physical reality", may never be entirely observable; one only has access to the measurement events $\mathcal{F}_y$. The mathematical operator performing measurements is thus part of the channel.

Information transmission has been studied for a long time, dating back to the nineteenth century [12]. However, the formulation of the communication problem in its modern mathematical form and its solution for one source and one destination is largely due to Claude Shannon [11]. In his *magnum opus* published in 1948, Shannon laid down the mathematical theory of communications, known as information theory [11].

Shannon makes a great deal of abstraction and introduces a number of new ideas when formulating and solving the point to point communication problem. Below we briefly review a few of the basic elements from information theory used in this thesis, for the

benefit of a reader not familiar with this area. The interested reader can consult [11,13,14] for a detailed discussion.

2.1.1 Statistical Regularity and the Concentration of Measure

We shall begin by examining the behavior of the sum S_n of n real random variables X_k with mean μ_k and finite variance σ_k^2,

$$S_n = X_1 + \cdots + X_n.$$

In general, if $|X_k| < c$ (almost surely), the probability distribution of S_n is supported in $[-nc, nc]$, and S_n is order of $\mathcal{O}(n)$ (almost surely). Let us square $X_1 - \mu_1 + \cdots + X_n - \mu_n$ and separate out the interaction terms

$$(S_n - \mathsf{E}S_n)^2 = \sum_{k=1}^{n}(X_k - \mu_k)^2 + \sum_{k=1}^{n}\sum_{\substack{l=1 \\ l\neq k}}^{n}(X_k - \mu_k)(X_l - \mu_l). \tag{2.1}$$

There are only n self-terms in (2.1), while the overwhelming $n^2 - n$ terms are interaction terms. For a general sequence of random variables X_k, asymptotically $(S_n - \mathsf{E}S_n)^2 \overset{\text{a.s.}}{\sim} \mathcal{O}(n^2)$. However it is a remarkable phenomenon that when X_k are pairwise independent, the interaction terms in (2.1), *i.e.*, the overwhelming number of terms, vanish on average, and $\mathsf{E}(S_n - \mathsf{E}S_n)^2 = \sum_{k=1}^{n}\sigma_k^2 = n\bar{\sigma}_n^2 \sim \mathcal{O}(n)$, where $\bar{\sigma}_n^2 = \sum_{k=1}^{n}\sigma_k^2/n < \infty$.

Observation 1 (Linearity of variance). A consequence of vanishing interaction terms on average in (2.1), is the linearity of variance

$$\mathrm{Var}\left(\sum_{k=1}^{n} X_k\right) = \sum_{k=1}^{n}\mathrm{Var}(X_k).$$

Thus in random quantities, unlike deterministic quantities, the linearity is on the variance, *i.e.*, on the square of the quantity, and not on the standard deviation, which has the units of the signal. □

From the linearity of variance we obtain that

$$\mathrm{VAR}\ (\frac{1}{n}S_n) = \frac{1}{n^2}\mathrm{VAR}\ (S_n) = \bar{\sigma}_n^2/n \to 0, \quad \text{as } n \to \infty.$$

That is to say, the fluctuations of $M_n = \frac{1}{n}S_n$ diminish in size as $n \to \infty$, and $M_n = \frac{1}{n}S_n$ would be highly concentrated around its mean. In particular, from the Chebyshev's

inequality,

$$M_n \xrightarrow{\mathrm{p}} \mathsf{E}M_n. \tag{2.2}$$

Observation 2 (Concentration of measure phenomenon [15]). Let X_k be a sequence of bounded random variables. The assumption that X_k are pairwise independent would make the probability distribution of the sum S_n highly concentrated around the mean $\mathsf{E}S_n$ in an interval of length $\mathcal{O}(\sqrt{n})$, much smaller than $\mathcal{O}(n)$ expected from deterministic quantities. □

This remarkable phenomenon is a direct consequence of the independence of X_k. Independent random variables tend to fall in the same region, and to push the sum S_n to the extremes $\mathcal{O}(n)$, variables X_k need to somehow "work together". This phenomenon of the concentration of measure is in fact more general than stated above, and is the cause of a variety of interesting results in the probability theory and statistics, including information theory, the subject of this thesis.

The simplest concentration result is the Law of Large Numbers (LLN) (2.2). The next in the hierarchy is the central limit theorem (CLT), stating that under further conditions, *e.g.*, when X_k are identically distributed,

$$S_n \xrightarrow{\mathrm{d}} \mathsf{E}S_n + \sqrt{n}Z_n, \tag{2.3}$$

where $Z_n \sim \mathcal{N}_{\mathbb{R}}(0, \bar{\sigma}_n^2)$ is a zero mean Gaussian RV with a finite variance. The LLN and the CLT, respectively, represent the zero-order and $\frac{1}{2}$-order asymptotic of the fluctuations of S_n as a function of n. There also exist other limit theorems with regard to the asymptotic behavior of S_n, notably the Law of Iterated Logarithm (LIL), sitting between LLN and CLT.

Remark 1. The linearity of the variance has a number of other significant consequences. It underlies the rules of the stochastic calculus, such as the form of the Taylor expansion for random functions or Ito lemma, in which the second order quantities $\mathrm{d}X^2$ are no longer negligible.

In general, a concentration of measure statement for M_n is an estimate of the following probability

$$p\left(|M_n - \mathsf{E}M_n| > \lambda\right) \tag{2.4}$$

in terms of λ and n. From CLT, in the limit $M_n - \mathsf{E}M_n \sim \mathcal{N}_{\mathbb{C}}\left(0, \frac{\bar{\sigma}^2}{n}\right)$. However, as illustrated in Fig. 2.2, the CLT describes only the bulk of the distribution of M_n within

$\frac{1}{\sqrt{n}}$ standard deviation from the mean (independent of the details of $p_{X_k}(x)$), and it is not valid for the description of the tail of $p_{M_n}(x)$ beyond this range (which generally depends on the details of $p_{X_k}(x)$). For a fixed λ, as $n \to \infty$ we eventually encounter the tail of the distribution, where the LLN and CLT are grossly ineffective.

To go beyond the LLN and CLT and estimate 2.4, concentration of measure inequalities are needed. Weak inequalities include the Markov inequality

$$p\left(|M_n - \mathsf{E}M_n| > \lambda\right) < \frac{1}{n\lambda} \sum_{k=1}^{n} \mathsf{E}|X_k - \mu_k|,$$

requiring no assumption on independence and giving no decay on n (linear decay in λ), and, by squaring the arguments in the Markov inequality, the Chebyshev's inequality

$$p\left(|M_n - \mathsf{E}M_n| > \lambda\right) < \frac{1}{n^2\lambda^2} \sum_{k=1}^{n} \sigma_k^2,$$

requiring pairwise independence and linear decay in n (quadratic decay in λ). Continuing this process by incorporating all higher order k moments, one obtains exponential decays $\exp(-nI(\lambda))$ in n, using various large deviation theorems, such as Chernoff bounds. The exponent $I(\lambda)$ is called the Cramer rate function.

Theorem 1 (Large Deviation)**.** 1. *Let X_n be a sequence of real-valued random variables. If the scaled cumulant generating function*

$$g(\lambda) = \lim_{n\to\infty} \frac{1}{n} \log \mathsf{E}_{X_n} e^{n\lambda X_n}$$

is differentiable in λ, then the probability density function of X_n for large n is

$$p_{X_n}(x) = e^{-nI(x)+o(n)},$$

where $o(n)/n \to 0$ and

$$I(x) = \sup_{\lambda\in\mathbb{R}} \{\lambda x - g(\lambda)\}. \tag{2.5}$$

2. *Let X_n be a sequence of* I.I.D. *bounded real-valued random variables with common distribution $p_X(x)$ and $\mathsf{E}X_n = \mu$. Then*

$$p\left(M_n > x\right) = e^{-nI(x)+o(n)} \quad x > \mu, \quad p\left(M_n < x\right) = e^{-nI(x)+o(n)} \quad x < \mu,$$

where $I(x)$ is given in (2.5) and $g(\lambda) = \log E_X e^{\lambda X}$ is the logarithmic moment generating function.

Proof. Part 1) is the Gärtner-Ellis theorem. It says that the dependency of the distribution of a sequence of random variables X_n, for which $g(\lambda)$ exists and is differentiable, must be exponential in n; see [16] for a proof. The utility of this theorem comes from the fact that in many cases one can compute $g(\lambda)$ without knowing $p_{X_n}(x)$ a priori. Part 2) is the Cramer's theorem and follows by applying part 1) to the mean of the sequence X_n,*i.e.*, substituting $X_n \to M_n = \sum X_n/n$ and simplifying $g(\lambda)$. □

Figs. 2.2 and 2.3 illustrate the concepts of the large deviation and rate functions when X_k are Gaussian and Bernoulli RVs. The sum S_n of n I.I.D. Gaussian or Bernoulli RVs seem to converge to a Gaussian distribution as n is increased. However looking at rate functions, the exponent of the distribution is quadratic only when X_k are Gaussian. For Bernoulli RVs, the rate function is only locally quadratic around the mean and deviates from that as λ is increased. Indeed, by Taylor expansion one always has a locally quadratic rate function and the resulting Gaussian approximation holds. These figures illustrate that one needs a large deviation inequality to estimate (2.4).

As noted earlier, the concentration of measure is a more general phenomenon than stated above. For instance, Talagrand concentration inequality asserts that it holds true as well for a convex Lipschitz function of independent RVs $F(X_1, \cdots, X_n)$, not necessarily the sum function [15].

Definition 2. A sequence x^n is $\lambda-$typical to a distribution $p_X(x)$ with respect to the function $F(x_1, x_2, \cdots, x_n)$ if it meets the concentration inequality $|F(x^n) - \mathsf{E}F(X^n)| < \lambda$, where $X_1, X_2, \cdots$ are I.I.D. $\sim p_X(x)$.

From Theorem 1 it follows that, with respect to $F(x^n) = \sum_1^n x_k/n$, chances that X^n drawn I.I.D. from $p_X(x)$ is not $\epsilon-$typical to $p_X(x)$ is within $e^{-nI(\mu \pm \epsilon)}$.

An immediate function of a random variable on a probability space is the probability function $p_X(x)$. In the next section, we choose F to be the probability function, or more conveniently, the logarithm of the probability $F(x_1, \cdots, x_n) = \log p(x_1, \cdots, x_n)$. For simplicity, we consider a DMC and apply the simplest (zero-order) concentration theorem: the law of large numbers.

2.1.2 Information Theory and Noise

The existence of the fundamental limits in communications is an application of the concentration of measure phenomenon to the sum of n independent random variables S_n.

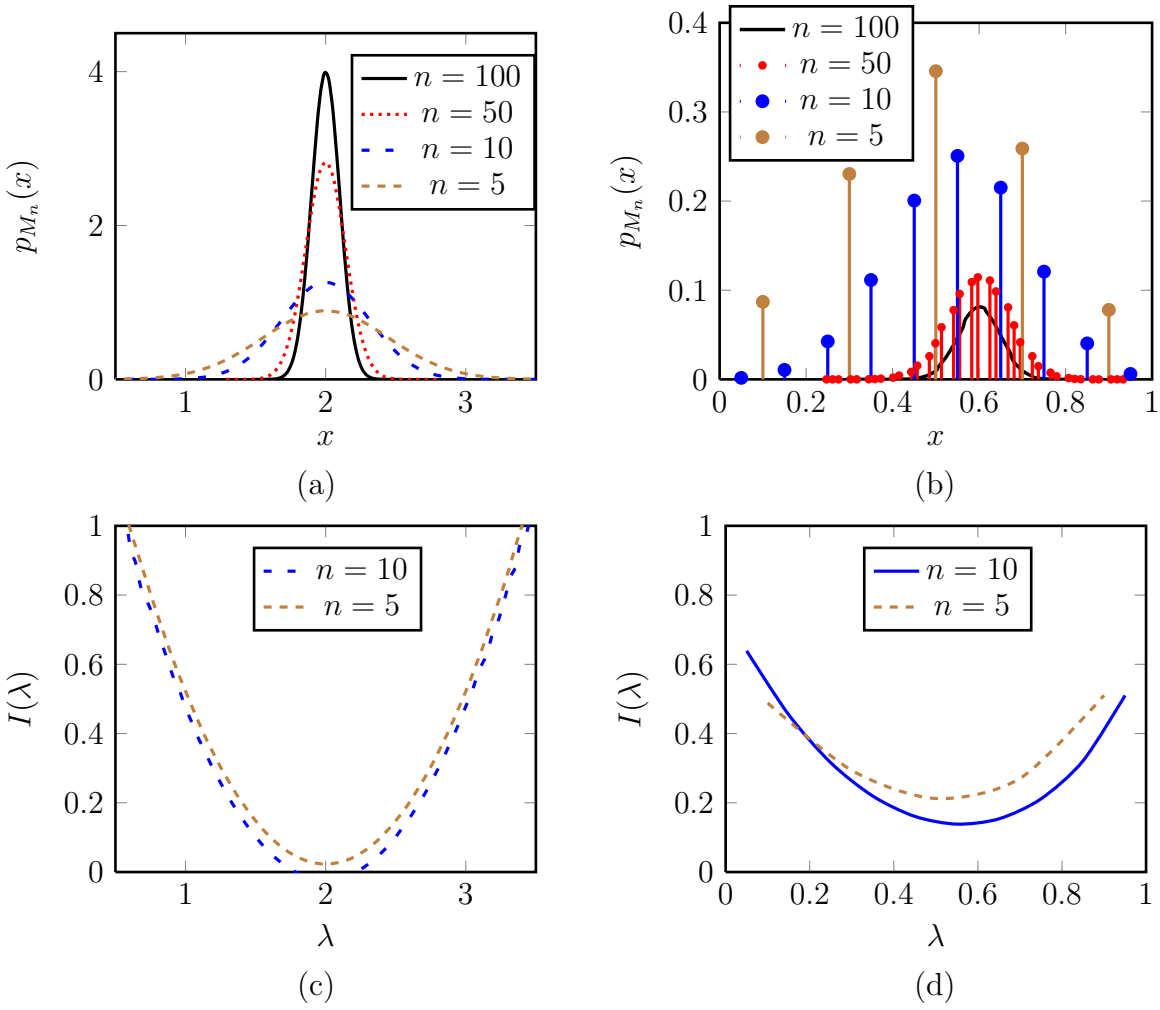

Figure 2.2: Distribution of M_n when (a) X_k I.I.D. $\sim \mathcal{N}_{\mathbb{R}}(0, 1)$, (b) X_k I.I.D. $\sim$ Bernoulli$(0, 0.6)$. (c) Rate function for part (a). (d) Rate function for part (b).

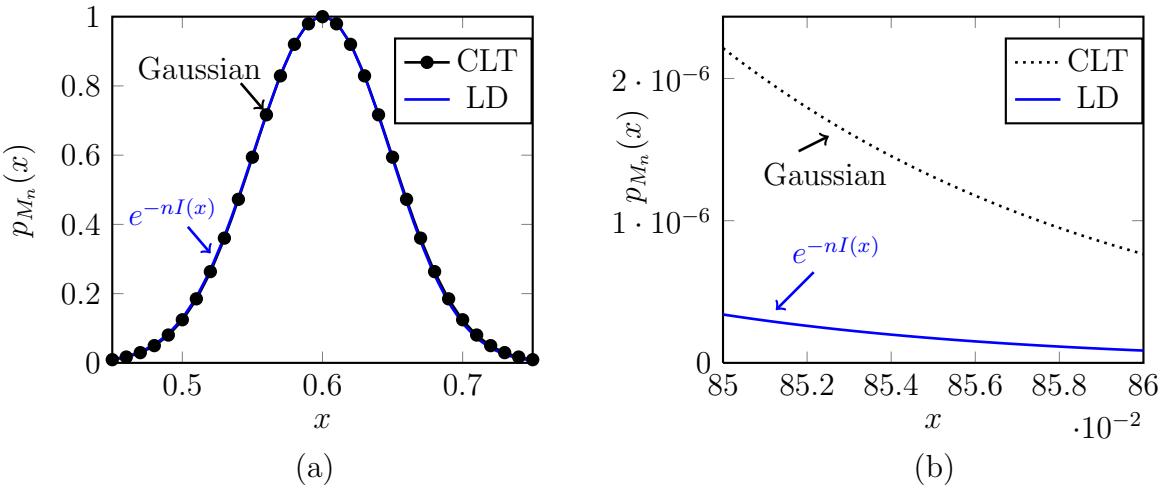

Figure 2.3: (a) Distributions obtained from CLT and large deviation (LD) both well describe the bulk of $p_{M_n}(x)$. Here X_k I.I.D. $\sim$ Bernoulli$(0, 0.6)$. (b) Only large deviation can approximate the tail of $p_{M_n}(x)$.

The LLN can be applied to see the existence of a capacity, while the concentration of measure inequalities can be used to analyze the probability of error asymptotically and make the argument precise. Below, we briefly re-derive the well-known channel coding theorem for one source and one destination [11].

Consider the single-shot communication problem where a single symbol $\omega_x \in \Omega_x$ is sent and a symbol $\omega_y \in \Omega_y$ is received. Given a measurement event $y \in F_y$ obtained at the output of the channel, the most probable $\omega_x \in \Omega_x$ giving rise to y is a solution of the maximum a posterior (MAP) estimation problem

$$\hat{\omega}_x(y, p_{\Omega_x}(\omega_x)) = \max_{\omega_x \in \Omega_x} p_{\Omega_x|F_y}(\omega_x|y).$$

A receiver implementing a MAP estimator is therefore the rule $y \to \hat{\omega}_x(y, p_{\Omega_x})$. The the single-shot problem under a MAP receiver has an average probability of error $P_e = E_{p_{\Omega_x}} P(\hat{\omega}_x \neq \omega_x)$, usually bounded away from zero. One can however obtain arbitrarily small probability of error, as prescribed by Shannon [11]. To summarize Shannon's result below, for simplicity we assume $\Omega_x = F_x = \{x_1, \cdots, x_{n_x}\}$, $\Omega_y = F_y = \{y_1, \cdots, y_{n_y}\}$, all having finite cardinalities.

A mathematical probability theory refers to physical reality through a frequency interpretation of the probability, *i.e.*, by replacing a distribution $p_X(x)$ by its empirical distribution, defined via a counting process. This motivates that in order to take advantage of the statistics provided by the channel law, and to see what these statistics mean in the first place, to consider the multiple-shot transmission problem, where a sequence

x^n drawn I.I.D. from $p_X(x)$ is transmitted. Since

$$p(x_1, \cdots, x_n) = \prod_{k=1}^{n} p_X(x_k),$$

the logarithm function is used to enable the use of the law of large numbers

$$\log p(x_1, \cdots, x_n) = \sum_{k=1}^{n} \log p_X(x_k) \xrightarrow{\text{p}} nE_X \log p_X(x) = -nH(X),$$

where $H(X) = -E \log p_X(x) = -\sum_{x \in \Omega} P_X(x) \log p_X(x) > 0$ is the entropy of the discrete distribution $p_X(x)$. It follows that $p(x_1, x_2, \cdots, x_n) \xrightarrow{\text{p}} 2^{-nH}$, a constant value and independent of the sequence. We thus obtain the following *Asymptotic Equipartition (AEP) Lemma*, which is at the center of information theory.

Lemma 2 (AEP)**.** *In sampling a distribution $p_X(x)$ independently $n \to \infty$ times, there are about $2^{nH(X)}$ typical sequences, all almost equiprobable with a constant probability near $2^{-nH(X)}$.*

The AEP asserts that as $n \to \infty$, as a result of the severe constraint imposed by the LLN, only a few events are typically observed compared to the total number of possibilities, all of them almost equally surprising. These are called typical sequences. We say x^n is $\epsilon-$typical to $p_X(x)$ if it is $\epsilon-$typical to that distribution with respect to the probability function $F(x^n) = p(x^n)$. The collection of $\epsilon-$typical sequences is the typical set A_ϵ^n. Theorem 1 ensures that if X^n I.I.D. $\sim p_X(x)$, then $p(x^n \notin A_\epsilon^n) = \exp\big(-nI(H(X) \pm \epsilon) + o(n)\big) \xrightarrow{\text{p}} 0$.

Example 1. Let $X \sim$ Bernoulli(p). Among 2^n possible sequences, $2^{nH(X)}$ are typical, where $H(X) = -p \log p - (1-p) \log(1-p)$. These are sequences of length n which have about np ones.

AEP lemma can also be applied to a conditional distribution, leading to the concept of *joint typicality*.

Corollary 3. *Let $P_{Y|X}(y|x)$ be a conditional distribution. For any input sequence X^n* I.I.D. *$\sim p_X(x)$, there are about $2^{nH(Y|X)}$ output typical sequences as $n \to \infty$, where*

$$H(Y|X) = \sum_{k=1}^{n_x} P_X(x_i) H(Y|X = x_i).$$

Proof. Let z^n be drawn I.I.D. from $p_X(x)$. Partition z^n into n_x sub-sequences, each containing one $x_i \in \Omega_x$ and having length n_i; $\sum_{i=1}^{n_x} n_i = n$. For each of these input sub-sequences, there are about $2^{n_i H(Y|X=x_i)}$ output typical subsequences. The number of output typical sequences of length n at the output is thus

$$\prod_{i=1}^{n_x} 2^{n_i H(Y|X=x_i)} = 2^{\sum_{i=1}^{n_x} n_i H(Y|X=x_i)} = 2^{\sum_{i=1}^{n_x} nP_X(x_i) H(Y|X=x_i)} = 2^{nH(Y|X)}. \tag{2.6}$$

Note that for each input typical sequence, the location of x_i's is fixed and that is what makes $H(Y|X)$ different from $H(Y)$. Allowing permutation in the counting process (2.6) will turn $H(Y|X)$ into (a larger quantity) $H(Y)$. □

Remark 2 (Finding the typical sequences). Let X be a random variable with finite alphabet size and distribution $p_X(x_i) = p_i, i = 1, \cdots, n_x$. The typical sequences of length n are all those sequences which have about np_1 symbol x_1, about np_2 symbols x_2, etc. A simple counting shows that the number of these sequences is

$$N = \binom{n}{np_1, \cdots, np_n} = \frac{n!}{(np_1)! \cdots (np_{n_x})!}.$$

Taking the $\log N$ and approximating sums by integrals (or using Stirling's formula), we obtain $N \approx 2^{nH(X)}$. Typical sequences are, asymptotically, permutations of one another, and the typical set can be obtained from one typical sequence. Hence, a typical set can simply be denoted by the notation $(n_1, \cdots, n_{n_x})$.

The typical sequences obtained from a conditional distribution can also be similarly described. Let $[p_{ij}]$ be a $n_x \times n_y$ probability matrix, representing a finite alphabet channel and assume that the channel input is drawn from a distribution $p_X(x_i) = p_i$. Associated with every (non-typical) input sequence $x^{np_i} = (x_i, x_i, \cdots, x_i)$ of length np_i, there is a typical set S_i determined by the probabilities of the i^{th} row of the channel matrix (*i.e.*, $2^{nH(Y|X=x_i)}$ output sequences having np_ip_{i1} symbols y_1, np_ip_{i2} symbols y_2, etc.). Let x^n be any input sequence, having symbols x_i at the index set I_i. The *conditional output typical set* arising from x^n consists of $2^{\sum_{i=1}^{n_x} n_i H(Y|X=x_i)}$ output sequences obtained from the Cartesian product $S_1 \times \cdots S_{n_x}$, keeping the index locations the same (thus permutations are only locally inside S_i). If x^n is a realization of a distribution $p_X(x)$, then there are $2^{nH(X)}$ input typical sequences, and associated with each, there is a conditional output typical set of size $2^{nH(Y|X)}$. The *output typical set* is the collection of all these conditional

output typical sets, with the cardinality

$$2^{nH(X)} \times 2^{nH(Y|X)} = 2^{nH(Y)},$$

where $H(Y) = H(X) + H(Y|X)$. The output typical set is thus the permutations of the conditional output typical sets, obtained *e.g.*, from one conditional output typical set associated with a particular input typical sequence. The difference between $H(Y)$ and $H(Y|X)$ is a permutation in the underlying counting sequences. Fig. 2.4 and Fig. 2.5 illustrate these concepts pictorially.

Lemma 4. *Let $p_{Y|X}(y|x)$ be a conditional distribution with an input alphabet $\Omega_x = \{a_1, \cdots, a_{n_x}\}$, x^n drawn* I.I.D. *from $p_X(x)$ an input ϵ-typical sequence, and y^n a resulting output sequence.*

1. *The probability that y^n obtained at the output is outside of the output typical set associated with x^n (y^n is not jointly typical with x^n) goes to zero as $n \to \infty$.*
2. *The probability that x^n is ϵ-typical with another distribution $q_X(x)$, $x \in \Omega_x$, is within $2^{-n(D(p||q)\pm\epsilon)+o(n)}$ for large n, where $D(p(x)|q(x))$ is the Kullback-Leibler distance between distributions p and q*

$$D(p_X(x)|q_X(x)) = \sum_x p_X(x) \log \frac{p_X(x)}{q_X(x)}.$$

3. *The probability that another randomly selected input sequence $\tilde{x}^n \neq x^n$ is jointly typical with y^n (giving rise to y^n) is within $2^{-n(I\pm\epsilon)}$, where $I = D(p_{X,Y}(x,y)|p_X(x)\, p_Y(y))$.*

Proof. 1) This probability vanishes following any concentration of measure theorem, *e.g.*, from Theorem 1, or AEP lemma. 2) This is Sanov's theorem. We can measure the empirical distribution of X by counting symbols in x^n, as $p_i = \sum_k \delta[x_k - a_i]/n$, $1 \leq i \leq n_x$, where $\delta[x]$ is the discrete Dirac function. By applying Part 2) of Theorem 1 in the vector form to estimate $p(\mathbf{p} \approx \mathbf{q})$, we obtain $D(p||q)$ as the rate function I. 3) Given x^n at the input, any other input sequence is independent of y^n and, from 2), the chance of another input sequence giving rise to y^n is within $2^{-n\left(D\left(p_{X,Y}(x,y)||p_X(x)p_Y(y)\right)\pm\epsilon\right)} = 2^{-n(I\pm\epsilon)}$. □

Remark 3. 1. Note that for input non-typical sequences, the size of the associated output typical set can be input dependent. However, the size of output typical sets associated with every input typical sequence is a constant $2^{nH(Y|X)}$, independent of the input.

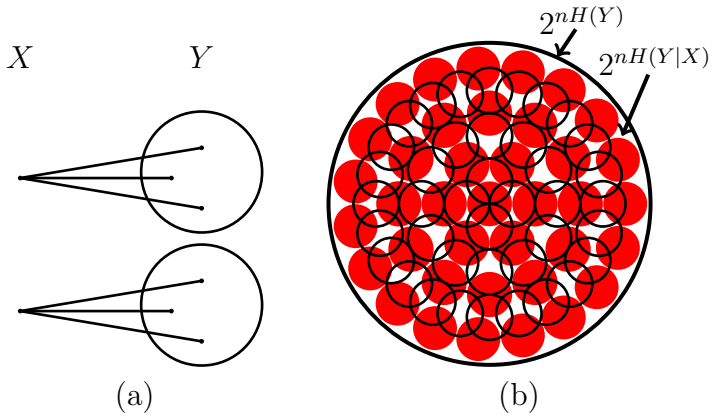

Figure 2.4: (a) For every input typical sequence (cause), there is a conditional output typical set (possible effects) with size $2^{nH(Y|X)}$. (b) Complete uniformization in the $n \to \infty$ dimensional space at the output of a generic communication channel as a result of the concentration of measure phenomenon (or AEP). The outermost big sphere has size $2^{nH(Y)}$ and shows the output typical set A_y; the small spheres represent the noise balls (conditional output typical sets) associated with an input typical sequence. The number of small spheres is $2^{nH(X)}$, each having size $2^{nH(Y|X)}$. The (red) filled spheres are a selection of the 2^{nI} spheres out of $2^{nH(X)}$ ones, packing the output space. The probability of $\mathbb{R}^n - A_y$ goes to zero as $n \to \infty$ from AEP lemma.

2. Note that there is no distinction between linear channels and nonlinear channels in the general argument made above. In high dimensions the "noise balls" (conditional typical sets) have the same size for any set of transition probabilities, regardless of where the statistics come from. This is simply because typical sequences are permutations of one another, essentially identical, and in any long input sequence the effects of "good" and "bad" symbols are averaged out.
3. In an asymptotic analysis, one can think of "typical" sequences as the only observable sequences.

It follows from the phenomenon of the concentration of measure (or AEP lemma) that a complete uniformization is achieved in the $n \to \infty$ dimensional space at the input and output of a conditional distribution $p_{Y|X}(y|x)$. That makes the the description of a conditional distribution, when extended in high dimensions, a uniform distribution over a finite set, *i.e.*, essentially a deterministic problem. These input output uniform sets are geometrically shown in Figs. 2.4 and 2.5.

This observation suggests transmitting a long block of data over a communication channel, so long that the statistical regularity is nearly achieved. There are about $2^{nH(X)}$ input typical sequences. For each received sequence y^n, there is a conditional input typical set of size $2^{nH(X|Y)}$. If each conditional input typical sets contains only one "signal", the

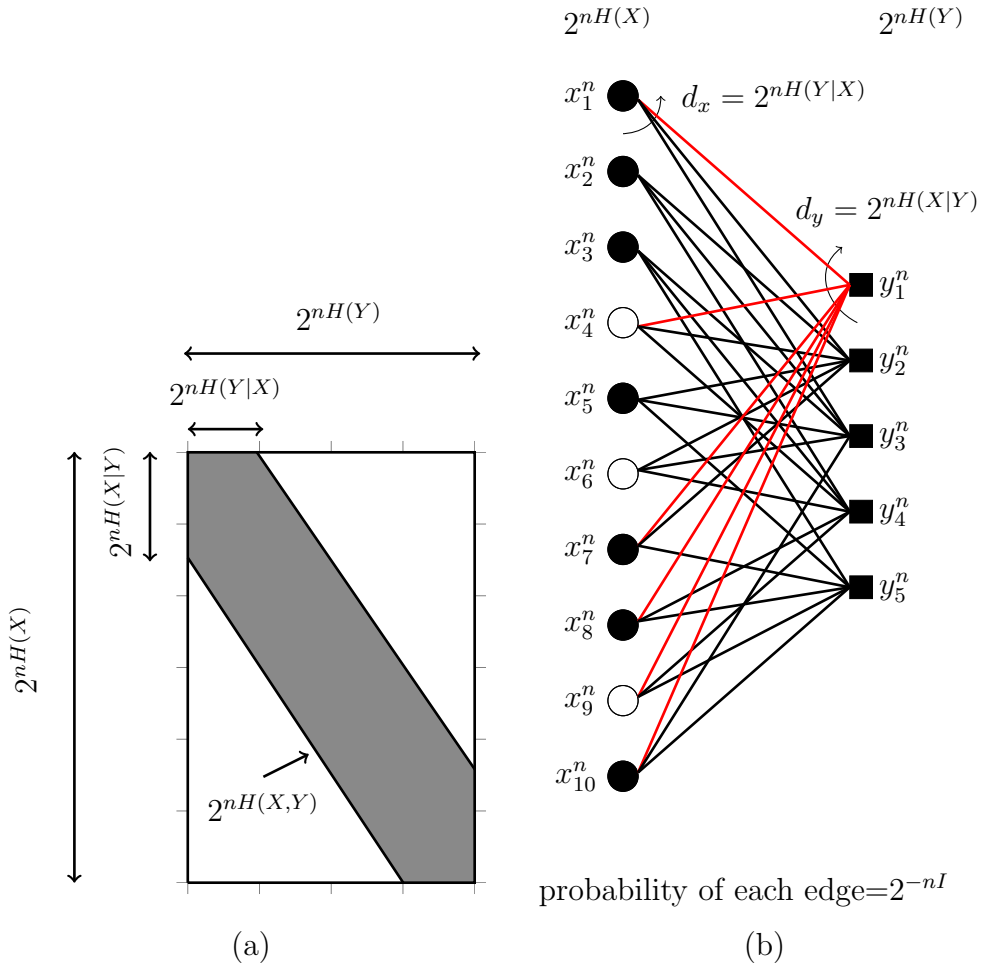

Figure 2.5: (a) Input, output, and jointly typical sequences. (b) A channel in n-dimensional space can be described on a regular bipartite graph. Left and right nodes represent, respectively, input and output typical (observable) sequences with degrees $2^{nH(Y|X)}$ and $2^{nH(X|Y)}$. The edges represent the cause and effect relationship between the input and output sequences; they indicate pairs (x^n, y^n) drawn I.I.D. from the joint distribution $p_{X,Y}(x, y)$. The input output nodes not connected are not in probabilistic relation with each other as $n \to \infty$. These are independent sequences drawn from the distribution $p_X(x)p_Y(y)$. There are total $2^{n(H(X)+H(Y))}$ possible pairs (x^n, y^n), but only $2^{nH(X,Y)}$ jointly typical pairs (edges). Thus in random selection of the nodes, the probability of getting an edge is 2^{-nI}. The white circles show 2^{nR} randomly selected codewords out of $2^{nH(X)}$ inputs. The received sequence y_1^n cannot be decoded unambiguously since it is connected to two codewords, while y_3^n can be decoded unambiguously. The decoder also fails if an output is connected to no codeword.

inverse map is unambiguous. The number of distinguishable input sequences is upper-bounded by

$$N \leq \frac{2^{nH(X)}}{2^{nH(X|Y)}} = 2^{n(H(X)-H(X|Y))} = 2^{nI(p_X(x))}.$$

The exponent $I(p_X(x)) := I\left(p_X(x), p_{Y|X}(y|x)\right)$ is called the mutual information functional

$$I\left(p_X(x)\right) = H(X) - H(X|Y) = D(p_{X,Y}(x,y)|p_X(x)p_Y(y)).$$

Channel capacity, representing the maximum achievable *information rate*, is defined as

$$C = \max_{p_X(x)} I\left(p_X(x)\right), \quad \text{bits per channel use.} \tag{2.7}$$

Below we show that one can indeed achieve rates arbitrary close to the above upper bound.

The set of input typical sequences form the rows of a $2^{nH(x)} \times n$ matrix, with elements that we draw from the capacity achieving input distribution. We select $2^{nR} \nearrow 2^{nC}$ input sequences from rows of this matrix, as our *codewords*. The set of codewords, a $2^{nR} \times n$ matrix, is the *codebook* M. This codebook is revealed to the receiver before communication starts. The encoder maps nR bits of the input data to a codeword of length n. Parameter R is thus the communication rate, $R = \log|M|/n$. The decoder receives a sequence y^n and lists its conditional input typical sequences according to the algorithm mentioned in Remark 2. If there is a unique codeword in this list, it is declared as the transmitted sequence, otherwise a failure is announced.

Since input typical sequences are equi-probable, it seems plausible that choosing codewords randomly (uniformly) likely leads to a well separated ensemble. The probability of error of a randomly selected codebook M can easily be estimated. Fig. 2.5 represents the input output sequences of a channel on a regular bipartite graph in the $n \to \infty$ dimensional space. Edges emerging from x^n are connected to nodes y^n which are statistically related to x^n, *i.e.*, pairs (x^n, y^n) are drawn from the joint distribution $p_{X,Y}(x^n, y^n)$. Suppose that codeword c_1^n has been transmitted, *e.g.*, x_4^n in Fig. 2.5. An error occurs if 1) y^n is not connected to c^1 (either there is no codeword at all, or there are codewords other than c^1 connected to y^n), or 2) some other codeword is connected to the y^n in addition to c^1. Events in case 1) mean that the received sequence is not jointly typical with c^1. The probability of this event $p_e^{(1)}(c_1^n)$ vanishes from Lemma 4(1). For case 2), the probability that a randomly selected input node is connected to y^n is $2^{nH(X|Y)}/2^{nH(X)} = 2^{-nI}$.

Hence the probability that in choosing 2^{nR} codewords randomly one or more wrong codewords is also connected to y^n is upper bounded by $(2^{nR}-1)2^{-nI}$, using the union bound. Clearly if $R < I$, $p_e^{(2)}(c_1^n) \to 0$. From the symmetry indicated by AEP lemma and random code construction, the probability of error averaged over all codewords is $\bar{p_e} = p_e(c_1^n) = p_e^{(1)}(c_1^n) + p_e^{(2)}(c_1^n)$ and hence vanishes as $n \to \infty$. Since this holds true for a random code, evidently there must exist at least one good code where $\bar{p_e} \to 0$.

The converse is also true: if $R = I + \epsilon$, in the limit there are infinitely many codeword nodes connected to any output node, and $p_e \to 1$. We thus get the following theorem indicating the significance of the capacity as the fundamental limit of information.

Theorem 5 (Channel Coding Theorem)**.** *In a DMC, all rates below capacity are achievable, i.e., for every $R < C$ there exists an encoder and decoder with $p_e \to 0$. Conversely no rate above capacity is achievable, i.e. if $p_e \to 0$ for any (n, k) code, then $R \leq C$.*

Proof. The proof of the forward part was outlined above. It essentially follows from the fact that in sampling a joint distribution $p_{X,Y}(x, y)$, X and Y are statistically related, and the chance that the distribution $p_X(x)p_Y(y)$ generates a pair (X^n, Y^n) obtained from $p_{X,Y}(x, y)$ is as small as $2^{-nD\left(p_{X,Y}(x,y)||p_X(x)p_Y(y)\right)} = 2^{-nI}$. In other words, a received sequence Y^n (drawn from $p_Y(y)$), "generates" input sequences according to $p_{X|Y}(x|y)$. The chances that a sequences statistically unrelated to Y^n, drawn from $p_X(x)$, generates Y^n, from the large deviation Theorem 1, is $2^{-nE_{p_Y}D\left(p_{X|Y}(x|y)||p_X(x)\right)} = 2^{-nI}$. Thus one can choose up to 2^{nI} signals before a decoder operating based on the joint typicality encounters a significant error. See [13] for details of the proof, specially the converse.

□

Remark 4. While the *sphere packing picture* shown in Fig. 2.4 is a helpful visualization aid to illustrate the concept of the capacity, it is useful only in the limit $n \to \infty$. In practice when n is finite, at rates close to the capacity these spheres indeed intersect with each other significantly, allowing higher number of packed spheres. The hard sphere packing picture of Fig. 2.4, typically pursued in algebraic coding, is not usually suitable for operation at rates close to the capacity.

The task of the communication over a given channel consists of finding the capacity C, as well as devising coding methods to achieve this limit. Although random block codes have good minimum distance properties, due to the lack of the structure, their decoding is complex. To manage complexity, modern capacity achieving codes enforce a sparsity structure on the codebook for efficient decoding, while still maintaining pseudo-randomness for good performance.

Remark 5 (Assumptions of information theory). Information theory is a consequence of the concentration of measure phenomenon. It thus relies on

1. the definition of the "probability"; and
2. assumptions of the concentration (*e.g.*, LLN), such as a sufficient independence.

There are various interpretations of "probability" such as, among others, notably the Kolmogorov axiomatization in mathematics and frequency interpretation in physics and engineering. The later, or a similar interpretation, is ultimately needed in order to refer to physical reality. In this case, the law of large numbers, and thus the channel coding theorem, emerges from the very definition of the probability as a statistically regulated counting process. However, modern probability theory uses the abstract mathematical definition of probability, encompassing many of these interpretations, as used earlier to illustrate the origin of the LLN. Here, too, one assumes a sufficient degree of independence between random variables and derives various notions of convergence for which $p_e^n \to 0$, such as the convergence in probability obtained from the weak LLN (leading to weak typicality), and almost sure convergence obtained from the strong LLN (leading to strong typicality). One can also consider information transmission under other notions of probability, different assumptions of concentration (though sufficient independence or its equivalent is needed), or physical models reflecting disturbance in different ways. In engineering, the independence assumption means that one can generate truly random data and one has the freedom to send blocks of data.

2.1.3 Communication Theory and Interference

The above discussion was largely in the context of the discrete memoryless channels. Information theory, however, can apply to all channels, including waveform channels. For waveform channels, first we try to *discretize* the channel if possible.

Let $L_W^2(\mathbb{R})$ denote the signal space of the functions with finite norm and bandlimited to W, with the inner product

$$\langle f, g \rangle = \int_{\mathbb{R}} f(t) g^*(t) dt.$$

The waveform additive white Gaussian noise channel is

$$\begin{aligned} &Y(t) = X(t) + N(t), \quad X(t), Y(t) \overset{\text{a.s.}}{\in} L_W^2(\mathbb{R}), \\ &\text{s.t.} \quad \mathsf{E} \frac{1}{\mathcal{T}} \int_0^{\mathcal{T}} |X(t)|^2 dt \le \mathcal{P}_0, \end{aligned} \tag{2.8}$$

where $X(t)$ and $Y(t)$ are processes whose realizations are respectively the input output signals, $N(t)$ is a stationary zero-mean white Gaussian noise with nonzero power spectral density $N_0/2$ in the frequency band $|f| < W$, $\mathcal{P}_0$ is the average signal power at the transmitter, and $\mathcal{T}$ is the communication time.

Let $\{e_n\}_{n\in\mathbb{N}}$ be an orthonormal basis for $L^2_W(\mathbb{R})$, for instance the set of sinc (Nyquist) functions $e_n = \mathrm{sinc}(2Wt - n)$. We can expand functions in (2.8) in this basis

$$X(t) = \sum_k X_k e_k, \quad Y(t) = \sum_k Y_k e_k, \quad N(t) = \sum_k N_k e_k,$$

where $\{X_k\}$ are signal degrees of freedom and N_k is I.I.D. $\sim \mathcal{N}_{\mathbb{R}}(0, N_0/2)$. Hence the waveform AWGN channel (2.8) is reduced to the discrete AWGN channel

$$\begin{aligned} Y_k &= X_k + N_k, \quad k = 1, 2, \cdots, \\ \mathsf{E}X_k^2 &\leq \frac{\mathcal{P}_0}{2W}. \end{aligned} \tag{2.9}$$

Thus instead of working with waveforms, one works with the set of scalar signal degrees of freedom $\{X_k\}_{k\in\mathbb{N}}$, *i.e.*, $X(t) \leftrightarrow \{X_k\}_{k\in\mathbb{N}}$. That is to say, the waveform channel (2.8) is discretized to a set of independent scalar parallel channels (2.9). Evaluating the capacity (2.7) (by replacing sums in the entropies with integrals), we obtain $C = W\log(1+\mathrm{SNR})$ bits/s, where $\mathrm{SNR} = \mathcal{P}_0/N_0W$.

Now consider the linear inter-symbol interference (ISI) channel

$$Y(t) = h(t) * X(t) + N(t), \tag{2.10}$$

where $h(t)$ is the channel filter and $*$ denotes convolution. If we proceed in a similar way as before, the dispersive effect of the channel filter $h(t)$ causes the degrees of freedom to couple together in the time domain, giving rise to ISI

$$Y_k = \langle e_k, h * X_k\rangle + \underbrace{\sum_{i\neq k} \langle e_k, h * X_i\rangle}_{\text{ISI}} + N_k.$$

However it is evident that the degrees of freedom in linear systems are essentially decoupled. For instance by taking the Fourier transform of (2.10), one obtains

$$\hat{Y}(f) = \hat{h}(f)\cdot\hat{X}(f) + \hat{N}(f), \quad |f| < W, \tag{2.11}$$

where noise remains white Gaussian in the frequency domain. The Fourier transform

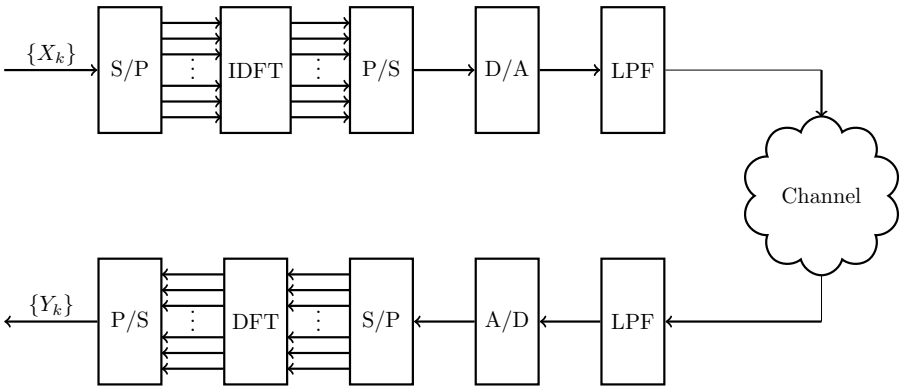

Figure 2.6: Orthogonal frequency-division channel model.

thus transforms the action of the convolution $*$ into a simple memoryless *multiplication operator* L_H in the frequency domain $\hat{Y}(f) = (L_H\hat{X})(f) + \hat{N}(f)$ (see Appendix A). The multiplication operator implies that all frequency components are independent of one another. The channel thus decomposes to a set of independent parallel scalar channels in the frequency domain.

Orthogonal frequency-division multiplexing works based on this idea, by discretizing (2.11) and encoding information in the spectrum of the signal $\hat{X}(f)$ rather than $X(t)$. The block diagram of a typical OFDM system is shown in Fig. 2.6.

In general, a conditional probability measure may not factorize into the product of the simpler conditional measures, such as scalar channels $\prod_k p_{Y|X}(y_k|x_k)$, under any transformation of the input output probability spaces. For waveform channels not factorizable, one can consider input functions $x(t)$ on a time mesh with size n on the interval $[-\mathcal{T}/2, \mathcal{T}/2]$ and replace the entropy in the definition of the capacity with the entropy rate

$$H(X(t)) = \lim_{\mathcal{T}\to\infty} \lim_{n\to\infty} \frac{1}{n} H(X_1, \cdots, X_n),$$

to obtain the capacity in bits per second. This approach is however generally difficult [17].

2.2 Evolution Equations

An evolution equation is a partial differential equation for an unknown function $q(t, z)$ of the form

$$q_z = K(q), \tag{2.12}$$

where $K(q)$ is an expression involving q and its derivatives with respect to t. In (2.12) and throughout this thesis, subscripts are used to denote partial derivatives with respect to the corresponding variable.

The evolution equation (2.12) is a PDE in $1+1$ dimensions, *i.e.*, one variable $t \in \mathbb{R}$ represents a temporal dimension and one variable $z \geq 0$ represents a spatial dimension. In most mathematical literature, the roles of z and t are interchanged, so rather than a spatial evolution as in (2.12), mathematicians study temporal evolution.

Evolution equations can be linear or nonlinear and dispersive or non-dispersive. Below we define these terminologies, frequently used in this thesis.

2.2.1 Dispersion Relations

Linear dispersion relation

Consider the evolution equation (2.12) when $K(q)$ is linear in q, *i.e.*,

$$q_z = p(\frac{\partial}{\partial t})q, \tag{2.13}$$

where $p(x)$ is a univariate polynomial $p(x) = \sum_{k=0}^{n} a_k x^k$.

A significant tool in the analysis of linear time-invariant systems is the Fourier transform. In this method variables are expressed as a linear combination of natural harmonics,

$$q(t,z) = \int\int Q(\omega,\beta) e^{j(\omega t - \beta z)} \mathrm{d}\omega \mathrm{d}\beta, \tag{2.14}$$

where ω is the signal frequency and β is the *wavenumber*.

Substituting (2.14) into (2.13), we obtain that β and ω depend on each other

$$\beta = jp(j\omega), \tag{2.15}$$

and (2.14) simplifies to

$$q(t,z) = \int Q(\omega) e^{j(\omega t - \beta(\omega) z)} \mathrm{d}\omega. \tag{2.16}$$

The relationship (2.15) between β, ω is called a *linear dispersion relation* and is often expressed as $\beta = \beta(\omega)$. Dispersion relations give valuable information about the character of the underlying equations. They illustrate how a medium responds to harmonics with various frequencies and wavenumbers.

The one-dimensional Fourier transform (2.16) shows that the solution of the linear

evolution equations is the superposition of *plane waves*,

$$q(t,z) = Ae^{j(\omega t - \beta(\omega) z)}. \tag{2.17}$$

In what follows, we consider the exponential (2.17) primarily a function of time t. Each plane wave is then a single tone frequency traveling in time with a speed $\beta(\omega)/\omega$ [sec/km], as z is increased. Hence, the speed of each frequency component depends on the frequency ω.

A simple way to find the dispersion relation of a linear evolution equation is to substitute the plane wave ansatz (2.17) into that equation and determine the β, ω binding.

Example 2 (heat equation). Consider the one-dimensional heat equation $q_z = c^2 q_{tt}$, where c is the diffusion coefficient and $q(t,z)$ represents the heat profile across a rod extending in *space* t, as *time* z goes on. Substituting the plane wave ansatz (2.17), we obtain the dispersion relation

$$j\beta = c^2\omega^2.$$

This is of course a special case of the dispersion relation for the linear constant coefficient evolution equation (2.13) given in (2.15).

□

One can also derive the original equation (2.13) from its dispersion relation (2.13) by the replacing β and ω by their corresponding derivatives

$$\beta \to j\frac{\partial}{\partial z} \quad \omega \to -j\frac{\partial}{\partial t}. \tag{2.18}$$

Thus linear constant coefficient equations are in one-to-one correspondence with their dispersion relations.

In many applications $q(t,z)$ is a passband signal with a spectrum centered at a carrier frequency ω_0 and a wavenumber β_0, and confined to a narrow bandwidth $W \ll \omega_0$, $\forall z$. In such cases, we often remove the carrier from the signal in (2.16) in order to describe the complex envelope of the signal

$$q(t,z) \;=\; e^{j(\omega_0 t - \beta_0 z)} \int Q(\omega) e^{j\{(\omega-\omega_0)t - (\beta-\beta_0)z\}} \mathrm{d}\omega.$$

Expanding the wavenumber in the frequency

$$\beta(\omega) = \beta_0 + \beta_1(\omega-\omega_0) + \frac{\beta_2}{2}(\omega-\omega_0)^2 + \cdots, \quad \beta_k = \frac{\mathrm{d}^k\beta}{\mathrm{d}\omega^k} \quad [\mathrm{sec^k/km}], \quad \mathrm{k} \geq 1,$$

we get

$$q(t,z) = e^{j(\omega_0 t - \beta_0 z)} \int Q(\omega) e^{j(\omega-\omega_0)\left\{(t-\beta_1 z) - \left(\beta_2(\omega-\omega_0)+\cdots\right)z\right\}} \mathrm{d}\omega. \tag{2.19}$$

If we introduce a retarded time $t' = t - \beta_1 z$, (2.19) is simplified to

$$q(t,z) = e^{j\omega_0(t'-v_p(\omega_0)z)} \int Q(\omega) e^{j(\omega-\omega_0)\left\{t'-v_g(\omega)z\right\}} \mathrm{d}\omega.$$

where

$$v_p = \frac{\beta_0}{\omega_0} - \beta_1 \quad [\text{sec/km}]$$

is the *phase velocity* or *the speed of the carrier*, and

$$v_g(\omega) = \beta_2(\omega - \omega_0)/2 + \cdots \quad [\text{sec/km}], \tag{2.20}$$

is the *group (envelope) velocity* or *the speed of the slowly varying envelope*. These speeds are measured in a frame of reference co-propagating with signal with the velocity β_1. In a stationary frame of reference, β_1 is added to these two speeds. Thus $\beta_0, \beta_1, \beta_2, \cdots$ respectively give carrier speed, envelope velocity (group velocity), the speed of the envelope of the envelope (group velocity dispersion), etc. Usually we are interested in the overall group velocity (2.20) depending on all β_k, $k \geq 1$.

The group velocity is a more significant concept than carrier velocity. Many evolution equations represent the complex envelope of the signal. One can simply think of group velocity as the signal velocity, or speed at which the energy propagates. While the carrier velocity is constant, group velocity is generally a function of the frequency.

Clearly, if $\beta_2 = \beta_3 = \cdots = 0$, all frequency components travel at the same speed. An equation is said to be dispersive if $\beta_k \neq 0$, for some $k \geq 2$. Since $v_g(\omega) \propto \omega$, high frequencies (blue) travel faster than low frequencies (red) and thus arrive at different times at a distance $z = \mathcal{L}$. Dispersion therefore can give rise to pulse broadening.

Nonlinear dispersion relations

The concept of the dispersion relation is difficult to extend to nonlinear evolution equations equally successfully. Nonlinear equations generally do not have plane wave solutions. Even if they do, the lack of a superposition principle does not allow generalizing a dispersion relation obtained from a plane wave ansatz to a general one.

For the nonlinear equations admitting plane wave solutions, dispersion relations still give important (partial) information about the behavior of the equation.

Example 3. Consider the evolution equation

$$jq_z = q_{tt} + 2q|q|^2, \tag{2.21}$$

where $q(t, z)$ is a complex function. Trying the ansatz (2.17), we obtain that plane wave solutions exist with the following dispersion relation and group velocity

$$\beta = 2|A|^2 - \omega^2, \quad v_g(\omega, A) = 2|A|^2/\omega - \omega. \tag{2.22}$$

As a result, a plane wave solution of (2.21) travel with a speed depending on both the wave frequency and amplitude. This, of course, does not mean that frequency components travels according to (2.22) in any solution of (2.21).

2.2.2 Classification of Evolution Equations

The evolution equation (2.12) can be linear or nonlinear and dispersive or nondispersive. A dispersion relation, if exists, can help to identify the type of the evolution equation.

The wavenumber of a medium can in general depend on both the frequency ω and signal q

$$\beta(\omega, q) = \overbrace{\beta_0 + \beta_1\omega}^{\text{travelling wave envelope}} + \overbrace{\beta_2\omega^2 + \cdots}^{\text{dispersion}} + \overbrace{f(q, \omega)}^{\text{nonlinearity}}, \quad f(0, \omega) = 0. \tag{2.23}$$

An evolution equation is linear if its wavenumber does not depend on the signal *i.e.*, $f = 0$ in (2.23). In this case, substituting $q(t, z) = \int Q(\omega, z)e^{j\omega t}\mathrm{d}\omega$ into (2.12), we get $Q_z = -j\beta(\omega)Q$. As a result, $q(t, z) = \int Q(\omega)e^{j(\omega t - \beta(\omega)z)}$, consistent with (2.16).

An evolution equation is dispersive if $\beta_k \neq 0$ in (2.23) for some $k \geq 2$. Thus the group velocity has a component depending on the frequency, leading to the group velocity dispersion. The equation has solutions whose frequency components travel at different speeds, leading due to changes in the the signal envelope during the evolution.

Below we give examples of various classes of evolution equations and discuss their pulse propagation behavior.

Linear Nondispersive Equations

An evolution equation is linear and nondispersive if its dispersion relation is

$$\beta = \beta_0 + \beta_1\omega.$$

In this case, from (2.16) the signal envelope is expressed as the superposition of the plane waves $\exp(j\omega(t-cz))$, all traveling with the same speed $c=\beta_1$. Thus the overall solution is $f(t-cz)$, where $f(t)$ is the initial data at $z=0$. As a result the solution of linear nondispersive equations are traveling waves, *i.e.*, waveforms that keep their shape, traveling at a constant speed c (stationary in the co-propagating reference). Fig. 2.7(a) shows a traveling wave propagating in a linear nondispersive medium.

Example 4 (One-dimensional wave equation in free space). Consider the one-dimensional wave equation $q_{zz}=c^2q_{tt}$, where $q(t,z)$ represents a wave in time t (*e.g.*, an electromagnetic field) propagating in the free space in the direction z with velocity c. Plugging in the plane wave ansatz (2.17), we obtain the dispersion relation

$$\beta=\pm c\omega.$$

As expected, the solution is the sum of the forward and backward traveling waves $\left(f(t-cz)+g(t+cz)\right)/2$ and experiences no dispersion. □

Linear Dispersive Equations

The dispersion relation of the linear dispersive equations is independent of the signal and at least quadratic in ω

$$\beta(\omega)=\beta_0+\beta_1\omega+\beta_2\omega^2+\cdots,$$

where $\beta_k\neq 0$ for some $k\geq 2$.

The dispersion coefficient β_2 can be positive or negative. Since the group velocity dispersion is $\beta_2(\omega-\omega_0)$ to the leading order, high frequencies travel faster than low frequencies if $\beta_2<0$ or slower if $\beta_2>0$. In both cases, this can lead to pulse broadening or pulse contraction in the time domain, depending on the input signal[1].

Fig. 2.7(b) shows an example of the wave propagation in a dispersive medium when $\beta_2<0$. Here a pulse initially at $z=0$ disperses to zero in the evolution, experiencing pulse broadening. While the signal energy (and perhaps additional conserved quantities) can be preserved in a dispersive equation, it can spread over a large time so that locally the signal energy is negligible in any finite time interval.

[1]In the frequency domain, a linear system could represent a low pass or a high pass filter, potentially leading to spectral broadening or contraction, depending on the definition of the bandwidth (*e.g.*, 99% bandwidth). However spectral broadening in the sense of creation of new frequencies does not occur. See also the footnote in page 44.

An example of a linear dispersive equation is the heat equation mentioned in Example 2. Solving the equation,

$$q(t,z) = h(t,z) * q(t,0) = \int Q(\omega,0)e^{j\omega(t-c^2\omega z)}\mathrm{d}\omega, \tag{2.24}$$

where the impulse $h(t,z)$ is a Gaussian function

$$h(t,z) = \frac{1}{\sqrt{4\pi c^2 z}} e^{-\frac{t^2}{4c^2 z}}.$$

It follows that $q(t,z)$ is the sum of the single tone frequencies traveling at speeds proportional to their frequencies. Integral (2.24) is a special case of (2.16).

Nonlinear Nondispersive Equations

Nonlinear nondispersive equations have solutions whose components in time travel with speeds depending on the signal in that time instance. The shape of the signal generally changes, but due to the nonlinearity not the dispersion. If the nonlinearity is set to zero, solutions are traveling waves. If a dispersion relation from a plane wave is obtained, it is linear in ω and depends on the signal

$$\beta = \beta_0 + \beta_1\omega + f(A,\omega).$$

Example 5. Consider the following nonlinear equation

$$q_z + \alpha q_t + \beta q q_t = 0. \tag{2.25}$$

The dispersion relation and the group velocity are

$$\beta = \omega(\alpha + \beta A), \quad v_g = \alpha + \beta A.$$

That is to say, samples of the signal with high amplitudes travel faster than those parts with small amplitudes. Note that a derivative term $\partial^k q/\partial t^k$ contributes to the dispersion only if $k \geq 2$. □

In many cases nonlinearity is memoryless and is best understood in the time domain. Fig. 2.7(c) shows the qualitative features of the pulse propagation in a nonlinear nondispersive equation where $v_q = q$, *i.e.*, $q(t,z) = q(t - q(t,z)z, 0)$. The top of the signal travels faster than the base of the signal, causing the initial pulse to tilt to the right. Pulse center $t = 0$ is mapped to a time t' at $z = 1$ satisfying $q(t') = t'$. It can be verified

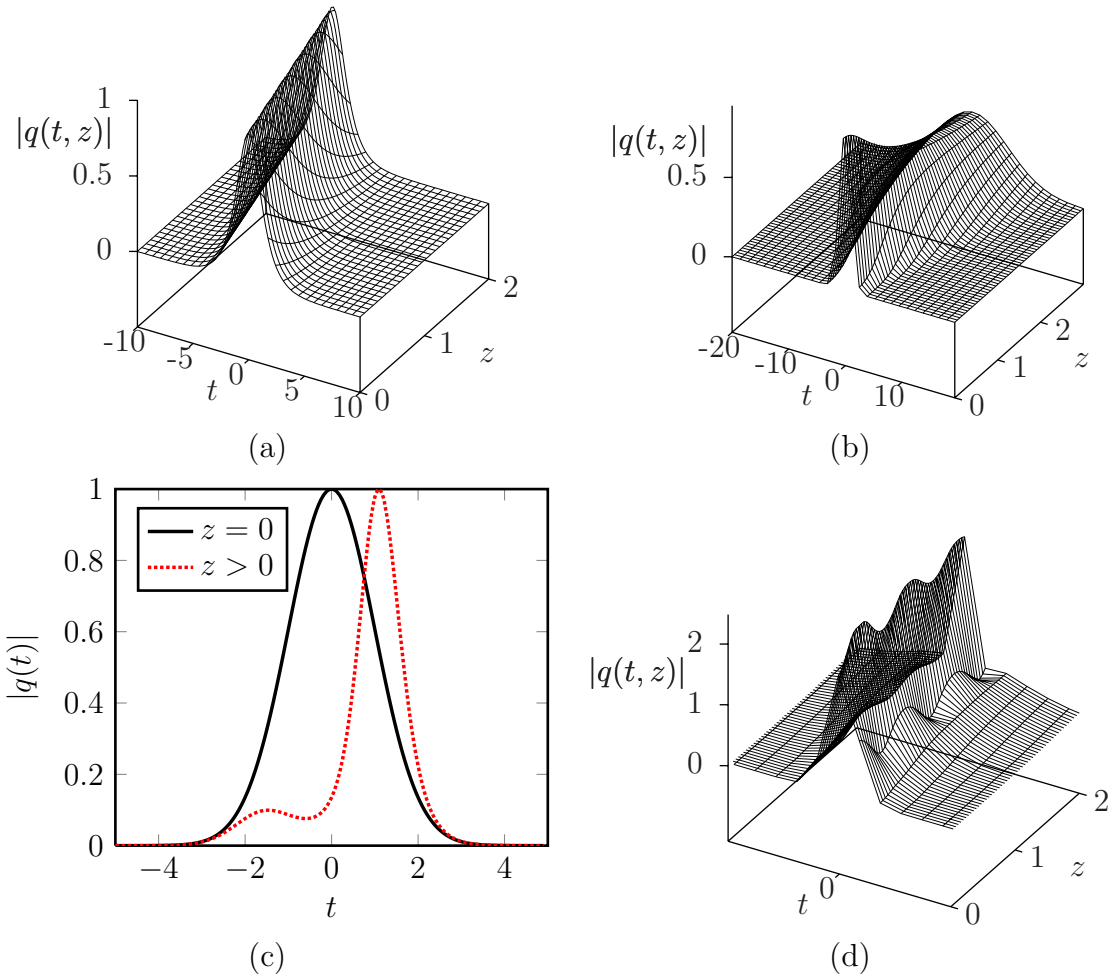

Figure 2.7: Wave propagation in a (a) linear nondispersive, (b) linear dispersive, (c) nonlinear nondispersive, and (d) nonlinear dispersive medium.

that (*e.g.*, in the case that z is small), the effect of the signal dependent shift is not simply titling the pulse, but distorting the waveform.

Example 6. In cases that $q(t, z)$ is complex, signal distortions may occur in the phase of the signal. Consider the following nonlinear equation

$$jq_z = 2|q|^2 q. \tag{2.26}$$

A dispersion relation exists, given by

$$\beta = 2|A|^2, \quad v_g = 2|A|^2/\omega.$$

Thus the speed of a single tone frequency depends on the intensity of that component.

It can be verified that the solution of (2.26) is

$$q(t,z) = q(t,0)e^{2j|q(t,0)|^2 z}.$$

Although the signal amplitude is preserved during the propagation, its phase is distorted according to the nonlinearity. There is no dispersion since $\beta_k = 0$, $k \geq 0$, although v_g depends on the frequency as well, due to the nonlinearity. □

Nonlinear Dispersive Equations

These equations generally have both elements of the nonlinearity and dispersion in the wavenumber expansion (2.23).

An example is (2.21), where the equation allows a plane wave solution, and the resulting wavenumber depends on the signal amplitude and frequency.

Example 7. Consider the nonlinear equation

$$q_z + q_{ttt} + qq_t = 0.$$

Unlike Example 2.21, a plane wave solution does not exist. However, it is evident that by setting the nonlinear term to zero, the equation is dispersive with dispersion relation $\beta = -\omega^3$. □

A nonlinear dispersive equation can be in the anomalous (focusing) or normal (defocusing) regime, depending on the signs of the dispersion and nonlinearity. In the anomalous regime, $\beta_2 < 0$ and the nonlinearity acts against the pulse broadening effects of the dispersion (see Fig. 2.7(d)). In this case, in the frequency domain plot, all frequencies travel towards the carrier, leading to pulse broadening in time. Since the wavenumber is a function of the signal intensity as well, if one has a signal whose shape in time is peaked at the center and decays at other times, like a Gaussian, there is a possibility that the entire wave packet travels at a constant speed. This corresponds to the formation of a certain traveling wave packets in the anomalous regime called solitons, similar to that in Fig. 2.7(a). In the normal regime, $\beta_2 > 0$ and all frequencies travel away from the carrier, leading to pulse compression in time. Thus if one has an inverted soliton signal, there is a possibility of obtaining a traveling wave packet (dark soliton).

Remark 6. Dispersion is best understood in the frequency domain, where its action is memoryless and multiplicative. The nonlinearity is usually memoryless and multiplicative in the time and is best understood in this domain. Nonlinear dispersive waves are

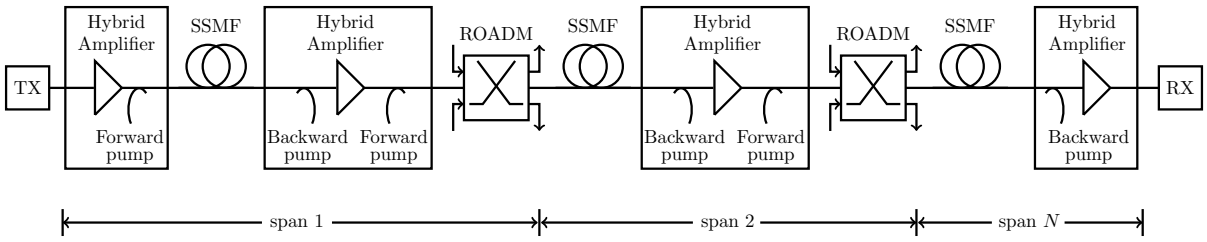

Figure 2.8: Fiber-optic communication system.

challenging to analyze because the degrees of freedom are coupled both in time and frequency. These equations often do not take simple forms in either time or usual frequency domains.

2.3 Lightwave Communications

The amount of information that can be transmitted on a signal is proportional to the carrier frequency (bandwidth $\sim$ carrier frequency). With the introduction of lasers in 1960s, it was speculated that a shift from the radio and microwave spectrum to optical frequencies near the infrared spectrum can significantly increase data rates. At wavelengths close to the visible light wavelengths, elements of the atmosphere contribute to a significant signal loss and random refractive index. This makes transmission of lightwaves over long distances in the exposed atmosphere nearly impractical. In search for a medium for the newly invented laser, optical fiber was suggested in 1966 [18].

Early fibers had significant loss and low-loss fibers were not made available until the 1970s. Fiber-optic communication systems initially used expensive repeaters in the 1980s to regenerate the signal. The advent of the optical amplifiers in 1987 [19, 20] and the wavelength-division multiplexing in mid 1990s subsequently revolutionized the fiber-optic communications.

Fig. 2.8 shows the block diagram of a typical optical communications system. Important components of such a system include laser sources, optical modulators, fiber segments, amplifiers, reconfigurable add-drop multiplexers (ROADMs), filters, and demodulators.

A laser source generates a coherent beam of light which is then modulated by the optical modulator. The transmitted signal is amplified in a lumped or distributed manner to keep the signal level constant over a fiber segment. At the receiver, a coherent detector measures signal quadratures of the channel of interest, which are subsequently used for the statistical detection. An important element in WDM optical fiber networks is

the ROADM. In these networks a fiber link has to be shared among many users, each operating at a distinct wavelength. The signals of the users are added or dropped by ROADMs. A WDM signal may be accessible at the transmitter only, receiver only, both or neither one. In the later case the signal enters and leaves the fiber link in an intermediate distance without even being noticed by the transmitter or the receiver.

Below, we very briefly explain the function of the components of the Fig. 2.8.

2.3.1 Components of a Fiber-optic System

Optical Fiber

Optical fiber used in the long-haul communications consists of a cylindrical core surrounded by a cladding, both usually made of the silica glass SiO_2. Silica glass has numerous desirable transmission, environmental, and mechanical properties, making it perfect for data communications. The fiber glass is so transparent that today it can be manufactured to carry a laser signal more than 15 km while maintaining half of its power. Lightwave communications systems have bandwidths of the order of THz, ideal for the core networking applications. Silica glass is as strong as steel and can be fabricated in μm diameters with high precision, and yet remarkably sturdy and flexible. It is hard to imagine a medium better suited to high data rate transmission than optical fiber.

In the communication systems considered in this thesis, the typical launched powers correspond to a large number of photons, and the classical theory of Maxwell equations would suffice to describe the light propagation, instead of the quantum mechanics. Indeed light transmission in optical fibers can be qualitatively explained via the total internal reflection phenomenon in geometric optics: the silica glass is doped to shape the refractive index so that the refractive index of the fiber core is higher than that of the cladding, either in a step wise manner or smoothly. If the angle of the incidental ray with the fiber axis is smaller than a critical angle, the total internal reflection occurs in the core cladding surface, confining the light inside the fiber [21].

In the following, we review two important parameters of the optical fiber.

Fiber Loss Until the 1970s, the fiber loss was so substantial ($\alpha > 20$ dB/km) that a lightwave signal could not be sent in the fiber more than a few kilometers. Traces of OH ions and heavy metal impurities left in the silica glass can contribute to a significant loss. Fig. 2.9 shows the graph of the fiber loss versus wavelength. Causes of the loss are either intrinsic, due to the infrared ($7.4\mu\text{m} < \lambda < 300\mu\text{m}$) and ultraviolet (10 nm $< \lambda < 0.4$ μm) absorptions occurring in the fused silica, or extrinsic due to impurities.

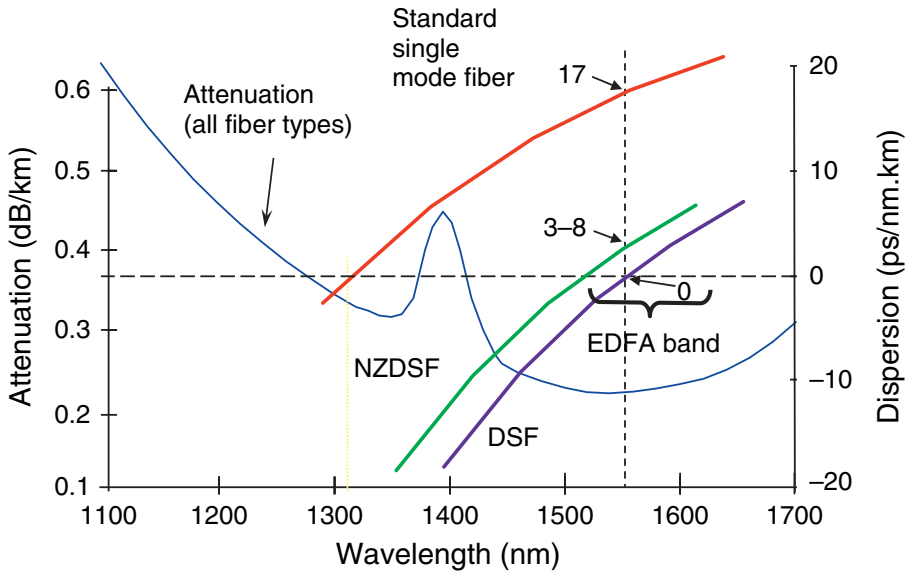

Figure 2.9: Fiber loss and dispersion versus wavelength (Courtesy of [1]).

A significant source of loss is the OH ions from water vapors left in the glass, whose harmonics contribute to the peak of the Fig. 2.9. At a wavelength close to $\lambda = 1.55$ μm loss has a minimum of about 0.2 dB /km.

To compensate for the power loss, fiber-optic communications systems use optical amplifiers. However, as we will see, these amplifiers introduce noise into the system. Thus one can trade perturbations caused by the loss with the fluctuations caused by the amplifiers.

Chromatic Dispersion As noted in Section 2.2.1, the dispersion (wavenumber) of a medium is generally frequency dependent. The first coefficient β_1 is a constant term in the speed and can be removed by introducing a retarded time. The second coefficient β_2 [sec^2/km] gives rise to the velocity of the envelope (2.20) and is called the *dispersion coefficient*. In the context of the optical fiber, it is often convenient to express β_2 in terms of the *dispersion parameter*

$$D = -\frac{2\pi c}{\lambda_0^2}\beta_2 \quad \text{ps/(nm.km)},$$

where c is the speed of light and λ_0 is the carrier wavelength. That is to say, in analogy with a horse race, there is a delay of D picoseconds after 1 km between two wavelengths of 1 nm apart. Positive and negative D correspond, respectively, to the anomalous (focusing) and normal (defocusing) regimes.

Fig. 2.9 shows the graph of the dispersion versus wavelength for a standard single

mode fiber. In addition to the coefficient β_2,, usually the third-order coefficient β_3 is also specified by the fiber manufacturers, expressed in terms of the *dispersion slope*

$$S = \frac{\mathrm{d}D}{\mathrm{d}\lambda} = \frac{4\pi c\beta_2}{\lambda^3} - \left(\frac{2\pi c}{\lambda^2}\right)^2 \beta_3.$$

The amount of the pulse broadening as a result of the dispersion is roughly $D\mathcal{L}\Delta\lambda$, where $\Delta\lambda$ is the wavelength resolution set by the laser spectral width [21]. For a standard single mode fiber with $D = 17$ ps/(nm.km), and a laser source with $\Delta\lambda = 0.1$ nm (*i.e.*, $\Delta f \approx 12.5$ GHz), the amount of the pulse broadening is 1700 ps in 1000 km, an ISI of $\sim$ 21 symbols for pulses with ~ 80 ps duration.

To suppress the effects of the dispersion, optical or electrical dispersion management (DM) is used. In optical dispersion management, segments of the fiber with positive and negative dispersion are used in cascade so that the signal is confined to its initial time window. In the electrical dispersion management, dispersion is compensated using digital signal processing at the transmitter, receiver or both. It has been demonstrated that optical systems greatly benefit from dispersion management in several ways. However, although the effects of the dispersion can be removed in the frequency domain, dispersion is coupled to the nonlinearity, and performing DM does not alleviate the impacts of the nonlinearity.

The wavenumber $\beta(\omega)$, loss coefficient $\alpha(\omega)$, refractive index $n(\omega)$, and material relative permittivity $\epsilon_r(\omega, \mathbf{E})$ can all be obtained from the susceptibility parameter χ

$$\begin{aligned} n(\omega, \mathbf{E}) &= 1 + \frac{1}{2}\Re\chi(\omega, \mathbf{E}), \\ \beta(\omega, \mathbf{E}) &= \omega n(\omega, \mathbf{E})/c, \\ \alpha(\omega) &= \frac{\omega}{nc}\Im\chi(\omega, 0), \\ \epsilon_r(\omega, \mathbf{E}) &= 1 + \chi(\omega, \mathbf{E}), \end{aligned}$$

where $\mathbf{E}$ is the electric field.

Optical Amplifiers

Optical amplifiers work as a result of the process of the *stimulated emission*, occurring *e.g.*, in a $p-n$ junction, due to the interaction of the light with matter. The same process also underlies the operation of the lasers, transistors, diodes, and integrated circuits.

Consider an n-type semiconductor, having excess electrons in the conduction band with excited state energy E_2, in contact with a p-type semiconductor, having holes in

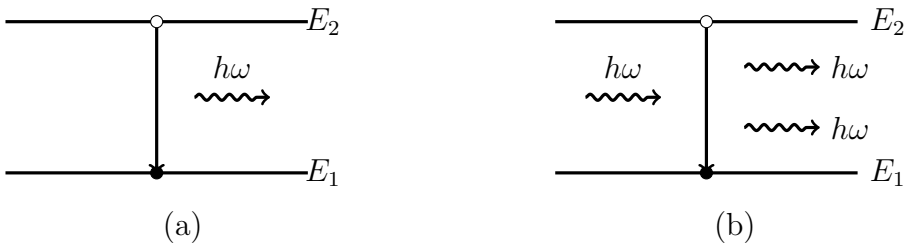

Figure 2.10: (a) Spontaneous emission. (b) Stimulated emission.

the valance band with ground state energy E_1. The $p-n$ junction is forward biased to reduce the width of the built-in voltage and establish a current. When an electron is absorbed from the excited state E_2 in a nearby hole at the lower state E_1, a photon with the frequency $\omega = (E_2 - E_1)/h$ is emitted. This can happen either spontaneously, in which photons are emitted with no external trigger and in random phases and directions, or stimulated by an external light source with frequency $\omega = (E_2 - E_1)/h$, in which the emitted photons are identical in phase, frequency and direction with the external photons.

Since in the stimulated emission the external and emitted photons are coherent, optical amplification can be realized. The amplification can be done in a discrete manner at several locations in the optical link using the erbium-doped fiber amplifiers (EDFAs) or continuously along the fiber using the Raman amplification.

Erbium-doped fiber amplifiers An EDFA consists of a short piece of fiber (a few tens of meters) doped with erbium ions or a similar dopant and optically pumped at 1.48 μm or 0.98 μm. While the amplification is achieved via the stimulated emission, some erbium ions move from the excited state to the ground state "spontaneously" as well, giving rise to the amplified spontaneous emission (ASE) noise.

The input output relationships of the signal before and after an EDFA located at distance z is

$$q(t, z^+) = Gq(t, z^-) + V(t)$$

where $G = e^{\alpha L_{\text{sp}}}$ is the amplifier gain in a span of fiber with length L_{sp} and loss coefficient α and $V(t)$ is the ASE noise. It has been demonstrated that the ASE noise is well modeled as additive white Gaussian with the power spectral density [22]

$$\text{PSD} = n_{\text{sp}} h\omega_0 (G - 1). \tag{2.27}$$

Here $n_{\text{sp}} \geq 1$ is the spontaneous emission efficiency factor, h is the Planck's constant, ω_0

Table 2.1: Fiber Parameters.

n_{sp}	1	spontaneous emission factor
h	$6.626 \times 10^{-34}\text{J} \cdot \text{s}$	Planck's constant
ω_0	193.55 THz	carrier frequency
α	0.046 km^{-1}	fiber loss (0.2 dB/km)
γ	1.27 $\text{W}^{-1}\text{km}^{-1}$	nonlinearity parameter

is the optical carrier frequency, and G is the amplifier gain. Typical fiber parameters are given in Table 2.1.

The efficiency of an EDFA is usually described by its noise figure, defined as the ratio of the SNRs at the amplifier input and output. It can be shown that

$$\text{NF} = 2n_{\text{sp}} - \frac{1}{G}\left(2n_{sp} - 1\right) < 2n_{\text{sp}}.$$

When $G \gg 1$, NF $\approx 2n_{sp}$ and the noise figure becomes a measure of n_{sp}. In general NF ≥ 0 dB , and for amplifiers where $G \gg 1$ and $n_{\text{sp}} = 1$, NF ≈ 3 dB .

The graph of the gain of an EDFA versus wavelength is peaked around 1.53 μm, and maintains a large gain in the optical C band 1.53 $\mu\text{m} \leq \lambda \leq 1.565$ μm (a window of 35 nm). Thus EDFAs can conveniently operate near the 1.55 μm system wavelength, where the fiber loss is minimum. The EDFA gain depends on the pumped power and can be as high as $30 - 50$ dB , with a noise figure NF $\approx 3 - 5$ dB and output power $10 - 25$ dBm.

Raman amplification In the distributed Raman amplification, the fiber itself, without doping, is used as a gain medium. Amplification is achieved thorough the process of *stimulated Raman scattering* (SRS). Raman pump units, placed at several locations in the optical link, inject high power fields in forward and backward directions. The incident field at frequency ω_{in} is absorbed by the silica glass, turning electrons in silica into oscillating dipoles, which in turn emit light at a lower frequency $\omega < \omega_{\text{in}}$. As before, the scattering process can be stimulated by an external light source of frequency ω, giving rise to distributed optical amplification . This keeps the signal power slightly varying around a constant mean along the fiber. The resulting ASE noise is Gaussian and white in space time

$$\mathsf{E}\{N(t,z)N^*(t',z')\} = \sigma_0^2\delta(t-t',z-z').$$

The noise power spectral density is obtained by taking the limit $L_{\text{sp}} \to 0$ of (2.27), obtaining

$$\sigma_0^2 = n_{\text{sp}}h\omega_0\alpha\mathcal{L},$$

where $\mathcal{L}$ is the total fiber length. The graph of the Raman gain versus frequency has a peak around 13.2 THz with a broad bandwidth as large as 8 THz. The pumped fields have high powers of a few watts, making the commercial development of distributed amplification challenging.

Optical Lasers

The optical source in long-haul high data rate systems is typically a semiconductor laser. A laser source is essentially an optical amplifier, operating based on the same principle of the stimulated emission, together with a feedback mechanism, to produce a powerful coherent beam of light. The output of a semiconductor laser source used in optical communications can have powers typically as high as few hundred milliwatts, concentrated around the signal frequency with a small *linewidth* (laser Δf before modulator due to phase noise, typically of order of MHz). We ignore the effects of the laser ASE noise and the non-zero laser linewidth in this thesis.

The bandwidth of a lightwave communications system, while depending on the bandwidth of all system components such as the laser source, fiber, amplifiers and network equipments, is usually limited by the bandwidth of the electronic circuits at the receiver.

2.3.2 Simplified Derivation of the NLS Equation

Derivation of the pulse propagation equation in optical fibers may be found in the standard text [21] or published papers. It is however useful to sketch a simplified derivation here to see the essence of the various terms in our channel model.

As mentioned earlier, pulse propagation in optical fibers is described by the classical theory of Maxwell equations. Canceling the magnetic fields in these equations, we obtain the well-known wave equation in the frequency domain

$$\nabla \times \nabla \times \widehat{\mathbf{E}} = -\mu_0 \omega^2 \widehat{\mathbf{D}}, \tag{2.28}$$

where $\mathbf{E}$ and $\mathbf{D}$ are the electric field and displacement vectors, μ_0 and ϵ_0 are, respectively, vacuum permittivity and permeability, and the hat symbol$\widehat{\ }$denotes the operation of the Fourier transform.

The displacement vector $\mathbf{D}$ depends on $\mathbf{E}$. Expanding $\mathbf{D}$ in terms of $\mathbf{E}$ in a vector

Volterra series (like a Taylor expansion for functionals)

$$\begin{aligned}\mathbf{D} &= \epsilon_0 \int_{-\infty}^{\infty} \epsilon_r^{(1)}(\tau)\mathbf{E}(t-\tau)\mathrm{d}\tau \\ &+ \int_{-\infty}^{\infty}\int_{-\infty}^{\infty}\int_{-\infty}^{\infty} \epsilon_r^{(3)}(\tau_1,\tau_2,\tau_3) : \mathbf{E}(t-\tau_1)\mathbf{E}(t-\tau_2)\mathbf{E}(t-\tau_2)\mathrm{d}\tau_1\tau_2\tau_3 + \cdots, \quad (2.29)\end{aligned}$$

where $\epsilon_r^{(k)}(\tau_1,\cdots,\tau_k)$ is the k^{th}-order permittivity kernel and following the inversion symmetry (centro-symmetry) of the SIO_2 crystal, the second-order kernel is zero. The notation $\epsilon_r^k : \mathbf{E}\cdots\mathbf{E}$ means a 3×1 vector whose each component is a product $E_{i_1}\cdots E_{i_k}$, $1 \le i_1,\cdots,i_k \le 6$, capturing interactions between the x, y, z components of the electric field and its conjugate at all times. For $k = 1$, the kernel ϵ_r^1 is simply a 3×3 matrix.

Assuming an isotropic wave propagation and ignoring the polarization birefringence, the tensors are diagonal and the wave propagation in each spatial coordinate is described independently by a scalar equation. The vector Volterra series (2.29) then reduces to a scalar Volterra series for each component, *e.g.*, $D := \mathbf{D}.\hat{\mathbf{x}}$ and $E := \mathbf{E}.\hat{\mathbf{x}}$

$$\begin{aligned}D &= \epsilon_0 \int_{-\infty}^{\infty} \epsilon_r^{(1)}(\tau)E(t-\tau)\mathrm{d}\tau \\ &+ \int_{-\infty}^{\infty}\int_{-\infty}^{\infty}\int_{-\infty}^{\infty} \epsilon_r^{(3)}(\tau_1,\tau_2,\tau_3)E(t-\tau_1)E^*(t-\tau_2)E(t-\tau_2)\mathrm{d}\tau_1\tau_2\tau_3 + \cdots. \quad (2.30)\end{aligned}$$

We remove the carrier $\exp(j(\omega-\omega_0)t)$ and assume that the envelope is slowly-varying so that the kernel $\epsilon_r^{(3)}(\tau_1,\tau_2,\tau_3)$ appears to be a delta function $\epsilon_r^{(3)}(\tau_1,\tau_2,\tau_3) = \epsilon_r^{(3)}\delta(\tau_1,\tau_2,\tau_3)$ with a constant coefficient $\epsilon_r^{(3)}$. This simplifies the nonlinear term to $\epsilon_r^{(3)}|E(t)|^2E(t)$. We then take the Fourier transform of the resulting equation. Given the small perturbative nature of the nonlinearity, we further assume that $|E(t)|^2$ is almost constant, so that $\widehat{E^3}(\omega) \approx |E|^2\widehat{E}(\omega)$. As a result, in the frequency domain we obtain the simple relation $\widehat{D} = \epsilon_0\epsilon_r\widehat{E}$, where

$$\epsilon_r(\omega,|E|^2) = \epsilon_r^{(1)}(\omega) + \epsilon_r^{(3)}|E|^2. \quad (2.31)$$

The wave equation (2.28) can be solved under (2.31). Assuming the separation of variables, we can express components of the envelope of $\mathbf{E}$ as $F(x,y)q(z,t)\exp(j(\omega_0 t - \beta_0 z))$. The cross section function F is separated out as in the linear cases. The space

derivatives $\partial/\partial x^2 + \partial/\partial y^2$ from $\nabla \times \nabla \times \mathbf{E}$ give F in terms of the Bessel functions. The second derivative of the remaining term $q(z,t)\exp(j(\omega_0 t - \beta_0 z))$ involves q_{zz}, q_z and q. For the slowly varying function q (in z), the curvature q_{zz} is ignored, and we obtain a dispersion relation for q

$$\beta(\omega, |q|) = \beta_0 + \beta_1(\omega - \omega_0) + \frac{1}{2}\beta_2(\omega - \omega_0)^2 + \cdots + \gamma|q|^2, \tag{2.32}$$

where $\gamma = \omega_0 n_2/(cA_{eff})$ is the Kerr nonlinearity coefficient and n_2 is the refractive index. The constant factor A_{eff} is the effective cross section and depends on $F(x,y)$ [21]. The terms $\beta - \beta_0$ and $(\omega - \omega_0)^k$ in the frequency represent, respectively, $-j\alpha/2 - j\partial/\partial z$ and and $j\partial/\partial t$ in the time. Multiplying (2.32) by q and making these substitutions, we obtain the nonlinear Schrödinger equation

$$q_z + \frac{\alpha}{2}q + \beta_1 q_t + \frac{j\beta_2}{2}q_{tt} = j\gamma|q|^2 q.$$

Note that the NLS equation is valid under the following assumptions:

- Signal bandwidth is much smaller than the carrier so that the higher order terms $(\omega - \omega_0)^k$ in the dispersion expansion are negligible at some k. This corresponds to a slowly varying envelope and is generally valid for pulses with duration $T > 1$ps.
- The medium is weakly nonlinear so that the cubic nonlinearity is a perturbation around the linear dispersion and the higher order nonlinear terms are negligible.
- The signal power is not too large so that other nonlinear phenomena, such as certain scattering processes not discussed here, can be ignored.

The NLS equation has been tested and used for many years now and it generally describes the experimental results very well.

Remark 7. Dispersion is due to the memory property of a dielectric and is reflected in the fact $p(t)$ depends on $E(t)$ in past and future, in the form of a convolution. This memory in turn, through the wave equation, implies nonuniform speeds across frequencies. Nonlinearity on the other hand is largely instantaneous, due to the dependency of the susceptibility to the intensity of the light.

Remark 8. Note that although the nonlinearity is locally a small perturbation around the dispersion, its effects are gradually accumulated with z.

2.4 Summary

Due to the inter-disciplinary subject of this thesis, we provided some of the necessary background in information theory, evolution equations and fiber-optic communications for the audience not familiar with some of these areas. Further details may be found in references made throughout this chapter.

Chapter 3

Origin of Capacity Limitations in Fiber-optic Networks

> It is a capital mistake to theorize before one has data.
>
> Sir Arthur Conan Doyle, A Study in Scarlet.

Recent studies on the information capacity of WDM optical fiber networks suggest that the spectral efficiency of such networks is ultimately limited by the inter-channel and intra-channel nonlinear interactions [7]. These interference distortions are deterministic and signal-dependent stochastic effects and grow with the input signal power, diminishing the capacity and the spectral efficiency at high signal-to-noise ratios. In these studies, the capacity, $\mathcal{C}$, increases with input power power, $\mathcal{P}$, reaching a peak at a certain critical input power, and then asymptotically vanishes as $\mathcal{P} \to \infty$ (see *e.g.*, [7] and references therein).

In this chapter, we briefly review the WDM model that is commonly used in these studies, as well as in the practical optical fiber systems. We briefly identify the origin of the capacity limitations in this model and explain that this method and similar ones, which are borrowed from linear system theories, are inappropriate for the communication over optical fiber networks. In particular the limitation of the capacity in the prior work is an artifact of these methods and some of the factors commonly believed to limit the achievable information rates are not indeed fundamental. In the subsequent chapters, we present a method that is able to fix these limitations and is fundamentally compatible with the structure of the nonlinear fiber optic channel, promising a higher spectral efficiency that keeps increasing beyond the critical input signal power associated

with linear transmission methods.

3.1 Capacity of WDM Optical Fiber Networks

Fiber-optic communication systems use wavelength-division multiplexing to transmit information. Similar to frequency-division multiplexing (FDM), in this method information is multiplexed in distinct wavelengths. This helps to separate the signal of the independent users in a network, where they have to share the same links between different nodes of the network.

Fig. 3.1 shows the system model for the part of an optical fiber network between a source and a destination. There are N fiber spans between multiple users at the transmitter (TX) and multiple users at the receiver (RX). The signal of some of these users is destined to a receiver other than the RX shown in Fig.3.1. As a result, at the end of each span there is a ROADM that may drop the signal of the some of the users or, if there are free frequency bands, add the signal of the potential external users. We are interested in evaluating the spectral efficiency of the fiber link from the TX to the RX.

Recall that the propagation of the complex envelope of a narrowband signal in each span of the fiber with distributed amplification is described by the stochastic nonlinear Schrödinger (NLS) equation [21, 23]

$$\frac{\partial Q(\tau,\ell)}{\partial \ell} + \frac{j\beta_2}{2}\frac{\partial^2 Q(\tau,\ell)}{\partial \tau^2} = j\gamma Q(\tau,\ell)|Q(\tau,\ell)|^2 + V(\tau,\ell), \quad 0 \le \ell \le < \mathcal{L}. \tag{3.1}$$

Here ℓ denotes distance (in km) along the fiber; the transmitter is located at $\ell = 0$, and the receiver is located at $\ell = \mathcal{L} = N\mathcal{L}_{\text{sp}}$. The symbol τ represents retarded time, measured in seconds, *i.e.*, $\tau = t - \beta_1 \ell$ where t is ordinary time and β_1 is a constant, and $Q(\tau,\ell)$ is the complex envelope of the signal propagating in the fiber. The coefficient β_2, measured in s^2/km, is called the chromatic dispersion coefficient, while γ, measured in $\text{W}^{-1}\text{km}^{-1}$, is the nonlinearity parameter. Finally, $V(\tau,\ell)$ is bandlimited white Gaussian noise with in-band spectral density σ_0^2 ($\text{W}/(\text{km}\cdot\text{Hz})$) and autocorrelation

$$\mathsf{E}\left\{V(\tau,\ell)V^*(\tau',\ell')\right\} = \sigma_0^2 \delta_W(\tau-\tau')\delta(\ell-\ell'),$$

where $\delta_W(x) = 2W\text{sinc}(2Wx)$. It is assumed that the transmitter is bandlimited to W

for all ℓ, $0 \leq \ell \leq \mathcal{L}$, and power limited to $\mathcal{P}_0$

$$\mathsf{E}\frac{1}{\mathcal{T}}\int_0^{\mathcal{T}} |Q_0(t)|^2 dt = \mathcal{P}_0.$$

The stochastic NLS equation (3.1) models both chromatic dispersion (captured by the $j\beta_2\partial^2 Q/\partial\tau^2$ term), which is responsible for temporal broadening, and the Kerr nonlinearity (captured by the $\gamma|Q|^2Q$ term), which is responsible for spectral broadening. Pulse propagation is governed by the tension between these effects and can be linearly dominated, nonlinearly dominated, or solitonic (in which case the two effects are balanced).[1] The NLS equation defines a nonlinear dispersive waveform channel from $Q(\tau, 0)$ at the transmitter to $Q(\tau, \mathcal{L})$ at the receiver.

We will find it convenient to work with the nonlinear Schrödinger equation (3.1) in a normalized form. By changing variables

$$q = \frac{Q}{\sqrt{P}}, \qquad z = \frac{l}{\mathcal{L}}, \qquad t = \frac{\tau}{T_0}, \tag{3.2}$$

with $T_0 = \sqrt{\frac{|\beta_2|\mathcal{L}}{2}}$ and $P = \frac{2}{\gamma\mathcal{L}}$, we get the normalized stochastic NLS equation

$$jq_z(t,z) = q_{tt} + 2|q(t,z)|^2 q(t,z) + v(t,z), \tag{3.3}$$

where

$$\mathsf{E}\left\{v(t,z)v^*(t',z')\right\} = \frac{\sigma_0^2}{PT_0}\delta_W(t-t')\delta(z-z').$$

Throughout this thesis, we primarily work with the normalized equation (3.3).

Stochastic partial differential equations (SPDEs) are usually interpreted via their equivalent integral representations. Integrating a function with unbounded variation is problematic, since *e.g.*, a Riemann approximation $\int_z^{z+\mathrm{d}z} g(z)\mathrm{d}B(z) \approx g(l)(B(z+\mathrm{d}z) - B(z))$, $l \in [z, z+\mathrm{d}z]$, where B is the Wiener process, would depend on the choice of l

[1] The action of a linear time-invariant system in the frequency domain is a multiplication by a filter H. This gives rise to separate amplitude and phase relations between input X and output Y (*e.g.*, $|Y| = |X||H|$). In contrast, the cubic nonlinearity in (3.3) is a triple convolution in the frequency domain, *i.e.*, an integral in which spectrum samples at various frequencies are (vectorially) added up with different angles (phases) controlled by dispersion. It follows that the nonlinearity converts phase modulations made by the dispersion to the amplitude modulations, leading to a constant exchange of information between amplitude and phase during the evolution. As a result, although the all-pass dispersion filter in (3.3) *individually* does not lead to any spectral broadening or narrowing, in the presence of a nonlinearity it can lead to such effects, thereby countering or amplifying the effects of the nonlinearity. The interaction between nonlinearity and dispersion can be understood via $q(t,z) = e^{-jz\partial_{tt}}q(t,0) - j\int_0^z e^{-j(z-z')\partial_{tt}}\left(2|q(t,z')|^2q(t,z') + v(t,z')\right)\mathrm{d}z'$, or its simplified (frequency domain) version (3.6).

(this ultimately comes from the linearity of variance stated in Observation 1). This leads to various interpretations for a SPDE, notably Ito and Stratonovich representations in which, respectively, $l = z$ and $l = z + \mathrm{d}z/2$ [24]. Due to conclusions made in this work, noise is treated only briefly in Section 6.5, where these conventions do not influence our results. Note that in the case that noise is bandlimited in time, the stochastic PDE is essentially a finite dimensional system and there is no difficulty in the rigorous interpretation of the stochastic NLS equation.

In a WDM optical system, the following signal is transmitted over the channel

$$q(t,0) = \sum_{k=1}^{N} \left(\sum_{l=1}^{WT} s_k^l \phi_l(t) \right) e^{jk2\pi Wt}, \quad 0 \le t \le T, \tag{3.4}$$

where s_k are the transmitted symbols, $\phi_l(t)$ are pulse shapes, $W \ge 1/T$ is the per channel bandwidth and N is the number of WDM channels. For illustration purpose, we can assume that each user sends an isolated pulse in the time interval $[0, T]$. Thus each user operates at a single frequency in a bandwidth $W = 1/T$ and $q(t,0) = \sum_1^N q_k(0) \exp(jk2\pi t/T)$, where $\{q_k(0)\}$ are the Fourier series coefficients at $z = 0$. When this signal is subject to an evolution, we have a Fourier series with variable coefficients

$$q(t,z) = \sum_{k=1}^{N} q_k(z) e^{j\frac{k2\pi t}{T}}. \tag{3.5}$$

Substituting the periodic solution (3.5) into (3.1), we get the NLS equation in the discrete frequency domain

$$\begin{aligned} j\frac{\partial q_k(z)}{\partial z} = & \underbrace{-4\pi^2 W^2 k^2 q_k(z)}_{\text{dispersion}} + \underbrace{2|q_k(z)|^2 q_k(z)}_{\text{SPM}} \\ & \underbrace{+ 2q_k(z) \sum_{l \neq k} |q_l(z)|^2}_{\text{XPM}} \\ & \underbrace{+ 2 \sum_{\substack{m \neq k \\ l \neq k}} q_m(z) q_l(z) q^*_{m+l-k}(z)}_{\text{FWM}} + v_k(z), \end{aligned} \tag{3.6}$$

in which v_k are the noise coordinates in frequency and we have identified the dispersion, self-phase modulation (SPM), cross-phase modulation (XPM) and four-wave mixing (FWM) terms in the frequency domain.

It is important to note that the optical WDM channel model is a (nonlinear) multi-

user *interference channel* [25]. The (inter-channel) interference terms are the XPM and FWM. There is no inter-symbol interference (ISI) in the isolated pulse transmission model (3.6) with one degree of freedom per user. However in a pulse train transmission model where $WT > 1$, replacing $\{q_k\}$ by $\{s_k\}$ via the inverse transform shows that the other two effects, the dispersion and SPM, cause inter-symbol interference (intra-channel interaction). Performance of a WDM transmission system depends on how interference and ISI are treated, and in particular the availability of the interference signals at the receiver. Several cases can be considered.

The SPM term of each user is available at the receiver for that user. Its deterministic part, if needed, can be removed, *e.g.*, by back propagation and its (signal-dependent) stochastic effects are handled by coding and optimal detection over a long block of data (*e.g.*, maximum likelihood sequence detection). ISI is therefore not a limitation to the capacity.

In contrast, a serious limitation to the capacity of optical fiber networks is the inter-channel interference. In optical fiber networks many users have to share the same optical fiber link. Each user has access to the signal in its own frequency band, and the signal of the users q_l, $l \neq k$, is generally unknown to the k^{th} user. In linear Gaussian channels there is no interference between users operating in disjoint frequency bands. In a nonlinear channel where, by definition, additively is not preserved under the action of the channel, multiplexing signals in a linear fashion, *e.g.*, by adding them in time or in frequency, leads to inter-channel interference.

In WDM optical systems, such linear frequency multiplexing is performed in ROADMs located in several locations throughout the fiber link. If multiplexing and demultiplexing is done only at the transmitter and receiver, one has access to the XPM and FWM interference terms. In this case interference is handled optimally by joint transmission and statistical detection, *e.g.*, using multiuser detection techniques. Such channel is essentially akin to a single user channel. Here one is expected to get an overall capacity similar to that of linear systems by joint transmission and detection.

Unfortunately in optical fiber networks it is not generally possible to perform joint transmission and detection. Many signals join and leave the optical link in intermediate distances without even being noticed by any user, leaving behind a residual nonlinear impact. The interference resulting from these signals is unavoidably treated as noise and ultimately limits the capacity of optical fiber networks.

Assuming the coefficients $q_k(z)$ remain independent in (3.6) during the evolution, the

XPM term is statistically regulated as $N \to \infty$

$$\sum_{l \neq k} |q_l(z)|^2 \to \frac{N-1}{N} \mathcal{P}_0 \to \mathcal{P}_0.$$

Thus the XPM does not influence the capacity of optical fibers significantly. The FWM on the other hand is cubic in signal and is not averaged out as XPM [26]. It is obvious that this interference will explode when increasing the common average power $\mathcal{P}$, ultimately overwhelming the signal and reducing the capacity to zero. The per degree of freedom capacity versus power curve $C(\mathcal{P})$ is noise-limited in low SNRs following $\log(1 + \text{SNR})$ and interference-limited in high SNRs, decreasing to zero [7, 26, 27]; see Fig. 3.2.

It follows that the information capacity of the nonlinear Schrödinger channel depends on the model assumed on this equation. One can assume a single-user or multiple-user channel with or without memory modeling. Below, we briefly elaborate on each case, essentially repeating the above argument.

Single-user discrete channels Capacity (bits/channel use) of a single user discrete channel (one complex degree of freedom) is a concave and non-decreasing function of the input average power (equality- or inequality-constraint). For a discrete memoryless channel this follows from the concavity of the mutual information as a function of the input distribution and the linearity of the cost constraint [28]. This, of course, holds true for any set of transition probabilities, including that obtained from nonlinear channels. Consider for instance the nonlinear channel

$$Y = X + X^2 N, \quad \mathsf{E}X^2 = \mathcal{P},$$

where random variables X, Y and N are, respectively, input, output, and noise. The power of the signal dependent additive noise term $X^2 N$ increases at a faster rate compared to the power of the signal term X. This, however, does not mean that the signal-dependent noise diminishes the capacity at high powers. In Shannon's argument, one is only concerned with typical sequences, in which the "good" and "bad" input symbols are averaged out. Nontypical sequences such as $(x_1, \cdots, x_1)$ may have variable output "noise balls", potentially large and increasing with x_1, but the noise balls associated with all input typical sequences have the same size in the sphere packing picture. In this sense, there is no distinction between linear and nonlinear channels when they are extended in time.

ISI in channels with memory Capacity of a single-user waveform channel is measured in bits per degree of freedom (equivalent to bits/s/Hz). Sending a large sinc wavetrain, as in (3.4) with $N = 1$, over the stochastic NLS equation, performing back propagation and maximum likelihood sequence detection at the receiver, one is expected to obtain a capacity that is nondecreasing with average input power. Thus the deterministic or stochastic intra-channel effects do not limit the capacity when joint transmission and detection of the degrees of freedom in time is computationally feasible. However assuming a discrete memoryless model for a nonlinear channel with memory such as the optical fiber, as often done in the literature, can potentially limit the capacity. This is explained below.

Note that, while the ISI is deterministic in traditional linear channels, for a nonlinear waveform channel, ISI can have a stochastic component as well. Even if a deterministic channel is a set of parallel non-interacting channels, noise addition, which usually becomes signal-dependent in the presence of a nonlinearity, can correlate these channels and bring the interference signals to the location of the channel of interest. Just as deterministic interference, this stochastic interference can limit the capacity of a nonlinear channel. This occurs only if the projection of the noise on the induced degrees-of-freedom is signal-dependent.

As a result if one sends the wavetrain (3.4) over the NLS channel and performs back propagation over the entire received block of data to remove the deterministic ISI, a net signal dependent noise is left over for each symbol

$$s_l^r = s_l^i + f(s_1^i, \cdots, s_{WT}^i, v), \quad l = 1, \cdots, WT,$$

where s_l^i and s_l^r are transmitted and received symbols and v is the noise. It is clear that performing isolated symbol detection, *e.g.*, per-symbol nearest neighbor mapping, has a capacity vanishing at high powers. This is in contrast to the application of the OFDM to linear ISI channels. The $\mathcal{C}(\mathcal{P})$ curve is, of course, similar to that of the linear systems if a maximum likelihood sequence detector (MLSD) is employed in which the sequence $(s_1^i, \cdots, s_{WT}^i)$ is jointly detected. The gains of using a MLSD are thus more pronounced in the nonlinear optical channel where the isolated detection poses a severe limitation to the capacity.

Interference in multi-user channels Here we are interested in the per user capacity and the sum rate of the multi-user channel. The per degree of freedom capacity of a continuous or discrete multi-user channel can potentially be decreasing with common

average power $\mathcal{P}$ if users interfere with one another and do not cooperate to manage this inter-channel interference. This can be an issue for linear channels as well; it is just a more serious issue for a strongly nonlinear channel such as the cubic NLS channel. The inter-channel interference is just the dual of the intra-channel ISI; the only difference is that cooperation and joint transmission and detection may not be physically possible among users. With users cooperating, one expects a nondecreasing per degree of freedom capacity similar to that of the linear systems. As we will see in this thesis, sometimes it is also possible to identify a set of non-interacting degrees-of-freedom for a nonlinear channel, giving rise to a transmission scheme in which the inter-channel interference does not limit the capacity.

Spectral broadening in nonlinear channels When a signal propagates in a nonlinear evolution equation, its spectrum can spread continuously. The amount of spectrum broadening depends on the pulse shape and generally is proportional to the signal power. While bits/symbol may increase with power, bit/sec/Hz may asymptotically vanish. Here we should divide bits/symbol to the maximum signal dimensions that admissible input signals occupy during the entire evolution. Spectral broadening is a serious issue in zero-dispersion fibers where the channel is strongly nonlinear [29]. In dispersive channels, it has been observed that pseudo-linear transmission does not suffer from a significant spectral broadening and this effect is not as significant [7]. Here one can simply divide the capacity by input bandwidth to obtain spectral efficiency.

3.2 The Importance of the Inter-channel Interference

From the above discussion it follows that while the intra-channel interference can be handled by memory modeling, the inter-channel interference ultimately limits the capacity of optical fiber networks. The current practice in fiber-optic communications is to send a linear sum of signals in time (pulse train) and in frequency (wavelength-division multiplexing) in the form of (3.4), both of which are poor ideas for the nonlinear fiber channel. Thus we identify ROADMs as the main culprit for the capacity limitation in optical fiber networks. These devices perform linear multiplexing of signals which is not consistent with the structure of the NLS equation, resulting in a severe interference that is subsequently treated as noise. A modification of these devices is needed so that the incoming signals are multiplexed in a nonlinear fashion, exciting noninteracting degrees

of freedom of the NLS equation. Note that the noise or intra-channel effects are not the primary reasons for the limitations of the capacity in the optical fiber networks and cannot bring down the $C(\mathcal{P})$ curve.

The effect of the interference when using the traditional frequency-division multiplexing in the nonlinear fiber channel is shown in Figs. 3.1 and 3.2. Here we have simulated transmission of 5 WDM channels over 2000 km of standard single-mode fiber with 100 spans. At the end of each span, a ROADM filters the channel of interest (COI) in the middle at 40 GHz bandwidth, and adds four side-band signals randomly from a common constellation (brown curves). At the output, the COI is filtered and back-propagated according to the inverse NLS equation. It can be seen that the nonlinear inter-channel interference is stronger at higher powers. Since this simulation is performed for isolated pulses per channel due to speed considerations, the per-channel power is increased by a factor of 5 to mimic the high energy nature of the pulse trains. Under a pulse train transmission, inter-channel interference effects are more significant.

It is clear from the Figs. 3.1-3.2 that as the average transmitted power is increased, the signal-to-noise ratio in the COI, and as a result the information rate, vanishes to zero. Note that this effect can simply be described by a SNR analysis at the receiver and one does not need a sophisticated information-theoretic analysis to illustrate it, unless exact numbers for the spectral efficiency are of interest. As it can seen from Fig. 3.1, the quality of the received signal in the COI degrades with power and taking the logarithm of the SNR gives the intended result fairly closely. The degradation of the capacity is simply because the real SNR is actually lower than the perceived SNR .

In the subsequent chapters it is shown that it is possible to exploit the integrability of the nonlinear Schrödinger equation and induce a k-user interference channel on the NLS equation so that both the deterministic inter-channel and inter-symbol interferences are zero for all users. This is done using the nonlinear Fourier transform and, in a special case, via a direct time domain approach. Such interference cancellation is a direct product of the integrability of the cubic nonlinear Schrodinger equation in $1+1$ dimensions, and is generally not doable for other types of nonlinearity (even if the nonlinearity is weaker!). The capacity or the spectral efficiency of the suggested method does not decline at the critical power associated with the linear methods. The scheme also has numerous other advantageous, desired in the communications networks.

Remark 9. Note that for the calculation of the capacity or the design of the optimal receiver it is not necessary to perform deterministic signal processing such as back propagation. For a communication study one is only concerned with transition probabilities, which include effects such as rotations or other deterministic transformations. Backprop-

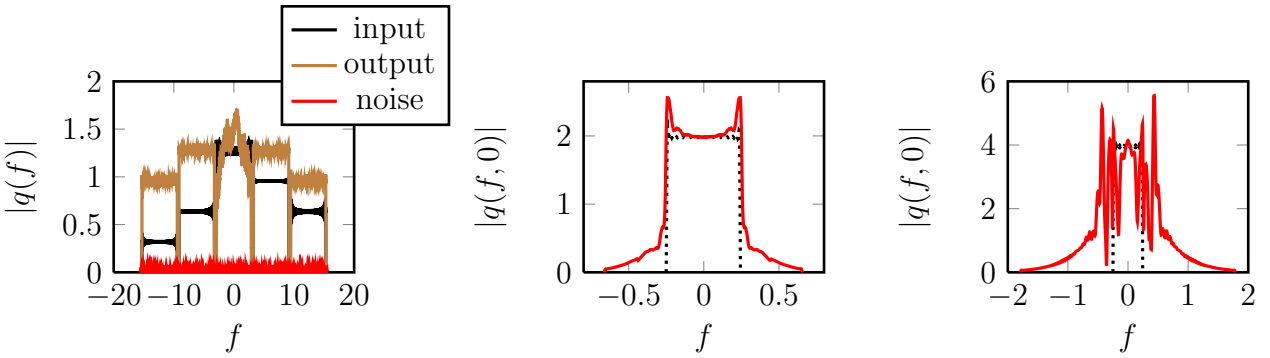

(a) (b) (c)

Figure 3.1: (a) 5 WDM channels in the frequency, with the channel of interest (COI) at the center. Neighbor channels are dropped and added at the end of the each span, creating a leftover interference for the COI. (b) Channel of interest at the input (dotted rectangle) and at the output after back propagation (solid curve). The mismatch is due to the fact that the back propagation is performed only on the channel of interest and the interference signals cannot be backpropagated. (c) Inter-channel interference is increased with signal level.

agation just aids the system engineer to simplify the task of the signal recovery, and it is likely suboptimal.

3.3 Summary

We reviewed important features of the WDM optical fiber networks pertinent to the capacity calculation. The achievable rates in such networks depend on the model assumed on the NLS equation, the method of the communication and how the noise, intra-channel interactions (ISI) and inter-channel interference are treated. Among these factors only the inter-channel interference can potentially bring down the $\mathcal{C}(\mathcal{P})$ due to the loss of the SNR. The signal-dependent noise (stochastic intra-channel effect) is handled by coding just as in linear systems, and the deterministic intra-channel interactions are not a fundamental limitation to the capacity either. We observed that the practice of using pulse trains and wavelength-division multiplexing both are ideas suitable for the traditional linear channels and are not necessarily appropriate for the nonlinear fiber channel. In particular, the decline of the capacity at high powers in the prior work is an artifact of using such methods incompatible with the structure of the NLS equation. The main culprit to the capacity limitation, when all other factors are addressed, are ROADMs which multiplex signals in a way not suitable for the NLS equation.

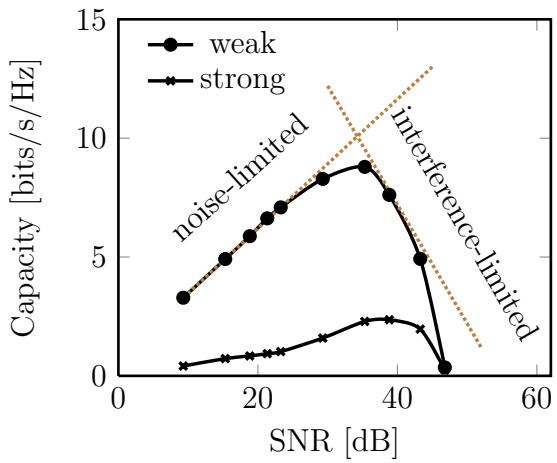

Figure 3.2: Spectral efficiency of WDM optical fiber transmission with weak and strong inter-channel interference.

Chapter 4

The Nonlinear Fourier Transform

> If people do not believe that mathematics is simple, it is only because they do not realize how complicated life is.
>
> John von Neumann

We shall begin developing the proposed nonlinear frequency-division multiplexing (NFDM) method mentioned earlier for communication over optical fiber networks. We consider a class of the evolution equations of the form (2.12), though throughout this thesis, the stochastic nonlinear Schrödinger equation (3.3) will be our primary and motivating illustrative example.

A nonlinear dispersive waveform channel such as (3.1) is a major departure from the classical additive white Gaussian noise and wireless fading channels in terms of analytical difficulty. Here the signal degrees-of-freedom couple together via the nonlinearity and dispersion in a complicated manner, making it difficult to establish the channel input-output map, even deterministically. Most current approaches assume a linearly-dominated regime of operation, or consider the nonlinearity as a small perturbation, and are geared towards managing and suppressing the (detrimental) effects of the nonlinear and dispersive terms. Inline dispersion management, digital backpropagation, and other forms of electronic pre-and post-compensation belong to this class of methods (see [7, 30–36] and references therein).

In this thesis we adopt a different philosophy. Rather than treating nonlinearity and dispersion as nuisances, we seek a transmission scheme that is fundamentally compatible with these effects. We effectively "diagonalize" the nonlinear Schrödinger channel with the help of the nonlinear Fourier transform, a powerful tool for solving *integrable* nonlinear

dispersive partial differential equations [9,10]. The NFT uncovers linear structure hidden in the one-dimensional cubic nonlinear Schrödinger equation, and can be viewed as a generalization of the (ordinary) Fourier transform to certain nonlinear systems.

With the help of the nonlinear Fourier transform, we are able to represent a signal by its discrete and continuous nonlinear spectra. While the signal propagates along the fiber based on the complicated NLS equation, the action of the channel on its spectral components is given by simple independent linear equations. Just as the (ordinary) Fourier transform converts a linear convolutional channel $y(t) = x(t) * h(t)$ into a number of parallel scalar channels, the nonlinear Fourier transform converts a nonlinear dispersive channel described by a *Lax convolution* (see Sec. 4.2) into a number of parallel scalar channels. This suggests that information can be encoded (in analogy with orthogonal frequency-division multiplexing) in the nonlinear spectra.

The nonlinear Fourier transform is intertwined with the existence of soliton solutions to the NLS equation. Solitons are pulses that retain their shape (or return periodically to their initial shape) during propagation, and can be viewed as system eigenfunctions, similar to the complex exponentials $e^{j\omega t}$, which are eigenfunctions of linear systems. An arbitrary waveform can be viewed as a combination of solitons, associated with the discrete nonlinear spectrum, and a non-solitonic (radiation) component, associated with the continuous nonlinear spectrum.

The goal of this chapter is to introduce the mathematical tools that underlie this approach to information transmission. These tools are sufficiently general to encompass not only the nonlinear Schrödinger equation, but also other completely integrable nonlinear dispersive PDEs. Thus, the transmission scheme described here can also be applied to any channel model in this general class. These tools are also described in mathematics and physics (see, e.g., [9, 10, 37]); here we attempt to extract those aspects of the theory that are relevant to the engineering aspects of the information transmission problem. In subsequent chapters, we will describe useful numerical methods and give performance results for actual fiber-optic systems.

The basic idea underlying this thesis has also been anticipated in [38]. Here the authors adopt a similar philosophy and use the inverse scattering transform (IST) to decode the amplitude of an isolated soliton-like pulse $A\text{sech}(t)$. There is however very limited development in [38] towards an optical system operating based on the IST. Motivated by the recent results in optical fiber networks showing that the spectral efficiency diminishes at high SNRs [39] and anticipating availability of high-performance computing devices and sophisticated receivers, in this thesis we conceive and develop an OFDM-type multi-user transmission technique by considering the IST as a nonlinear Fourier trans-

form. Note that, as mentioned earlier and will be clarified later on, the advantages of the IST method in point to point channels are limited to the stability and robustness of the spectral invariants and few other desirable properties. The important advantage of using the IST for communications, or insights drawn from that, occurs in a multi-user scenario where the underlying interference is severe and cannot be addressed, at least in a straightforward manner, using the techniques already in place.

4.1 A Brief History of the Nonlinear Fourier Transform

The nonlinear Fourier transform (also known as the inverse scattering transform or IST) is a method for solving certain nonlinear dispersive partial differential equations. These are integrable PDEs, *i.e.*, nonlinear differential equations exhibiting certain hidden linearity. There are several integrable equations having physical significance, among which is the NLS equation. The IST method was a result of extensive efforts in theoretical physics and applied mathematics in the 1960s, closely associated with the notion of solitons and is often used to predict their existence and properties in integrable models [9, 10].

In the 1950s, in one of the first dynamical-systems simulations performed on a computer [40], Fermi, Pasta and Ulam performed a numerical experiment to understand why solids have finite heat conductivity. They modeled the solid as a lattice with point masses at the lattice points coupled with springs each having a quadratic nonlinearity. To their surprise, rather than observing an equipartition of energy among all modes, energy cycled periodically among a few low-order modes. Such behavior implies that the nonlinear oscillator behaves somehow linearly.

In the 1960s, Zabusky and Kruskal showed that the equations of motion for the Fermi-Pasta-Ulam lattice in the continuum limit is a remarkable PDE called the Korteweg-de Vries (KdV) equation [41], known in the study of water waves. The KdV equation for the evolution of a real-valued pulse $q(t, z)$ as a function of time t and distance z is

$$q_z = qq_t + q_{ttt}. \tag{4.1}$$

Zabusky and Kruskal found that (4.1) has pulse-like solutions whose shape is preserved (or varies periodically) during propagation. Furthermore, they made the surprising observation that when two such pulses are launched towards each other, despite their nonlinear interaction, they pass through each other without changing their shape. Zabusky and Kruskal coined the term *soliton* for such solutions, in recognition of their particle-like

properties [41].

The spectacular properties of these solutions greatly excited the mathematics and physics communities and many researchers started to study solitons. In a celebrated paper [42], Gardner, Greene, Kruskal and Miura uncovered some of the deep structure underlying the KdV equation which is responsible for solitons and their unusual properties. The authors of [42] were studying the celebrated linear Schrödinger equation from quantum mechanics, given by

$$\psi_z(t,z) = \psi_{tt}(t,z) + g(t,z)\psi(t,z)/3, \tag{4.2}$$

where $\psi(t,z)$ is the wave-function and $g(t,z)$ is an external potential. They found that if one takes the solution $q(t,z)$ of the KdV equation (4.1) as the external potential in (4.2), then the eigenvalues of the Schrödinger operator

$$H = \frac{\partial^2}{\partial t^2} + g(t,z)/3 \tag{4.3}$$

remain invariant during the evolution in z! Based on this critical observation, they developed a method to recover the external potential $g(t,z) = q(t,z)$ by solving an inverse problem for (4.2). The method analytically predicts soliton solutions for the KdV equation, as observed earlier by Zabusky and Kruskal through numerical computations. They had in fact found the IST for the special case of the KdV equation.

It was not immediately clear if the method developed in [42] could be generalized to other nonlinear PDEs, since it is not obvious if there exists a certain auxiliary operator, like the Schrödinger operator H, whose eigenvalues are preserved during the evolution. In a landmark paper published in 1968 [43], Lax put the theory on a firm mathematical footing. In particular, he established the mathematical relationship between the auxiliary operators with invariant eigenvalues (now called Lax pairs) and the original nonlinear equation. Once a Lax pair for a nonlinear PDE is found, a method along the lines of [42] can be applied to solve that PDE.

Shortly afterwards, in 1972, Zakharov and Shabat found a Lax pair for the NLS equation in one spatial dimension [23], and thus established that this equation, too, could be solved in the same manner. Details of this method for the NLS equation were subsequently developed by Ablowitz and others (see [9] and references therein), who also referred to this scheme as the "nonlinear Fourier transform". After these discoveries from the 1960s and 70s, research into solitons became an established area of research, lying at the intersection of applied mathematics and nonlinear physics.

Nonlinear PDEs solvable by the NFT are called integrable equations or exactly solvable models [44]. These are usually Hamiltonian systems having an infinite number of conserved quantities, and include the KdV, NLS, modified KdV, and sine-Gordon equations, the Toda lattice, among others [9, 10]. These equations all exhibit similar properties, including the existence of soliton solutions. Signal processing problems (e.g., detection and estimation) involving soliton signals in the Toda lattice and similar models have been considered by Singer [45].

4.2 Canonical Lax Form for Exactly Solvable Models

4.2.1 Lax Pairs and Evolution Equations

We wish to consider linear differential operators whose eigenvalues are invariant during an evolution [43]. More precisely, we consider such operators defined in terms of a signal $q(t, z)$ where the eigenvalues of the operator remain constant even as q evolves (in z) according to some evolution equation.

To facilitate the discussion, it is useful to imagine a linear operator represented as a matrix; however, we must keep in mind that, when moving from finite-dimensional spaces to infinite-dimensional spaces (of e.g., functions and operators), some results do not carry over necessarily. The relevant properties of linear operators needed for this thesis are reviewed in Appendix A.

Let $L(z)$ be a square matrix whose entries are functions of z. Clearly, the eigenvalues of this matrix are in general functions of z too. However, for some matrices, it might be the case that while the entries of the matrix change with z, the eigenvalues remain constant (independent of z). Such a matrix, if diagonalizable, should be similar to a constant diagonal matrix Λ, i.e., $L(z) = G(z)\Lambda G^{-1}(z)$, for some similarity transformation $G(z)$.

This idea generalizes to operators. Let $\mathcal{H}$ be a Hilbert space, let $\mathcal{D}$ be some domain that is dense in $\mathcal{H}$, and let $L(z) : \mathcal{D} \to \mathcal{H}$ be a family of linear operators indexed by a parameter z [46]. If the eigenvalues of $L(z)$ do not depend on z, then we refer to $L(z)$ as an *isospectral* family of operators. If diagonalizable, it follows that for each z, $L(z)$ is similar to a multiplication operator Λ (the operator equivalent of a diagonal matrix; see Appendix A), i.e., $L(z) = G(z)\Lambda G^{-1}(z)$, for some operator $G(z)$.

Assuming that $L(z)$ varies smoothly with z, we can consider the rate of the change

(with respect to z) of $L(z)$. We have

$$\begin{aligned}\frac{\mathrm{d}L(z)}{\mathrm{d}z} &= G'\Lambda G^{-1} + G\Lambda\left(-G^{-1}G'G^{-1}\right)\\ &= G'G^{-1}\left(G\Lambda G^{-1}\right) - \left(G\Lambda G^{-1}\right)G'G^{-1}\\ &= M(z)L(z) - L(z)M(z) = [M,L]\,,\end{aligned} \tag{4.4}$$

where $G' = \mathrm{d}G(z)/\mathrm{d}z$, $M = G'G^{-1}$, and $[M,L] \triangleq ML - LM$ is the *commutator bracket*. In other words, every diagonalizable isospectral operator $L(z)$ satisfies the differential equation (4.4).

Conversely, suppose $M(z)$ is given and the (unknown) diagonalizable operator $L(z)$ evolves according to (4.4) with initial condition $L(0) = G_0\Lambda_0 G_0^{-1}$. Let $G(z)$ be the (unique invertible) solution to $G' = MG$ with $G(0) = G_0$. One can easily verify that $L(z) = G(z)\Lambda_0 G(z)^{-1}$ satisfies (4.4). Since the solution to a first-order differential equation is unique [47], we see that $L(z)$ is an isospectral family.

The characterization of isospectral operators is therefore summarized in the following lemma [43].

Lemma 6. *Let $L(z)$ be a diagonalizable operator. Then $L(z)$ is isospectral if and only if it satisfies*

$$\frac{\mathrm{d}L}{\mathrm{d}z} = [M,L], \tag{4.5}$$

for some operator M. If L is self-adjoint (so that L is unitarily equivalent to a multiplication operator, i.e., $L = G\Lambda G^*$), then M must be skew-Hermitian, i.e., $M^* = -M$.

Proof. The proof was outlined above. The skew-Hermitian property of M can be shown by differentiating $GG^* = I$. □

It is important to note that L and M do not have to be independent and can depend on a common parameter, e.g., a function $q(t,z)$, as illustrated in Fig. 4.1. The isospectral property of the solution is unchanged. The commutator bracket $[M,L]$ in (4.5) can create nonlinear evolution equations for $q(t,z)$ in the form

$$\frac{\partial q}{\partial z} = K(q),$$

where $K(q)$ is some, in general nonlinear, function of $q(t,z)$ and its time derivatives. An example of this is the KdV equation.

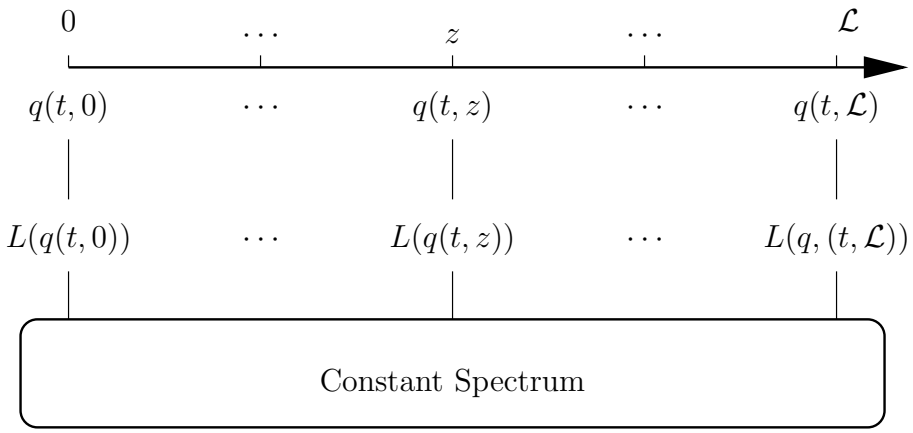

Figure 4.1: An isospectral flow: the spectrum of L is held invariant even as $q(t,z)$ evolves.

Example 8 (KdV equation). Let $D = \frac{\partial}{\partial t}$ denote the time-derivative operator, and let $q(t,z)$ be a real-valued function. Finally, let

$$\begin{aligned} L &= D^2 + \frac{1}{3}q, \text{ and let} \\ M &= 4\left(D^3 + \frac{1}{4}Dq + \frac{1}{4}qD\right). \end{aligned} \tag{4.6}$$

The Lax equation $L_z = [M, L]$ is easily simplified to

$$\frac{1}{3}q_z - \frac{1}{3}\left(q_{ttt} + qq_t\right) + (\text{some terms})D \equiv \mathbf{0}, \tag{4.7}$$

where $\mathbf{0}$ is the zero operator. The zero-order term of this equation as a polynomial in D, which must be zero, produces the KdV equation $q_z = q_{ttt} + qq_t$. Using $(D^k)^* = (-1)^k D$ (provable by integration by parts), it is easy to see that L and M are self-adjoint and skew-Hermitian, respectively, since they are real valued and involve even and odd powers of $\mathcal{D}$, respectively. The eigenvalues of L are thus preserved from Lemma 6. Note that the L operator in this example is precisely the (linear) Schrödinger operator H given in (4.3). □

Definition 3. A pair of operators L and M, depending on z, are called a Lax pair (L, M) if they satisfy (4.5). Following Lemma 6, the eigenvalues of the L operator are independent of z.

4.2.2 The Zero-Curvature Condition

The eigenvalues of the operator L, which are constant in an isospectral flow, are defined via

$$Lv = \lambda v. \tag{4.8}$$

Taking the z derivative of (4.8) and using the Lax equation $L_z = [M, L]$, we obtain $(L - \lambda I)(v_z - Mv) = 0$. Since $L - \lambda I$ vanishes only on eigenvectors of L, it must be that $v_z - Mv$ is proportional to an eigenvector, i.e., $v_z - Mv = \alpha v$, $\alpha \in \mathbb{C}$. The choice of α does not influence the results of future sections; thus for simplicity we set $\alpha = 0$. It follows that an eigenfunction $v(t, z)$ evolves based on the linear equation

$$v_z = Mv. \tag{4.9}$$

Furthermore, it is often more convenient to re-write (4.8) as

$$v_t = Pv, \tag{4.10}$$

for some operator P. The relationship between P and L can be derived (if necessary) by combining $(DI - P)v = 0$ with $(L - \lambda I)v = 0$, obtaining

$$P = \Sigma(L - \lambda I) + DI, \tag{4.11}$$

where Σ is some invertible operator, and $D = \frac{\partial}{\partial t}$ as in Example 8.

Combining equations (4.9) and (4.10) by using the equality of mixed derivatives, i.e., $v_{tz} = v_{zt}$, the Lax equation (4.5) is reduced to the *zero-curvature condition* [10]

$$P_z - M_t + [P, M] = 0. \tag{4.12}$$

Note that the nonlinear equation derived from (4.12) results as a compatibility condition between the two linear equations (4.9) and (4.10). This shows that certain nonlinear equations possess a "hidden linearity" in the form of (4.9) and (4.10).

Following the work of Zakharov and Shabat on the NLS equation [23], Ablowitz et al. [48] suggested that for many equations of practical significance, the operator P can be fixed as

$$P = \begin{pmatrix} -j\lambda & r(t,z) \\ s(t,z) & j\lambda \end{pmatrix}, \tag{4.13}$$

where $r(t, z)$ and $s(t, z)$ are functions—depending on $q(t, z)$—to be determined to produce

a given nonlinear evolution equation. From (4.11) this corresponds to the L operator

$$L = j \begin{pmatrix} D & -r(t,z) \\ s(t,z) & -D \end{pmatrix}, \tag{4.14}$$

with $\Sigma = \mathrm{diag}(j, -j)$. In this case, both L and P operate on 2×1 vector functions.

Equation (4.10), with P as in (4.13), is known as the *AKNS system* (after the authors of [48]) and is central in the study of the nonlinear Fourier transform [10]. The important special case where $r(t,z) = q(t,z)$ and $s(t,z) = -q^*(t,z)$ is generally known as the *Zakharov-Shabat system*. We will refer to (4.8), (4.9) and (4.10) as the L-, M-, and P-equations, respectively. Throughout this thesis, we will assume that the domain of L, P, and M are subsets of the Hilbert space $L^2(\mathbb{R})$, denoted here by $\mathcal{H}$, depending on the particular structure of that operator.

Example 9 (sine-Gordon equations). Let $r(t,z) = -s(t,z) = \frac{1}{2}q_t(t,z)$ in (4.13) and let

$$M = \frac{j}{4\lambda} \begin{pmatrix} \cos(q) & -\sin(q) \\ -\sin(q) & -\cos(q) \end{pmatrix}. \tag{4.15}$$

Then the zero-curvature equation is simplified to $q_{tz} = \sin(q)$. Taking $r = s = \frac{1}{2}q_t$ and M as

$$M = \frac{j}{4\lambda} \begin{pmatrix} \cosh(q) & -\sinh(q) \\ \sinh(q) & -\cosh(q) \end{pmatrix}. \tag{4.16}$$

gives $q_{tz} = \sinh(q)$. □

Example 10 (Nonlinear Schrödinger equation). Take $r = q$, $s = -q^*$ and

$$M = \begin{pmatrix} 2j\lambda^2 - j|q(t,z)|^2 & -2\lambda q(t,z) - jq_t(t,z) \\ 2\lambda q^*(t,z) - jq_t^*(t,z) & -2j\lambda^2 + j|q(t,z)|^2 \end{pmatrix}.$$

The zero-curvature equation is simplified to $jq_z(t,z) = q_{tt}(t,z) + 2|q(t,z)|^2 q(t,z)$. □

Example 11 (KdV equation revisited). Let $r = \frac{2}{\sqrt{3}}q$, $s = -\frac{1}{4\sqrt{3}}$ and

$$M = \begin{pmatrix} 4j\lambda^3 - \frac{j\lambda q}{3} + \frac{q_t}{6} & -\frac{8\lambda^2 q}{\sqrt{3}} - \frac{4}{\sqrt{3}}j\lambda q_t + \frac{2q^2}{3\sqrt{3}} + \frac{2q_{tt}}{\sqrt{3}} \\ \frac{\lambda^2}{\sqrt{3}} - \frac{q}{12\sqrt{3}} & -4j\lambda^3 + \frac{j\lambda q}{3} - \frac{q_t}{6} \end{pmatrix}. \tag{4.17}$$

The zero-curvature equation leads to $q_z = qq_t + q_{ttt}$. □

It should be noted from Examples 8 and 11 that the choice of L and M giving rise to a given nonlinear equation is not unique. Obviously one can scale L, or add a constant to L

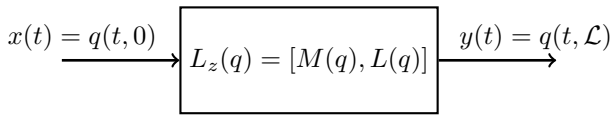

Figure 4.2: A system defined by Lax convolution.

or M. In addition, both the Lax equation (4.5) and (4.8) are unchanged under orthogonal transformations, i.e., replacing L and M with $\Sigma L \Sigma^T$ and $\Sigma M \Sigma^T$, respectively, where Σ is a (constant) orthogonal matrix, i.e., $\Sigma^T \Sigma = I$. Note further that it may be possible to choose two Lax pairs (L_1, M_1) and (L_2, M_2) for a given equation such that L_1 is self-adjoint and L_2 is not self-adjoint. The eigenvalues of L_1 and L_2 are, respectively, real and complex; see Appendix A.

4.2.3 Lax Convolution and Integrable Communication Channels

Linear systems traditionally have been described by linear constant coefficient differential equations. An example is the one-dimensional heat equation $q_z = c^2 q_{tt}$, where c is the diffusion coefficient and $q(t, z)$ represents the heat profile across a rod extending in *space* t, as *time* z goes on. From a systems point of view, this defines a linear time-invariant system from input $x(t) = q(t, 0)$ at $z = 0$ to the output $y(t) = q(t, \mathcal{L})$ at some $z = \mathcal{L}$. The role of z is therefore just a parameter and once fixed (to $z = \mathcal{L}$), the system is described by an impulse response (or a Green function) $h(t; \mathcal{L})$, representing the underlying (linear) convolution.

Following this analogy, we wish to define a system in terms of a Lax pair (L, M). Here, L and M are parametrized by a waveform $q(t, z)$. Such a system accepts a waveform $x(t) = q(t, 0)$ at its input and produces a waveform $y(t) = q(t, \mathcal{L})$ at its output, according to the evolution equation induced by $L_z = [M, L]$. The time-domain input-output map is thus given by an evolution equation of the form $q_z = K(q)$, obtainable from the Lax equation (4.5) (or its equivalent (4.12)). We refer to such a system as an *integrable system*. Note that an integrable system is completely characterized by the two operators (L, M) and the parameter $z = \mathcal{L}$, independent of the signals. We denote such a system using the triple $(L, M; \mathcal{L})$.

Definition 4 (Lax Convolution)**.** We refer to the action of an integrable system $S = (L, M; \mathcal{L})$ on the input $q(t, 0)$ as the Lax convolution of q with S. We write the system output as $q(t, \mathcal{L}) = q(t, 0) * (L, M; \mathcal{L})$. See Fig. 4.2.

Definition 5 (Integrable communication channels)**.** A waveform communication channel $C : x(t) \times v(t,z) \to y(t)$ with inputs $x(t) \in L^1(\mathbb{R})$ and space-time noise $v(t,z) \in L^2(\mathbb{R}, \mathbb{R}^+)$, and output $y(t) \in L^1(\mathbb{R})$, is said to be *integrable* if the noise-free channel is an integrable system.

Note that noise can be introduced into an integrable system in a variety of ways. In what follows, we assume that the signal-to-noise ratio is not too small, so that the stochastic system may justifiably be considered as a perturbation of the deterministic system. Furthermore, in this thesis we limit ourselves to integrable channels with additive noise, i.e.,

$$q_z = K(q) + v(t,z), \quad q(t,0) = x(t), \quad q(t,\mathcal{L}) = y(t),$$

where $v(t,z)$ is distributed band-limited noise. Note that this model is *not* in general equivalent to one in which noise is added (in lumped fashion) at the channel output. Here, the noise is distributed in space, and so interacts with the signal (in a potentially very complicated manner) according to the given evolution equation.

In this thesis, we develop a scheme for communication over integrable channels. By various choices of Lax pair (L, M), one can construct a variety of interesting channel models, mostly nonlinear, which go beyond the linear channel models typically studied in data communications. Interestingly, some linear channels can also be analyzed using this nonlinear spectral approach advocated here [49]. The central application (and motivation) for this work is fiber-optic communication, in which the channel model is given by the nonlinear Schrödinger equation (3.1), and for which a Lax pair was given in Example 10. In what follows, we first discuss the deterministic (noise-free) case and later treat noise as a perturbation of the deterministic system.

4.3 Nonlinear Fourier Transform

In this section, we assume that a function $q(t,\cdot) \in L^1(\mathbb{R})$ is given, and we define its nonlinear Fourier transform with respect to a given Lax operator L. As the notation $q(t,\cdot)$ implies, in this and the next section, the variable z can take on any value in the range $[0, \mathcal{L}]$ and is irrelevant in the forward and inverse transforms. We shall therefore omit the index z in what follows.

As previously noted, for concreteness we carry through the development of the NFT

for the case of the NLS equation (3.3), for which the P- and M-equations are given by

$$v_t = P(\lambda, q)v = \begin{pmatrix} -j\lambda & q(t,z) \\ -q^*(t,z) & j\lambda \end{pmatrix} v, \tag{4.18}$$

$$\begin{aligned} v_z &= M(\lambda, q)v \\ &= \begin{pmatrix} 2j\lambda^2 - j|q(t,z)|^2 & -2\lambda q(t,z) - jq_t(t,z) \\ 2\lambda q^*(t,z) - jq_t^*(t,z) & -2j\lambda^2 + j|q(t,z)|^2 \end{pmatrix} v, \end{aligned} \tag{4.19}$$

respectively. Here the P-equation is the Zakharov-Shabat system.

The nonlinear Fourier transform (and its inverse) are defined solely in terms of the temporal P-equation (4.18). The spatial M-equation (4.19) is used in a brief, and critical, propagation step, but plays no role in the definition of the nonlinear Fourier transform.

If for a given $\lambda \in \mathbb{C}$, the operator $L - \lambda I$, here equivalent to $DI - P$ representing (4.18), is not invertible, we say that λ belongs to the spectrum of L and $v(t, \lambda)$ represents its associated eigenfunction. In finite-dimensional Hilbert spaces of matrices the spectrum is a discrete finite set, called eigenvalues. This may no longer be true in infinite-dimensional spaces of operators, where the eigenvalues (if they exist) may only be one part of the spectrum. See Appendix A.

The nonlinear Fourier transform of a signal $x(t)$ with respect to an operator L in a Lax pair is defined via the spectral analysis of the L operator, which we consider next.

4.3.1 Canonical Eigenvectors and Spectral Coefficients

We wish to study solutions of (4.18), in which vectors $v(t)$ are considered as elements of the vector space $\mathcal{H}$. We begin by equipping the vector space $\mathcal{H}$ with a symplectic bilinear form $\mathcal{H} \times \mathcal{H} \mapsto \mathbb{C}$, which, for any *fixed* value of $t \in \mathbb{R}$, is defined as

$$\langle v(t), w(t) \rangle_s = v_1(t)w_2(t) - v_2(t)w_1(t). \tag{4.20}$$

Let us also define the adjoint of any vector v in H as

$$\tilde{v}(t) = \begin{pmatrix} v_2^*(t) \\ -v_1^*(t) \end{pmatrix}.$$

The following properties hold true for all v and w in H:

- $\tilde{\tilde{v}} = -v$;
- $\langle v, v \rangle_s = 0$;
- $\langle v, w \rangle_s = -\langle w, v \rangle_s$;

- $\langle \tilde{v}, v \rangle_s = -\langle v, \tilde{v} \rangle_s = |v_1|^2 + |v_2|^2$;
- $\frac{\mathrm{d}}{\mathrm{d}t}\langle v, w \rangle_s = \langle v_t, w \rangle_s + \langle v, w_t \rangle_s$;
- for every 2×2 matrix A, $\langle Av, w \rangle_s + \langle v, Aw \rangle_s = \mathrm{tr}(A)\langle v, w \rangle_s$.

There are generally infinitely many solutions v of (4.18) for a given $\lambda \in \mathbb{C}$, parametrized by the set of all possible boundary conditions. These solutions form a subspace E_λ of continuously differentiable 2×1 vector functions (an eigenspace).

Lemma 7. *For all vectors $v(t)$ and $w(t)$ in E_λ,*

1. *$\tilde{v} \in E_{\lambda^*}$, i.e., $\tilde{v}_t = P(\lambda^*, q)\tilde{v}$;*
2. *$\langle v(t), w(t) \rangle_s$ is a constant, independent of t;*
3. *If $\langle v(t), w(t) \rangle_s \neq 0$, then v and w are linearly independent and form a basis for E_λ;*
4. *$\dim(E_\lambda) = 2$.*

Proof: Property 1) follows directly from (4.18). To see 2), note that $\frac{\mathrm{d}}{\mathrm{d}t}\langle v, w \rangle_s = \langle v_t, w \rangle_s + \langle v, w_t \rangle_s = \langle Pv, w \rangle_s + \langle v, Pw \rangle_s = \mathrm{tr}(P)\langle v, w \rangle_s = 0$. To see 3), fix t and let $u(t) \in E_\lambda$, then $u(t) = a(t)v(t) + b(t)w(t)$ for some $a(t)$ and $b(t)$. Taking the symplectic inner product of both sides with w and v, we get $a(t) = \langle u, w \rangle_s / \langle v, w \rangle_s$ and $b(t) = \langle u, v \rangle_s / \langle w, v \rangle_s$. From Property 2, $\langle u, w \rangle_s$, $\langle v, w \rangle_s$, $\langle u, v \rangle_s$, and $\langle w, v \rangle_s$ are all independent of t. It follows that a and b are also independent of t. Finally, 4) follows from 3). □

An important conclusion of Lemma 7 is that any two linearly independent solutions u and w of (4.18) provide a basis for the solution space. To choose two such solutions, we examine the behavior of the equation at large values of $|t|$. If we assume that $q(t, \cdot) \to 0$ as $|t| \to \infty$, then, as $|t| \to \infty$ (4.18) is reduced to

$$v_t \to \begin{pmatrix} -j\lambda & 0 \\ 0 & j\lambda \end{pmatrix} v, \qquad \text{for large } |t|,$$

which has a general solution

$$v(t, \lambda) \to \left[\alpha e^{-j\lambda t}, \beta e^{j\lambda t}\right]^T, \quad \alpha, \beta \in \mathbb{C}.$$

Two possible boundary conditions, bounded in the upper half complex plane ($\Im(\lambda) > 0$), are

$$v^1(t, \lambda) \to \begin{pmatrix} 0 \\ 1 \end{pmatrix} e^{j\lambda t}, \quad t \to +\infty \tag{4.21}$$

$$v^2(t, \lambda) \to \begin{pmatrix} 1 \\ 0 \end{pmatrix} e^{-j\lambda t}, \quad t \to -\infty. \tag{4.22}$$

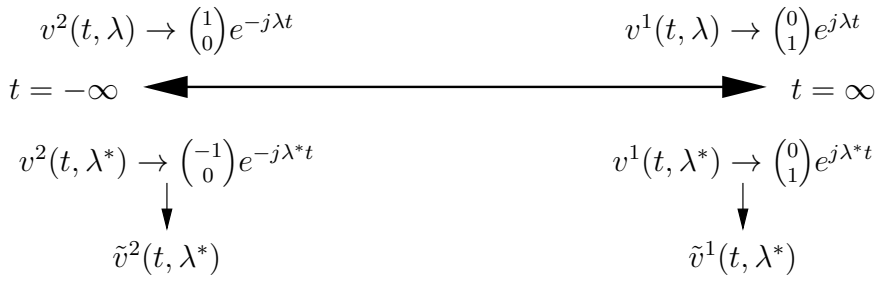

Figure 4.3: Boundary conditions for the canonical eigenvectors.

We solve (4.18) for a given λ under the boundary conditions (4.21)-(4.22), and denote the resulting solutions for all $t \in \mathbb{R}$ as $v^1(t,\lambda)$ and $v^2(t,\lambda)$. We can also solve (4.18) for λ^* under the adjoint boundary conditions

$$v^1(t,\lambda^*) \to \begin{pmatrix} 0 \\ 1 \end{pmatrix} e^{j\lambda^* t}, \quad t \to +\infty, \tag{4.23}$$
$$v^2(t,\lambda^*) \to \begin{pmatrix} -1 \\ 0 \end{pmatrix} e^{-j\lambda^* t}, \quad t \to -\infty,$$

giving rise to two solutions $v^1(t,\lambda^*)$ and $v^2(t,\lambda^*)$. From Lemma 7 we have that $\tilde{v}^1(t,\lambda^*)$ and $\tilde{v}^2(t,\lambda^*)$ are elements of E_λ. These four eigenfunctions $v^1(t,\lambda)$, $v^2(t,\lambda)$, $\tilde{v}^1(t,\lambda^*)$, and $\tilde{v}^2(t,\lambda^*)$, all of them elements of E_λ, are called *canonical eigenvectors*. Fig. 4.3 illustrates the canonical eigenvectors at their boundaries.

Lemma 8. *Canonical eigenvectors satisfy:*

1. $\langle \tilde{v}^1(t,\lambda^*), v^1(t,\lambda \rangle_s = \langle \tilde{v}^2(t,\lambda^*), v^2(t,\lambda) \rangle_s = 1$*;*
2. $\{v^1(t,\lambda), \tilde{v}^1(t,\lambda^*)\}$ *and* $\{v^2(t,\lambda), \tilde{v}^2(t,\lambda^*)\}$ *are independent sets in* E_λ*.*

Proof: 1) Since $\langle \tilde{v}^1, v^1 \rangle_s$ is independent of t, using (4.21) and (4.23), $\langle \tilde{v}^1(t,\lambda^*), v^1(t,\lambda) \rangle_s = \langle \tilde{v}^1(+\infty,\lambda^*), v^1(+\infty,\lambda) \rangle_s = 1$. 2) Follows from 1) and Lemma 7. □

Choosing $\tilde{v}^1(t,\lambda^*)$ and $v^1(t,\lambda)$ as a basis of E_λ, one can project $v^2(t,\lambda), \tilde{v}^2(t,\lambda^*) \in E_\lambda$ on this basis to obtain

$$v^2(t,\lambda) = a(\lambda)\tilde{v}^1(t,\lambda^*) + b(\lambda)v^1(t,\lambda), \tag{4.24}$$
$$\tilde{v}^2(t,\lambda^*) = b^*(\lambda^*)\tilde{v}^1(t,\lambda^*) - a^*(\lambda^*)v^1(t,\lambda), \tag{4.25}$$

where $a(\lambda) = \langle v^2, v^1 \rangle_s$ and $b(\lambda) = \langle \tilde{v}^1, v^2 \rangle_s$. A crucial property, following from Lemma 7, is that $a(\lambda)$ and $b(\lambda)$ are time-independent. The time-independent complex scalars $a(\lambda)$ and $b(\lambda)$ are called the *nonlinear Fourier coefficients* [9, 10].

Since the nonlinear Fourier coefficients are time independent, to facilitate computing them, for simplicity we can send t to, e.g., $+\infty$ where $v^1(+\infty, \lambda)$ and $\tilde{v}^1(+\infty, \lambda^*)$ are known. The other two canonical eigenvectors v^2 and $\tilde{v}^2$ are then propagated from their boundary values $v^2(-\infty, \lambda)$ and $\tilde{v}^2(-\infty, \lambda^*)$ at $t = -\infty$ according to $v_t^2 = P(\lambda, q)v^2$ and $\tilde{v}_t^2 = P(\lambda^*, q)\tilde{v}^2$ to obtain $v^2(\infty, \lambda)$ and $\tilde{v}^2(\infty, \lambda^*)$. At this stage, we have available all four canonical eigenvectors at one time, namely,

$$\left\{v^2(+\infty, \lambda), \tilde{v}^2(+\infty, \lambda), v^1(+\infty, \lambda), \tilde{v}^1(+\infty, \lambda)\right\}.$$

We can now project $v^2(+\infty, \lambda)$ and $\tilde{v}^2(+\infty, \lambda)$ onto the basis $v^1(+\infty, \lambda)$ and $\tilde{v}^1(+\infty, \lambda)$ according to (4.24)-(4.25) to obtain

$$\left[v^2(+\infty, \lambda), \tilde{v}^2(+\infty, \lambda)\right] = \left[\tilde{v}^1(+\infty, \lambda), v^1(+\infty, \lambda)\right] S, \tag{4.26}$$

where

$$S = \begin{pmatrix} a(\lambda) & b^*(\lambda^*) \\ b(\lambda) & -a^*(\lambda^*) \end{pmatrix}. \tag{4.27}$$

The matrix S is called the scattering matrix and contains the nonlinear Fourier coefficients [9, 10]. It is a function of $q(t, \cdot)$ and says how the solution to (4.18) is scattered from $t = -\infty$ to $t = +\infty$. More precisely, the field $v^2(-\infty, \lambda) = [1, 0]^T e^{-j\lambda t}$ is applied at $t = -\infty$, where q is absent. This field evolves forward in time according to (4.18), interacts with the signal (which can be viewed as an "obstacle") at finite values of t, and subsequently propagates towards $t = +\infty$, where again q is absent. The field at $t = +\infty$ is measured and gives information about the "obstacle" as seen from a distance. Although not obvious from the development so far, we shall see in Section 4.6 that the information measured at $t = +\infty$, captured by $a(\lambda)$ and $b(\lambda)$, is *complete*, in the sense that from this information we can retrieve $q(t, \cdot)$ entirely. In view of this interpretation, the nonlinear Fourier transform was historically referred to as the *inverse scattering transform*.

4.3.2 The Nonlinear Fourier Transform

The projection equations (4.24) and (4.25) that give $a(\lambda)$ and $b(\lambda)$ are well-defined if $\lambda \in \mathbb{R}$. From Lemma 7, Property 1), we observe that the eigenspace is symmetric in λ, i.e., if λ is an eigenvalue then so is λ^*. Thus it is sufficient to consider the upper half complex plane $\mathbb{C}^+ = \{\lambda | \Im(\lambda) > 0\}$. In this region, the boundary conditions on the

basis vectors v^1 and $\tilde{v}^1$ at $t = \infty$ decay and blow up, respectively. As a result, (4.24) is consistent in $\mathbb{C}^+$ only if $a(\lambda) = 0$. Eigenvalues in $\mathbb{C}^+$ are therefore identified as the zeros of the complex function $a(\lambda)$ and they form the discrete (point) spectrum of the signal. We will see in the next section that the discrete spectrum corresponds to soliton pulses.

Lemma 9. *If $q(t) \in L_1(\mathbb{R})$, $a(\lambda)$ is an analytic function of λ on $\mathbb{C}^+$.*

Proof: From Lemma 10 in Section 4.6, if $q(t) \in L_1(\mathbb{R})$ the scaled canonical eigenvectors $v^1(t,\lambda)e^{-j\lambda t}$ and $v^2(t,\lambda)e^{j\lambda t}$ are analytic functions of λ in $\mathbb{C}^+$. Since

$$a(\lambda) = \langle v^2, v^1 \rangle_s = \langle v^2 e^{j\lambda t}, v^1 e^{-j\lambda t} \rangle_s,$$

is a combination of two analytic functions in $\mathbb{C}^+$, it is analytic in the same region. (Note, however, that $b(\lambda)$, which is a combination of functions analytic in disjoint regions in $\mathbb{C}$, may not be analytic in either of those regions.) □

A consequence of Lemma 9 is that the zeros of $a(\lambda)$ in $\mathbb{C}^+$ are isolated points [50]. It follows that the Zakharov-Shabat operator for the NLS equation has two types of spectra. The discrete (or point) spectrum, which occurs in $\mathbb{C}^+$, is characterized by those $\lambda_j \in \mathbb{C}^+$ satisfying

$$a(\lambda_j) = 0, \ j = 1, 2, \ldots, N.$$

The discrete spectrum corresponds to solitons, and in this case (4.24) reduces to

$$v^2(t, \lambda_j) = b(\lambda_j) v^1(t, \lambda_j).$$

The continuous spectrum, which in general includes the whole real line $\Im(\lambda) = 0$, corresponds to the non-solitonic (or radiation) component of the signal. The continuous spectrum is the component of the NFT which corresponds to the ordinary Fourier transform, whereas the discrete spectrum has no analogue in linear systems theory. The reader is referred to Appendix A for a number of examples illustrating various notions of the spectrum associated with bounded linear operators; Example 18 is particularly relevant to the discussion here.

To distinguish between the discrete and continuous spectra, we find it convenient to refer to discrete spectral values of λ using the symbol λ_j (with a subscript). Continuous spectral values are denoted as λ (without a subscript). In general, $\lambda_j \in \mathbb{C}^+$, whereas $\lambda \in \mathbb{R}$.

For the purpose of developing the inverse transform, we find it sufficient to work with

the ratios

$$\hat{q}(\lambda) = \frac{b(\lambda)}{a(\lambda)}, \quad \tilde{q}(\lambda_j) = \frac{b(\lambda_j)}{a'(\lambda_j)},$$

where $a'(\lambda_j)$ denotes the derivative $\frac{\mathrm{d}a(\lambda)}{\mathrm{d}\lambda}\Big|_{\lambda=\lambda_j}$.

We can now formally define the nonlinear Fourier transform of a signal with respect to a given Lax operator L as follows.

Definition 6 (Nonlinear Fourier transform [9, 37])**.** Let $q(t)$ be a sufficiently smooth function in $L_1(\mathbb{R})$. The nonlinear Fourier transform of $q(t)$ with respect to a given Lax operator L consists of the continuous and discrete spectral functions $\hat{q}(\lambda) : \mathbb{R} \mapsto \mathbb{C}$ and $\tilde{q}(\lambda_j) : \mathbb{C}^+ \mapsto \mathbb{C}$ where

$$\hat{q}(\lambda) = \frac{b(\lambda)}{a(\lambda)}, \quad \tilde{q}(\lambda_j) = \frac{b(\lambda_j)}{a'(\lambda_j)}, j = 1, 2, \ldots, N,$$

in which λ_j are the zeros of $a(\lambda)$. Here, the spectral coefficients $a(\lambda)$ and $b(\lambda)$ are given by

$$a(\lambda) = = \lim_{t\to\infty} v_1^2 e^{j\lambda t}, \tag{4.28}$$

$$b(\lambda) = = \lim_{t\to\infty} v_2^2 e^{-j\lambda t}, \tag{4.29}$$

where $v^2(t, \lambda)$ is a solution of (4.18) under the boundary condition (4.22). □

To obtain the continuous spectral function $\hat{q}(\lambda)$, $\lambda \in \mathbb{R}$, it is not necessary to obtain $a(\lambda)$ and $b(\lambda)$ separately. For convenience, one can instead write an explicit differential equation

$$\begin{aligned} \frac{\mathrm{d}y(t,\lambda)}{\mathrm{d}t} + q(t)e^{2j\lambda t}y^2(t,\lambda) + q^*(t)e^{-2j\lambda t} &= 0, \\ y(-\infty,\lambda) &= 0, \end{aligned} \tag{4.30}$$

and obtain $\hat{q}(\lambda) = \lim_{t\to\infty} y(t, \lambda)$.

Analogously, one can solve the second-order differential equation

$$\begin{aligned} \frac{\mathrm{d}^2 z(t,\lambda)}{\mathrm{d}t^2} - \left(2j\lambda + \frac{q_t}{q}\right)\frac{\mathrm{d}z(t,\lambda)}{\mathrm{d}t} + |q|^2 z(t,\lambda) &= 0, \\ z(-\infty,\lambda) = 1, \quad \frac{\mathrm{d}z(-\infty,\lambda)}{\mathrm{d}t} &= 0, \end{aligned} \tag{4.31}$$

and obtain $a(\lambda) = \lim_{t\to\infty} z(t, \lambda)$. The discrete spectrum is obtained as the zeros of $a(\lambda)$.

Remark 10. The NFT is generally operator specific and thus is defined with respect to an

L operator. However many known equations can be represented by the AKNS operator (4.14).

Just like the ordinary Fourier transform, the nonlinear Fourier transform can be computed analytically only in a few cases. An example is given in the next subsection.

4.3.3 Example: Nonlinear Fourier Transform of a Rectangular Pulse

Consider the rectangular pulse

$$q(t) = \begin{cases} A, & t \in [t_1, t_2]; \\ 0, & \text{otherwise.} \end{cases}$$

Let $T = t_2 - t_1$ and $T' = t_2 + t_1$.

In this case $P(\lambda, q)$ is time-independent when $t \in [t_1, t_2]$, and (4.18) under the boundary condition (4.22) can be easily solved in closed form. The canonical eigenvector v^2 is given by

$$v^2(t, \lambda) = \exp[(t - t_1)P]v^2(t_1, \lambda), \quad v^2(t_1, \lambda) = \begin{pmatrix} 1 \\ 0 \end{pmatrix} e^{-j\lambda t_1}.$$

It follows that

$$v^2(\infty, \lambda) = v^2(t_2, \lambda) = \exp(PT)v^2(t_1, \lambda),$$

where

$$\begin{aligned} \exp(PT) &= \exp\left\{ \begin{bmatrix} -j\lambda & q \\ -q^* & j\lambda \end{bmatrix} T \right\} \\ &= \begin{bmatrix} \cos(\Delta T) - j\frac{\lambda}{\Delta}\sin(\Delta T) & \frac{A}{\Delta}\sin(\Delta T) \\ \frac{-A^*}{\Delta}\sin(\Delta T) & \cos(\Delta T) + j\frac{\lambda}{\Delta}\sin(\Delta T) \end{bmatrix}, \end{aligned}$$

with $\Delta = \sqrt{\lambda^2 + |A|^2}$. The spectral coefficients are obtained from (4.28) and (4.29) as

$$\begin{aligned} a(\lambda) &= \left(\cos(\Delta T) - j\frac{\lambda}{\Delta}\sin(\Delta T) \right) e^{j\lambda T}, \\ b(\lambda) &= \frac{-A^*}{\Delta}\sin(\Delta T) e^{-j\lambda T'}. \end{aligned}$$

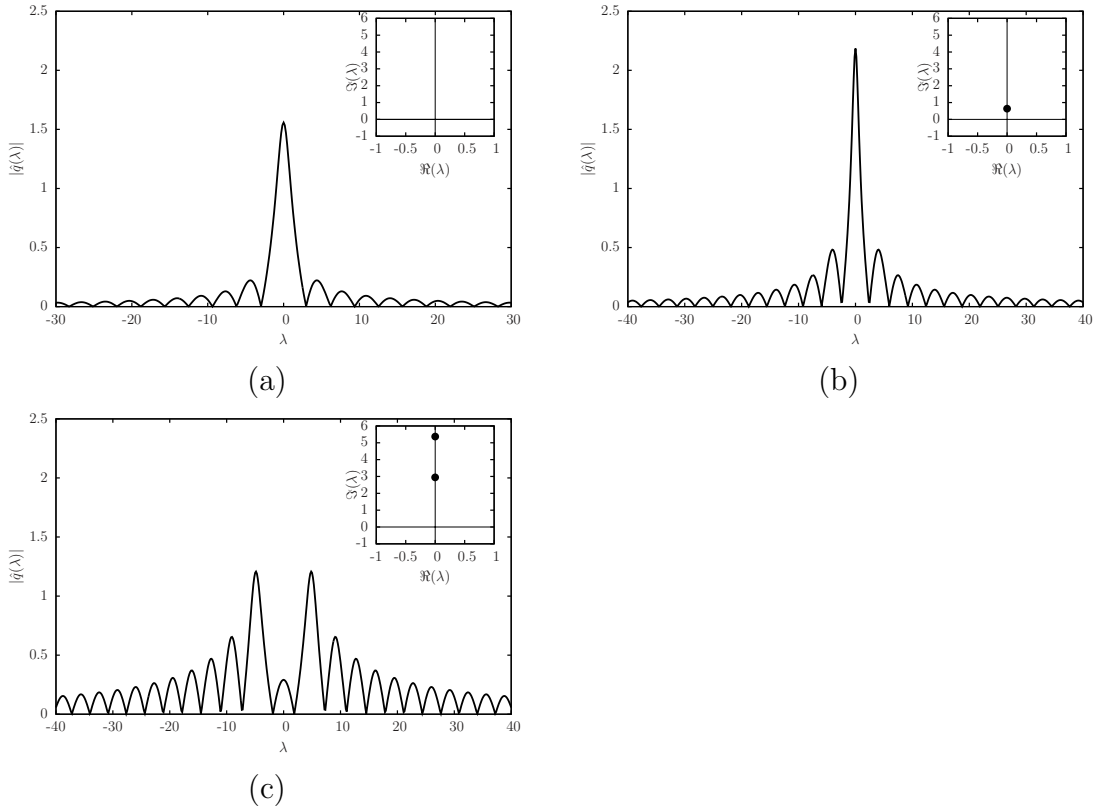

Figure 4.4: Discrete and continuous spectra of a square wave signal with $T = 1$, and (a) $A = 1$, (b) $A = 2$, (c) $A = 6$.

The zeros of $a(\lambda)$ in $\mathbb{C}^+$, which satisfy

$$j \tan(T\sqrt{|A|^2 + \lambda^2}) = \sqrt{1 + \frac{|A|^2}{\lambda^2}},$$

give rise to the discrete spectrum. The continuous spectrum is given by

$$\hat{q}(\lambda) = \frac{A^*}{j\lambda} e^{-2j\lambda t_2} \left(1 - \frac{\Delta}{j\lambda} \cot(\Delta T)\right)^{-1}.$$

Note that as $A \to 0$, $\Delta \to \lambda$, and one can see that in the limit of $AT \ll 1$ there is no discrete spectrum. Furthermore, the continuous spectrum tends to

$$\hat{q}(\lambda) = -A^* T e^{-j\lambda T'} \text{sinc}(2Tf), \quad \lambda = 2\pi f,$$

which is just the ordinary Fourier transform of the $q(t)$.

Fig. 4.4 shows the two spectra for $T = 1$ and various values of A. For small A, there is no discrete spectrum and the continuous spectrum is essentially just the ordinary Fourier

transform of $q(t)$. As A is increased, the continuous spectrum deviates from the ordinary Fourier transform and one or more discrete mass points appear on the $j\omega$ axis.

4.3.4 Elementary Properties of the Nonlinear Fourier Transform

Let $q(t) \leftrightarrow (\widehat{q}(\lambda), \widetilde{q}(\lambda_k))$ be a nonlinear Fourier transform pair. The following properties are proved in Appendix C.1.

1. (The ordinary Fourier transform as limit of the nonlinear Fourier transform): If $||q||_{L_1} \ll 1$, there is no discrete spectrum and $\widehat{q}(\lambda) \to Q(\lambda)$, where $Q(\lambda)$ is the ordinary (linear) Fourier transform of $-q^*(t)$

$$Q(\lambda) = -\int_{-\infty}^{\infty} q^*(t) e^{-2j\lambda t} \mathrm{d}t.$$

2. (Weak nonlinearity): If $|a| \ll 1$, then $\widehat{aq}(\lambda) \approx a\widehat{q}(\lambda)$ and $\widetilde{aq}(\lambda_k) \approx a\widetilde{q}(\lambda_k)$. In general, however, $\widehat{aq}(\lambda) \neq a\widehat{q}(\lambda)$ and $\widetilde{aq}(\lambda_k) \neq a\widetilde{q}(\lambda_k)$.
3. (Constant phase change): $\widehat{e^{j\phi}q(t)}(\lambda) = e^{j\phi}\widehat{q(t)}(\lambda)$ and $\widetilde{e^{j\phi}q(t)}(\lambda_k) = e^{j\phi}\widetilde{q(t)}(\lambda_k)$.
4. (Time dilation): $\widehat{q(\frac{t}{a})} = \widehat{|a|}q(a\lambda)$ and $\widetilde{q(\frac{t}{a})} = \widetilde{|a|}q(a\lambda_k)$;
5. (Time shift): $q(t - t_0) \leftrightarrow e^{-2j\lambda t_0}\,(\widehat{q}(\lambda,)\widetilde{q}(\lambda_k))$;
6. (Frequency shift): $q(t)e^{-2j\omega t} \leftrightarrow (\widehat{q}(\lambda - \omega), \widetilde{q}(\lambda_k - \omega))$;
7. (Lax convolution): If $q_2(t) = q_1(t) * (L, M; \mathcal{L})$, then $\widehat{q_2}(\lambda) = H(\lambda, \mathcal{L})\widehat{q_1}(\lambda)$ and $\widetilde{q_2}(\lambda_k) = H(\lambda, \mathcal{L})\widetilde{q_1}(\lambda_k)$. For the NLS equation, the channel filter is $H(\lambda, \mathcal{L}) = \exp(-4j\lambda^2\mathcal{L})$.
8. (Parseval identity): $\int_{-\infty}^{\infty} \|q(t)\|^2 \,\mathrm{d}t = \hat{E} + \tilde{E}$, where

$$\hat{E} = \frac{1}{\pi}\int_{-\infty}^{\infty} \log\left(1 + |\hat{q}(\lambda)|^2\right) \mathrm{d}\lambda, \quad \tilde{E} = 4\sum_{j=1}^{N} \Im\left(\lambda_j\right).$$

   The quantities $\hat{E}$ and $\tilde{E}$ represent the energy contained in the continuous and discrete spectra, respectively.

In addition, we have the following properties related to the nonlinear Fourier transform

1. (Causality and layer-peeling property): Let $q_1(t)$ and $q_2(t)$ be two signals with non-overlapping support, *e.g.*, signals in a pulse train. Without loss of generality, assume that $q_1(t)$ is supported on $t \leq t_0$, and that $q_2(t)$ is supported on $t > t_0$. If

(a_1, b_1) and (a_2, b_2) are, respectively, the nonlinear Fourier coefficients of $q_1(t)$ and $q_2(t)$, then the nonlinear Fourier coefficients of $q_1(t) + q_2(t)$ are given by

$$\begin{aligned}(a(\lambda), b(\lambda)) &= (a_1(\lambda), b_1(\lambda)) \circ (a_2(\lambda), b_2(\lambda)) \\ &\triangleq \big(a_1(\lambda)a_2(\lambda) - b_1(\lambda)b_2^*(\lambda^*), a_1(\lambda)b_2(\lambda) + b_1(\lambda)a_2^*(\lambda^*)\big).\end{aligned}$$

That is to say, if we slice the signal in time in consecutive portions according to a mesh $-\infty < \cdots < t_{-1} < t_0 < t_1 < \cdots < \infty$, the nonlinear Fourier coefficients satisfy the Markov property

$$\{a_k(\lambda), b_k(\lambda); q(t), t_k < t < t_{k+1}\} \to (a_{k+1}(\lambda), b_{k+1}(\lambda)),$$

where $(a_k(\lambda), b_k(\lambda))$ are the spectral coefficients calculated from $q(t)$ in $-\infty < t < t_k$.

2. (Purely imaginary eigenvalues) If $||q||_{L_1} < \frac{\pi}{2}$, then there is no discrete spectrum. If $q(t)$ is real, nonnegative, piecewise smooth, and single-lobe (non-decreasing for $t < t_0$ and non-increasing for $t > t_0$), then there are precisely $N = \lfloor \frac{1}{2} + \frac{||q(t)||_{L_1}}{\pi} - \epsilon \rfloor$ eigenvalues, all purely imaginary and simple [51].

4.4 Evolution of the Nonlinear Fourier Transform

Derivation of the evolution of the nonlinear Fourier transform of a signal propagating based on the NLS equation proceeds straightforwardly. As $q(t, z)$ propagates, the eigenvalues of L are preserved and the eigenvectors of L propagate based on (4.19). Assuming that $q(t, z)$ and its time-derivative vanish at $t = \pm\infty$ for all $z \leq \mathcal{L}$ during the propagation, then as $t \to \infty$ (4.19) is reduced to

$$v_z(t, z) \to \begin{pmatrix} 2j\lambda^2 & 0 \\ 0 & -2j\lambda^2 \end{pmatrix} v(t, z). \tag{4.32}$$

Thus the boundary conditions (4.21) and (4.22) are transformed to

$$\begin{aligned} v^1(t, \lambda) &\to \begin{pmatrix} 0 \\ 1 \end{pmatrix} e^{j\lambda t} e^{-2j\lambda^2 z}, \quad t \to +\infty, \\ v^2(t, \lambda) &\to \begin{pmatrix} 1 \\ 0 \end{pmatrix} e^{-j\lambda t} e^{2j\lambda^2 z}, \quad t \to -\infty. \end{aligned}$$

These transformed boundary conditions are not consistent with the boundary conditions (4.21) and (4.22) used to define the canonical eigenvectors, due to the additional factors $e^{\pm 2j\lambda^2 z}$. As a result, the evolution of the canonical eigenvectors from $z = 0$, according to $v_z = Mv$, does not lead to the canonical eigenvectors at $z = \mathcal{L}$. However, by proper scaling, one can obtain the canonical eigenvectors at any z.

For instance, focusing on $v^2(t, \lambda; z)$, and changing variables to $u^2(t, \lambda; z) = v^2(t, \lambda; z)e^{-2j\lambda^2 z}$, we obtain $u_t^2 = Pu^2$ with boundary condition (4.22) for all z. Consequently, $u^2(t, \lambda; z)$ is a canonical eigenvector for all z. By transforming (4.32), the evolution equation for u is asymptotically (at $t = +\infty$) given by

$$u_z^2(\infty, \lambda; z) = \begin{pmatrix} 0 & 0 \\ 0 & -4j\lambda^2 z \end{pmatrix} u^2(\infty, \lambda; z),$$

which gives

$$\begin{aligned} u_1^2(\infty, \lambda; z) &= u_1^2(\infty, \lambda; 0) \\ u_2^2(\infty, \lambda; z) &= u_2^2(\infty, \lambda; 0)e^{-4j\lambda^2 z} \end{aligned}$$

Using expressions (4.28) and (4.29) we obtain

$$\begin{aligned} a(\lambda, z) &= \lim_{t\to\infty} u_1^2(t, \lambda; z)e^{j\lambda t} = \lim_{t\to\infty} u_1^2(t, \lambda; 0)e^{j\lambda t} = a(\lambda, 0) \\ b(\lambda, z) &= \lim_{t\to\infty} u_2^2(t, \lambda; z)e^{-j\lambda t} = \lim_{t\to\infty} u_2^2(t, \lambda; 0)e^{-4j\lambda^2 z}e^{-j\lambda t} \\ &= b(\lambda, 0)e^{-4j\lambda^2 z}. \end{aligned}$$

In turn, the nonlinear Fourier transform propagates according to

$$\begin{aligned} \widehat{q(t, z)}(\lambda) &= e^{-4j\lambda^2 z}\widehat{q(t, 0)}(\lambda), \\ \widetilde{q(t, z)}(\lambda_j) &= e^{-4j\lambda_j^2 z}\widetilde{q(t, 0)}(\lambda_j), \\ \lambda_j(z) &= \lambda_j(0), \qquad j = 1, 2, \ldots, N. \end{aligned} \tag{4.33}$$

Note that, since $a(\lambda, z)$ is preserved under the evolution (i.e., is independent of z), the number of the discrete eigenvalues—which are zeros of $a(\lambda)$—are also preserved.

In summary, we see that the operation of the Lax convolution in the nonlinear Fourier domain is described by a simple multiplicative (diagonal) operator, much in the same way that the ordinary Fourier transform maps $y(t) = x(t) * h(t)$ to $Y(\omega) = X(\omega) \cdot H(\omega)$. The channel filter in (4.33) is $\exp(-4j\lambda^2 z)$.

4.5 An Approach to Communication over Integrable Channels

Since the nonlinear Fourier transform of a signal is essentially preserved under Lax convolution, one can immediately conceive of a nonlinear analogue of orthogonal frequency division multiplexing (OFDM) for communication over integrable channels. We refer to this scheme as nonlinear frequency division multiplexing (NFDM). In this scheme, the input output channel model is given by

$$\begin{aligned}\hat{Y}(\lambda) &= H(\lambda)\hat{X}(\lambda) + \hat{Z}(\lambda)\\ \tilde{Y}(\lambda_j) &= H(\lambda_j)\tilde{X}(\lambda_j) + \tilde{Z}(\lambda_j),\end{aligned}$$

where $\hat{X}(\lambda) = \hat{q}(\lambda, 0)$ and $\tilde{X}(\lambda_j) = \tilde{q}(\lambda, 0)$ are spectra at the input of the channel, $\hat{Y}(\lambda) = \hat{q}(\lambda, z)$ and $\tilde{Y}(\lambda_j) = \tilde{q}(\lambda, z)$ are spectra at the output of the channel, $\hat{Z}(\lambda)$ and $\tilde{Z}(\lambda_j)$ are effective noises in the spectral domain, and the *channel filter* is

$$H(\lambda) = e^{-4j\lambda^2 z}.$$

A bandlimited Gaussian noise in time domain generally maps to non-Gaussian noise processes in the spectral domain.

The proposed scheme consists of two steps.

- *The inverse nonlinear Fourier transform at the transmitter (INFT).* At the transmitter, information is encoded in the nonlinear spectra of the signal according to a suitable constellation on $\left(\hat{X}(\lambda), \tilde{X}(\lambda_j)\right)$. The time domain signal is generated by taking the inverse nonlinear Fourier transform,

  $$q(t) = \text{INFT}\left(\hat{X}(\lambda), \tilde{X}(\lambda)\right),$$

  and is sent over the channel. (The INFT is described formally in the next section.)
- *The forward nonlinear Fourier transform at the receiver (NFT).* At the receiver, the (forward) nonlinear Fourier transform of the signal,

  $$\left(\hat{Y}(\lambda), \tilde{Y}(\lambda)\right) = \text{NFT}(q(t, z))$$

  is taken and the resulting spectra are compared against the transmitted spectra according to some metric $d\left(\hat{X}(\lambda), \tilde{X}(\lambda); \hat{Y}(\lambda), \tilde{Y}(\lambda)\right)$.

As $q(t, 0)$ propagates in the time domain based on the complicated nonlinear equa-

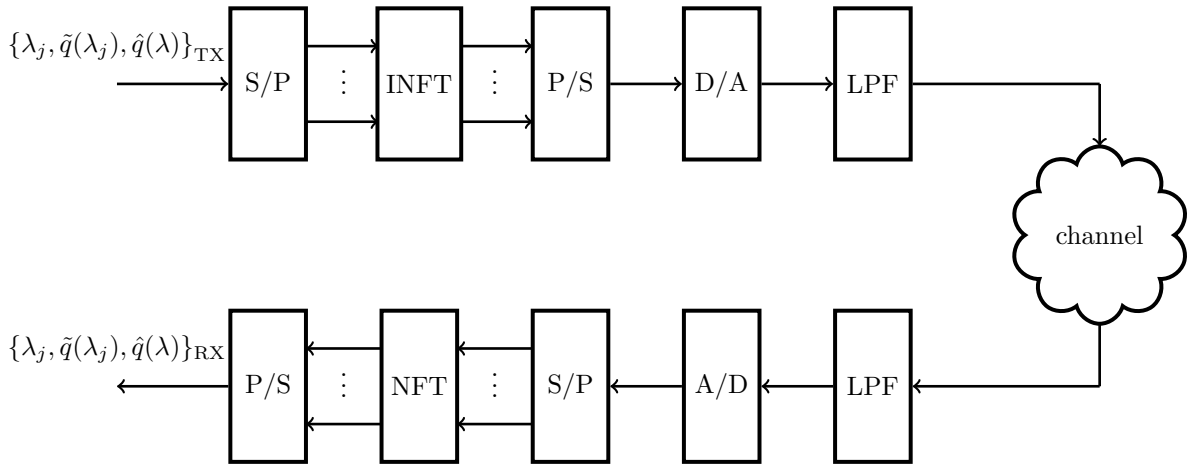

Figure 4.5: Nonlinear frequency-division channel model.

tion, it is significantly distorted and, among other distortions, undergoes intersymbol interference (ISI) in a very complicated manner. Despite this, the nonlinear spectra of the signal, $\left(\hat{X}(\lambda), \tilde{X}(\lambda_j)\right)$, are essentially held invariant during propagation, up to a complex-valued scale factor (see (4.33)). All the nonlinear spectral components propagate independently of each other, and the channel is decomposed into a number of linear parallel independent channels of the form $y_k = c_k x_k + n_k$, where n_k denotes the effective noise in the kth channel. By diagonalizing the channel in this way, the ISI is removed in the spectral domain.

In this scheme, as in linear OFDM, communication objectives, such as constellation design, coding and modulation are entirely formulated in the spectral domain. All available degrees of freedom, i.e., $\{\lambda_j, \tilde{X}(\lambda_j), \hat{X}(\lambda)\}$ can be generally modulated. Time domain constraints can be translated to constraints in the spectral domain. A power constraint, for instance, can be exactly transformed to a power constraint in the spectral domain with the help of the Parseval Identity. A bandwidth limitation is not directly and simply expressed in the nonlinear spectral domain; however, it appears that the nonlinear spectrum of a signal bandlimited to W is indeed confined, approximately, to a vertical strip in the real line and the upper half complex plane, with a width proportional to the W.

Fig. 4.5 illustrates the NFDM channel model that we use in this thesis for data transmission over integrable channels such as optical fibers.

4.6 Inverse Nonlinear Fourier transform

In this section, we describe the inverse nonlinear Fourier transform, which is a method for recovering the signal $q(t,\cdot)$ from its nonlinear Fourier transform $(\hat{q}(\lambda), \tilde{q}(\lambda_j))$. This is the opposite of what was done in the Section 4.3, and it gives further important insight into the mechanism of the NFT. As in Section 4.3, the value of z is irrelevant here and the index z is thus suppressed.

4.6.1 Riemann-Hilbert Factorization

In the 1950s, before the publication of Gardner [42], a method for retrieving the potential $q(t)$ in the linear Schrödinger equation from the knowledge of the scattering matrix S was already known in quantum mechanics. It was later realized that this method is an instance of a *Riemann-Hilbert problem* in complex analysis [10, 37]. Alternatively, the same task can be accomplished using the *Gelfand-Levitan method* [10], a different approach developed earlier in the context of inverse problems for Sturm-Liouville differential equations. Although either of these methods can be used for solving the inverse problem, in this thesis we will use the Riemann-Hilbert method.

To begin, canonical eigenvectors can be found in two ways. On the one hand, they are related to $q(t)$ through the Zakharov-Shabat system (4.18). One can solve (4.18) to explicitly express the canonical eigenvectors as a series involving $q(t)$. On the other hand, canonical eigenvectors are related to the nonlinear Fourier transform via the projection equations (4.24)-(4.25). The latter are two equations for four unknowns and in general cannot be solved. However, the unique properties of the canonical eigenvectors, which are analytic in disjoint regions of the complex plane, will allow us to find them in terms of the nonlinear Fourier transform. Note that this second derivation does not explicitly depend on $q(t)$; however, by equating the canonical eigenvectors obtained from these two derivations, we can relate the signal $q(t)$ to its nonlinear Fourier transform $(\hat{q}(\lambda), \tilde{q}(\lambda_j))$.

We find it helpful to briefly introduce the tool that we employ in this section, namely the Riemann-Hilbert factorization problem in complex analysis.

Definition 7 (Riemann-Hilbert factorization)**.** The Riemann-Hilbert factorization problem consists of finding two complex functions $f^-(z)$ and $f^+(z)$, respectively, analytic inside and outside of a closed contour C in the complex plane, such that on C they satisfy the boundary condition $f^+(z) = g(z)f^-(z)$ for some given $g(z)$.

It $g(z)$ satisfies a Hölder condition, it is possible to find both $f^+(z)$ and $f^-(z)$ everywhere in the complex plane from the given boundary condition. In Appendix B, we

provide a brief overview of this problem and its solution. See [52] for more discussion.

4.6.2 The Inverse Transform

The inverse transform maps the two spectral functions $(\hat{q}(\lambda), \tilde{q}(\lambda_j))$ to the signal $q(t)$.

As noted, we need to express the canonical eigenvectors in terms of the nonlinear Fourier transform. Below we will find it more convenient to work with canonical eigenvectors subject to fixed boundary conditions. Scaling the canonical eigenvectors as $V^2 = v^2 e^{j\lambda t}$, $\tilde{V}^2(t,\lambda^*) = \tilde{v}^2(t,\lambda^*)e^{-j\lambda t}$, $V^1 = v^1 e^{-j\lambda t}$ and $\tilde{V}^1(t,\lambda^*) = \tilde{v}^1(t,\lambda^*)e^{j\lambda t}$, the projection equations (4.24) and (4.25) are transformed to

$$V^2(t,\lambda) = a(\lambda)\tilde{V}^1(t,\lambda^*) + b(\lambda)e^{2j\lambda t}V^1(t,\lambda), \tag{4.34}$$

$$\tilde{V}^2(t,\lambda^*) = -a^*(\lambda^*)V^1(t,\lambda) + b^*(\lambda^*)e^{-2j\lambda t}\tilde{V}^1(t,\lambda^*). \tag{4.35}$$

Lemma 10. *If $q \in L^1(\mathbb{R})$, then $V^1(t,\lambda)$ and $V^2(t,\lambda)$ are analytic functions of λ in the upper half complex plane $\mathbb{C}^+ = \{z \in \mathbb{C} : \Im(z) > 0\}$ while $\tilde{V}^1(t,\lambda^*)$ and $\tilde{V}^2(t,\lambda^*)$ are analytic functions of λ in the lower half complex plane $\mathbb{C}^- = \{z \in \mathbb{C} : \Im(z) < 0\}$.*

Proof. See Appendix C.2. □

Rearranging (4.34)-(4.35) gives

$$\begin{aligned}&\begin{pmatrix} V^1(t,\lambda) & V^2(t,\lambda) \end{pmatrix} \\ &= \begin{pmatrix} \tilde{V}^1(t,\lambda^*) & \tilde{V}^2(t,\lambda^*) \end{pmatrix} \begin{pmatrix} \frac{b^*(\lambda^*)}{a^*(\lambda^*)}e^{-2j\lambda t} & \frac{1}{a^*(\lambda^*)} \\ \frac{-1}{a^*(\lambda^*)} & -\frac{b(\lambda)}{a^*(\lambda^*)}e^{-2j\lambda t} \end{pmatrix}.\end{aligned} \tag{4.36}$$

Since $\begin{pmatrix} V^2 & V^1 \end{pmatrix}$ and $\begin{pmatrix} \tilde{V}^2(t,\lambda^*) & \tilde{V}^1(t,\lambda^*) \end{pmatrix}$ are analytic, respectively, in the upper and lower half-planes, (4.36) defines a matrix Riemann-Hilbert problem.

Solution of the Riemann-Hilbert factorization problem (4.36) is given in Appendix C.4. Omitting the details, the following linear system of equations, known as the Riemann-

Hilbert system, is obtained:

$$\begin{aligned}
\tilde{V}^1(t,\lambda^*) &= \begin{pmatrix}1\\0\end{pmatrix} + \sum_{i=1}^{N} \frac{\tilde{q}(\lambda_i)e^{2j\lambda_i t}V^1(t,\lambda_i)}{\lambda-\lambda_i} \\
&\quad + \frac{1}{2\pi j}\int_{-\infty}^{\infty} \frac{\hat{q}(\zeta)e^{2j\zeta t}V^1(t,\zeta)}{\zeta-(\lambda-j\epsilon)}\mathrm{d}\zeta, \\
V^1(t,\lambda) &= \begin{pmatrix}0\\1\end{pmatrix} - \sum_{i=1}^{N} \frac{\tilde{q}^*(\lambda_i^*)e^{-2j\lambda_i^* t}\tilde{V}^1(t,\lambda_i^*)}{\lambda-\lambda_i^*} \\
&\quad + \frac{1}{2\pi j}\int_{-\infty}^{\infty} \frac{\hat{q}^*(\zeta^*)e^{-2j\zeta t}\tilde{V}^1(t,\zeta^*)}{\zeta-(\lambda+j\epsilon)}\mathrm{d}\zeta,
\end{aligned}$$

$$\begin{aligned}
\tilde{V}^1(t,\lambda_m^*) &= \begin{pmatrix}1\\0\end{pmatrix} + \sum_{i=1}^{N} \frac{\tilde{q}(\lambda_i)e^{2j\lambda_i t}V^1(t,\lambda_i)}{\lambda_m^*-\lambda_i} \\
&\quad + \frac{1}{2\pi j}\int_{-\infty}^{\infty} \frac{\hat{q}(\zeta)e^{2j\zeta t}V^1(t,\zeta)}{\zeta-\lambda_m^*}\mathrm{d}\zeta, \quad m=1,\ldots,N, \\
V^1(t,\lambda_m) &= \begin{pmatrix}0\\1\end{pmatrix} - \sum_{i=1}^{N} \frac{\tilde{q}^*(\lambda_i^*)e^{-2j\lambda_i^* t}\tilde{V}^1(t,\lambda_i^*)}{\lambda_m-\lambda_i^*} \\
&\quad + \frac{1}{2\pi j}\int_{-\infty}^{\infty} \frac{\hat{q}^*(\zeta^*)e^{-2j\zeta t}\tilde{V}^1(t,\zeta^*)}{\zeta-\lambda_m}\mathrm{d}\zeta, \\
&\quad m=1,\ldots,N.
\end{aligned} \tag{4.37}$$

This is a system of $2N+2$ linear equations for $2N+2$ discrete and continuous canonical eigenvectors $\{V^1(t,\lambda_m)\}_{m=1}^N$, $\{\tilde{V}^1(t,\lambda_m)\}_{m=1}^N$, and $V^1(t,\lambda)$ and $\tilde{V}^1(t,\lambda)$ as a function of the Fourier transform $(\hat{q}(\lambda),\tilde{q}(\lambda_j))$.

Next, the canonical eigenvectors are related to the signal $q(t)$. By inspecting the Zakharov-Shabat system (4.18), it is shown in Appendix C.3 that for $|\lambda| \gg 1$

$$V^1(t,\lambda) = \begin{pmatrix} \frac{1}{2j\lambda}q(t) \\ 1 + \frac{1}{2j\lambda}\int_{-\infty}^{\infty}|q(t)|^2\mathrm{d}t \end{pmatrix} + O(\lambda^{-2}). \tag{4.38}$$

It now becomes easy to recover the signal $q(t)$ from the nonlinear Fourier transform $(\hat{q}(\lambda),\tilde{q}(\lambda_j))$. Eigenvector V^1 is related to q via (4.38) for $|\lambda| \gg 1$, and is related to the nonlinear Fourier transform via the second equation in (4.37). Approximating $1/(\lambda-\zeta)$

and $1/(\lambda - \lambda_i)$ by $-1/\lambda + O(\lambda^{-2})$ in the second equation of (4.37) for $|\lambda| \gg 1$ and comparing V_1^1 with V_1^1 in (4.38), we obtain

$$q^*(t) = 2j \sum_{i=1}^{N} \tilde{q}(\lambda_i) e^{2j\lambda_i t} V_2^1(t, \lambda_i) - \frac{1}{\pi} \int_{-\infty}^{\infty} \hat{q}(\lambda) e^{2j\lambda t} V_2^1(t, \lambda) \mathrm{d}\lambda. \tag{4.39}$$

This represents $q(t)$ as a function of the nonlinear Fourier transform.

In summary, given $(\hat{q}(\lambda), \tilde{q}(\lambda_j))$, we first solve the Riemann-Hilbert system to find the eigenvector V^1. For this purpose, one can discretize the system (4.37) and solve a linear system of equations of the form

$$Ax = b,$$

for appropriate A and b. This is done for each fixed t_i to determine the samples of $V^l(t_i, \lambda)$ at that time. Then, V^1, $\hat{q}$ and $\tilde{q}$ are substituted in (4.39) to obtain the signal $q(t)$.

Note that this inverse transform is taken only once at the transmitter to synthesize the desired pulse shapes. It is only the forward transform which needs to be taken in real time at the receiver.

The mathematical tools developed in this chapter are used in the subsequent chapters to present further details pertaining the application of the suggested scheme in data transmission over integrable channels. In the next chapter, numerical methods are presented to compute NFT. An important special case occurs when the continuous spectrum is zero. This corresponds to N-soliton signals, where the inverse NFT can be carried out in several ways. N-solitons are discussed in Chapter 6.

4.7 Summary

The nonlinear Fourier transform of a signal with respect to an operator L in a Lax pair consists of continuous and discrete spectral functions $\hat{x}(\lambda)$ and $\tilde{x}(\lambda_j)$, obtainable by solving the eigenproblem for the L operator. The NFT maps a Lax convolution to a multiplication operator in the spectral domain. Using the nonlinear Fourier transform, we propose a transmission scheme for integrable channels, termed nonlinear frequency-division multiplexing, in which the information in encoded in the nonlinear spectrum of the signal. The scheme is an extension of traditional OFDM to any channel generated by

a Lax pair. An example is the optical fiber channel, in which signals propagate according to the nonlinear Schrödinger equation. The class of integrable channels, though nonlinear and often complicated, are somehow "linear in disguise," and thus admit the proposed nonlinear frequency-division multiplexing transmission scheme.

Chapter 5

Numerical Methods For Computing the NFT

> The purpose of computing is insight, not numbers.
>
> Richard Hamming

The nonlinear Fourier transform of a signal $q(t)$ is a pair of functions: the *continuous spectrum* $\hat{q}(\lambda)$, $\lambda \in \mathbb{R}$, and the *discrete spectrum* $\tilde{q}(\lambda_j)$, $\Im\lambda_j > 0$, $j = 1, \ldots, \mathsf{N}$. The NFT arises in the study of integrable waveform channels as defined in Chapter 4. In such channels, signals propagate (in a potentially complicated manner) according to a given integrable evolution equation, whereas the nonlinear Fourier transform of the signal propagates according to a (simple) multiplication operator.

In Chapter 4, we proposed *nonlinear frequency-division multiplexing* (NFDM), a scheme that uses the nonlinear Fourier transform for data communication over integrable channels. NFDM extends traditional orthogonal frequency division multiplexing (OFDM) to channels generatable by a Lax pair. An example is the optical fiber channel, where signal propagation is modeled by the (integrable) nonlinear Schrödinger (NLS) equation. In general, the channel input-output relations in the NFT domain are (see Chapter 4)

$$\begin{aligned} \hat{Y}(\lambda) &= H(\lambda)\hat{X}(\lambda) + \hat{Z}(\lambda), \\ \tilde{Y}(\lambda_j) &= H(\lambda_j)\tilde{X}(\lambda_j) + \tilde{Z}(\lambda_j), \end{aligned}$$

where $\hat{X}(\lambda)$ and $\tilde{X}(\lambda_j)$ are continuous and discrete spectra at the input of the channel, $\hat{Y}(\lambda)$ and $\tilde{Y}(\lambda_j)$ are spectra at the output of the channel, and $\hat{Z}(\lambda)$ and $\tilde{Z}(\lambda_j)$ represent

noise. The channel filter $H(\lambda)$ for the NLS equation is given by $H(\lambda) = \exp(-4j\lambda^2 z)$.

NFDM is able to deal directly with nonlinearity and dispersion, without the need for additional compensation at the transmitter or receiver. In this scheme, information is encoded in the nonlinear spectrum at the channel input, and the corresponding time-domain signal is transmitted. At the receiver, the NFT of the received signal is computed, and the resulting spectra $\hat{Y}(\lambda)$ and $\tilde{Y}(\lambda_j)$ are subsequently used to recover the transmitted information.

Similar to the ordinary Fourier transform, while the NFT can be computed analytically in a few cases, in general, numerical methods are required. Such methods must be robust, reliable and fast enough to be implemented in real time at the receiver. In this chapter, we suggest and evaluate the performance of a number of numerical algorithms for computing the forward NFT of a given signal. Using these algorithms, we then perform extensive numerical simulations to understand the behavior of the nonlinear spectrum for various pulse shapes and parameters commonly used in data communications.

We are aware of no published work presenting the NFT of various signals numerically, for different pulse shapes and parameters. Such work is necessary to clarify the structure of the nonlinear spectrum and help in its understanding. In part, this has been due to the fact that the NFT has largely remained a theoretical artifice, and practical implementation of the NFT as an applied tool has not yet been pursued in engineering.

We review the relevant literature in Section 5.1 and suggest new schemes for the numerical evaluation of the NFT. Although these methods are general and work for the AKNS system [48], for the purpose of illustration, we specialize the AKNS system to the Zakharov-Shabat system. All these methods are put to test in cases where analytical formulae exist and are compared with one another in Section 5.5. Only some of these methods will be chosen for the subsequent numerical simulations; these are the layer-peeling method, Ablowitz-Ladik integrable discretization, and the spectral matrix eigenvalue scheme. These methods are used in the next sections to numerically compute the nonlinear Fourier transform of a variety of practical pulse shapes encountered in data communications.

5.1 The Nonlinear Fourier Transform

Details of the nonlinear Fourier transform can be found in Chapter 4. Here we briefly recall a few essential ingredients required in the numerical computation of the forward transform. As noted earlier, we illustrate numerical methods in the context of the Zakharov-Shabat system, which is a Lax operator for the nonlinear Schrödinger equation.

For later use, we recall that the slowly-varying complex envelope $q(t,z)$ of a narrow-band small-amplitude signal propagating in a dispersive weakly-nonlinear medium, such as an optical fiber, satisfies the cubic nonlinear Schrödinger equation. By proper scaling, the equation can be normalized to the following dimensionless form in $1+1$ dimensions:

$$jq_z = q_{tt} + 2|q|^2 q. \tag{5.1}$$

Here t denotes retarded time, and z is distance.

The NFT for an integrable evolution equation starts by finding a *Lax pair* of operators L and M such that the evolution equation arises as the compatibility condition $L_z = [M, L] = ML - LM$. For the NLS equation, we may take operator L as

$$L = j \begin{pmatrix} \frac{\partial}{\partial t} & -q(t,z) \\ -q^*(t,z) & \frac{\partial}{\partial t} \end{pmatrix}. \tag{5.2}$$

(The corresponding M operator can be found in Chapter 4.)

The NFT is defined via the spectral analysis of the L operator (5.2). The spectrum of L is found by solving the eigenproblem $Lv = \lambda v$, where λ is an eigenvalue of L and v is its associated eigenvector. It can be shown that the operator L in (5.2) has the *isospectral flow* property, *i.e.*, its spectrum is invariant even as q evolves according to the NLS equation.

The eigenproblem $Lv = \lambda v$ can be simplified to

$$v_t = \begin{pmatrix} -j\lambda & q(t) \\ -q^*(t) & j\lambda \end{pmatrix} v. \tag{5.3}$$

Note that the z-dependence of q is suppressed in (5.3) (and throughout this chapter), as this variable comes into play only in the propagation of the signal, not in the definition and computation of the NFT.

Assumption 1. Throughout this thesis we assume that (a) $q \in L^1(\mathbb{R})$, and (b) $q(t)$ is supported in the finite interval $[T_1, T_2]$. □

The set of eigenvectors v associated with eigenvalue λ in (5.3) is a two-dimensional subspace E_λ of the continuously differentiable functions. We define the adjoint of a vector $v = [v_1(t), v_2(t)]^T$ as $\tilde{v} = [v_2^*(t), -v_1^*(t)]^T$. If $v(t,\lambda^*)$ is an element of E_{λ^*}, then $\tilde{v}(t,\lambda^*)$ is an element of E_λ. It can be shown that any pair of eigenvectors $v(t,\lambda)$ and $\tilde{v}(t,\lambda^*)$ form a basis for E_λ (see Section 4.3.1). Using Assumption 1(b), we can select an eigenvector

$v^1(t,\lambda)$ to be a solution of (5.3) with the boundary condition

$$v^1(T_2,\lambda) = \begin{pmatrix} 0 \\ 1 \end{pmatrix} e^{j\lambda T_2}.$$

The basis eigenvectors v^1 and $\tilde{v}^1$ are called *canonical eigenvectors*.

Having identified a basis for the subspace E_λ, we can project any other eigenvector v^2 on this basis according to

$$v^2(t,\lambda) = a(\lambda)\tilde{v}^1(t,\lambda) + b(\lambda)v^1(t,\lambda). \tag{5.4}$$

Following Assumption 1(b), a particular choice for v^2 is made by solving the system

$$v_t = \begin{pmatrix} -j\lambda & q(t) \\ -q^*(t) & j\lambda \end{pmatrix} v, \quad v(T_1,\lambda) = \begin{pmatrix} 1 \\ 0 \end{pmatrix} e^{-j\lambda T_1}, \tag{5.5}$$

in which we dropped the superscript 2 in v^2 for convenience. By solving (5.5) in the interval $[T_1, T_2]$ for a given λ and obtaining $v(T_2,\lambda)$, the nonlinear Fourier coefficients $a(\lambda)$ and $b(\lambda)$ can be obtained by considering (5.4) at $t = T_2$. The resulting coefficients obtained in this manner are

$$\begin{aligned} a(\lambda) &= v_1(T_2)e^{j\lambda T_2}, \\ b(\lambda) &= v_2(T_2)e^{-j\lambda T_2}. \end{aligned} \tag{5.6}$$

The NFT of a signal $q(t)$ consists of a continuous spectral function defined on the real axis $\lambda \in \mathbb{R}$

$$\hat{q}(\lambda) = \frac{b(\lambda)}{a(\lambda)}, \quad \lambda \in \mathbb{R},$$

and a discrete spectral function defined on the upper half complex plane $\mathbb{C}^+ = \{\lambda : \Im(\lambda) > 0\}$

$$\tilde{q}(\lambda_j) = \frac{b(\lambda_j)}{\mathrm{d}a(\lambda)/\mathrm{d}\lambda|_{\lambda=\lambda_j}},\ j = 1, \cdots, \mathsf{N},$$

where λ_j are eigenvalues and correspond to the (isolated) zeros of $a(\lambda)$ in $\mathbb{C}^+$, *i.e.*, $a(\lambda_j) = 0$.

From the discussions made, in order to compute the nonlinear spectrum of $q(t)$, the system of differential equations (5.5) needs to be solved in the interval $[T_1, T_2]$. Except

for special cases, (5.5) needs to be solved numerically.

Numerical methods for the calculation of the forward nonlinear Fourier transform are divided into two classes in this chapter:

1. Methods which estimate the continuous spectrum by directly integrating the Zakharov-Shabat system; see Section 5.2.
2. Methods which find the (discrete) eigenvalues. Two approaches are suggested in this thesis for this purpose. Similar to the continuous spectrum estimation, we can integrate the Zakharov-Shabat system numerically and obtain $a(\lambda)$. To find zeros of $a(\lambda)$, the scheme is often supplemented with a search method to locate eigenvalues in the upper half complex plane. One can also discretize and rewrite the Zakharov-Shabat system in the interval $[T_1, T_2]$ as a (large) matrix eigenvalue problem; see Section 5.3.

We begin by discussing methods which estimate the continuous spectrum.

5.2 Numerical Methods for Computing the Continuous Spectrum

In this section, we assume that $\lambda \in \mathbb{R}$ is given and provide algorithms for calculating the nonlinear Fourier coefficients $a(\lambda)$ and $b(\lambda)$. The continuous spectral function is then easily computed as the ratio $\hat{q}(\lambda) = b(\lambda)/a(\lambda)$. This process can be repeated to compute the spectral amplitudes for any desired finite set of continuous frequencies λ.

5.2.1 Forward and Central Discretizations

The most obvious method to attempt to solve (5.5) is the first-order Euler method or one of its variations [53].

Recall that the signal $q(t)$ is supported in the finite time interval $[T_1, T_2]$, and partition this interval uniformly according to the mesh $T_1 < T_1 + \epsilon < \cdots < T_1 + N\epsilon = T_2$ with size N, *i.e.*, with $\epsilon = (T_2 - T_1)/N$. Let $q[k] \triangleq q(k\epsilon)$ and let

$$P[k] \triangleq \begin{pmatrix} -j\lambda & q[k] \\ -q^*[k] & j\lambda \end{pmatrix}. \tag{5.7}$$

Integrating both sides of (5.5) from $k\epsilon$ to $(k+1)\epsilon$ and assuming that the right hand side

is constant over this interval, we get

$$\begin{aligned} v[k+1] &= v[k] + \epsilon P[k]v[k], \quad k = 0, \ldots, N, \\ v[0] &= \begin{pmatrix} 1 \\ 0 \end{pmatrix} e^{-j\lambda T_1}. \end{aligned} \tag{5.8}$$

Equation (5.8) is iterated from $k = 0$ to $k = N$ to find $v[N]$. The resulting vector is subsequently substituted in (5.6) to obtain $a(\lambda)$ and $b(\lambda)$.

We have implemented the Euler method for the calculation of the nonlinear Fourier transform of a number of pulse shapes. Unfortunately, the one-step Euler method does not produce satisfactory results for affordable small step sizes ϵ.

One can improve upon the basic Euler method by considering the *central difference iteration* [53],

$$v[k+1] = v[k-1] + 2\epsilon P[k]v[k].$$

This makes the discretization second-order, *i.e.*, the error $v(T_1 + k\epsilon) - v[k]$ is of order $\mathcal{O}(\epsilon^2)$. Here an additional initial condition is required too, which can be obtained, e.g., by performing one step of the regular forward difference (5.8).

5.2.2 Fourth-order Runge-Kutta Method

One can also employ higher-order integration schemes such as the Runge-Kutta methods. Improved results are obtained using the fourth-order Runge-Kutta method [54–56]. However it takes significant time to estimate the spectrum using such higher order numerical methods in real-time. Since the method, with its typical parameters, is quite slow and does not outperform some of the schemes suggested in the following sections, we do not elaborate on this method here; see [53] for details. However, for comparison purposes we will include this scheme in our numerical simulations given in Section 5.5.

5.2.3 Layer-peeling Method

In Section 4.3.3 of Chapter 4, we have calculated the nonlinear spectra of a rectangular pulse. One can approximate $q(t)$ as a piece-wise constant signal and use the layer-peeling property of the nonlinear Fourier transform to estimate the spectrum of any given signal. Let $a[k]$ and $b[k]$ be the nonlinear Fourier coefficients of $q(t)$ in the interval $[T_1, k\epsilon)$, and $x[k]$ and $y[k]$ coefficients in the small (rectangular) region $[k\epsilon, k\epsilon + \epsilon)$. The iterations of

the layer-peeling method read

$$\begin{aligned}(a[k+1], b[k+1]) &= (a[k], b[k]) \circ (x[k], y[k]), \\ (a[0], b[0]) &= (1, 0),\end{aligned} \tag{5.9}$$

where the $\circ$ operation is defined as in [57]

$$\begin{aligned}a[k+1] &= a[k]x[k] - b[k]\bar{y}[k], \\ b[k+1] &= a[k]y[k] + b[k]\bar{x}[k],\end{aligned}$$

in which

$$\begin{aligned}x[k] &= \left(\cos(D\epsilon) - j\frac{\lambda}{D}\sin(D\epsilon)\right) e^{j\lambda(t[k]-t[k-1])}, \\ y[k] &= \frac{-q_k^*}{D}\sin(D\epsilon)e^{-j\lambda(t[k]+t[k-1])},\end{aligned}$$

and $\bar{x}[k](\lambda) = x^*[k](\lambda^*)$, $\bar{y}[k](\lambda) = y^*[k](\lambda^*)$, $D = \sqrt{\lambda^2 + |q[k]|^2}$. The desired coefficients are obtained as $a := a[N]$ and $b := b[N]$. Note that the exponential factors in $x[k]$ and $y[k]$ enter in a telescopic manner. As a result, for the numerical implementation, it is faster to drop these factors and just scale the resulting $a[N]$ and $b[N]$ coefficients by $\exp(j\lambda(T_2 - T_1))$ and $\exp(-j\lambda(T_2 + T_1))$, respectively. This, however, reduces the accuracy as it involves the product of large and small numbers.

We are motivated by [37] in which the layer-peeling identity (5.9) is mentioned as a property of the nonlinear Fourier transform. An equivalent presentation of this method is given in [56, 58, 59] as well.

Note further that a different numerical method, but with the same name (layer-peeling), exists in geophysics and fiber Bragg design [60]; however this method is not related to the problem considered here.

We shall see in Section 5.5 that the layer-peeling method gives remarkably accurate results in estimating the nonlinear Fourier transform.

5.2.4 Crank-Nicolson Method

In the Crank-Nicolson method, the derivative of the evolution parameter is approximated by a finite-difference approximation, e.g., forward discretization, and other functions are

discretized by taking their average over the end points of the discretization interval:

$$\frac{v[k+1]-v[k]}{\epsilon} = \frac{1}{2}\left(P[k]v[k] + P[k+1]v[k+1]\right),$$

where $P[k]$ is defined in (5.7). This implicit iteration can be made explicit

$$\begin{aligned} v[k+1] &= (I - \frac{\epsilon}{2}P[k+1])^{-1}(I + \frac{\epsilon}{2}P[k])v[k], \\ k &= 0, \ldots, N \end{aligned}$$

with initial condition (5.8). As we will see, this simple scheme too gives good results in estimating the nonlinear spectrum.

5.2.5 The Ablowitz-Ladik Discretization

Ablowitz-Ladik discretization is an integrable discretization of the NLS equation in time domain [61, 62]. In this section, we suggest using the Lax pairs of the Ablowitz-Ladik discretization of the NLS equation for solving the Zakharov-Shabat eigenproblem in the spectral domain [63].

Discretization sometimes breaks symmetries, making the discrete version of an integrable equation no longer integrable. A consequence of symmetry-breaking is that quantities that are conserved in the continuous model may no longer be invariant in the discretized equation. A completely integrable Hamiltonian system with an infinite number of conserved quantities might have a discretized version with no, or few, conserved quantities. The discrete equation therefore does not quite mimic the essential features of the original equation if the step size is not small enough.

However, for some integrable equations, discretizations exist which are themselves completely integrable Hamiltonian systems, *i.e.*, they possess an infinite number of conserved quantities and are linearizable by a Lax pair, and therefore are solvable by the nonlinear Fourier transform. Such developments exist for the NLS and Korteweg-de Vries (KdV) equations.

For the NLS equation, the integrable discrete version was introduced by Ablowitz and Ladik [61]. To illustrate the general idea, let us replace $1 \pm j\lambda\epsilon$ for small ϵ with $e^{\pm j\lambda\epsilon}$ in the forward discretization method (5.8) (the opposite of what is usually done in practice). Let $z = e^{-j\lambda\epsilon}$ represent the discrete eigenvalue, $Q[k] = q[k]\epsilon$, and

$$R[k] = \begin{pmatrix} z & Q[k] \\ -Q^*[k] & z^{-1} \end{pmatrix}. \tag{5.10}$$

The Ablowitz-Ladik iteration is

$$v[k+1] = R[k]v[k], \quad v[0] = \begin{pmatrix} 1 \\ 0 \end{pmatrix} e^{-j\lambda T_1}. \tag{5.11}$$

Under this z transformation, the upper half complex plane in λ domain is mapped to the exterior of the unit circle in the z domain. The continuous spectrum therefore lies on the unit circle $|z| = 1$, while the discrete spectrum lies outside of the unit circle $|z| > 1$.

One can rewrite the R-equation (5.10) in the eigenvalue form $Lv[k] = zv[k]$, with the following L operator

$$L = \begin{pmatrix} \mathcal{Z} & -Q[k] \\ -Q^*[k-1] & \alpha[k-1]\mathcal{Z}^{-1} \end{pmatrix}, \tag{5.12}$$

where $\alpha[k] = 1 + |Q[k]|^2$, and $\mathcal{Z}$ is the shift operator, *i.e.*, $\mathcal{Z}^{-1}x[k] = x[k-1]$, $k \in \mathbb{Z}$. To the first order in ϵ, $\alpha[k] \approx 1$ and (5.12) can be simplified to

$$L = \begin{pmatrix} \mathcal{Z} & -Q[k] \\ -Q^*[k] & \mathcal{Z}^{-1} \end{pmatrix}. \tag{5.13}$$

Given the L operator (5.13), one can consider the M operator of the continuous NLS equation and modify its elements such that the compatibility equation $L_z = [M, L]$ represents a discretized version of the NLS equation. It is not hard to verify that after doing so we are led to an M operator resulting in the following discrete integrable NLS equation

$$\begin{aligned} j\frac{\mathrm{d}q[k]}{\mathrm{d}z} = &\frac{q[k+1] - 2q[k] + q[k-1]}{\epsilon^2} \\ &+ |q[k]|^2(q[k+1] + q[k-1]). \end{aligned} \tag{5.14}$$

Here the space derivative remains intact and the signal $q[k]$ is discretized in time, in such a way that the nonlinearity is somehow averaged among three time samples. In the continuum limit $\epsilon \to 0$, (5.14) approaches the continuous NLS equation and its merits lie in the fact that it is integrable for any ϵ, not just in the limit $\epsilon \to 0$. For example, soliton pulses can be observed in this model for any ϵ. The equation has its own infinite number constants of motion, approaching integrals of motion in the continuum limit. The operator M which leads to (5.14), and the details of the nonlinear Fourier transform for (5.14) can be found in [9, 61].

We conclude that the Ablowitz-Ladik discretization can be used not only as a means

to discretize the NLS equation in the time domain, but also as a means to solve the continuous-time Zakharov-Shabat system in the spectral domain. This is a non-finite-difference discretization, capable of dealing with oscillations $\exp(\pm j\lambda t)$ in the Zakharov-Shabat system, which greatly enhances the accuracy of the one-step finite-difference methods.

Following the Tao and Thiele's approach [37] and [54], we can also normalize the $R[K]$ matrix

$$v[k+1] = \frac{1}{\sqrt{1+|Q[k]|^2}} \begin{pmatrix} z & Q[k] \\ -Q[k]^* & z^{-1} \end{pmatrix} v[k]. \tag{5.15}$$

The scale factor does not change the spectrum significantly, since it is canceled out in the ratios $\hat{q} = b/a$ and $\tilde{q} = b/a'$, and also its effects are second order in ϵ. However, numerically, normalization may help in reducing the numerical error. In subsequent sections, we refer to (5.11) as the Ablowitz-Ladik method (AL1) and to (5.15) as the modified Ablowitz-Ladik method (AL2).

5.3 Methods for Calculating the Discrete Spectrum

In order to compute the discrete spectrum, the zeros of $a(\lambda)$ in the upper half complex plane must be found. One way to visualize this is to assume a two-dimensional mesh in $\mathbb{C}^+$ and determine a at all mesh points. Discrete eigenvalues are then easily identified by looking at the graph of $|a(\lambda)|$; in many cases they correspond to deep and narrow "wells" corresponding to the zeros of the magnitude of a.

As noted earlier, two types of methods are suggested to calculate the point spectrum.

1. One can use the integration-based algorithms mentioned in Section 5.2 which calculate nonlinear Fourier coefficients, and search for eigenvalues using a root finding method, such as the Newton-Raphson method. Such methods require good initial points and one needs to be careful about convergence [53].
2. It is also possible to rewrite the spectral problem for an operator as a (large) matrix eigenvalue problem. The point spectrum of the operator can be found in this way too.

5.3.1 Search Methods

To calculate the discrete spectral amplitude $\tilde{q} = b/a'$, we require $\mathrm{d}a/\mathrm{d}\lambda$ as well. As we will show, information about the derivative of a can be updated recursively along with

the information about a, without resorting to approximate numerical differentiation.

Recall that the nonlinear Fourier coefficient $a(\lambda)$ is given by (5.6)

$$a(\lambda) = v_1[N]e^{j\lambda t[N]}.$$

Taking the derivative with respect to λ, we obtain

$$\frac{\mathrm{d}a(\lambda)}{\mathrm{d}\lambda} = \left((v_1[N])' + jT_2 v_1[N]\right) e^{j\lambda t[N]}.$$

We can update the derivative information $\mathrm{d}v/\mathrm{d}\lambda$ along with v. In methods of Section 5.2, the transformation of eigenvectors from $t[k]$ to $t[k+1]$ can be generally represented as

$$v[k+1] = A[k]v[k],$$

for some suitable one-step update matrix A_k (which varies from method to method). Differentiating with respect to λ and augmenting v with $v' = \mathrm{d}v/\mathrm{d}\lambda$, we get the iterations

$$v[k+1] = A[k]v[k], \tag{5.16}$$
$$v'[k+1] = A'[k]v[k] + A[k]v'[k], \tag{5.17}$$

with initial conditions

$$v[0] = \begin{pmatrix} 1 \\ 0 \end{pmatrix} e^{-j\lambda t[0]}, \quad v'[0] = \begin{pmatrix} -jt[0] \\ 0 \end{pmatrix} e^{-j\lambda t[0]}.$$

The derivative matrix A' depends on the method used.

For the forward discretization scheme:

$$A' = M_1 = \begin{pmatrix} -j & 0 \\ 0 & j \end{pmatrix} \epsilon.$$

For the Crank-Nicolson scheme:

$$A' = \frac{1}{2}\left(I + M_2\right)^{-1}\left(I + \left(I + M_2\right)^{-1}\left(I - M_2\right)\right) M_1,$$

where

$$M_2 = \begin{pmatrix} \frac{1}{2}j\lambda & -\frac{1}{2}q[k] \\ \frac{1}{2}q^*[k] & -\frac{1}{2}j\lambda \end{pmatrix} \epsilon.$$

For the Ablowitz-Ladik method:

$$A' = \begin{pmatrix} -jz & 0 \\ 0 & jz^{-1} \end{pmatrix} \epsilon.$$

The desired coefficients are obtained at $k = N$ as follows

$$\begin{aligned} a(\lambda) &= v_1[N] e^{j\lambda t[N]}, \\ b(\lambda) &= v_2[N] e^{-j\lambda t[N]}, \\ a'(\lambda) &= \left(v_1'[N] + jt[N] v_1[N]\right) e^{j\lambda t[N]}. \end{aligned}$$

Similarly, the layer-peeling iteration can be augmented to update $a'(\lambda)$ as well:

$$\begin{aligned} a[k+1] &= a[k]x[k] - b[k]\bar{y}[k], \\ b[k+1] &= a[k]y[k] + b[k]\bar{x}[k], \\ a'[k+1] &= a'[k]x[k] + a[k]x'[k] - (b'[k]\bar{y}[k] + b[k]\bar{y}'[k]), \\ b'[k+1] &= a'[k]y[k] + a[k]y'[k] + b'[k]\bar{x}[k] + b[k]\bar{x}'[k], \\ a[0] &= 1, \quad b[0] = a'[0] = b'[0] = 0, \end{aligned} \tag{5.18}$$

where

$$\begin{aligned} x[k] &= \cos(D\epsilon) - j\frac{\lambda}{D}\sin(D\epsilon), \\ y[k] &= \frac{-q_k^*}{D}\sin(D\epsilon), \\ x'[k] &= -\frac{j\lambda^2\epsilon}{D^2}\cos(D\epsilon) - \left(\frac{j+\lambda\epsilon}{D} - \frac{j\lambda^2}{D^3}\right)\sin(D\epsilon), \\ y'[k] &= -\frac{q_k^*\lambda}{D^3}\left(D\epsilon\cos(D\epsilon) - \sin(D\epsilon)\right). \end{aligned}$$

The expressions for $\bar{x}'[k]$ and $\bar{y}'[k]$ are similar, with j replaced with $-j$ and $q[k]$ replaced with $-q^*[k]$.

With the derivative information being available, the Newton-Raphson method is a good scheme to search for the location of the (discrete) eigenvalues. The iteration for the complex-valued Newton-Raphson scheme is

$$\lambda_{k+1} = \lambda_k - \alpha_k \frac{a(\lambda_k)}{a'(\lambda_k)}, \tag{5.19}$$

where α_k is some step size modifier; usually $\alpha_k = 1$. The iteration stops if λ_k is almost

stationary, *i.e.*, if $|\alpha\frac{a}{a'}| < \delta$ for a small δ. In practice, the quadratic convergence of the scheme is often very fast and occurs in just a few iterations.

In data communications, since noise is usually small, the points in the transmitted constellation can (repeatedly) serve as the initial conditions for (5.19). In this case, convergence is usually achieved in a couple of iterations. For an unknown signal, random initial conditions are chosen. In either case, one or more sequence of Newton iterations have to be performed for any single eigenvalue.

To make sure that all of the eigenvalues are found, we can check the trace formula for $n = 1, 2, 3$. The trace formula is a time frequency identity relating the hierarchy of infinitely many conserved quantities to the spectral components.

In general, the trace formula represents a time domain conserved quantity as the sum of discrete and continuous spectral terms:

$$E^{(k)} = E^{(k)}_{\text{disc}} + E^{(k)}_{\text{cont}},$$

where

$$E^{(k)}_{\text{disc}} = \frac{4}{k}\sum_{i=1}^{\mathsf{N}} \Im\left(\lambda_i^k\right),$$
$$E^{(k)}_{\text{cont}} = \frac{1}{\pi}\int_{-\infty}^{\infty} \lambda^{k-1}\log\left(1+|\hat{q}(\lambda)|^2\right)d\lambda,$$

and where $E^{(k)}$ are time domain conserved quantities (functionals of the signal). The first few conserved quantities are energy

$$E^{(1)} = \int_{-\infty}^{\infty} |q(t,z)|^2 dt,$$

momentum

$$E^{(2)} = \frac{1}{2j}\int_{-\infty}^{\infty} q(t)\frac{\mathrm{d}q(t)}{\mathrm{d}t}dt,$$

and Hamiltonian

$$E^{(3)} = \frac{1}{(2j)^2}\int_{-\infty}^{\infty}\left(|q(t)|^4 - \left|\frac{\mathrm{d}q(t)}{\mathrm{d}t}\right|^2\right)\mathrm{d}t.$$

For $n = 1$, the trace formula is a kind of Parseval's identity (Plancherel's theorem), representing the total energy of the signal in time as the sum of the energy of the discrete and continuous spectral functions. When satisfied, the Parseval's identity ensures that all of the signal energy has been accounted for.

We first calculate the continuous spectrum and its "energy terms" for a sufficiently fine mesh on the real λ axis. The energy difference $E_{\text{error}} = \left|\left|E^{(k)} - E^{(k)}_{\text{cont}}\right|\right|$ gives an estimate on the number of missing eigenvalues. When a new eigenvalue λ is found, this error is updated as $E_{\text{error}} := \left|\left|E^{(k)} - E^{(k)}_{\text{cont}} - \frac{4}{k}\Im\lambda^k\right|\right|$. The process is repeated until E_{error} is less than a small prescribed tolerance value.

To summarize, given the signal $q(t)$, its nonlinear Fourier transform can be computed based on Algorithm 1.

5.3.2 Discrete Spectrum as a Matrix Eigenvalue Problem

The methods mentioned in Section 5.3.1 find the discrete spectrum by searching for eigenvalues in the upper half complex plane. Sometimes it is desirable to have all eigenvalues at once, which can be done by solving a matrix eigenvalue problem [55, 63]. These schemes obviously estimate only (discrete) eigenvalues and do not give information on the rest of the spectrum. Since the matrix eigenvalue problem can be solved quickly for small-sized problems, it might take less computational effort to compute the discrete spectrum in this way. In addition, one does not already need the continuous spectrum to estimate the size of the discrete spectrum. On the other hand, for large matrices that arise when a large number of signal samples are used, the matrix eigenproblem (which is usually not Hermitian) is slow and it may be better to find the discrete spectrum using the search-based methods. The matrix-based methods also have the disadvantages that they can generate a large number of spurious eigenvalues, and one may not be able to restrict the algorithm for finding eigenvalues of a matrix to a certain region of the complex plane.

Below we rewrite some of the methods mentioned in the Section 5.2 as a regular matrix eigenvalue problem, for the computation of the discrete spectrum.

Algorithm 1 Numerical Nonlinear Spectrum Estimation

Sample the signal at a sufficiently small step size ϵ.
Fix a sufficiently fine mesh M on the real λ axis.
for each $\lambda \in M$ **do**
Iterate (5.16) from $k = 0$ to $k = N$ to obtain $v[N]$.
Compute the continuous spectral amplitude

$$\rho(\lambda) = \frac{v_2[N]}{v_1[N]} e^{-2j\lambda t[N]}.$$

end for
Initialize the error $e = ||E - E_{\text{cont}}||$.
while $|e| > \epsilon_1$ **do**
Choose $\lambda_0 \in \mathcal{D}$ randomly, where $\mathcal{D}$ is a prescribed region in $\mathbb{C}^+$.
Set $i = 0$;
repeat
Iterate (5.16)-(5.17) from $k = 0$ to $k = N$ to obtain $v[N]$ and $v'[N]$, and perform a Newton-Raphson update

$$\lambda_{i+1} = \lambda_i - \Delta\lambda, \quad \Delta\lambda = \alpha_i \frac{v_1[N]}{v_1'[N] + jt[N]v_1[N]}$$

if If $\lambda_{i+1} \notin \mathcal{D}$ **then**
choose $\lambda_0 \in \mathcal{D}$ randomly.
Set $i := -1$.
end if
Set $i := i + 1$.
until $|\Delta\lambda| < \epsilon_2$ and $i > 0$
λ_i is an eigenvalue and the associated spectral amplitude is

$$\tilde{q}(\lambda_i) = \frac{v_2[N]}{v_1'[N] + jt[N]v_1[N]} e^{-2j\lambda_i t[N]}.$$

Update $e := ||E - E_{\text{cont}} - E_{\text{disc}}||$, where $E_{\text{disc}} = [4\Im\lambda_i, 2\Im\lambda_i^2, \frac{4}{3}\Im\lambda_i^3]$.
end while

Central-difference Eigenproblem

The matrix eigenvalue problem can be formulated in the time domain or the frequency domain [55]. Consider the Zakharov-Shabat system in the form $Lv = \lambda v$

$$j \begin{pmatrix} \frac{\partial}{\partial t} & -q \\ -q^* & -\frac{\partial}{\partial t} \end{pmatrix} v = \lambda v. \tag{5.20}$$

In the time domain, one can replace the time derivative $\partial/\partial t$ by the central finite-difference matrix

$$D = \frac{1}{2\epsilon} \begin{pmatrix} 0 & 1 & 0 & \cdots & -1 \\ -1 & 0 & 1 & \cdots & 0 \\ & & & \cdots & \\ 0 & 0 & -1 & 0 & 1 \\ 1 & 0 & 0 & -1 & 0 \end{pmatrix},$$

and expand (5.20) as

$$j \begin{pmatrix} D & -\mathrm{diag}(q[k]) \\ -\mathrm{diag}(q^*[k]) & -D \end{pmatrix} v[k] = \lambda v[k]. \tag{5.21}$$

The point spectrum is contained in the eigenvalues of the matrix in the left hand side of (5.21).

Eigenvalues of a real symmetric or Hermitian matrix can be found relatively efficiently, owing to the existence of a complete orthonormal basis and the stability of the eigenvalues. In this case, a sequence of unitary similarity transformations $A_{k+1} = PA_kP^T$ can be designed, using, for instance, the QR factorization, the Householder transformation, *etc.*, to obtain the eigenvalues rather efficiently [64].

Unfortunately, most of the useful statements about computations using Hermitian matrices cannot usually be generalized to non-Hermitian matrices. As a result, the eigenvalues of a non-Hermitian matrix (corresponding to a non-self-adjoint operator) are markedly difficult to calculate [64, 65]. Running a general-purpose eigenvalue calculation routine on (5.21) is probably not the most efficient way to get eigenvalues. Next we make suggestions to simplify the non-Hermitian eigenproblem (5.21) by exploiting its structure.

The diagonal matrix in the lower left corner of (5.21) can be made zero by applying elementary row operations and using the entries of the D matrix. Since elementary row operations, as in Gauss-Jordan elimination, generally change the eigenvalues, the

corresponding column operations are also applied to induce a similarity transformation. In this way, an upper-Hessenberg matrix is obtained in $\mathcal{O}(N)$ operations, as compared to a sequence of Householder transformations with $\mathcal{O}(N^3)$ operations and $\mathcal{O}(N^2)$ memory registers. The eigenvalues of the resulting complex upper-Hessenberg matrix can subsequently be found using QR iterations.

Ablowitz-Ladik Eigenproblem

We can also rewrite the Ablowitz-Ladik discretization as a matrix eigenvalue problem. Using the L operator (5.13), we obtain

$$v_1[k+1] - Q[k]v_2[k] = zv_1[k], \tag{5.22}$$
$$-Q^*[k-1]v_1[k] + \alpha[k-1]v_2[k-1] = zv_2[k], \tag{5.23}$$

which consequently takes the form

$$\begin{pmatrix} U_1 & -\mathrm{diag}(Q[k]) \\ -\mathrm{diag}(Q^*[k-1]) & U_2^T \end{pmatrix} v = zv,$$

in which

$$U_1 = \begin{pmatrix} 0 & 1 & 0 & \cdots & 0 \\ 0 & 0 & 1 & \cdots & 0 \\ & & & \cdots & \\ 0 & 0 & 0 & 0 & 1 \\ 1 & 0 & 0 & 0 & 0 \end{pmatrix},$$

$$U_2 = \begin{pmatrix} 0 & \alpha[1] & 0 & \cdots & 0 \\ 0 & 0 & \alpha[2] & \cdots & 0 \\ & & & \cdots & \\ 0 & 0 & 0 & 0 & \alpha[N-1] \\ \alpha[N] & 0 & 0 & 0 & 0 \end{pmatrix},$$

and $\mathrm{diag}(Q[k]) = \mathrm{diag}\left(Q[0], \cdots, Q[N]\right)$, $\mathrm{diag}(Q^*[k-1]) = \mathrm{diag}\left(Q^*[N], Q^*[0] \cdots, Q^*[N-1]\right)$. Note that all shifting operations are cyclic, so that all vector indices k remain in the interval $0 \leq k \leq N$.

It is not very different to consider the more simplified L operator (5.12) instead of (5.13). This corresponds to the above discretization with $U_2 := U_1$ and $-Q^*[k-1]$ replaced with $-Q^*[k]$. Similarly, one can rewrite the normalized Ablowitz-Ladik iteration

as a matrix eigenvalue problem. This corresponds to (5.23) where instead of having $\alpha[k-1]$, $v_1[k+1]$ is multiplied by $\alpha[k]$ in the first equation, *i.e.*, U_1 and U_2 are interchanged.

Spectral Method

In the frequency domain, one can approximate derivatives with the help of the Fourier transform. Let us assume that

$$v(t) = \sum_{k=-\frac{M}{2}}^{\frac{M}{2}} \begin{pmatrix} \alpha_k \\ \beta_k \end{pmatrix} e^{\frac{j2k\pi t}{T}}, \quad q(t) = \sum_{k=-\frac{M}{2}}^{\frac{M}{2}} \gamma_k e^{\frac{j2k\pi t}{T}},$$

where $T = T_2 - T_1$. Then the Zakharov-Shabat system is

$$-\alpha_k \frac{2\pi k}{T} - j \sum_{m=-\frac{M}{2}}^{\frac{M}{2}} \gamma_{k-m}\beta_m = \lambda\alpha_k,$$
$$-j \sum_{m=-\frac{M}{2}}^{\frac{M}{2}} \gamma^*_{-k+m}\alpha_m + \beta_k \frac{2\pi k}{T} = \lambda\beta_k.$$

Thus we obtain

$$\begin{pmatrix} \Omega & \Gamma \\ -\Gamma^H & -\Omega \end{pmatrix} \begin{pmatrix} \boldsymbol{\alpha} \\ \boldsymbol{\beta} \end{pmatrix} = j\lambda \begin{pmatrix} \boldsymbol{\alpha} \\ \boldsymbol{\beta} \end{pmatrix},$$

where $\boldsymbol{\alpha} = [\alpha_{-\frac{M}{2}}, \ldots, \alpha_{\frac{M}{2}}]^T$, $\boldsymbol{\beta} = [\beta_{-\frac{M}{2}}, \ldots, \beta_{\frac{M}{2}}]^T$, $\Omega = -\frac{2\pi}{T}\mathrm{diag}(-\frac{M}{2}, \ldots, \frac{M}{2})$ and

$$\Gamma = -j \begin{pmatrix} \gamma_0 & \gamma_{-1} & \cdots & \gamma_{-\frac{M}{2}} & 0 & 0 & \cdots & 0 \\ \gamma_1 & \gamma_0 & \gamma_{-1} & \cdots & \gamma_{-\frac{M}{2}} & 0 & \cdots & 0 \\ & & \ddots & & \ddots & & \ddots & \\ \gamma_{\frac{M}{2}} & \gamma_{\frac{M}{2}-1} & & \cdots & & & \gamma_{-\frac{M}{2}+1} & \gamma_{-\frac{M}{2}} \\ 0 & \gamma_{\frac{M}{2}} & \gamma_{\frac{M}{2}-1} & & \cdots & & & \gamma_{-\frac{M}{2}+1} \\ & & \ddots & & \ddots & & \ddots & \\ 0 & \cdots & 0 & \gamma_{\frac{M}{2}} & \gamma_{\frac{M}{2}-1} & \cdots & \gamma_0 & \gamma_{-1} \\ 0 & 0 & \cdots & 0 & \gamma_{\frac{M}{2}} & \gamma_{\frac{M}{2}-1} & \cdots & \gamma_0 \end{pmatrix}.$$

The point spectrum is thus found by looking at the eigenvalues of the matrix

$$A = \begin{pmatrix} \Omega & \Gamma \\ -\Gamma^H & -\Omega \end{pmatrix}.$$

5.4 Running Time, Convergence and Stability of the Numerical Methods

The numerical methods discussed in this chapter are first-order matrix iterations and therefore the running time of all of them is $\mathcal{O}(N)$ multiplications and additions per eigenvalue. This corresponds to a complexity of $\mathcal{O}(N^2)$ operations for the calculation of the continuous spectrum on a mesh with N eigenvalues. The exact number of operations depends on the details of the implementation and the memory requirement of the method. All iterative methods thus take about the same time asymptotically, albeit with different coefficients.

An important observation is that, while the Fast Fourier Transform (FFT) takes $\mathcal{O}(N \log_2 N)$ operations to calculate the spectral amplitudes of a vector with length N at N equispaced frequencies, the complexity of the methods described in this chapter to compute the continuous spectrum are $\mathcal{O}(N^2)$. Similarly, it takes $\mathcal{O}(\mathsf{N}N)$ operations to calculate the discrete spectrum. In other words, so far we do not exploit the potentially repetitive operations in our computations.

It is evident from (5.6) that as $T_2 \to \infty$, $v_1[k]$ should grow as $\sim \exp(-j\lambda T_2)$ so that $a(\lambda)$ is a finite complex number. The canonical eigenvector $v[k; T_1, T_2]$ thus has an unbounded component as $T_2 \to \infty$ (*i.e.*, $||v[k]|| \to \infty$). One can, however, normalize v_1 and v_2 according to

$$\begin{aligned} u_1 &= v_1 e^{j\lambda t} \\ u_2 &= v_2 e^{-j\lambda t}, \end{aligned}$$

and transform (5.5) to

$$u_t = \begin{pmatrix} 0 & q(t)e^{2j\lambda t} \\ -q^*(t)e^{-2j\lambda t} & 0 \end{pmatrix} u, \quad u(T_1, \lambda) = \begin{pmatrix} 1 \\ 0 \end{pmatrix}. \tag{5.24}$$

The desired coefficients are simply $a(\lambda) = u_1(T_2)$ and $b(\lambda) = u_2(T_2)$. Consequently, if one is interested in obtaining eigenvectors $v[k]$ in addition to the coefficients $a(\lambda)$ and $b(\lambda)$, the discretization of the normalized system (5.24) has better stability properties:

$$\begin{aligned} (a[k+1], b[k+1]) &= \begin{pmatrix} 1 & Q[k]z^{-2k} \\ -Q^*[k]z^{2k} & 1 \end{pmatrix} (a[k], b[k]) \\ (a[0], b[0]) &= (1, 0)\,. \end{aligned} \tag{5.25}$$

The nonlinear Fourier coefficients are obtained as $a := a[N]$ and $b := b[N]$. The discrete nonlinear Fourier transform mentioned in [37] is thus the forward discretization of the normalized Zakharov-Shabat system (5.24).

We are interested in the convergence of $v[k]$ (or $a(\lambda)$ and $b(\lambda)$) as a function of N for fixed values of T_1 and T_2. That is to say, we require that the error $e = ||v(k\epsilon) - v[k]|| \to 0$ as $N \to \infty$ (for fixed T_1 and T_2). The (global) error in all methods described in this chapter is at least $\mathcal{O}(\epsilon)$, and therefore all these methods are convergent.

Some of these methods are, however, not stable. This is essentially because the Zakharov-Shabat system in its original form has unbounded solutions, *i.e.*, $||v(t)|| \to \infty$ as $t \to \infty$. Errors can potentially be amplified by the unstable system poles. One should be cautious about the normalized system (5.24) as well. For example, forward discretization of the normalized system (5.25) gives a first-order iteration $x[k+1] = A[k]x[k]$. The eigenvalues of the matrix $A[k]$ in this method are

$$s_{1,2} = 1 \pm j\epsilon|q[k]|.$$

It follows that the forward discretization of (5.24) gives rise to eigenvalues outside of the unit disk, $|s| > 1$. As a result, first-order discretization of (5.24) are also unstable. In cases where $|s| > 1$, we can consider normalizing the iterations by dividing $A[k]$ by $\sqrt{\det A[k]}$ (in the case of (5.25), dividing the right-hand side by $\sqrt{1 + |Q[k]|^2}$). The resulting iteration has eigenvalues inside the unit disk. For $\epsilon \ll 1$ the effect is only second-order in ϵ, however it helps in managing the numerical error if larger values of ϵ are chosen.

An issue pertinent to numerical methods is chaos. Chaos and numerical instability of finite-difference discretizations has been observed in [66] for the sine-Gordon equation, which is also integrable and shares a number of basic properties with the NLS equation. In [67], the authors conclude that the standard discretizations of the cubic nonlinear Schrödinger equation may lead to spurious numerical behavior. This instability is deeply related to the homoclinic orbits of the NLS equation, *i.e.*, it occurs if the initial signal $q(t, z = 0)$ is chosen to be close to the homoclinic orbit of the equation. It disappears only if the step size is made sufficiently small, which can be smaller than what is desired in practice.

It is shown in [67] that the Ablowitz-Ladik discretization of the NLS equation (in time) has the desirable property that chaos and numerical instability, which are sometimes present in finite-difference discretizations of the NLS equation, do not appear at all. Though these results are for the original time-domain equations, the issue can occur in

the spectral eigenvalue problem (5.5) as well, if the signal $q[k]$ is close to a certain family of functions (related to $\sin \omega t$ and $\cos \omega t$). Therefore, among discretizations studied, the Ablowitz-Ladik discretization of the Zakharov-Shabat system is immune to chaos and its resulting numerical instability. This is particularly important in the presence of amplifier noise, where chaos can be more problematic.

5.5 Testing and Comparing the Numerical Methods

In this section, we test and compare the ability of the suggested numerical schemes to estimate the nonlinear Fourier transform (with respect to the Zakharov-Shabat system) of various signals. Numerical results are compared against analytical formulae, in a few cases where such expressions exist. Our aim is to compare the speed and the precision of these schemes for various pulse shapes in order to determine which ones are best suited for subsequent simulation studies.

To derive the analytical formulae, recall that the continuous spectral function can be written as $\hat{q}(\lambda) = \lim_{t\to\infty} y(t,\lambda)$, in which $y(t,\lambda)$ satisfies [57]

$$\begin{aligned} \frac{\mathrm{d}y(t,\lambda)}{\mathrm{d}t} + q(t)e^{2j\lambda t}y^2(t,\lambda) + q^*(t)e^{-2j\lambda t} = 0, \\ y(-\infty,\lambda) = 0. \end{aligned} \tag{5.26}$$

Similarly, one can solve the second-order differential equation

$$\begin{aligned} \frac{\mathrm{d}^2 z(t,\lambda)}{\mathrm{d}t^2} - \left(2j\lambda + \frac{q_t}{q}\right)\frac{\mathrm{d}z(t,\lambda)}{\mathrm{d}t} + |q|^2 z(t,\lambda) = 0, \\ z(-\infty,\lambda) = 1, \quad \frac{\mathrm{d}z(-\infty,\lambda)}{\mathrm{d}t} = 0, \end{aligned} \tag{5.27}$$

and obtain $a(\lambda) = \lim_{t\to\infty} z(t,\lambda)$. The zeros of $a(\lambda)$ form the discrete spectrum.

In the following, the discrete spectrum is found and compared using the following matrix-based schemes:

1. central difference method;
2. spectral method;
3. Ablowitz-Ladik (AL) discretization (AL1);
4. AL discretization with normalization (AL2).

In the matrix-based schemes, the entire point spectrum is found at once by solving a matrix eigenvalue problem.

The complete spectrum is found using search-based methods:

1. forward discretization method;
2. fourth-order Runge-Kutta scheme;
3. layer-peeling methods;
4. Crank-Nicolson method;
5. AL discretization;
6. AL discretization with normalization.

In search-based methods, the Newton method is used together with the trace formula to find both discrete and continuous spectra.

Each of the following pulses is sampled uniformly using a total of n samples in a time window containing at least 99.99% of the pulse energy.

5.5.1 Satsuma-Yajima Pulses

One signal with known spectrum is the Satsuma-Yajima pulse [68]

$$q(t) = A\text{sech}(t).$$

Solving the initial value problem (5.5) (or (5.26)) analytically, the following continuous spectral function is obtained [68]

$$\hat{q}(\lambda) = -\frac{\Gamma(-j\lambda + \frac{1}{2} + A)\Gamma(-j\lambda + \frac{1}{2} - A)}{\Gamma^2(-j\lambda + \frac{1}{2})} \frac{\sin(\pi A)}{\cosh(\pi\lambda)}.$$

The discrete spectrum is the set of zeros of $a(\lambda)$ *i.e.*, poles of $\hat{q}(\lambda)$ (when analytically extended in $\mathbb{C}^+$). Recalling that $\Gamma(x)$ has no zeros and is unbounded for $x = 0, -1, -2, \ldots$, it follows that the discrete spectrum consists of $\mathsf{N} = \lfloor A + \frac{1}{2} - \epsilon \rfloor$ eigenvalues, located at $(A - \frac{1}{2})j, (A - \frac{3}{2})j, \ldots$. In the special case in which A is an integer, $A = \mathsf{N}$, the Satsuma-Yajima pulse is a pure N-soliton with N eigenvalues, and the continuous spectral function is zero.

Figs. 5.1, 5.2 and 5.3 give the numerical results for $A = 2.7$, $N = 2^{10}$. Fig. 5.1 shows that, in this example, the spectral and central difference methods produce good results among the matrix-based methods in estimating the discrete eigenvalues $\lambda = 0.2j, 1.2j, 2.2j$. All methods generate a large number of spurious eigenvalues along the real axis. This behavior might be viewed as a tendency of the algorithms to generate the continuous spectrum too. However the spurious eigenvalues do not disappear completely even when the continuous spectrum is absent (when A is an integer); only their range becomes more limited. The spurious eigenvalues across the real axis can easily be filtered, since their imaginary part has negligible amplitude. The AL methods, with

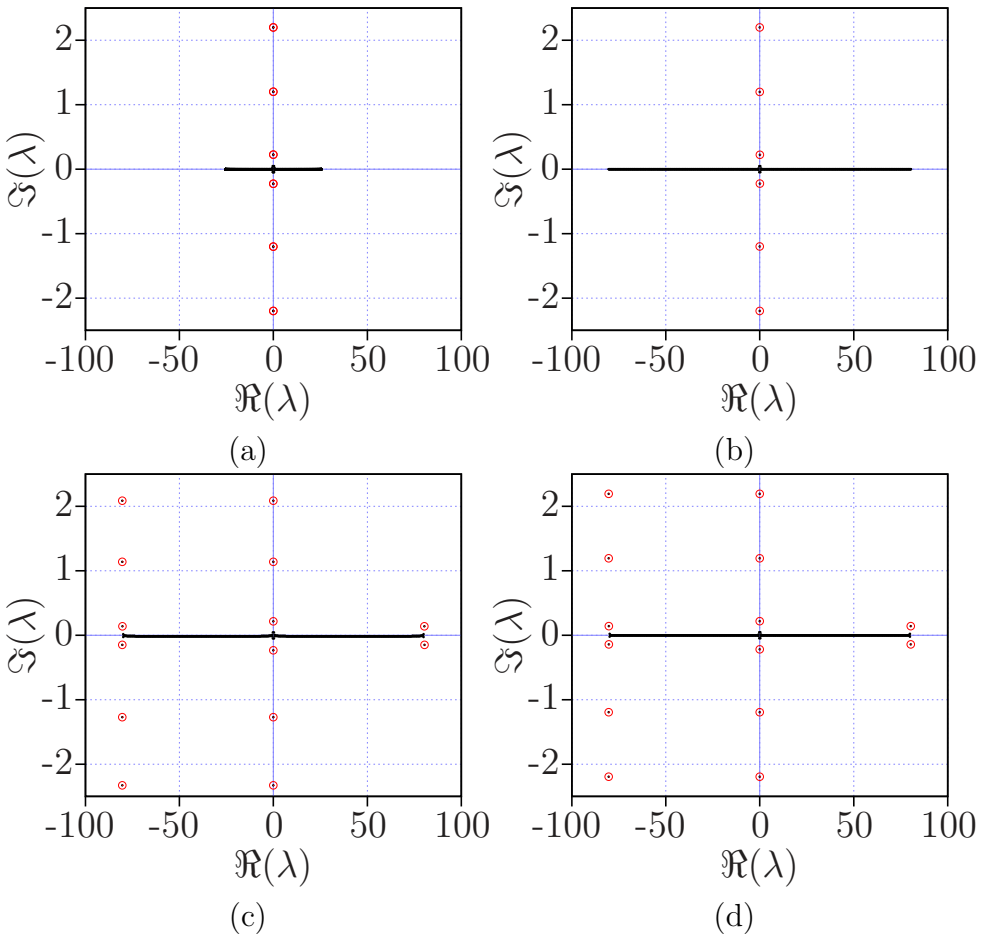

Figure 5.1: Discrete spectrum of the Satsuma-Yajima pulse with $A = 2.7$ using (a) central difference method, (b) spectral method, (c) Ablowitz-Ladik scheme, (d) modified Ablowitz-Ladik scheme.

and without normalization, produce the same eigenvalues plus another vertical line of spurious eigenvalues having a large negative real part. Normalization in the AL scheme does not make a significant difference in this example.

Fig. 5.2 shows the accuracy of the various matrix-based methods in estimating the smallest and largest eigenvalues of $q = 2.7\text{sech}(t)$ in terms of the number of the sample points N. As the number of sample points N is decreased, the spectral and central difference methods maintain reasonable precisions, while the accuracy of the AL schemes quickly deteriorates. One can check that in these cases, the error in the approximation $e^{j\lambda\Delta t} \sim 1 + j\lambda\Delta t$ becomes large (since $\Delta t \gg 1$).

The spectral method is generally more accurate than the other matrix-based methods. The AL discretizations seem to perform well as long as $\lambda\Delta t \ll 1$, *i.e.*, when estimating eigenvalues with small size or when $N \geq 200$. The AL discretization eventually breaks down at about $N = 50$ as the analogy between the continuous and discrete NLS equation

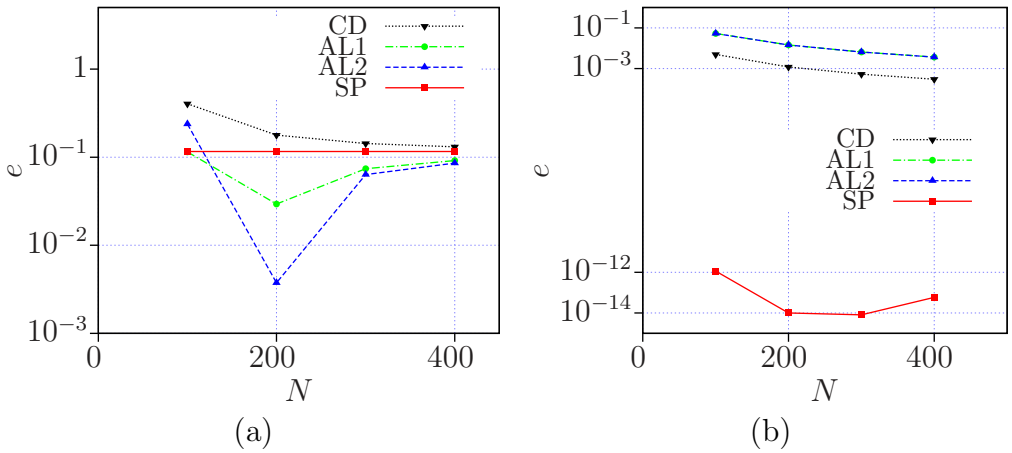

Figure 5.2: Error in estimating (a) the smallest eigenvalue and (b) the largest eigenvalue of the Satsuma-Yajima pulse $q(t) = 2.7\text{sech}(t)$ as a function of the number of sample points N using matrix eigenvalue methods. The Ablowitz-Ladik method 1 is the method of Section 5.3.2 with no normalization, and the Ablowitz-Ladik method 2 is the same scheme with normalization.

is no longer justified at such low resolutions, whereas other schemes continue to track the eigenvalues to some accuracy. In other words, what the AL methods find at such small values of N is the spectrum of the discrete soliton-bearing NLS equation, which is not a feature of finite-difference discretizations. (In fact, it is essential for this algorithm to deviate from the finite-difference discretizations as N is reduced, to produce appropriate solitons with few samples.) The running time of all matrix eigenvalue methods is about the same.

Search-based methods can be used to estimate the point spectrum as well. Here we use the Newton method with random initial points to locate eigenvalues in $\mathbb{C}^+$. Naturally, we limit ourselves to a rectangular region in the complex plane, slightly above the real axis to avoid potential spurious eigenvalues. Since the number of eigenvalues is not known a priori, the continuous spectrum is found first so as to give an estimate of the energy of the discrete spectrum. It is essential that the continuous spectrum is estimated accurately so that a good estimate of the energy of the discrete spectrum can be obtained. Once this energy is known, and a suitable (rectangular) search region in $\mathbb{C}^+$ is chosen, the Newton method is often able to locate all of the discrete eigenvalues using just a few iterations.

Fig. 5.3 shows the accuracy of the searched-based methods in estimating the largest eigenvalue of the signal $q(t) = 2.7\text{sech}(t)$. The Runge-Kutta, layer-peeling and Crank-Nicolson methods have about the same accuracy, followed closely by forward discretization. Since this is the largest eigenvalue, the AL schemes are not quite as accurate. As noted above, comparison at smaller values of N is not illustrative, as the AL estimate

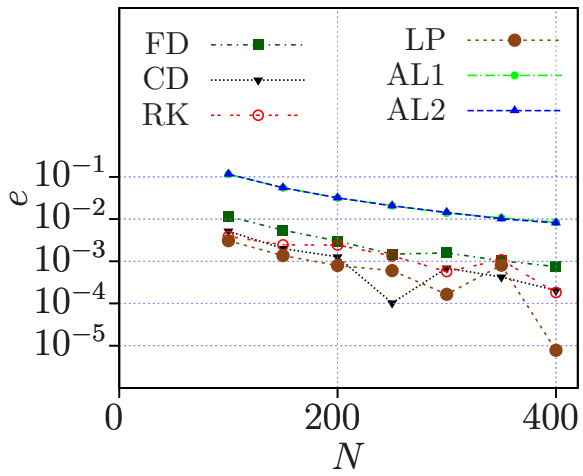

Figure 5.3: Error in estimating the largest eigenvalue of Satsuma-Yajima pulse $q(t) = 2.7\text{sech}(t)$ as a function of the number of sample points N using search-based methods.

quickly deviates from $\lambda_{\max}$ of the continuous signal.

The Runge-Kutta method, at the accuracies shown in the above graphs, is of course very slow, and is not a practical method to implement. The running time for the other schemes is approximately the same. Search-based methods take an order of magnitude more time than matrix-based methods when N is small. These methods fail when N becomes too small ($N < 200$), since the large error in estimating the energy terms of the continuous spectrum negatively influences the stopping criteria and consequently degrades the Newton increments. For large N, on the other hand, the QR factorization, which takes $\mathcal{O}(N^3)$ operations in calculating the eigenvalues of a matrix, becomes quite slow and restricts the use of matrix-based methods.

The same conclusions are observed for various choices of real or complex parameter A. As $|A|$ is increased, as before, the spectral and finite-difference schemes produce the correct eigenvalues, and the AL methods generate the same eigenvalues plus an additional vertical strip of spurious eigenvalues. The range of the spurious eigenvalues across the real axis remains about the same. As the phase of A is increased, the true (non-spurious) eigenvalues remain the same in all methods (as expected analytically), while some of the vertical spurious eigenvalues in the AL schemes move from left to right or vice versa. The spectral and finite-difference schemes are relatively immune to these additional spurious eigenvalues. Normalization of the AL method sometimes produces slightly fewer spurious eigenvalues across the real axis, as can be seen in Figs. 5.1(c)-(d).

5.5.2 Rectangular Pulse

Consider the rectangular pulse

$$q(t) = \begin{cases} A & t \in [T_1, T_2] \\ 0 & \text{otherwise} \end{cases}. \tag{5.28}$$

It can be shown that the continuous spectrum is given by [57]

$$\hat{q}(\lambda) = \frac{A^*}{j\lambda} e^{-2j\lambda t} \left(1 - \frac{D}{j\lambda} \cot(D(T_2 - T_1))\right),$$

where $D = \sqrt{\lambda^2 + |A|^2}$. To calculate the discrete spectrum, the equation (5.27) is reduced to a simple constant coefficient second-order ODE

$$\frac{\mathrm{d}^2 z}{\mathrm{d}t^2} - 2j\lambda \frac{\mathrm{d}z}{\mathrm{d}t} + |A|^2 z = 0, \quad z(T_1) = 1, z'(T_1) = 0.$$

It is easy to verify that the eigenvalues are the solutions of

$$e^{2j(T_2 - T_1)\sqrt{\lambda^2 + |A|^2}} = \frac{\lambda + \sqrt{\lambda^2 + |A|^2}}{\lambda - \sqrt{\lambda^2 + |A|^2}}. \tag{5.29}$$

Following the causality and the layer-peeling property of the NFT, one can generalize the above result to piece-wise constant pulses. This is the basis of the layer-peeling method of Section 5.2.3.

Fig. 5.4(a)-(b) show the results of numerically computing the discrete spectrum of a rectangular pulse with parameters $A = 2$, $T_2 = -T_1 = 1$. The exact eigenvalue is found to be $\lambda = 1.5713j$, by numerically finding the roots of (5.29) using the Newton-Raphson method. No other eigenvalue is found under a large number of random initial conditions. All methods generate the desired eigenvalue together with a large number of spurious eigenvalues across the real axis. The central-difference scheme visibly generates fewer spurious eigenvalues. The Ablowitz-Ladik schemes produce two more eigenvalues with a large negative real part.

Fig. 5.5 compares the precision of various methods in estimating the nonlinear spectrum of the rectangular pulse with $A = 2$, $T_2 = -T_1 = 1$. The modified AL scheme performed the same as the basic AL scheme, and hence we do not include the modified AL scheme in the graphs.

Convergence to the discrete spectral amplitudes generally occurs much more slowly than convergence to the eigenvalues. Fig. 5.6(a) shows the precision of various methods

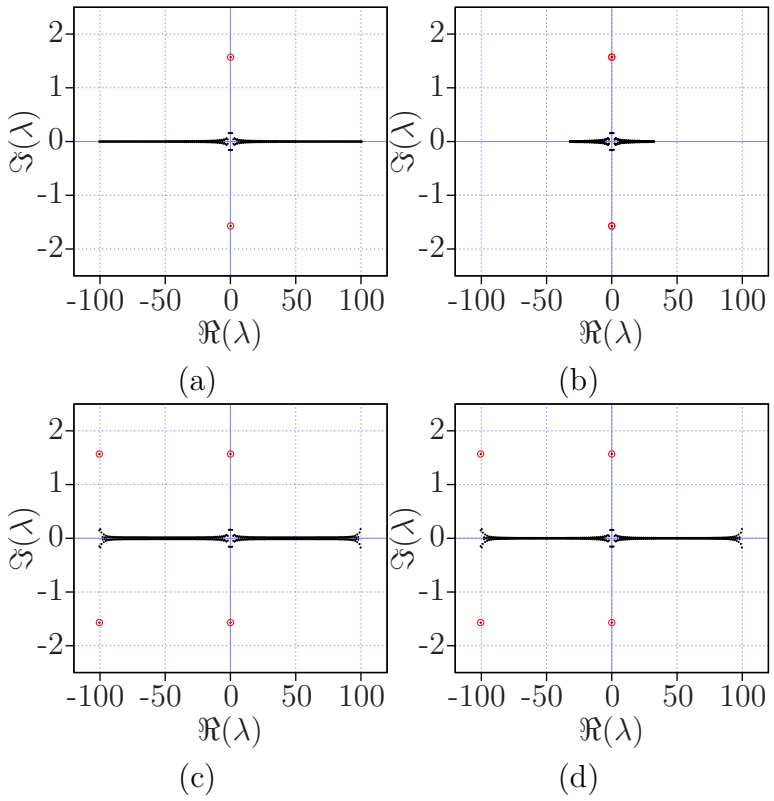

Figure 5.4: Discrete spectrum of the rectangular pulse (5.28) with $A = 2$, $T_2 = -T_1 = 1$ using (a) Fourier method, (b) central difference method, (c) Ablowitz-Ladik scheme, (d) modified Ablowitz-Ladik scheme.

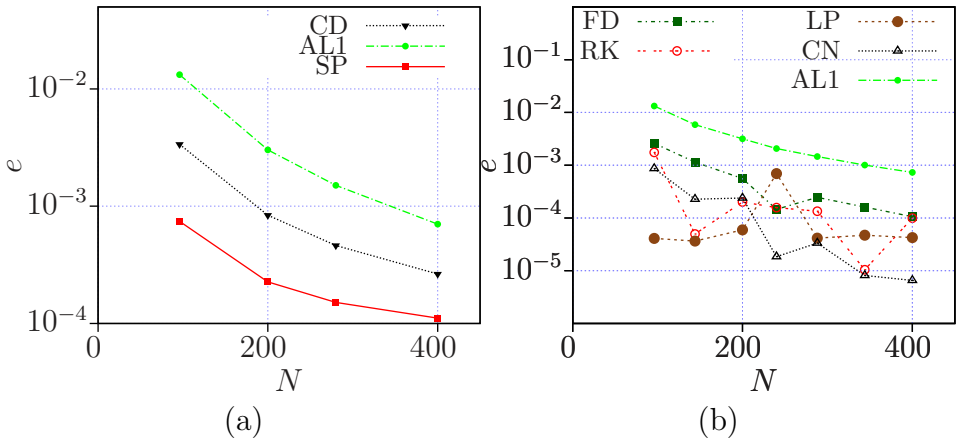

Figure 5.5: Error in estimating the largest eigenvalue of the rectangular pulse $q(t) = 2\text{rect}(t)$ as a function of the number of sample points N using (a) matrix-based methods and (b) search-based methods.

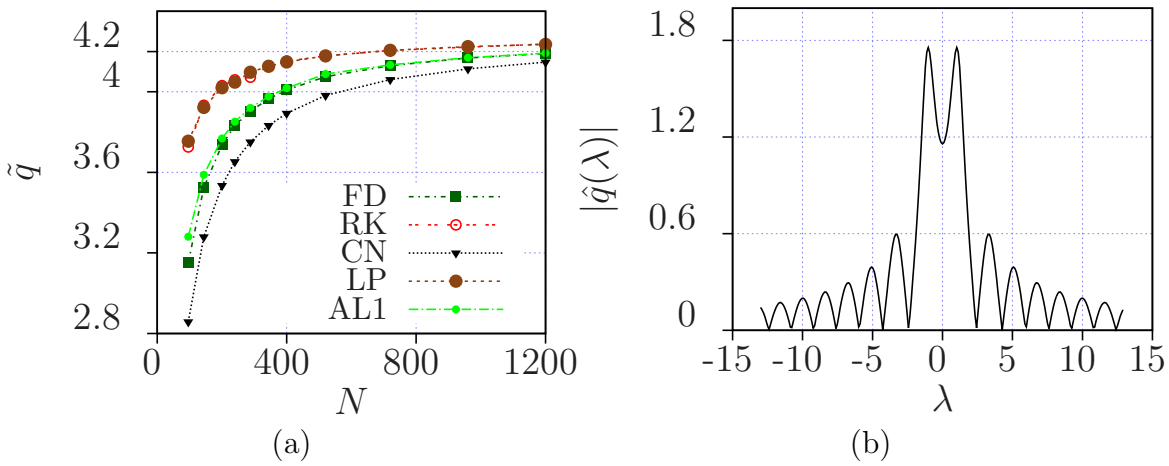

Figure 5.6: (a) Convergence of the discrete spectral amplitude for the rectangular pulse $q(t) = 2\text{rect}(t)$ as a function of the number of sample points N. Factor $-j$ is not shown in the figure. (b) Continuous spectrum.

in estimating the discrete spectral amplitude of the rectangular wave with $A = 2$, $T_2 = -T_1 = 1$. It can be seen that convergence does not occur until $N > 1000$. Fig. 5.6(b) shows the continuous spectrum for the same function. All methods produced essentially the same continuous spectrum, except for some very slight variations near zero frequency.

As $|A|$ is increased, more eigenvalues appear on the imaginary axis. The distance between these eigenvalues becomes smaller as $|\lambda|$ is increased. All methods produce similar results, with the Ablowitz-Ladik methods reproducing the purely imaginary eigenvalues at spurious locations with large real part. Phase addition has no influence on any of these methods, as expected analytically.

5.5.3 N-Soliton Pulses

We consider an 4-soliton pulse with discrete spectrum

$$\begin{aligned} \tilde{q}(-1+0.25j) = 1, \quad \tilde{q}(1+0.25j) = -j, \\ \tilde{q}(-1+0.5j) = -1, \quad \tilde{q}(1+0.5j) = j. \end{aligned} \tag{5.30}$$

The 4-soliton is generated by solving the Riemann-Hilbert linear system of equations with zero continuous spectrum [57] and can be seen in Fig. 5.7(a). Figs. 5.8(a)-(d) show the discrete spectrum of the signal using various matrix-based methods. The relative accuracy of these schemes in estimating the eigenvalue $\lambda = 1+0.5j$ is shown in Fig. 5.7(b). A very similar graph is obtained for other eigenvalues. Iterative methods fare similarly

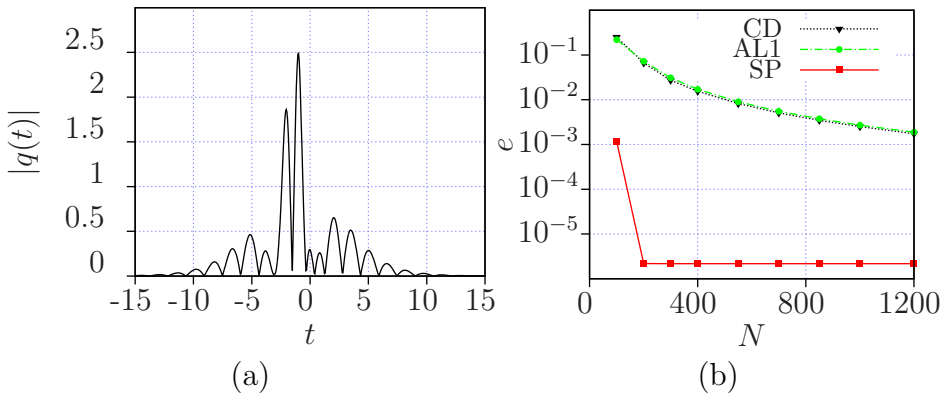

Figure 5.7: (a) Amplitude profile of a 4-soliton pulse with spectrum (5.30). (b) Error in estimating the eigenvalue $\lambda = 1 + 0.5j$.

and their performance is shown in Fig. 5.9(b).

The convergence of the discrete spectral amplitudes $\tilde{q}(\lambda_j)$ is not quite satisfactory. Discrete spectral amplitudes associated with eigenvalues with small $|\Im(\lambda_j)|$ can be obtained with reasonable accuracy, although the convergence of $\tilde{q}(\lambda_j)$ is slower than the convergence of the eigenvalues themselves. On the other hand, discrete spectral amplitudes associated with eigenvalues with large $|\Im(\lambda)|$ are extremely sensitive to the location of eigenvalues and even slight changes in eigenvalues lead to radically different estimates for the spectral amplitudes. In fact, as the energy of the pulse is increased by having eigenvalues with large $|\Im(\lambda)|$, the Riemann-Hilbert system becomes ill-conditioned. Therefore the discrete spectral amplitudes cannot generally be obtained using the methods discussed in this chapter. It is illustrative to see the surface of $|a(\lambda)|$ in Fig. 5.21. The eigenvalues sometimes correspond to deep and narrow wells in the surface of $|a(\lambda)|$, and sometimes they correspond to flat minima. In cases that they correspond to narrow wells, the derivative $a'(\lambda)$ is sensitive to the location of eigenvalues, leading to sensitivities in $\tilde{q}(\lambda_j)$. It is also clear from (5.18) that $a'(\lambda)$ is proportional to λ^2 and thus is sensitive to λ.

Note that $\tilde{q}(\lambda_j)$ do not appear in the trace formula, and in particular they do not contribute to the signal energy. This part of the NFT controls the time center of the pulse and influences the signal phase too. Due to dependency on the time center of the signal and the fact that time center can hardly be used for digital transmission, the values of $\tilde{q}(\lambda_j)$ appear to be numerically chaotic and cannot carry much information. For this reason, we do not discuss these quantities in detail.

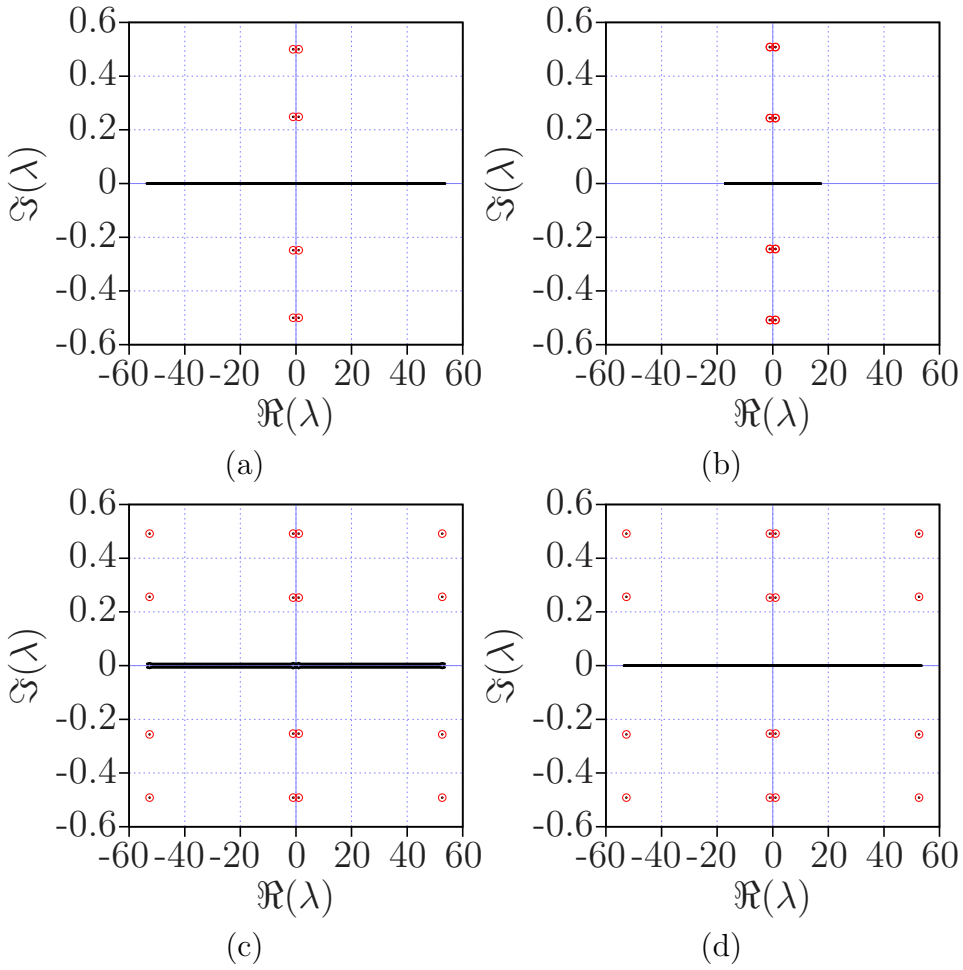

Figure 5.8: Discrete spectrum of N-soliton pulse with spectrum (5.30) using (a) Fourier method, (b) central difference method, (c) Ablowitz-Ladik scheme, and (d) modified Ablowitz-Ladik scheme.

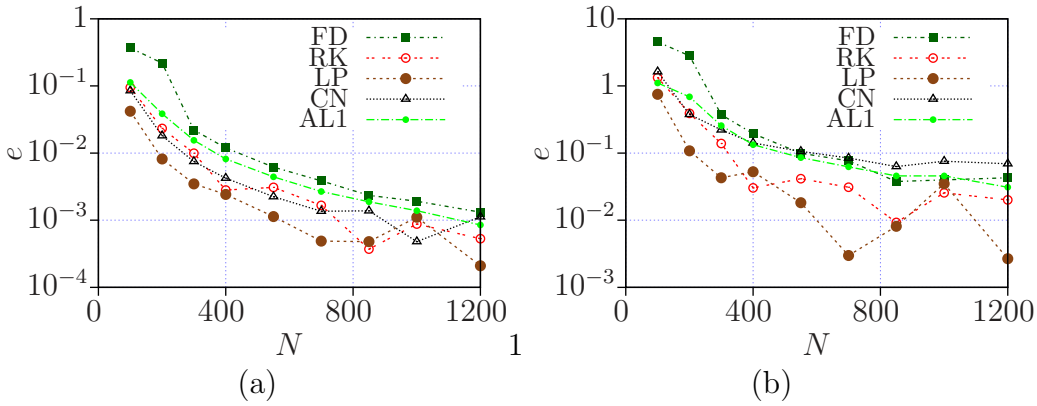

Figure 5.9: (a) Error in estimating the eigenvalue $\lambda = -1 + 0.25j$ in a 4-soliton using search-based methods. (b) Error in estimating the discrete spectral amplitude $|\tilde{q}| = 1$.

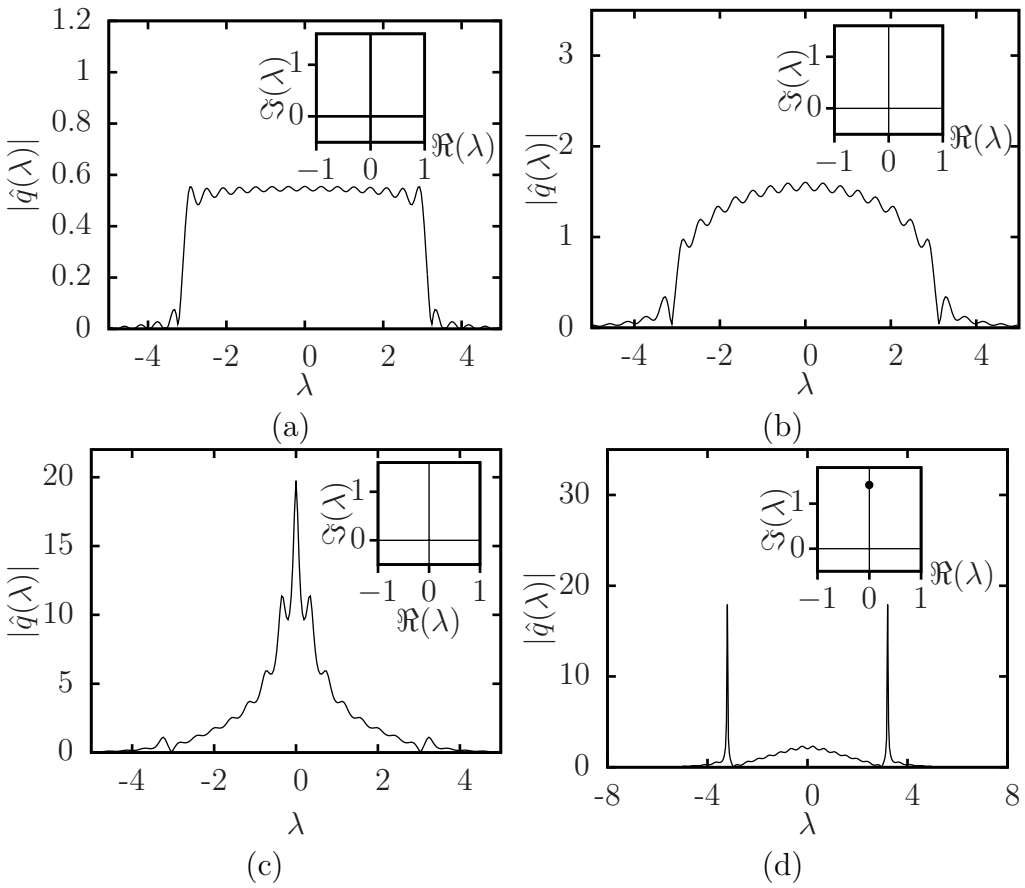

Figure 5.10: Nonlinear Fourier transform of a sinc function with amplitude $A = 1, 2, 3, 4$.

5.6 Nonlinear Fourier Transform of Pulses in Data Communications

In this section, we use the numerical methods discussed in Section 5.1 to compute the nonlinear Fourier transform of signals typically used in optical fiber transmission. The emphasis is on sinc functions as they constitute signal degrees of freedom, but we also consider raised-cosine functions, sech signals, and Gaussian pulses. In particular, we study the effect of the amplitude and phase modulation on the structure of the nonlinear spectra. We will also discuss the spectrum of wavetrains formed by sinc functions.

Since the layer-peeling and the spectral methods give accurate results in estimating the nonlinear spectra, they are chosen for subsequent simulations.

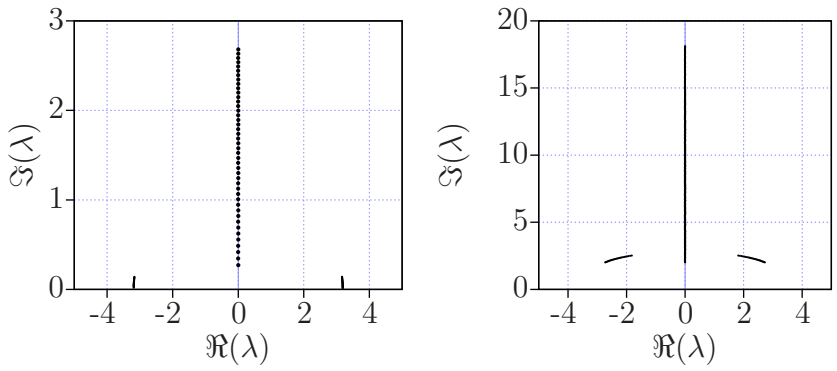

(a) (b)

Figure 5.11: Locus of eigenvalues of the sinc function under amplitude modulation: (a) $A = 0$ to $A = 5$, (b) $A = 0$ to $A = 20$.

5.6.1 Amplitude and Phase Modulation of Sinc Functions

Fig. 5.10 shows the spectrum of $y(t) = A\text{sinc}(2t)$ under amplitude modulation. It can be seen that a sinc function is all dispersive as A is increased from zero, until about $A = \pi$ ($||q||_{L_1} = 1.2752\pi$) where a new eigenvalue emerges from the origin. Starting from $A = 0$, the continuous spectrum is a rectangle, resembling the ordinary Fourier transform $-\mathcal{F}(q^*(t))(2\lambda)$. As A is increased, the continuous spectral function is narrowed until $A = \pi$, where it looks like a delta function and its energy starts to deviate from the energy of the time domain signal. As $A > \pi$ is further increased, the dominant eigenvalue on the $j\omega$ axis moves up until $A = 1.27\pi$, where $\lambda_1 = 1.4234j$ and a new pair of eigenvalues emerges, starting from $\lambda_{23} = \pm 3.2 + 0.05j$. When the newly created eigenvalues are not pronounced enough, for instance in this example when transiting from $A = \pi$ to $A = 1.27\pi$, numerical algorithms have difficulties in determining whether these small emerging eigenvalues are part of the spectrum or not. Here it appears that for $\pi < A < 1.27\pi$ there is just one dominant purely imaginary eigenvalue moving upward. At $A = 1.27\pi$, λ_{23} emerge and move up in the complex plane as A is increased. An important observation is that the sinc function appears to have not only purely imaginary eigenvalues, but also a pair of symmetric eigenvalues with nonzero real part emerging at high values of A; see Fig. 5.11(b). This means that, for example, a sinc function (viewed in the time domain) contains a stationary "central component" plus two small "side components" which travel to the left and right if the sinc function is subject to the NLS flow. The locus of the eigenvalues of the function $A\text{sinc}(2t)$ as a result of variations in A is given in Fig. 5.11.

It follows that the sinc function is a simple example of a real symmetric pulse whose

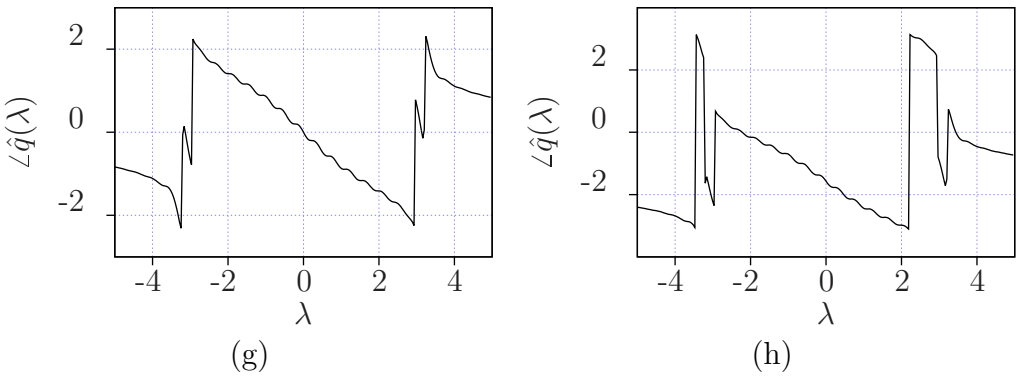

Figure 5.12: Phase of the continuous spectrum of a sinc function when: (a) $A = 4$, (b) $A = 4j$.

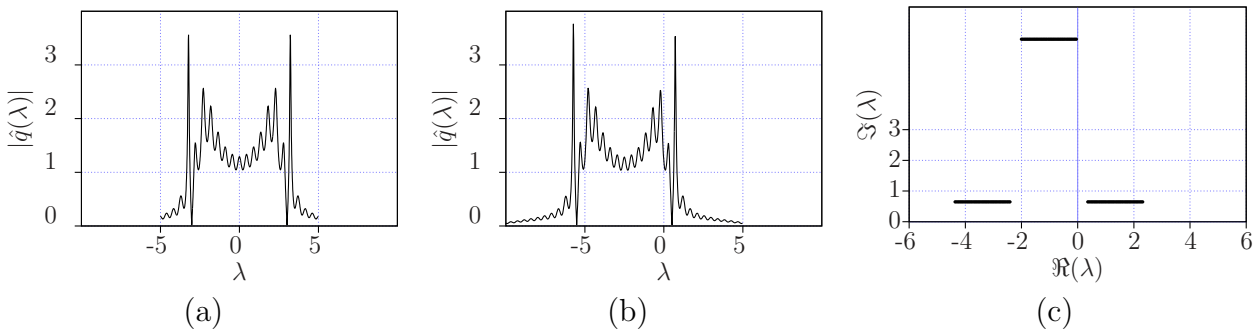

Figure 5.13: (a) Amplitude of the continuous spectrum with no carrier. (b) Amplitude of the continuous spectrum with carrier frequency $\omega = 5$. The phase graph is also shifted similarly with no other change ($\Delta\lambda = 2.5$). (c) Locus of the eigenvalues of a sinc function with amplitude $A = 8$ as the carrier frequency $\exp(-j\omega t)$ varies.

eigenvalues are not necessarily purely imaginary, as conjectured for a long time. However if $q(t)$ is real, non-negative, and "single-lobe", then there are exactly $\mathsf{N} = \lfloor \frac{1}{2} + \frac{||q||_{L_1}}{\pi} - \epsilon \rfloor$ eigenvalues, all purely imaginary [51].

Under phase modulation, in the form of adding a constant phase term to the signal, the eigenvalues and the magnitude of the continuous spectrum remained unchanged. Vertical shift in the phase of the continuous spectrum as a result of phase modulation can be seen in Fig. 5.12.

We may also examine the effect of time-dependent phase changes. The effect of linear chirp, of the form $\exp(j\omega t)$, is shown in picture Fig. 5.13. Linear chirp results in just a shift of the discrete and continuous spectrum to the left or the right, depending on the sign of the chirp.

It is interesting to observe the effect of a quadratic chirp. The locus of eigenvalues that result due to changes in the quadratic phase $q\exp(j\omega t^2)$ has been studied in [51] for Gaussian pulses. In our sinc function example, in the case that there is one discrete

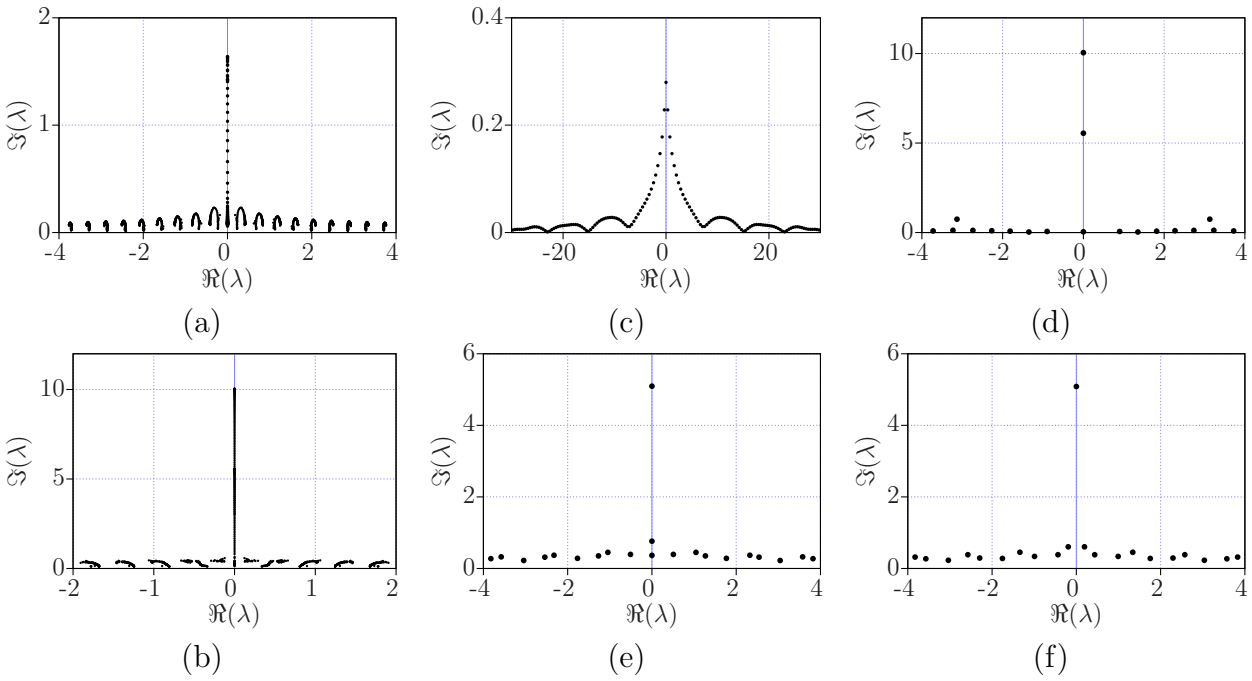

Figure 5.14: Eigenvalues of $Ae^{-j\omega t^2}\text{sinc}(2t)$: (a) locus of eigenvalues for $A = 4$ and $\omega = 0.5$ to $\omega = 50$, (b) locus of eigenvalues for $A = 12$ and $\omega = 0$ to $\omega = 50$, (c) eigenvalues for $A = 4$ and $\omega = 15$, (d) eigenvalues for $A = 12$ and $\omega = 0.50$, (e) eigenvalues for $A = 12$ and $\omega = 41.39$ just before collision, (f) eigenvalues for $A = 12$ and $\omega = 41.43$ after collision.

eigenvalue in the chirp-free case (such as when $A = 4$), increasing ω will move the eigenvalue on the $j\omega$ axis upward, but then the eigenvalue move down again and is absorbed in the real axis. Fig. 5.14(c) shows the moment before the eigenvalue is absorbed into the real axis. Note that the eigenvalues off the $j\omega$ axis are considered to be spurious; their number increases as the number of sample points is increased.

A more interesting behavior is observed when $A = 12$. Here, there are two eigenvalues on the $j\omega$ axis: $\lambda_1 \approx 10.0484j$, $\lambda_2 = 5.5515j$, together with $\lambda_{3,4} = \pm 3.1315 + 0.7462j$ (Fig 5.14(d)). As ω is increased, λ_1 and λ_2 move down and a fifth eigenvalue λ_5 emerges from the real axis and moves upwards on the $j\omega$ axis. Eventually, at about $\omega = 41.41$, λ_2 and λ_5 "collide" and move out of the $j\omega$ axis to the left and right. If ω is further increased, λ_2 and λ_5 are absorbed into the real axis; see Fig. 5.14.

Collision of eigenvalues also occurs with time dilation. Signal $q(t) = \text{sinc}(at)$ has 3 eigenvalues on the $j\omega$ axis for $a = 0.1$, plus two small eigenvalues on two sides of the $j\omega$ axis (Fig 5.16(b)). As a is increased, the smaller eigenvalue on the $j\omega$ axis comes down and a new eigenvalue is generated at the origin, moving upward. These two eigenvalues collide at $0.12j$ ($a = 0.1330$) and are diverted to the first and second quadrant, and

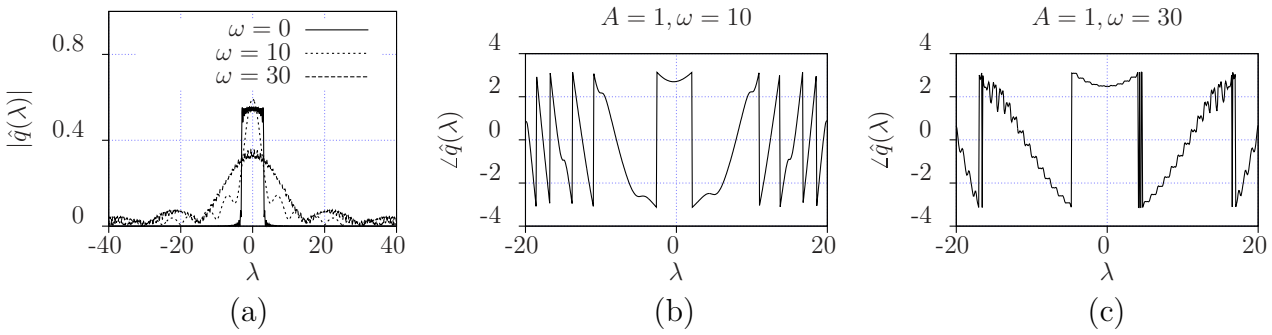

Figure 5.15: (a) Nonlinear spectral broadening as a result of quadratic phase modulation $Ae^{j\omega t^2}\text{sinc}(2t)$ with $A = 1$ and $\omega = 0$, 10 and 30. (b) Phase of the continuous spectrum when $A = 1$ and $\omega = 10$. (c) Phase of the continuous spectrum when $A = 1$ and $\omega = 30$.

eventually absorbed in the real axis at about $\Re\lambda = \pm 0.32$ ($\omega = 0.1990$), Fig. 5.16(c)-(d)). As a is decreased, more eigenvalues appear on the $j\omega$ axis and fewer on the real axis (Fig. 5.16(e)-(f)). Note that the eigenvalues are not necessarily on the $j\omega$ axis. For example, the signal $y = \text{sinc}(0.1370t)$ clearly has eigenvalues $\lambda_1 = 0.8684j$, $\lambda_2 = 0.5797j$, $\lambda_{3,4} = \pm 0.1055 + 0.1210i$.

Fig. 5.15 shows the nonlinear spectrum of a sinc pulse under a quadratic chirp modulation, given by $Ae^{j\omega t^2}\text{sinc}(2t)$, is broadened as ω varies.

The effect of time dilation on the continuous spectrum can be seen in Fig. 5.17. It can be observed that increasing bandwidth a, will increase the continuous range of real nonlinear frequencies, leading to bandwidth expansion.

5.6.2 Sinc Wavetrains

The nonlinear spectrum of a wavetrain can take on a complicated form, just like its ordinary Fourier transform counterpart. Eigenvalues of a two-symbol train, for instance, depend on the amplitude and phase of the two signals, and their separation distance.

We first analyze the case in which there are only two sinc functions located at the fixed Nyquist distance from each other, *i.e.*, $y(t) = a_1\text{sinc}(2t + \frac{1}{2}) + a_2\text{sinc}(2t - \frac{1}{2})$. For $a_1 = a_2 = 2$ the spectrum consists of a single eigenvalue $\lambda = 0.3676j$ and a number of spurious eigenvalues as shown in Fig. 5.18(a). As the phase of a_2 is increased from $\theta = 0$ to $\theta = \pi$, the eigenvalues moves off the $j\omega$ axis to the left and a new eigenvalue emerges from the real axis in the first quadrant. Eigenvalues at $\theta = \pi$ are $\pm 1.3908 + 0.3287i$. The resulting locus of eigenvalues is shown in Fig. 5.18(b). Figs 5.18(c)-(d) depict similar graphs when both a_1 and a_2 change.

Next we study the locus of the discrete spectrum as a function of pulse separation for fixed amplitudes. If the amplitude of the sinc functions is increased sufficiently,

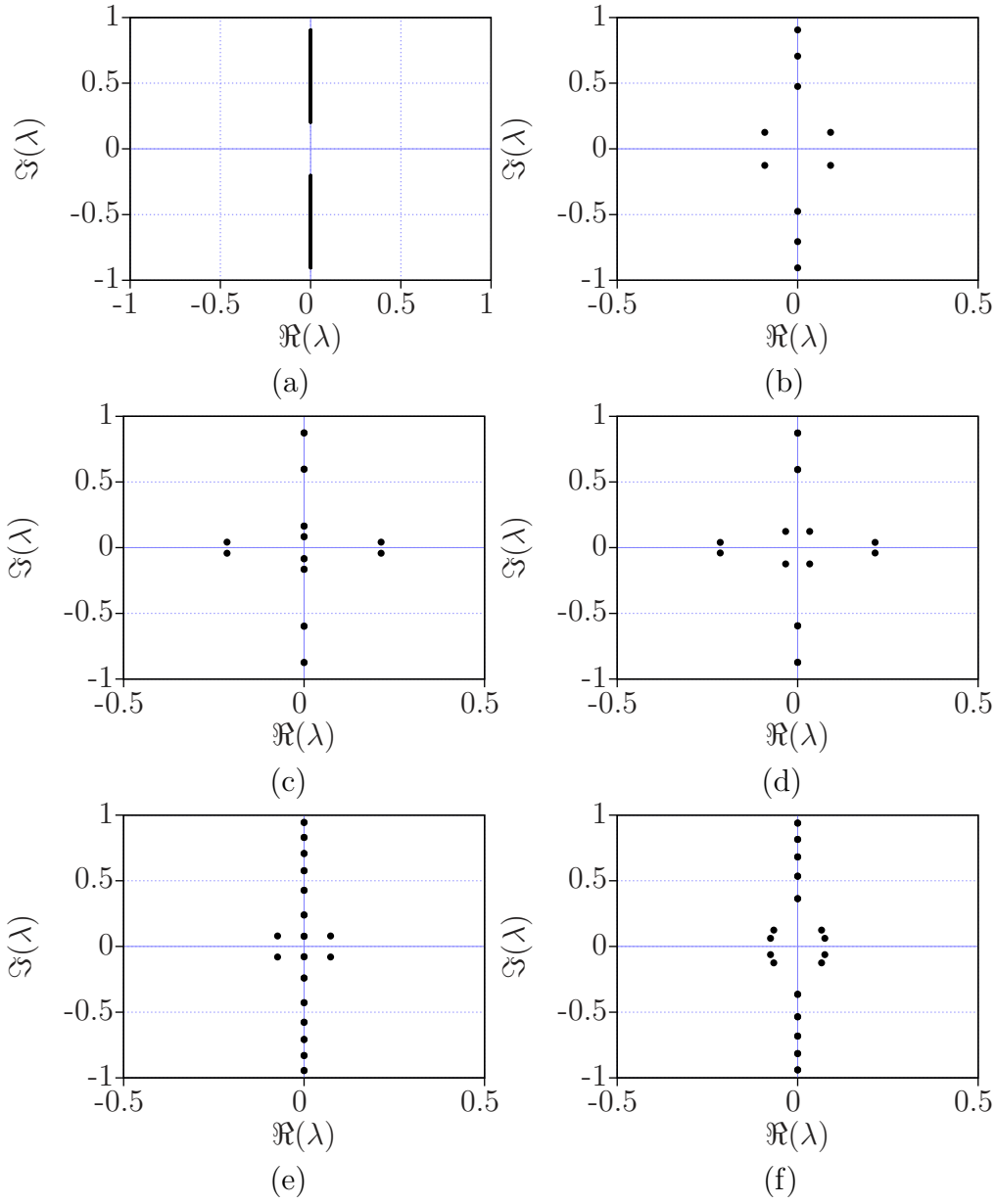

Figure 5.16: Locus of eigenvalues of $\mathrm{sinc}(at)$ as the bandwidth varies (a) from $a = 0.1$ to $a = 0.6$. (Eigenvalues with small $\Im\lambda$ are not shown here.) (b) Eigenvalues for $a = 0.1$. (c) Eigenvalues before collision and (d) after collision. (e) Eigenvalues for $a = 0.06$ before collision and (f) for $a = 0.065$ after collision.

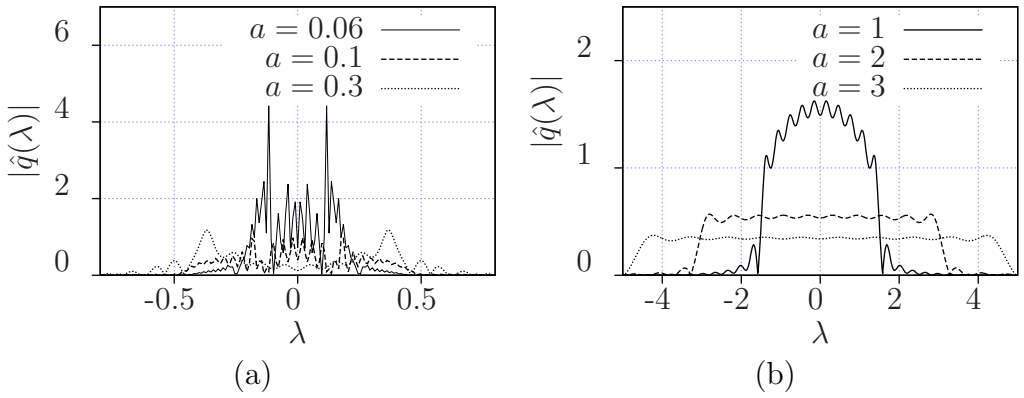

Figure 5.17: Bandwidth expansion in $\text{sinc}(at)$ for (a) $a = 0.06$, $a = 0.1$, $a = 0.3$ (b) $a = 1$, $a = 2$, $a = 3$.

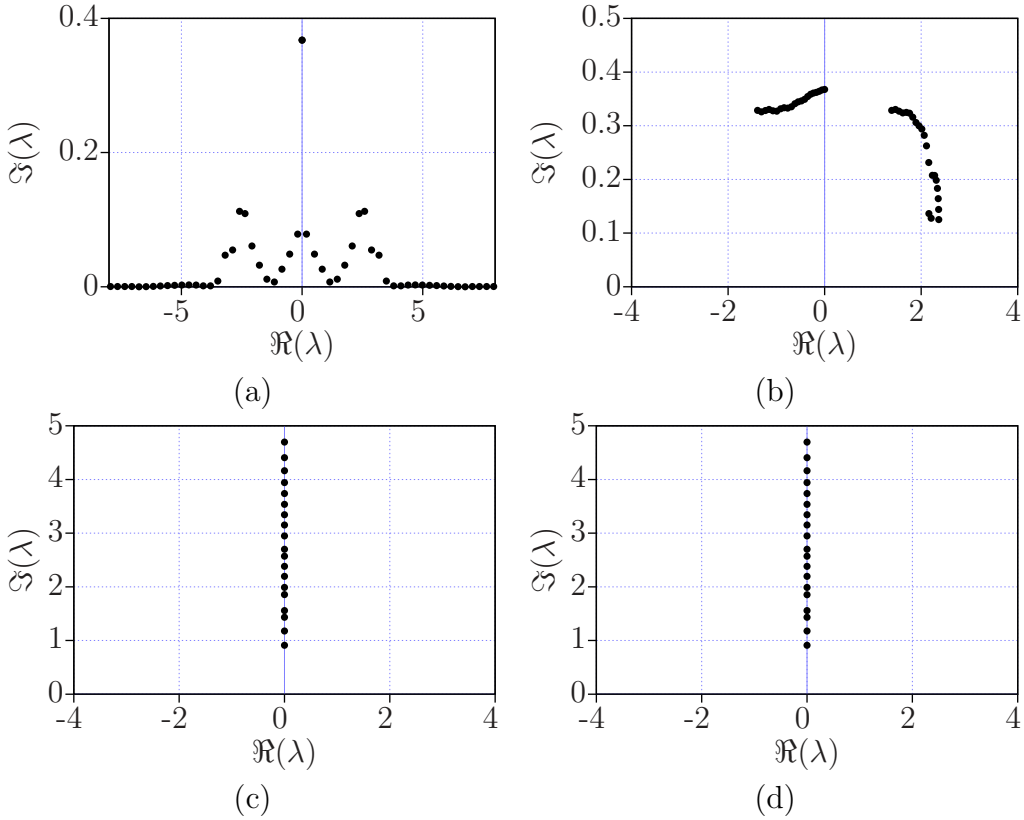

Figure 5.18: Discrete spectrum of $y(t) = a_1\text{sinc}(2t - \frac{1}{2}) + a_2\text{sinc}(2t + \frac{1}{2})$ for (a) $a_1 = a_2$, (b) $a_1 = 2$, $a_2 = 2e^{j\theta}$ for $-\pi < \theta \leq \pi$, (c) $a_1 = 2$, $0 \leq a_2 \leq 6$, (d) $a_1 = 4j$, $0 \leq a_2 \leq 6$.

eigenvalues appear off the real axis and form a locus as the distance between pulses varies. Fig. 5.19(a) shows the locus of eigenvalues of $y(t) = 4\text{sinc}(2t+\tau) + 4\text{sinc}(2t-\tau)$ as τ changes between zero to 5. At $\tau = 0$, eigenvalues are $\lambda_1 = 6j$, $\lambda_{2,3} = \pm 2.3618 + 0.6476i$ and $\lambda_{4,5} = \pm 3.2429 + 0.0815i$. As the distance between pulses is increased, λ_1 rapidly decreases, and at about $\tau = 0.25$, where $\lambda_1 = 4.3j$, the eigenvalues with non-zero real parts are absorbed into the real axis at $\Re\lambda = -3$. As τ is further increased, λ_1 decreases further, until $\tau = 0.4$ where $\lambda_1 = 2.4j$ and two new eigenvalues emerge at locations $\Re\lambda = \pm 3.12$ going up and towards the $j\omega$ axis. These eigenvalues return, before reaching the $j\omega$ axis, to be absorbed into the real axis, while new eigenvalues are generated again from the real axis. At $\tau = 0.7$ eigenvalues are $\lambda = 2j$, $\pm 1 + j$. At some point, the newly created eigenvalues are not absorbed into the real axis, but they reach the $j\omega$ axis and collide. A collision occurs, for instance, at $\tau = 1.05$. One of these eigenvalues goes down to be absorbed into the origin, and the other one, interestingly, goes up to be united with the maximum eigenvalue on the $j\omega$ axis (*i.e.*, to create one eigenvalue with multiplicity two). Increasing the distance further does not change the location of this eigenvalue, which from now is fixed at $\lambda = 1.4j$, but just changes the pattern of lower level eigenvalues. The collision does not occur when the amplitudes of the signals are smaller; see Fig. 5.19 (b) for the locus of the eigenvalues when the amplitude of the two sinc functions is 2.

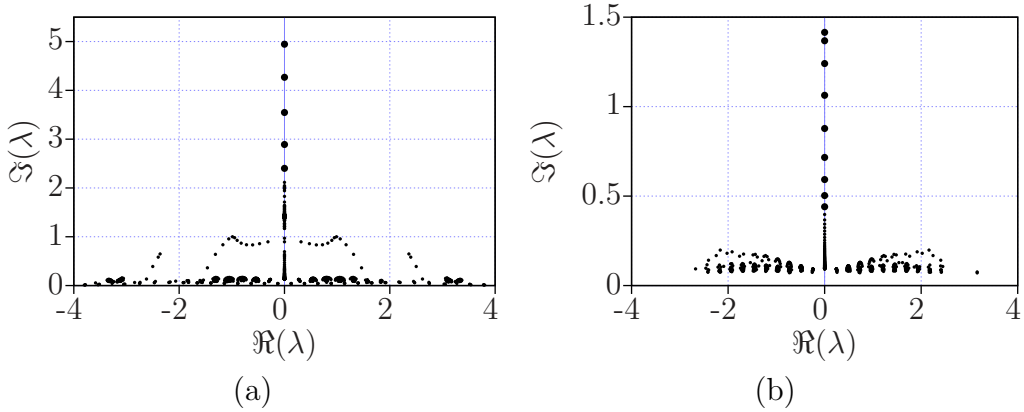

Figure 5.19: (a) The locus of the discrete spectrum of $y(t) = 4\text{sinc}(2t+\tau) + 4\text{sinc}(2t-\tau)$ as a function of $0 \leq \tau \leq 5$. (b) The locus of the discrete spectrum of $y(t) = 2\text{sinc}(2t+\tau) + 2\text{sinc}(2t-\tau)$ as a function of $0 \leq \tau \leq 5$.

For wavetrains with a larger number of signals, the number of eigenvalues increases proportionally. We generate these wavetrains randomly and examine the region to which the spectrum is confined. Fig. 5.20 shows the locus of the discrete spectrum of all sinc wavetrains with 16 signals. All 16 signal degrees of freedom in the bandlimited signal are

modulated here. The effect of the bandwidth constraint in the nonlinear spectral domain can seen in this picture.

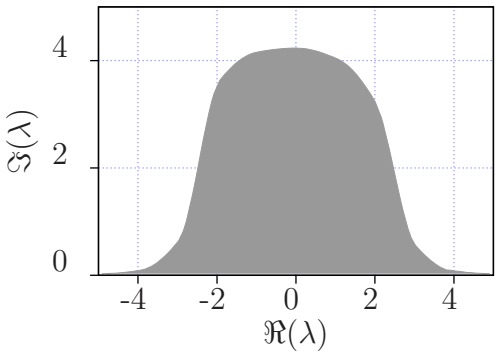

Figure 5.20: Effect of the bandwidth constraint on the location of the eigenvalues of a sinc wavetrain containing 16 pulses having random amplitudes.

5.6.3 Preservation of the Spectrum of the NLS Equation

It is crucial to ensure that the spectrum found by the numerical methods, such as those discussed in the previous sections, is in fact correct. While it proved difficult to do so consistently and efficiently, there are various tests to increase one's confidence in the truth of the output of the numerical methods. Taking the inverse nonlinear Fourier transform in the continuous-time domain and comparing the resulting function in time with the original signal is generally quite cumbersome and not always feasible. One quick test is to examine a time frequency identity, such as the trace formula for $n = 1, 2, 3, \ldots$ as used in this chapter. The first few conserved quantities in this identity can be written explicitly. One should allow higher tolerance values in the trace formula for large n, as the discrete terms in this identity involve λ^n and thus are increasingly more sensitive to the eigenvalues. Another test is to subject the signal to the flow of an integrable equation, such as the NLS equation, and check that the discrete spectrum is preserved and the spectral amplitudes are scaled appropriately according to that equation. In this section, we let the signal propagate according to the NLS equation and compare the spectra at $z = 0$ and $z = \mathcal{L}$ for various $\mathcal{L}$.

Fig. 5.21 shows examples of the spectra of a number of pulses at $z = 0$ and $z = \mathcal{L}$ evolving according to the NLS equation (5.1). The distances mentioned in the graphs in km correspond to a standard optical fiber with parameters in Table 2.1.

Note that in all these examples discrete the spectrum is completely preserved, and the continuous spectral amplitudes undergo a phase change properly. Compared to Gaussian and raised-cosine examples, whose nonlinear Fourier transform can be found easily, the

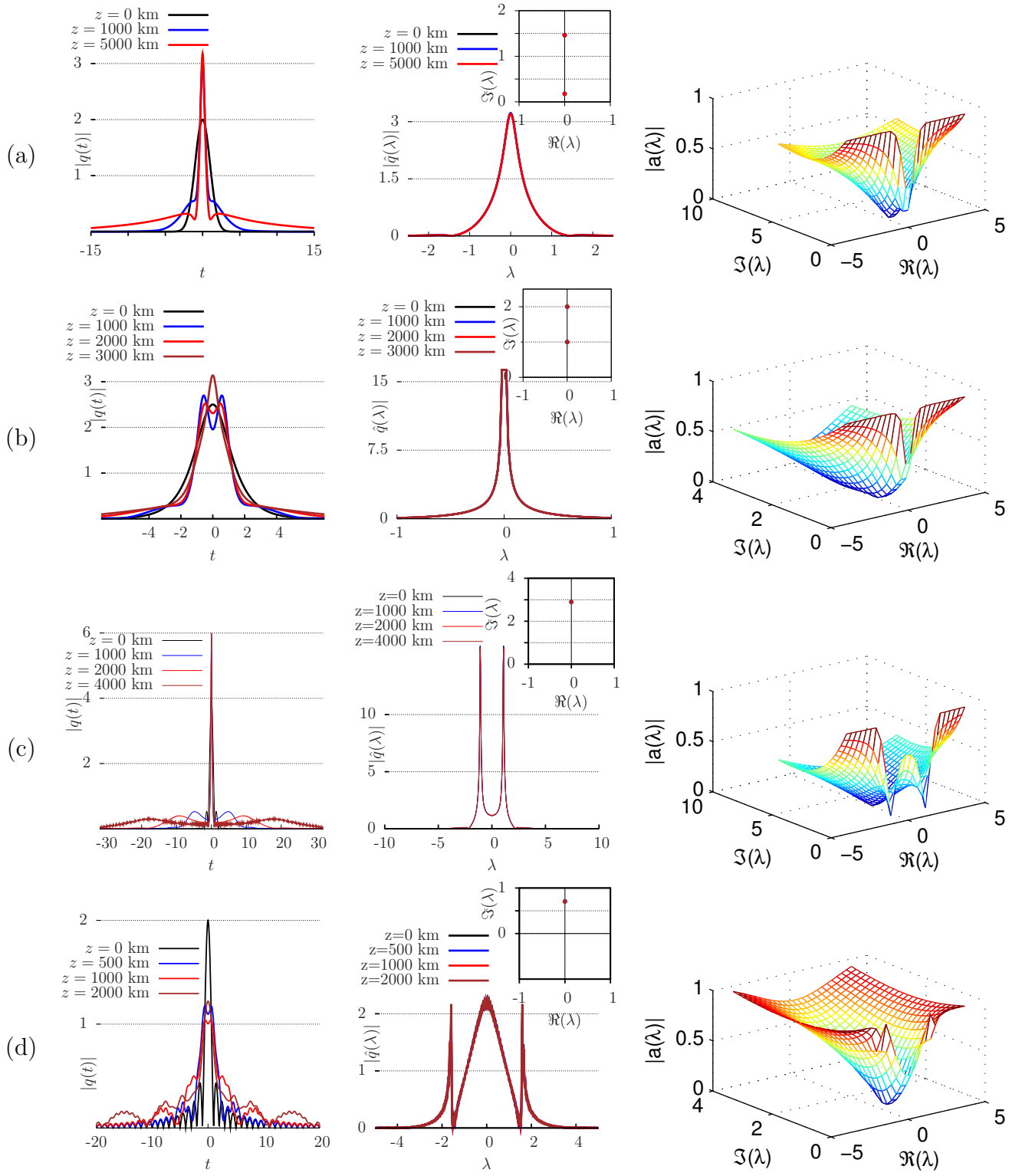

Figure 5.21: Propagation of pulses along an optical fiber in the time domain (left), in the nonlinear Fourier transform domain (middle), and showing the surface of $|a(\lambda)|$ (right). The pulses are (a) Gaussian pulse, (b) Satsuma-Yajima pulse, (c) raised-cosine pulse, (d) sinc pulse. The zeros of $|a(\lambda)|$ correspond to eigenvalues in $\mathbb{C}^+$.

discrete spectrum of sinc functions is much more challenging to find. This is because the non-dominant eigenvalues off the $j\omega$ axis have small imaginary parts for typical parameters and are not sufficiently distinguished. They also have large real parts, increasing the search region. Sinc functions are thus not the best examples to illustrate the application of the NFT in optical fibers. We studied these ideal pulses primarily because of their fundamental utility in digital communications.

5.7 Summary

In this chapter, we have suggested and compared a variety of numerical methods for the computation of the nonlinear Fourier transform of a signal defined on the entire real line. A straightforward finite-difference discretization, such as the forward discretization, does not often produce satisfactory results. Among the methods studied in this chapter, the layer-peeling and spectral methods gave accurate results in estimating the continuous and discrete spectrum over a wide class of examples.

Given a waveform without having prior knowledge of the location of the discrete eigenvalues, we suggest the use of matrix-based methods to compute the discrete spectrum. If, on the other hand, the location of the eigenvalues is known approximately (as in data-communication problems, where the eigenvalues are chosen at the transmitter from a finite set) a search-based method is recommended.

Although the eigenvalues and the continuous spectral function can be calculated with great accuracy, the discrete spectral amplitudes are quite sensitive to the location of the eigenvalues, even in the absence of noise. These discrete amplitudes control the time center of the pulse, and are therefore sensitive to timing jitter. For data communication purposes it follows that, whereas the presence or absence of the eigenvalue itself may allow for robust information transmission, encoding information in the time center of the pulse, *i.e.*, in the discrete spectral amplitudes, is unlikely to be viable.

Using these numerical methods, we studied the influence of various signal parameters on the nonlinear Fourier transform of a number of pulses commonly used in data communications. We found, for example, that the spectrum of an isolated normalized sinc function with amplitude A is purely continuous for the $A < \pi$. However, as the pulse amplitude is increased, dominant eigenvalues appear on the $j\omega$ axis, together with pairs of symmetric eigenvalues having nonzero real part.

In general, amplitude variations result in variations in the location of the eigenvalues and the shape of the continuous spectrum. Eigenvalues follow particular trajectories in the complex plane. Phase variations, on the other hand, influence only the phase of the

spectrum, not the location of the eigenvalues. One important observation, which may be beneficial for the design of data communication systems, is that the nonlinear spectrum of bandlimited pulses appears to be confined to a vertical strip in the complex plane with a width proportion to the signal bandwidth.

This chapter has only scratched the surface of a potentially rich research area. The development of efficient and robust numerical techniques suitable for various engineering applications of the nonlinear Fourier transform will require significant additional effort. A problem of particular interest is the development of a "fast" nonlinear Fourier transform method that would be the analog of the FFT.

Chapter 6

Discrete and Continuous Spectrum Modulation

> Few things are harder to put up with than a good example.
>
> Mark Twain

In the previous chapters it was suggested to exploit the integrability and use the nonlinear Fourier transform to transmit information over integrable communication channels, such as the optical fiber channel. In this transmission scheme information is encoded in the nonlinear Fourier transform of the signal, consisting of a discrete and a continuous spectral function. In this chapter, we provide further detail on the nonlinear spectrum modulation and determine gains achievable via modulating the spectral invariants of the nonlinear Schrödinger equation. Since the guard time between pulses can be large in a dispersive system, a large number of discrete spectral degrees of freedom should be eventually modulated. This corresponds to an implementation of the inverse nonlinear Fourier transform from a suitably chosen $2N$ complex discrete spectral degrees of freedom to an N-soliton pulse in time domain. We examine various ways to generate such N-solitons for $N \gg 1$ for nonlinear transmission over optical fiber networks. The resulting method compatible with the channel nonlinearity can have significant potential for long-haul fiber data transmission.

After describing the structure of the NFT transmitter, we give some examples showing how to use the nonlinear Fourier transform for data transmission, improving upon the classical soliton systems. The nonlinear Fourier transform of a signal with respect to a Lax operator consists of discrete and continuous spectral functions, in one-to-one correspondence with the signal [57]. In this chapter, we mostly consider the important

special case where the continuous spectrum is zero, examining data transmission schemes conceived by modulating the discrete spectrum.

An important step in developing a communication theory of waveform channels is to appropriately discretize the channel and identify a suitable set of degrees of freedom. The NFT provides a means to discretize integrable nonlinear dispersive waveform channels. The proposed nonlinear frequency-division multiplexing (NFDM) scheme can be considered as a generalization of orthogonal frequency-division multiplexing (OFDM) to integrable nonlinear dispersive communication channels. The advantages of NFDM arise from the following:

1. NFDM removes inter-channel interference (cross-talk) between users of a network sharing the same fiber channel;
2. NFDM removes inter-symbol interference (ISI) (intra-channel interactions) for each user;
3. spectral invariants as carriers of data are remarkably stable and noise-robust features of the NLS flow;
4. with NFDM, information in each channel of interest can be conveniently read anywhere in a network without knowledge of the distance or any information about other users.

Modulating the discrete spectrum corresponds to multisoliton transmission and detection. Fiber-optic communications using fundamental solitons (*i.e.*, 1-solitons) has faced numerous challenges in the past decades. The spectral efficiency of current soliton systems is typically quite low. Solitons interact with each other and in the presence of noise the system-reach is limited by the Gordon-Haus effect [69]. Despite solutions suggested to alleviate these limitations [69], the industry currently considers the use of more traditional pulse-shapes, such as sinc and raised-cosine pulses, which may not be particularly compatible with the structure of the nonlinear Schrödinger (NLS) equation [39], which governs pulse transmission in optical fibers.

This chapter improves upon the classical soliton systems by using multisoliton pulse shapes as carriers of data. While a fundamental soliton can be modulated, detected and analyzed in the time domain, multisolitons are best understood via their nonlinear spectrum in the complex plane. In this chapter, these pulses are obtained by implementing a simplified inverse NFT at the transmitter, and are demodulated at the receiver by recovering their spectral invariants using the forward NFT. Numerical methods for the calculation of the forward NFT are discussed in Chapter 5. Here we discuss the inverse NFT for the case that the continuous spectrum is zero.

It can be observed numerically that the discrete spectrum of a long random wavetrain,

e.g., that formed from a sinc basis, appears to contain most of the wavetrain energy. This implies that a sample function from a stationary bandlimited stochastic process $x(t)$, $-T/2 < t < T/2$ is approximately a multisoliton as $T \to \infty$. The fact that a large class of input signals of interest are indeed multisolitons implies that the desirable properties of such signals (or issues such as interactions and timing jitters) exist to the same extent for multisolitons and, in fact, are better understood in the context of the latter. Since parameters of a multisoliton naturally do not interact with one another, there is potentially a great advantage in directly modulating these parameters. Sending an N-soliton train for large N and detecting it at the receiver with the help of the NFT, the interaction of the individual components is no longer problematic.

There is a vast body of literature on solitons in mathematics, physics, and engineering; see, e.g., [9, 10, 69] and references therein. Classical, path-averaged and dispersion-managed fundamental 1-solitons are well-studied in fiber optics [69]. The existence of optical N-soliton pulses in optical fibers is also well known [69]. These results however mostly study the pulse propagation properties of an N-soliton pulse, are usually limited to small N (e.g. $N = 2, 3$), and consider specific isolated input signals (e.g., inputs of the form $A\text{sech}(t)$). Since N-solitons are naturally defined in the nonlinear spectral domain, in general they are best decoded with the help of the nonlinear Fourier transform. With the exception of few papers, we are aware of no other work using soliton trains or the nonlinear Fourier transform for data transmission. See [45] for an early interesting work on multi-solitons and the inverse scattering transform and [70] for a more recent (in progress) publication. The general viewpoint taken in this chapter is similar to that of [45].

6.1 Background

6.1.1 System Model

As before, we consider a standard single-mode (SSM) fiber with dispersion coefficient β_2, nonlinearity parameter γ and length $\mathcal{L}$. We thus consider again the normalized stochastic NLS equation (3.3) of Chapter 4, with parameters given in Table 2.1. We do not perform dispersion compensation, although the NLS equation is integrable for both positive and negative dispersions.

6.1.2 The Discrete Spectral Function

Here we briefly recall the definition of the discrete spectral function in the context of the nonlinear Schrödinger equation. We first consider the deterministic version of (3.3), where the noise is zero. Later, we will treat noise as a perturbation of the noise-free equation.

The nonlinear Fourier transform of a signal in (3.3) arises via spectral analysis of the operator

$$L = j \begin{pmatrix} \frac{\partial}{\partial t} & -q(t) \\ -q^*(t) & -\frac{\partial}{\partial t} \end{pmatrix} = j \left(D\Sigma_3 + Q \right), \tag{6.1}$$

where $D = \frac{\partial}{\partial t}$,

$$Q = \begin{pmatrix} 0 & -q \\ -q^* & 0 \end{pmatrix}, \text{ and } \Sigma_3 = \begin{pmatrix} 1 & 0 \\ 0 & -1 \end{pmatrix}.$$

Let $v(t, \lambda)$ be an eigenvector of L with eigenvalue λ. Following Chapter 4, the discrete spectral function of the signal propagating according to (3.3) is obtained by solving the the Zakharov-Shabat eigenproblem $Lv = \lambda v$, or equivalently

$$v_t = \begin{pmatrix} -j\lambda & q(t) \\ -q^*(t) & j\lambda \end{pmatrix} v, \quad v(-\infty, \lambda) = \begin{pmatrix} 1 \\ 0 \end{pmatrix} e^{-j\lambda t}, \tag{6.2}$$

where the initial condition was chosen based on the assumption that the signal $q(t)$ vanishes as $|t| \to \infty$. The system of ordinary differential equations (6.2) is solved from $t = -\infty$ to $t = +\infty$ to obtain $v(+\infty, \lambda)$. The nonlinear Fourier coefficients $a(\lambda)$ and $b(\lambda)$ are then defined as

$$\begin{aligned} a(\lambda) &= \lim_{t \to \infty} v_1(t, \lambda) e^{j\lambda t}, \\ b(\lambda) &= \lim_{t \to \infty} v_2(t, \lambda) e^{-j\lambda t}. \end{aligned}$$

Finally, the discrete spectral function is defined on the upper half complex plane $\mathbb{C}^+ = \{\lambda : \Im(\lambda) > 0\}$:

$$\tilde{q}(\lambda_j) = \frac{b(\lambda_j)}{a(\lambda_j)}, \; j = 1, \cdots, N,$$

where λ_j are the isolated zeros of $a(\lambda)$ in $\mathbb{C}^+$, *i.e.*, solutions of $a(\lambda_j) = 0$. The continuous spectral function is defined on the real axis $\lambda \in \mathbb{R}$ as $\hat{q}(\lambda) = b(\lambda)/a(\lambda)$.

6.2 Modulating the Discrete Spectrum

Let the nonlinear Fourier transform of the signal $q(t)$ be represented by

$$q(t) \longleftrightarrow (\hat{q}\,(\lambda), \tilde{q}(\lambda_j))\,.$$

When the continuous spectrum $\hat{q}(\lambda)$ is set to zero, the nonlinear Fourier transform consists only of discrete spectral functions $\tilde{q}(\lambda_j)$, *i.e.*, N complex numbers $\lambda_1, \ldots, \lambda_N$ in the upper half complex plane $\mathbb{C}^+$ together with the corresponding N complex spectral amplitudes $\tilde{q}(\lambda_1), \ldots, \tilde{q}(\lambda_N)$. In this case, the inverse nonlinear Fourier transform can be worked out in closed-form, giving rise to N-soliton pulses [71]. The resulting expressions, however, quickly get complicated when $N > 2$. As a consequence, analytical results tend to be limited to low-order solitons.

One can, however, create and modulate these multisolitons numerically. In this section we study various schemes for the implementation of the inverse NFT at the transmitter when $\hat{q} = 0$.

6.2.1 Discrete Spectrum Modulation by Solving the Riemann-Hilbert System

The inverse nonlinear Fourier transform can be obtained by solving a Riemann-Hilbert system of integro-algebraic equations or, alternatively, by solving the Gelfand-Levitan-Marchenko integral equations. Great simplifications occur when $\hat{q}(\lambda)$ is zero. For instance, in this case the integral terms in the Riemann-Hilbert system vanish and the integro-algebraic system of equations is reduced to an algebraic linear system, whose solution gives rise to N-soliton pulses.

Let $V(t, \lambda_j)$ and $\tilde{V}(t, \lambda_j^*)$ denote the scaled eigenvectors associated with λ_j and λ_j^* defined by their boundary conditions at $+\infty$ (they are denoted by V^1 and $\tilde{V}^1$ in Chapter 4). Setting the continuous spectral function $\hat{q}(\lambda)$ to zero in the Riemann-Hilbert system of Chapter 4, we obtain an algebraic system of equations

$$\begin{aligned}
\tilde{V}(t, \lambda_m^*) &= \begin{pmatrix} 1 \\ 0 \end{pmatrix} + \sum_{i=1}^{N} \frac{\tilde{q}(\lambda_i) e^{2j\lambda_i t} V(t, \lambda_i)}{\lambda_m^* - \lambda_i}, \\
V(t, \lambda_m) &= \begin{pmatrix} 0 \\ 1 \end{pmatrix} - \sum_{i=1}^{N} \frac{\tilde{q}^*(\lambda_i) e^{-2j\lambda_i^* t} \tilde{V}(t, \lambda_i^*)}{\lambda_m - \lambda_i^*}.
\end{aligned} \tag{6.3}$$

Define

$$\begin{aligned}
\mathbf{V}_{2\times N} &= \begin{pmatrix} V(t,\lambda_1) & V(t,\lambda_2) & \cdots & V(t,\lambda_N) \end{pmatrix}, \\
\tilde{\mathbf{V}}_{2\times N} &= \begin{pmatrix} \tilde{V}(t,\lambda_1^*) & \tilde{V}(t,\lambda_2^*) & \cdots & \tilde{V}(t,\lambda_N^*) \end{pmatrix}, \\
\mathbf{K}_{N\times N} &= \begin{pmatrix} \frac{\tilde{q}_1 e^{2j\lambda_1 t}}{\lambda_1^*-\lambda_1} & \frac{\tilde{q}_1 e^{2j\lambda_1 t}}{\lambda_2^*-\lambda_1} & \cdots & \frac{\tilde{q}_1 e^{2j\lambda_1 t}}{\lambda_N^*-\lambda_1} \\ \frac{\tilde{q}_2 e^{2j\lambda_2 t}}{\lambda_1^*-\lambda_2} & \frac{\tilde{q}_2 e^{2j\lambda_2 t}}{\lambda_2^*-\lambda_2} & \cdots & \frac{\tilde{q}_2 e^{2j\lambda_2 t}}{\lambda_N^*-\lambda_2} \\ \vdots & \vdots & \ddots & \vdots \\ \frac{\tilde{q}_N e^{2j\lambda_N t}}{\lambda_1^*-\lambda_N} & \frac{\tilde{q}_N e^{2j\lambda_N t}}{\lambda_2^*-\lambda_N} & \cdots & \frac{\tilde{q}_N e^{2j\lambda_N t}}{\lambda_N^*-\lambda_N} \end{pmatrix}, \\
(\mathbf{J}_1)_{2\times N} &= \begin{pmatrix} 1 & 1 & \cdots & 1 \\ 0 & 0 & \cdots & 0 \end{pmatrix}, \\
(\mathbf{J}_2)_{2\times N} &= \begin{pmatrix} 0 & 0 & \cdots & 0 \\ 1 & 1 & \cdots & 1 \end{pmatrix}, \\
\mathbf{e}_{N\times 1} &= \begin{pmatrix} 1 & 1 & \cdots & 1 \end{pmatrix}^T, \\
\mathbf{J}_{2\times N} &= \mathbf{J}_2 - \mathbf{J}_1\mathbf{K}^* = \begin{pmatrix} -\mathbf{e}^T\mathbf{K}^* \\ \mathbf{e} \end{pmatrix}, \\
\mathbf{F}_{N\times 1} &= \begin{pmatrix} \tilde{q}_1 e^{2j\lambda_1 t} & \tilde{q}_2 e^{2j\lambda_2 t} & \cdots & \tilde{q}_N e^{2j\lambda_N t} \end{pmatrix}^T.
\end{aligned}$$

In this notation, the algebraic equations (6.3) are simplified to

$$\tilde{\mathbf{V}} = \mathbf{J}_1 + \mathbf{V}\mathbf{K} \qquad \mathbf{V} = \mathbf{J}_2 - \tilde{\mathbf{V}}\mathbf{K}^*. \tag{6.4}$$

Note that $\mathbf{K}^*$ is the complex conjugate of $\mathbf{K}$ (not Hermitian). Therefore

$$\mathbf{V} = (\mathbf{J}_2 - \mathbf{J}_1\mathbf{K}^*)\,(\mathbf{I}_N + \mathbf{K}\mathbf{K}^*)^{-1} = \mathbf{J}\,(\mathbf{I}_N + \mathbf{K}\mathbf{K}^*)^{-1},$$

and $\mathbf{V}_2 = \mathbf{e}^T\,(\mathbf{I}_N + \mathbf{K}\mathbf{K}^*)^{-1}$. The N-soliton formula is given by

$$q(t) = -2j\mathbf{e}^T\,(\mathbf{I}_N + \mathbf{K}^*\mathbf{K})^{-1}\,\mathbf{F}^*. \tag{6.5}$$

The right hand side is a complex scalar and has to be evaluated for every t to determine samples of $q(t)$ everywhere.

Example 12. It is useful to see the (scaled) eigenvectors for a single soliton with spectrum

$\tilde{q}(\frac{\alpha+j\omega}{2}, z) = \tilde{q}_0 e^{2\alpha\omega z} e^{-j(\alpha^2-\omega^2)z}$ and the eigenvector

$$v(t, \lambda; z) = \frac{1}{2}\text{sech}[\omega(t - t_0)] \begin{pmatrix} e^{-j\Phi} \\ e^{\omega(t-t_0)} \end{pmatrix}, \tag{6.6}$$

where $\Phi = \alpha t + (\alpha^2 - \omega^2)z - \angle\tilde{q}_0 - \frac{\pi}{2}$ and $t_0 = \frac{1}{\omega}\log\frac{|\tilde{q}_0|}{\omega} - 2\alpha z$. The celebrated equation for the single soliton obtained from (6.5) is

$$q(t) = -j\omega e^{-j\alpha t} e^{-j\phi_0} \text{sech}\left(\omega(t \pm t_0)\right). \tag{6.7}$$

From the phase-symmetry of the NLS equation, the factor $-j$ in (6.7) can be dropped. The real and imaginary part of the eigenvalue are the frequency and amplitude of the soliton. Note that the discrete spectral amplitude $\tilde{q}(\lambda)$ is responsible for the phase and time-center of the soliton.

6.2.2 Discrete Spectrum Modulation via the Hirota Bilinearization Scheme

It is also possible to generate multisolitons without solving a Riemann-Hilbert system or directly using the NFT. A method which is particularly analytically insightful is the Hirota direct method [71]. It prescribes in some sense a *nonlinear superposition* for integrable equations.

The Hirota method for an integrable equation works by introducing a transformation of the dependent variable q to convert the original nonlinear equation to one or more *homogeneous bilinear* PDEs. For integrable equations, the nonlinearity usually is canceled or separated out. The resulting bilinear equations have sum of exponentials solutions. Computationally, bilinear equations are solved perturbatively by expanding the unknowns in terms of the powers of a small parameter ϵ. For integrable equations, this series truncates, rendering approximate solutions of various orders to be indeed exact. The bilinearization transformation has been found for many integrable equations [71], taking on similar forms that usually involve the derivatives of the logarithm of the transformed variable.

Let us substitute $q(t, z) = \frac{G(t,z)}{F(t,z)}$, where, without loss of generality, was may assume that $F(t, z)$ is real-valued. To keep track of the effect of nonlinearity, let us restore the nonlinearity parameter γ in the NLS equation. Plugging into the resulting NLS equation

$$jq_z = q_{tt} + 2\gamma|q|^2 q,$$

we get

$$\begin{aligned} j\left(G_z F - F G_z\right) &= F G_{tt} - 2F_t G_t - G F_{tt} \\ &\quad + 2\frac{F_t^2 + \gamma|G|^2}{F} G \\ &= F G_{tt} - 2F_t G_t + G F_{tt} \\ &\quad + 2\frac{F_t^2 + \gamma|G|^2 - F F_{tt}}{F} G, \end{aligned} \tag{6.8}$$

where we have added and subtracted $2GF_{tt}$. Equation (6.8) is trilinear in F and G. It can be made bilinear by setting

$$\begin{aligned} j(G_z F - G F_z) &= F G_{tt} - 2F_t G_t + G F_{tt}, \\ F_t^2 + \gamma|G|^2 - F F_{tt} &= 0. \end{aligned} \tag{6.9}$$

It is very convenient (though not necessary) to organize (6.9) using the Hirota D operator

$$D_t^n(a(t), b(t)) = \left(\frac{\partial}{\partial t} - \frac{\partial}{\partial t'}\right)^n a(t) b(t')|_{t=t'},$$

as

$$(jD_z + D_t^2) F G = 0, \tag{6.10}$$

$$D_t^2 F F = 2\gamma|G|^2. \tag{6.11}$$

Note that the D-operator acts on a pair of functions to produce another function. Note further that (6.10) does not depend on the nonlinearity parameter γ. That is to say, the nonlinearity has been separated from equation (6.10). For some other integrable equations (e.g., the Korteweg-de Vries equation for which one gets only one bilinear PDE), the nonlinearity parameter is in fact canceled completely.

Because (6.10) and (6.11) are homogeneous in the order of derivatives that occur in each term, exponential functions are candidate solutions. This suggests that F and G can be expanded (linearized) as

$$\begin{aligned} F(t,z) &= f^0(t,z) + \epsilon f^{(1)}(t,z) + \epsilon^2 f^{(2)}(t,z) + \cdots, \\ G(t,z) &= g^0(t,z) + \epsilon g^{(1)}(t,z) + \epsilon^2 g^{(2)}(t,z) + \cdots, \end{aligned}$$

for some small parameter ϵ. We then obtain

$$\begin{aligned}
FG &= f^{(0)}g^{(0)} + \epsilon\left(f^{(0)}g^{(1)} + f^{(1)}g^{(0)}\right) \\
&\quad + \epsilon^2\left(f^{(0)}g^{(2)} + f^{(1)}g^{(1)} + f^{(2)}g^{(0)}\right) + \cdots, \\
F^2 &= (f^{(0)})^2 + 2\epsilon f^{(0)}f^{(1)} + \epsilon^2\left(2f^{(0)}f^{(2)} + f^{(1)^2} + \right) + \cdots, \\
|G|^2 &= |g^{(0)}|^2 + \epsilon\left(g^{(0)}g^{(1)^*} + g^{(0)^*}g^{(1)}\right) \\
&\quad + \epsilon^2\left(g^{(0)}g^{(2)^*} + g^{(2)}g^{(0)^*} + |g^{(1)}|^2\right) + \cdots,
\end{aligned}$$

which can then be substituted into (6.10)-(6.11). Equating like powers of ϵ, one obtains bilinear equations for sub-components $f^{(i)}g^{(j)}$ using the D operator. As shown below (for the NLS), this series truncates for integrable systems and exact solutions of various finite order are obtained. To begin finding unknowns recursively, we can set initially $f^{(0)} = 1$.

The zero-order term in (6.10) gives $jg_z^{(0)} + g_{tt}^{(0)} = 0$ or $g^{(0)} = ce^{X_0}$, where $X_0 = 2j\lambda_0 t - k_0 z + \phi_0$. Here $\lambda_0 = (\alpha + j\omega)/2$ is the eigenvalue, $k_0 = 4j\lambda_0^2$, and ϕ_0 is a constant phase related to the spectral amplitude ($\phi_0 = \log(\tilde{q}/\omega^2)$). The zero-order term in (6.11) gives $c = 0$, and thus $g^{(0)} = 0$. At this stage, we can set the higher order terms to zero and get the trivial solution $q = 0$.

The ϵ term in (6.10) gives $g^{(1)} = \alpha e^{X_1}$. The corresponding term in (6.11) gives $2D_t^2 f^{(1)} = 0$, or $f^{(1)} = 0$.

The ϵ^2 term in (6.11) is $D_t^2 f^{(2)} = 2|g^{(1)}|^2$, or $2f_{tt}^{(2)} = 2|g^{(1)}|^2$. Trying $f^{(2)} = \alpha e^{X_1 + X_1^*}$, we get $\alpha = (\lambda - \lambda^*)^{-2}/4$. At this stage, we can set other higher order unknowns to zero and get the one soliton solution (choosing $\epsilon = 1$)

$$\begin{aligned}
F(t,z) &= 1 + \frac{1}{4(\lambda - \lambda^*)^2} e^{X_1 + X_1^*}, \\
G(t,z) &= e^{X_1}, \\
q(t,z) &= \left(e^{-X_1} + \frac{1}{4(\lambda - \lambda^*)^2} e^{X_1^*}\right)^{-1} \\
&= \omega \mathrm{sech}\left[\omega\left(t - 2\alpha z - t_0\right)\right] e^{j\alpha t - j(\alpha^2 - \omega^2)z}.
\end{aligned}$$

where $t_0 = \log(|\tilde{q}|/\omega)/\omega$.

We can continue to find higher order solitons. The ϵ^2 term in (6.10), *i.e.*, $(jD_z + D_t^2)1.g_2 = 0$, gives $g_2 = \alpha_2 e^{X_2}$.

In general, we have

$$F(t,z) = \sum_{\mathbf{m}=0,1} D_1(\mathbf{m}) \exp\left(\mathbf{m}\cdot\mathbf{x} + \mathbf{m}^T\Phi\mathbf{m}\right),$$
$$G(t,z) = \sum_{\mathbf{m}=0,1} D_2(\mathbf{m}) \exp\left(\mathbf{m}\cdot\mathbf{x} + \mathbf{m}^T\Phi\mathbf{m}\right),$$

where $\mathbf{m} = [m_i]_{i=1}^{2N}$, $m_i = \{0,1\}$, $\mathbf{x} = [X_i]_{i=1}^{2N}$, $X_i = \omega_i t - k_i z + X_i(0)$, $k_i = j\omega_i$, $X_{i+N} = X_i^*$, $\Phi = [\phi_{ij}]_{i,j=1}^{2N}$,

$$\phi_{ij} = \begin{cases} 0 & i \geq j \\ -2\log(\omega_i + \omega_j) & \substack{i=1,2,\cdots,N \\ j=N+1,N+2,\cdots,2N} \\ -2\log(\omega_i - \omega_j) & \substack{i=N+1,\cdots,2N \\ j=N+1,N+2,\cdots,2N} \end{cases}$$

and

$$D_1(\mathbf{m}) = \begin{cases} 1 & \sum_{i=1}^{N} m_i = \sum_{i=1}^{N} m_{i+N} \\ 0 & \text{otherwise} \end{cases},$$

$$D_2(\mathbf{m}) = \begin{cases} 1 & \sum_{i=1}^{N} m_i = 1 + \sum_{i=1}^{N} m_{i+N} \\ 0 & \text{otherwise} \end{cases}.$$

Note that, using the identity $\partial_{tt}\log F = \frac{F_{tt}F - F_t^2}{F^2}$, (6.11) is reduced to $|q(t,z)|^2 = \gamma^{-1}\partial_{tt}\log F$. The amplitude of q is thus captured by the real-valued function F, while G contains the phase of the signal.

Two important observations follow from the Hirota method. Firstly, multisoliton solutions of the NLS equation in the F,G domain ($q = G/F$) are the summation of exponentially decaying functions $\beta(\alpha)e^{-\alpha t}e^{j\omega t}$, each located at a frequency ω. That is to say, while plane waves $e^{j(\omega t - kz)}$ are the natural basis functions that solve linear PDEs, for integrable systems, exponentially decaying functions are suitable. The addition of the decaying factor $e^{-\alpha t}$ (when $t > 0$) is the point at which the nonlinear Fourier transform diverges from the linear Fourier transform [58]. Secondly, for each individual soliton term, the Hirota method adds two-way interaction terms, three-way interaction terms, etc., until all the interactions are accounted for. In this way, the interference between individual components is removed, as shown schematically in Fig. 6.1. Tables 6.1 and

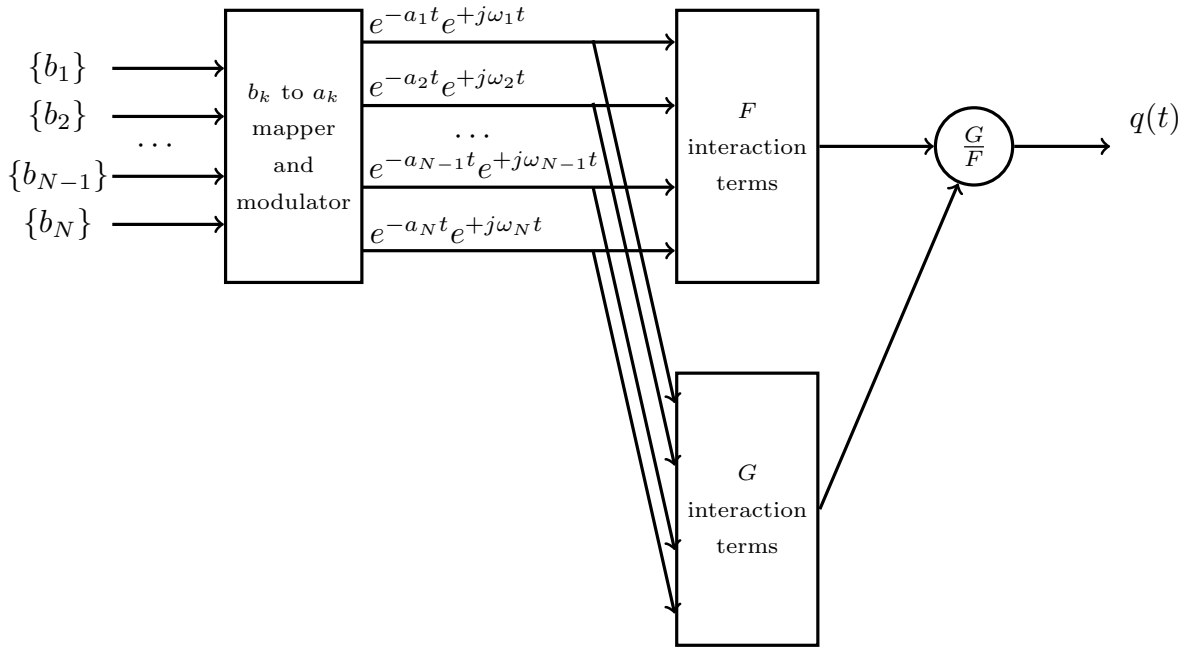

Figure 6.1: (a) Hirota modulator in creating N-solitons.

Table 6.1: The structure of the interaction terms in F.

	F
$N=1$	$1+e^{X_1+X_1^*}$
$N=2$	$1+e^{X_1+X_1^*}+e^{X_2+X_2^*}+e^{X_1+X_2^*}+e^{X_2+X_1^*}$
$N=3$	$1+e^{X_1+X_1^*}+e^{X_2+X_2^*}+e^{X_3+X_3^*}+\left(e^{X_1+X_2^*}+e^{X_2+X_1^*}+e^{X_1+X_3^*}+e^{X_3+X_1^*}+e^{X_2+X_3^*}+e^{X_3+X_2^*}\right)+$ $\left(e^{X_1+X_2+X_1^*+X_2^*}+e^{X_1+X_2+X_1^*+X_3^*}+e^{X_1+X_2+X_2^*+X_3^*}+e^{X_1+X_3+X_1^*+X_2^*}+e^{X_1+X_3+X_1^*+X_3^*}+e^{X_1+X_3+X_2^*+X_3^*}\right.$ $\left.+e^{X_2+X_3+X_1^*+X_3^*}+e^{X_2+X_3+X_1^*+X_2^*}+e^{X_2+X_3+X_2^*+X_3^*}\right)+e^{X_1+X_2+X_3+X_1^*+X_2^*+X_3^*}$

6.2 show these interaction terms for $N=1,2,3$.

While the Hirota method reveals important facts about the structure of the NLS equation, it may not be the best method to compute multisolitons numerically. There are $\binom{2N}{N}\sim 2^{2N}$ and $\binom{2N}{N+1}\sim 2^{2N}$ terms in F and G respectively, and unless one truncates the interaction terms at some step, the complexity quickly grows, making it hard to compute N-solitons for $N\geq 10$.

6.2.3 Recursive Discrete Spectrum Modulation Using Darboux Transformation

Multisoliton solutions of the NLS equation can be constructed recursively using the Darboux transformation (DT). The Darboux transformation, originally introduced in the

Table 6.2: The structure of the interaction terms in G.

	G
$N=1$	$e^{X_1}+e^{X_1^*}$
$N=2$	$e^{X_1}+e^{X_1^*}+e^{X_1+X_2+X_1^*}+e^{X_1+X_2+X_2^*}$
$N=3$	$e^{X_1}+e^{X_2}+e^{X_3}+\left(e^{X_1+X_2+X_1^*}+e^{X_1+X_2+X_2^*}+e^{X_1+X_2+X_3^*}+e^{X_1+X_3+X_1^*}+e^{X_1+X_3+X_2^*}+e^{X_1+X_3+X_3^*}\right.$ $\left.e^{X_2+X_3+X_1^*}+e^{X_2+X_3+X_2^*}+e^{X_2+X_3+X_3^*}\right)+\left(e^{X_1+X_2+X_3+X_1^*+X_2^*}+e^{X_1+X_2+X_3+X_2^*+X_3^*}+e^{X_1+X_2+X_3+X_2^*+X_3^*}\right)$

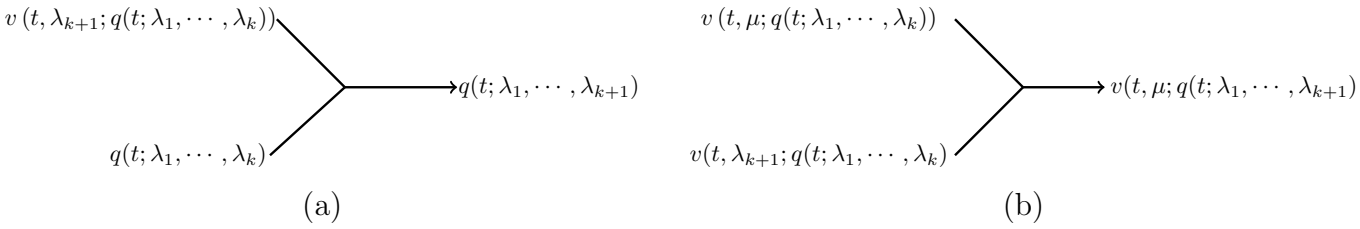

Figure 6.2: (a) Signal update. (b) Eigenvector update.

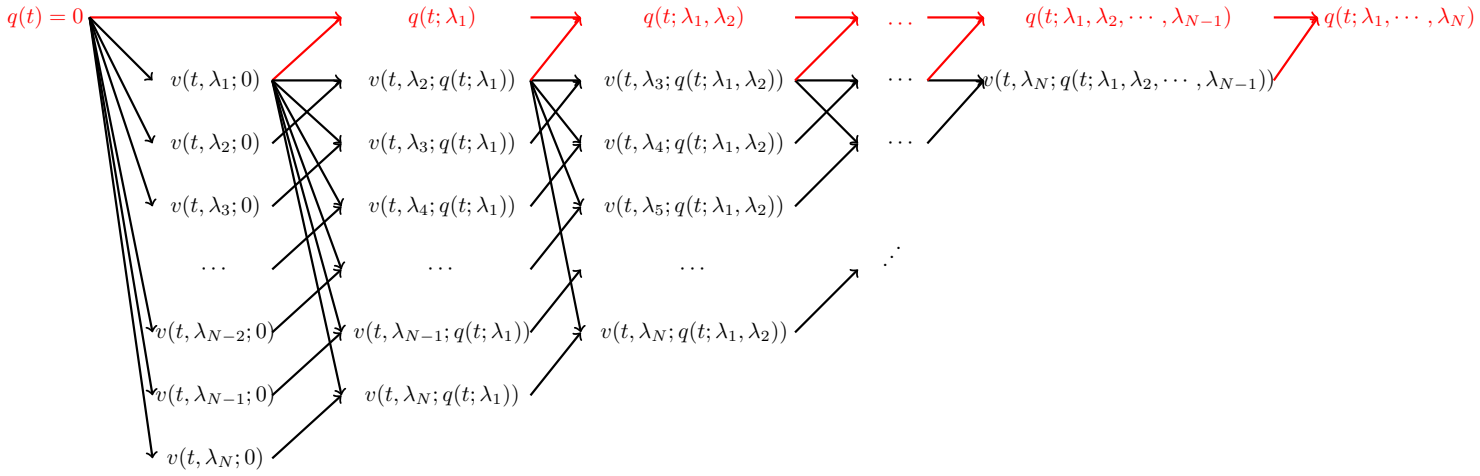

Figure 6.3: Darboux iterations for the construction of an N-soliton.

context of the Sturm-Liouville differential equations and later used in the nonlinear integrable systems, provides the possibility to construct from one solution of an integrable equation another solution [72]. For instance, one can start from the trivial solution $q=0$ of the NLS equation, and recursively obtain all higher order N-soliton solutions. This approach is particularly suited for numerical implementation.

Let $x(t,\lambda;q)$ denote a solution of the system

$$\begin{aligned} x_t &= P(\zeta,q)x, \\ x_z &= M(\zeta,q)x, \end{aligned} \tag{6.12}$$

for the signal q and complex number $\zeta = \lambda$ (not necessarily an eigenvalue of q), where the P and M operators were defined in Chapter 4. It is clear that $\tilde{x} = [x_2^*, -x_1^*]^T$ satisfies (6.12) for $\zeta \to \zeta^*$, and furthermore, by cross-elimination, q is a solution of the integrable equation underlying (6.12).

The statement of the Darboux theorem is as follows.

Theorem 11 (Darboux Transformation)**.** *Let $\phi(t, \lambda; q)$ be a known solution of* (6.12)*, and set $\Sigma = S\Gamma S^{-1}$, where $S = [\phi(t, \lambda), \tilde{\phi}(t, \lambda)]$ and $\Gamma = diag(\lambda, \lambda^*)$. If $v(t, \mu; q)$ satisfies* (6.12)*, then $u(t, \mu; \tilde{q})$ obtained from the Darboux transform*

$$u(t, \mu; \tilde{q}) = (\mu I - \Sigma)\, v(t, \mu; q), \tag{6.13}$$

satisfies (6.12) *for*

$$\tilde{q} = q - 2j(\lambda^* - \lambda)\frac{\phi_2^* \phi_1}{|\phi_1|^2 + |\phi_2|^2}. \tag{6.14}$$

Furthermore, both q and $\tilde{q}$ satisfy the integrable equation underlying the system (6.12)*.*

Proof. See Appendix D. □

The Darboux transform thus provides a means to construct from one solution of an integrable equation q, another solution $\tilde{q}$ according to (6.14). Theorem 11 immediately provides the following observations.

1. From $\phi(t, \lambda; q)$ and $v(t, \mu; q)$, we can obtain $u(t, \mu; \tilde{q})$ according to (6.13). If μ is an eigenvalue of q, then μ is an eigenvalue of $\tilde{q}$ as well. Furthermore, since $u(t, \mu = \lambda; \tilde{q}) = 0$, λ is also an eigenvalue of $\tilde{q}$. It follows that the eigenvalues of $\tilde{q}$ are the eigenvalues of q together with λ, *i.e.*, λ is added to the eigenvalues of q.
2. $\tilde{q}$ is a new solution of the NLS equation obtained from q, and $u(t, \mu; \tilde{q})$ is one of its eigenvectors.

These observations suggest a two-step iterative algorithm to generate N-solitons pulses, as illustrated in the Figs. 6.2-6.3. Denote a k-soliton pulse with eigenvalues $\lambda_1, \lambda_2, \cdots, \lambda_k$ by $q(t; \lambda_1, \lambda_2, \cdots, \lambda_k) := q^{(k)}$.

Eigenvector update:

$$\begin{aligned} v_1(t, \lambda_j, q^{(k+1)}) = -\Big\{ &(\lambda_j - \lambda_{k+1})|v_1(t, \lambda_{k+1}, q^{(k)})|^2 + (\lambda_j - \lambda_{k+1}^*)|v_2(t, \lambda_{k+1}, q^{(k)})|^2 \Big\} v_1(t, \lambda_j, q^{(k)}) \\ &+ (\lambda_{k+1}^* - \lambda_{k+1}) v_1(t, \lambda_{k+1}, q^{(k)}) v_2^*(t, \lambda_{k+1}, q^{(k)}) v_2(t, \lambda_j, q^{(k)}), \end{aligned} \tag{6.15}$$

$$v_2(t,\lambda_j,q^{(k+1)}) = -\Big\{(\lambda_j-\lambda_{k+1}^*)|v_1(t,\lambda_{k+1},q^{(k)})|^2 + (\lambda_j-\lambda_{k+1})|v_2(t,\lambda_{k+1},q^{(k)})|^2\Big\}v_2(t,\lambda_j,q^{(k+1)})$$
$$-(\lambda_{k+1}-\lambda_{k+1}^*)v_1^*(t,\lambda_{k+1},q^{(k)})v_2(t,\lambda_{k+1},q^{(k)})v_1(t,\lambda_j,q^{(k)}), \tag{6.16}$$

for $k = 1,\cdots,N$ and $j = k,\cdots,N$.

Signal update:

$$q^{(k+1)} = q^{(k)} - 2j(\lambda_{k+1}^*-\lambda_{k+1}) \times \frac{v_1(t,\lambda_{k+1},q^{(k)})v_2^*(t,\lambda_{k+1},q^{(k)})}{||v(t,\lambda_{k+1},q^{(k)})||^2}. \tag{6.17}$$

Note that $v(t,\lambda_j,q^{(k+1)})$ can also be obtained directly by solving the Zakharov-Shabat system for $q^{(k+1)}$. It is however more efficient to update the required eigenvector from (6.15)-(6.16). N-solitons can be constructed from the trivial solution $q = 0$. The first column of Fig. 6.3 is chosen to be the (non-canonical eigenvector) $v(t,\lambda_j) = [Ae^{-j\lambda_j t}, Be^{j\lambda_j t}]^T$ and iterations are initialized from these vectors to find all $k-$solitons, $k \leq N$. The coefficients A and B control the spectral amplitudes and the shape of the pulses. For a single soliton $A = \exp(j\angle\tilde{q})$ and $B = |\tilde{q}|$.

6.3 Evolution of the Discrete Spectrum

Recall that the imaginary and real parts of the eigenvalues correspond, respectively, to soliton amplitude and frequency. If the real part of the eigenvalue $\Re\lambda$ is zero, the N-soliton does not travel (with respect to a traveling observer) while propagating. The individual components of an N-soliton pulse with non-zero frequencies travel in retarded time with speeds proportional to $\Re\lambda_i$ (frequency).

The manner of N-soliton propagation thus depends on the choice of the eigenvalues. An N-soliton signal is essentially composed of N single solitons coupled together, similar to a molecule which groups a number of atoms. If the discrete spectrum of the signal lies completely on the imaginary axis, the pulse preserves its shape or periodically oscillates during the evolution. If the eigenvalues have non-zero real parts, various components travel at different speeds and eventually when $z \to \infty$ the N-soliton decomposes into N separate solitons

$$q(t,z) \to \sum \omega_i e^{-j(\alpha_i t + k_i z + \phi_0)}\text{sech}(\omega_i(t - t_i - \alpha_i z)),$$

where $\lambda = (\alpha_i + j\omega_i)/2$ is the eigenvalue, $k_i = (\alpha_i^2 - \omega_i^2)/2$, and t_i is the time center. This breakdown of a signal to its individual components, while best observed in the case of multisolitons, is simply a result of group velocity dispersion and exists for all pulses

similarly. The extent of breakdown and shift depends on a variety of factors, such as launch power, length of the fiber, number of mass points, fiber dispersion, and dispersion-management schemes. If dispersion is not managed, the effects of pulse broadening must be carefully considered.

6.4 Demodulating the Discrete Spectrum

To demodulate a multisoliton pulse, the eigenproblem (6.2) needs to be solved. There is limited work in the mathematical literature concerning the numerical solution of the Zakharov-Shabat spectral problem (6.2). In Chapter 5, we have suggested methods by which the nonlinear Fourier transform of a signal may be computed numerically. In particular, here we use the layer-peeling and Ablowitz-Ladik methods described in Chapter 5 to estimate the discrete spectrum.

Recall that the layer-peeling method works by approximating $q(t)$ as a piece-wise constant signal and using the layer-peeling property of the nonlinear Fourier transform mentioned in [37]. Let $q(t)$ be defined in the interval $[T_1, T_2]$. The layer-peeling iteration is given as

$$\begin{aligned} a[k+1] &= a[k]x[k] - b[k]\bar{y}[k], \\ b[k+1] &= a[k]y[k] + b[k]\bar{x}[k]. \end{aligned}$$

where

$$x[k] = \left(\cos(\epsilon D) - j\frac{\lambda}{D}\sin(\epsilon D)\right)e^{j\lambda\epsilon}, \tag{6.18}$$

$$y[k] = \frac{-q_k^*}{D}\sin(D\epsilon)e^{-2j\lambda t}, \tag{6.19}$$

and $\bar{x}[k](\lambda) = x^*[k](\lambda^*)$, $\bar{y}[k](\lambda) = y^*[k](\lambda^*)$, $D = \sqrt{\lambda^2 + |q[k]|^2}$.

The layer-peeling scheme can be used along with the Newton-Raphson method to search for the eigenvalues of $q(t)$ in the upper-half complex plane $\mathbb{C}^+$. The reader is referred to Chapter 5 for further details.

6.5 Statistics of the Spectral Data

Unfortunately, the generalized NLS equation that includes an additive space-time noise term is generally not integrable. The addition of noise also disturbs the vanishing or

periodic boundary conditions usually assumed in the development of the nonlinear Fourier transform. However, since the amplified spontaneous emission noise in optical fibers is quite small compared to the signal level for SNR >10 dB , one can treat the effects of noise as a small perturbation of the signal, and still safely use the NFT.

Calculation of the exact statistics can be quite cumbersome. This is essentially because the NLS equation with additive noise, unlike the noise-free equation, has little or no structure, giving rise to complicated variational representations for the noise statistics. Even if such exact results are available, they are poorly suited for data communications studies. One can however approximate or bound these statistics using a perturbation theory, or simulate them on a computer.

Remark 11. In the special case that the noise is real and multiplicative and only a function of distance, *i.e.*, the signal is multiplied by a real-valued multiplicative random variable at each (discrete) point in the fiber, the resulting equation is still integrable and the theory of the nonlinear Fourier transform can be used with no approximation. We conjecture that exact statistics of the spectral data can be found in this case.

Remark 12. Note that the generalized NLS equation that includes a loss term is also not integrable. Note, however, that loss is traded with the distributed Raman amplification noise, and once including perturbations resulting from the noise, the effect of the fiber loss can approximately be ignored (though the nature of these two perturbations are different).

Noise can be added in a discrete or continuous manner. In the case of the discrete (lumped) noise addition resulting from the erbium-doped fiber amplifiers, the randomness is on initial conditions and, assuming a finite time interval, the NFT is exact whether the input pulse is deterministic or random. We refer to this type of the stochasticity where the randomness comes from the initial conditions and not the medium as the *homogeneous randomness*.

If noise is injected continuously throughout the fiber as a result of distributed Raman amplification (DRA), one has a *non-homogeneous noise*. Here we can discretize the fiber into a large number of small fiber segments and add lumped noise at the end of each segment. The injected noises act as random perturbations of the initial data at the input of each segment. The DRA can thus be approximately treated similar to the lumped noise case. This is justified in the view that when simulating the stochastic NLS equation, the step size in the split-step Fourier method can be as large as the distance between EDFA amplifiers, *i.e.*, the dynamic of the pulse propagation under DRA and a large number of EDFAs is about the same. Other non-homogeneous distortions can also be treated similarly.

In this section, we study the effect of the these two types of perturbations on the NFDM channel model. We assume that the noise vanishes, or is negligible, as $|t| \to \infty$ and has a finite energy such that the signal remains absolutely integrable almost surely.

6.5.1 Homogeneous Noise

The NFT arises in the spectral analysis of the L operator (6.1). We can easily analyze the perturbations of the eigenvalues λ as a result of the changes in the signal $q(t)$.

Let us denote the noise-free nonlinear Fourier transform of $q(t)$ by $(\hat{q}(\lambda), \tilde{q}(\lambda_j))$. As the signal $q(t)$ is perturbed to $q(t) + \epsilon N(t)$ for some small parameter ϵ and (normalize) noise process $N(t)$, the (discrete) eigenvalues and spectral amplitudes slightly deviate from their nominal values. Separating the signal and noise terms, the perturbed v and λ satisfy

$$(L + \epsilon R)v = \lambda v, \qquad R = \begin{pmatrix} 0 & N \\ -N^* & 0 \end{pmatrix}, \tag{6.20}$$

where R is the noise matrix. The study of the stochastic nonlinear Fourier transform is thus a perturbation theory of the non-self-adjoint operator (6.20). Here we need to measure the variation of the eigenvalues and eigenvectors as the operator L is changed from L to $L + \epsilon R$.

Perturbation theory of Hermitian operators is well-studied in the quantum mechanics (*e.g.*, by E. Schrödinger). The Zakharov-Shabat operator (6.20) is however non-self-adjoint. Unfortunately most useful properties of the self-adjoint operators do not carry to the non-self-adjoint operators, particularly due to the lack of a complete orthonormal basis. Thus the perturbation of the spectral data for the NLS equation is more difficult than that for the KdV equation. In both cases (deterministic) perturbation analysis of the IST already exists in the literature [73–76]. These are however mostly deterministic results and the distribution of the scattering data is still lacking in the literature. A very interesting work is [77] in which authors calculate the distribution of the spectral data for the special case that channel has no noise and the input is a white Gaussian stochastic process.

Since in this Section we are only interested in finding the noise in eigenvalues (and not discrete spectral amplitudes whose perturbation analysis can be complicated), a simple small noise approximation, given below, is sufficient.

For the non-self adjoint operators L, the orthogonality that we require is between the space of left and right eigenvectors of L associated with distinct eigenvalues; that is to

say, between eigenvectors of L associated with λ and eigenvectors of the adjoint operator L^* associated with $\mu \neq \lambda^*$. Let us equip the space of eigenvectors with the usual L^2 inner product

$$\langle u, v \rangle = \int_{-\infty}^{\infty} (u_1 v_1^* + u_2 v_2^*)\, dt. \tag{6.21}$$

It can be easily verified that the operator $\Sigma_3 L$ is self-adjoint, *i.e.*, $\langle u, \Sigma_3 L v \rangle = \langle \Sigma_3 L u, v \rangle$, where $\Sigma_3 = \text{diag}(1, -1)$ is the Pauli matrix.

We use a *small noise approximation* method, expanding unknown variables in noise level ϵ [24] as

$$v(t) = v^{(0)}(t) + \epsilon v^{(1)}(t) + \epsilon^2 v^{(2)}(t) + \cdots \tag{6.22}$$

$$\lambda = \lambda^{(0)} + \epsilon \lambda^{(1)} + \epsilon^2 \lambda^{(2)} + \cdots . \tag{6.23}$$

We assume these variables are analytic functions of ϵ so that above series are convergent (without the need to renormalize [24]). Plugging (6.22)-(6.23) into (6.20) and equating the like powers of ϵ, we obtain

$$Lv^{(0)} = \lambda^{(0)} v^{(0)}, \tag{6.24}$$

$$(L - \lambda^{(0)}) v^{(1)} = -(R - \lambda^{(1)}) v^{(0)}, \tag{6.25}$$

$$(L - \lambda^{(0)}) v^{(2)} = -(R - \lambda^{(1)}) v^{(1)} + \lambda^{(2)} v^{(0)}, \tag{6.26}$$

$$\vdots\ .$$

The first term gives that $v^{(0)}$ and $\lambda^{(0)}$ are eigenvalue and eigenvector of the (nominal) operator L. To eliminate v_1 from the second equation, we take the inner product on both sides of (6.24) with some vector u; the left hand side of the resulting expression is

$$\langle u, (L - \lambda^{(0)}) v^{(1)} \rangle = \langle (L - \lambda^{(0)})^* u, v^{(1)} \rangle = \langle (L^* - \lambda^{(0)*}) u, v^{(1)} \rangle. \tag{6.27}$$

To have (6.27) vanish, we can choose u to be an eigenvector of the adjoint operator L^* associated with an eigenvalue $\mu = \lambda^{(0)*}$, *i.e.*, $(L^* - \lambda^{(0)*}) u = 0$. Since $L^*(q) = L(-q)$, if $Lv = \lambda^{(0)} v$, it can be verified that $L^* u = \lambda^{(0)} u$ for $u = [v_1, -v_2] = \Sigma_3 v$. Choosing $u := u^{(0)} = \Sigma_3 v^{(0)}(t, \lambda^*)$

$$\lambda^{(1)} = \frac{\langle u^{(0)}, R v^{(0)} \rangle}{\langle u^{(0)}, v^{(0)} \rangle}.$$

Using similar calculations we obtain $\lambda^{(2)}$

$$\lambda^{(2)} = \frac{\langle u, Rv^{(1)}\rangle}{\langle u, v^{(0)}\rangle} - \lambda^{(1)}\frac{\langle u, v^{(1)}\rangle}{\langle u, v^{(0)}\rangle},$$

and so on.

To summarize, the fluctuations of discrete eigenvalues is given by

$$\hat{\lambda}_n = \lambda_n + \epsilon\frac{\langle u_n, Rv_n\rangle}{\langle u_n, v_n\rangle} + O(\epsilon^2), \quad n = 1, 2, \cdots, N.$$

It follows that the perturbation of the eigenvalues is distributed, to the first order, according to a zero mean complex Gaussian distribution.

To find higher order fluctuations of eigenvalues, $v^{(k)}$, $k \geq 1$, need to be found as well. This is done by expanding $v^{(k)}$ in the eigenspace of L associated with all eigenvalues and using the orthogonality of left and right eigenspaces. Since the operator L is not self-adjoint under the $L^2(\mathbb{R})$ inner product, this calculation is a little more elaborate than the case that L is self-adjoint (where a complete orthonormal basis exists).

6.5.2 Non-homogeneous Noise and Other Perturbations

Consider the perturbed NLS equation

$$jQ_z = Q_{tt} + 2|Q|^2Q + \epsilon V(t, z), \tag{6.28}$$

where ϵ is a small parameter (noise level), and $V(t, z)$ represents the combined effects of the signal loss and the distributed noise. Here we will make the *a priori* assumption that sample paths of the stochastic process possess sufficient regularity and we do not discuss the well-posedness properties of (6.28).

Let us represent (6.28) with the same L and M of the noise-free equation and now let λ vary with time. The equality of mixed derivatives $v_{tz} = v_{zt}$ gives

$$\begin{pmatrix} -j\lambda_z & Q_z + jQ_{tt} + 2j|Q|^2Q \\ -Q_z^* + jQ_{tt}^* + 2j|Q|^2Q^* & j\lambda_z \end{pmatrix} v = 0.$$

This, upon re-arranging and using (6.28), simplifies to

$$\lambda_z v = \epsilon\bar{R}v, \quad \bar{R} = -R.$$

Note that, as before, we do not have $v(t, z)$ a priori because, according to (6.1), it

depends on the noisy signal $q(t,z)$ and $\lambda(z)$, both of which are unknown. However, if the noise level ϵ is small, we can expand $v(t,z)$ and λ in powers of ϵ as (6.22) and (6.23) to obtain $(\lambda^{(0)})_z = 0$ and $\bar{R}v^{(0)} = (\lambda^{(1)})_z v^{(0)}$ (*i.e.*, $(\lambda^{(1)})_z$ appears as a time-independent eigenvalue of $\bar{R}(t)$). Taking the inner-product with $u^{(0)} = \Sigma_3 v^{(0)}(t,\lambda^*)$ on both sides of $\bar{R}v^{(0)} = (\lambda^{(1)})_z v^{(0)}$, we obtain the first order variation of eigenvalues

$$(\lambda_1)_z = \frac{\langle u^{(0)}, \bar{R}v^{(0)}\rangle}{\langle u^{(0)}, v^{(0)}\rangle}. \tag{6.29}$$

It follows from (6.29) that the distribution of deviation of the eigenvalues is approximately a zero-mean conditionally Gaussian random variable. The variance of this random variable is signal dependent, and although eigenvectors of an N-soliton can be represented as a series from Darboux transform, it is best calculated numerically if $N \geq 2$.

Example 13. Consider the single soliton of Example 12. It can be verified that $\langle \Sigma_3 v(t,\lambda^*), v(t,\lambda)\rangle = \frac{\omega}{2}(1+\frac{\omega^2}{|\tilde{q}|^2}) = \frac{1}{\omega}$, where we assumed $|\tilde{q}| = \omega$ so that the soliton is centered at $t_0 = 0$. Furthermore

$$\begin{aligned}
&\langle v(t,\lambda^*), \bar{R}v(t,\lambda)\rangle = -\int (v_1(t,\lambda^*)v_2^*(t,\lambda)N^* + v_2(t,\lambda^*)v_1^*(t,\lambda)N)\,\mathrm{d}t \\
&= -\int \frac{1}{2}\mathrm{sech}(\omega t)(v_2(t,\lambda^*) + v_2^*(t,\lambda))\Re\bar{N} + j\int \frac{1}{2}\mathrm{sech}(\omega t)(v_2(t,\lambda^*) - v_2^*(t,\lambda))\Im\bar{N}\mathrm{d}t \\
&= -\frac{1}{2}\int \mathrm{sech}(\omega t)\Re\bar{N}\mathrm{d}t - \frac{j}{2}\int \mathrm{sech}(\omega t)\tanh(\omega t)\Im\bar{N}\mathrm{d}t,
\end{aligned}$$

where $\bar{N} = N\exp(j\Phi)$ has the same statistics as N. It follows that

$$\alpha_z = -\int \mathrm{sech}(\tau)\Re\bar{N}\mathrm{d}\tau, \tag{6.30}$$

$$\omega_z = -\int \mathrm{sech}(\tau)\tanh(\tau)\Im\bar{N}\mathrm{d}\tau. \tag{6.31}$$

The Gordon-Haus effect easily follows from the α_z equation. Note that in fiber optics noise is added to the signal, *i.e.*, $V \to jV$.

6.6 Spectral Efficiencies Achievable by Modulating the Discrete Spectrum

We turn now to the numerical study of N-solition data transmission schemes, providing simulation results to quantify the gains that are achievable. The baseline system is assumed to be a classical on-off keying soliton transmission in which in any symbol period

T_s either zero or a fundamental soliton is sent. To improve upon the classical binary soliton transmission system, two or more discrete mass points are packed in a time interval which an on-off keying soliton system occupies, while keeping the bandwidth requirements same. The location of the eigenvalues and the values of the discrete spectral amplitudes can be jointly modulated for this purpose. We shall see that the effective useful region in the upper-half plane to exploit the potential of discrete eigenvalue modulation is limited by a variety of factors. As noted earlier, in this chapter, we discuss modulating the continuous spectrum just briefly.

Since modulating the nonlinear spectrum translates to pulses with variable width, power, and bandwidth, we take the average time, average power, and the maximum bandwidth to properly convert bits per symbol to bits/s and bits/sec/Hz. We start by continuously modulating one eigenvalue in a given region (*i.e.*, a classical soliton with amplitude and phase drawn from a multiple ring constellation). We next consider multisoliton systems with a number of constellations on eigenvalues and discrete spectral amplitudes. We compare the achievable spectral efficiencies (and in some cases bit error rates) with those of an on-off-keyed single-soliton communication system.

Throughout this section, we consider a 2000 km single mode single channel optical link in which fiber loss is perfectly compensated in a distributed manner using the Raman amplification. Dispersion compensation is not applied, as it is an advantage of the method that no dispersion management or nonlinearity compensation is required. We let pulses interact naturally, as atoms in a molecule, and perform all operations on such groups. The method however works for dispersion managed fibers as well, and in general with any operation that does not change integrability. Typical simulation parameters are given in Table 2.1.

6.6.1 Spectral Efficiency of 1-Soliton Systems

Soliton transmission systems typically do not have high spectral efficiencies. This is because the amplitude and the width of a single soliton are inversely related, and hence they require a lot of time or bandwidth per degree of freedom provided. Errors in a soliton transmission system occur either because of the Gordon-Haus timing jitter effect (which is the primary source of the error if not managed) or amplitude (energy) fluctuations. Following the Galilean invariance [9], the Gordon-Haus effect exists for all kind of pulses to the same extent and is not specific to solitons. This classical effect can be suppressed with the help of the suitably designed filters, and as a result is ignored in this section.

Let first consider a classical soliton system with only one eigenvalue $\lambda = (\alpha + j\omega)/2$.

The joint density $f_{A,\Omega}(\alpha,\omega)$ can be obtained from (6.30)-(6.31) or just directly by extracting the dynamics of α and ω from the stochastic NLS equation, resulting to a pair of coupled stochastic ordinary differential equations. For instance, multiplying the stochastic NLS equation (6.28) by q^*, subtracting from its conjugate, integrating over time, and using the integration by parts in the dispersion term, we get

$$\frac{\partial E}{\partial z} = 2\Im \int_{-\infty}^{\infty} q(\tau,z)Z(\tau,z)\mathrm{d}\tau, \tag{6.32}$$

where $E(z) = \int |q(\tau,z)|^2\mathrm{d}\tau$ is the energy, and $Z = -N^*$ is a noise process similar to N. Thus energy fluctuations is a signal-dependent Gaussian random variable $E(z) \sim \mathcal{N}_{\mathbb{R}}\big(E(0), \sigma^2 \int E(z)\mathrm{d}z\big) \approx \mathcal{N}_{\mathbb{R}}(E(0), \sigma^2 z E(0))$. Ignoring the energy of the continuous spectrum, we have $E \approx 2\omega$ and

$$\omega(z) = \omega(0) + \sigma\sqrt{\frac{z\omega(0)}{2}}\mathcal{N}_{\mathbb{R}}(0,1)\,. \tag{6.33}$$

The conditional probability density function (PDF) $f_{\Omega|\Omega_0}(\omega|\omega_0)$ is easily derived

$$f(\omega|\omega_0) = \frac{1}{\sqrt{\pi\sigma^2 z\omega_0}} e^{-\frac{(\omega-\omega_0)^2}{\sigma^2 z\omega_0}}. \tag{6.34}$$

The the PDF of $r = \sqrt{\omega(z)}$ is approximately a Rician distribution

$$\begin{aligned} f(r|r_0) &= \frac{r}{\sigma^2} e^{-\frac{r^2+r_0^2}{2\sigma^2}} I_0\Big(\frac{rr_0}{\sigma^2}\Big) \\ &\approx \frac{1}{\sqrt{2\pi\sigma^2}} e^{-\frac{(r-r_0)^2}{2\sigma^2}}, \quad r, r_0 \geq \sigma, \end{aligned} \tag{6.35}$$

which is signal-independent in high SNRs.

Note that we are interpreting the stochastic NLS equation as a soliton-bearing system in the limit that noise is small. A soliton of the deterministic NLS equation launched into a system described by the stochastic NLS equation would have, of course, a growing continuous spectrum too and, in addition, a very small chance of creating additional solitons out of noise at some distance, or collapsing into the real axis in the λ plane. All these effects are negligible if the energy of the launched soliton is large enough and the propagation distance is not exceedingly long. where the Gaussian approximation is valid in the limit $\mathcal{P} \gg \sigma^2$. The non-Gaussian part of the PDF could also be taken into account, however this would be of little value in the evaluation of the capacity as it is quite negligible and complicates mutual information optimization.

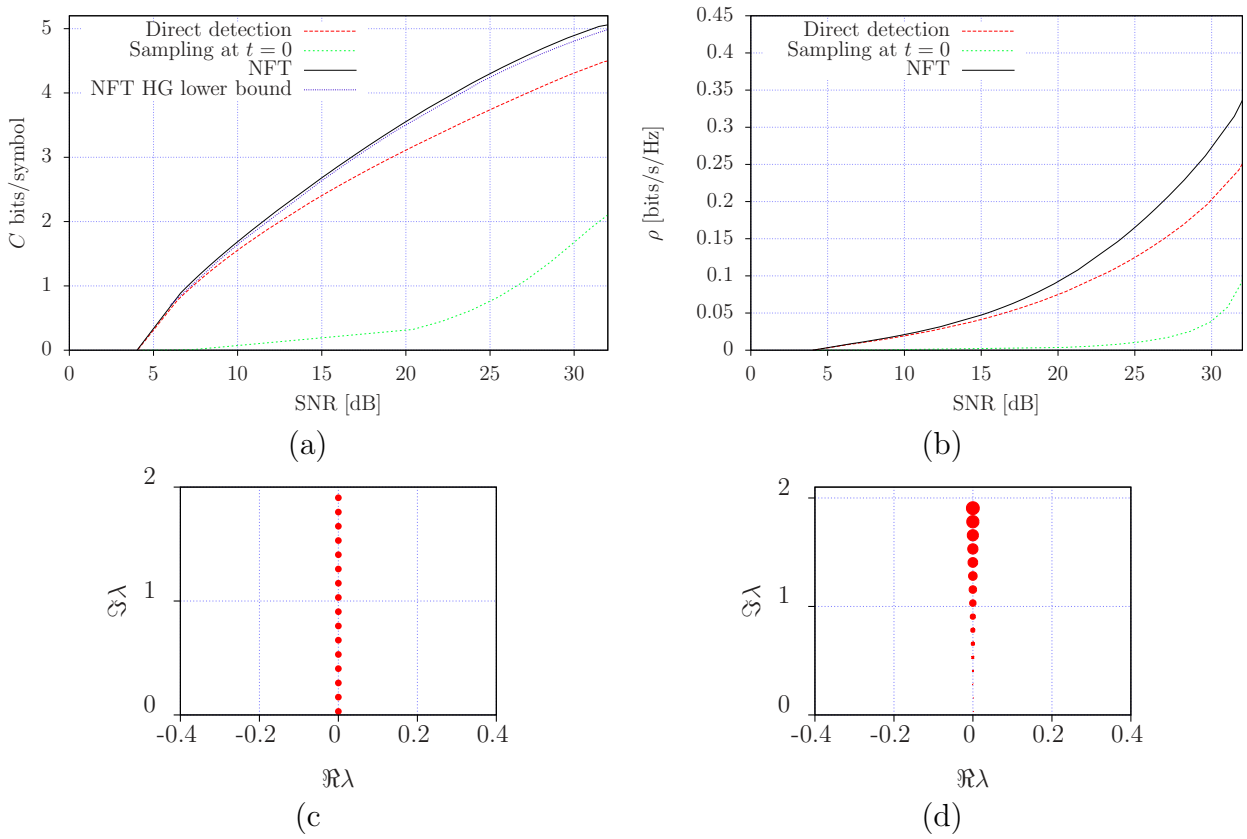

Figure 6.4: (a) Capacity (bits/symbol) and, (b) spectral efficiency (bits/s/Hz), of soliton systems using direct detection, sampling, and the NFT methods. (c) Eigenvalue constellation. (d) Noise balls at the receiver in the NFT approach. The signal-dependency of the noise balls can be seen *e.g.*, through (6.33).

In [29] we have shown that a half-Gaussian density

$$f(\omega_0) = \frac{1}{\sqrt{2\pi P}} e^{-\frac{\omega_0^2}{2P}}, \quad \omega_0 \geq 0,$$

gives the asymptotic capacity for (6.34)

$$C \sim \frac{1}{2} \log(1 + \text{SNR }) - \frac{1}{2},$$

where $\text{SNR } = \frac{\mathcal{P}}{\sigma^2}$.

Translating capacity in bits/symbol to the spectral efficiency in bits/s/Hz depends on the receiver architecture. Assuming that the receiver is able to decode pulses with

variable widths, the spectral efficiency $\rho(\mathcal{P})$ is obtained by

$$\begin{aligned} \rho(\mathcal{P}) &= \max_{\substack{f(\omega_0) \\ \omega_0 \in S}} \frac{1}{\mathsf{E}T(\omega_0)BW(S)} I(\omega;\omega_0), \\ \mathsf{E}P(\omega_0) &\leq \mathcal{P}, \end{aligned} \tag{6.36}$$

where $T(\omega_0)$ and $P(\omega_0)$ are the width and the power of a single soliton with amplitude ω_0 and $BW(S) = \max_{\omega_0 \in S} BW(\omega_0)$ is the maximum passband bandwidth that the signal set S requires for transmission (set by the $\min S$). For a one soliton signal, we have approximately

$$T(\omega_0) = \frac{7}{\omega_0}, \quad P(\omega_0) = \frac{\omega_0^2}{6.2}, \quad BW(\omega_0) = 0.95\omega_0, \tag{6.37}$$

where the width $T(\omega_0)$ includes a guard time, four times the full width at half maximum power FWHM, so as to minimize the intra-channel interactions.

Using (6.37), the maximum spectral efficiency of a baseline on-off keying system is obtained to be about $\rho \approx 0.15$ bits/s/Hz at the average power $P_0 = 0.16$ mW. Note that the spectral efficiency problem (6.36) is not convex and hence finding the global optimum may prove to be challenging. Here we simply optimize mutual information and scale it by $\mathsf{E}T(\omega) \times BW_{\max}(S)$ evaluated at the capacity achieving input distribution.

Fig. 6.4 shows that capacity and the spectral efficiency of a 1-soliton system with amplitude modulation using various detection methods. Note that since we do not solve the optimization problem (6.36), the spectral efficiencies shown in the Fig. 6.4(b) are only lower bounds to the actual achievable values. Fig. 6.4(c)-(d) shows the transmitted constellation and the noise balls at the receiver. The actual number of signal levels is 64 in the simulations. Calculation of the approximate capacity is performed using the Arimoto-Blahut algorithm and is confirmed by numerical interior point optimization.

6.6.2 Spectral Efficiency of 2-Soliton Systems

To illustrate how the NFT method works, we start off by a simple example.

Modulating Eigenvalues

Consider the following signal set with 4 elements.

$$\begin{aligned} S_1 &: 0, \\ S_2 &: \tilde{q}(0.5j) = 1, \\ S_3 &: \tilde{q}(0.25j) = 0.5, \\ S_4 &: \tilde{q}(0.25j, 0.5j) = (1, 1). \end{aligned} \tag{6.38}$$

We compare this with a standard on-off keying soliton transmission system, consisting of S_1 and S_2, providing about $\rho_0 = 0.33$ bits/sec/Hz spectral efficiency at $P_0 = 0.1876$ mW and $R_0 = 7.42$ Gbits/sec data rate (see Table. 6.3 and its description). Note that the noise level is so small compared to the imaginary part of the eigenvalues that with few eigenvalues performance evaluation is essentially a deterministic analysis.

Table 6.3 shows the energy, duration, power and the bandwidth of the signals in (6.38). The resulting constellation has the average power $0.46P_0$ and the average time duration $1.65T_1$, where P_0 and T_1 are power and time duration of the fundamental soliton. Therefore the new signal sets provides about $\frac{\log 4}{1.65T_1W_0} = 1.2121 \times \rho_0$ bits/sec/Hz and operates at $R = 1.2121 \times R_0$ for about the same average power $(0.5P_0)$. Note that without S_4 the average power would be higher and in addition the improvement in the spectral efficiency is slightly smaller compared to the on-off keying system. Signal S_4 is the new signal that NFT method adds to what other methods can also include. Signals such as S_4 do not cost much in terms of time $\times$ maximum bandwidth product, while they add additional elements to the signal set. Such additional signals can generally be decoded only with the help of the nonlinear Fourier transform.

In this example, the receiver needs to estimate the pulse-duration. This can be done in many ways, *e.g.*, using the NFT computations already performed: zeros of the signal

signal	energy	duration FWHM	99% duration	power	bandwidth
S_1	0	T_0	T_1	0	W_0
S_2	E_0	T_0	T_1	P_0	W_0
S_3	$0.5\ E_0$	$2T_0$	$2T_1$	$0.25P_0$	$0.5W_0$
S_4	$1.5\ E_0$	$4.25T_0$	$2.58T_1$	$0.58P_0$	$0.5W_0$

Table 6.3: Parameters of the signal set in Section. 6.6.2. Here $E_0 = 4\times0.5 = 2$, $T_0 = 1.763$ at FWHM power, $T_1 = 5.2637$ (99% energy), $P_0 = 0.38$ and $W_0 = 0.5714$. The scale parameters are $T_0' = 25.246$ ps and $P_0' = 0.5$ mW at dispersion 0.5 ps/(nm $-$ km).

in time can be detected when $[v_1^2 e^{j\lambda t}, v_2^2 e^{-j\lambda t}]$ reaches a constant value in steady state. This can be checked at times $t = T_1$, $t = 2T_1$ and $t = 2.58T_1$. If one of the signals is zero at the end of another signal, one can monitor the energy of the continuous spectrum to make sure that it is small. If symbol duration is fixed to be the maximum $2.58T_1$, the addition of S_3 and S_4 increases both time interval and cardinality of signal set such that the spectral efficiency and data rate remained to be same ($\log(6)/2.58$), while operating at 77% of the on-off keying signal power.

Since solitons with purely imaginary eigenvalues do not suffer from major temporal or spectral broadening, there would be no major performance loss at the end of the fiber.

Modulating both Eigenvalues and Spectral Amplitudes

We can improve upon the previous example by modulating the spectral amplitudes too. Consider the following signal set

$$\begin{aligned} S_1 &: 0, \\ S_2 - S_5 &: \tilde{q}(0.5j) = \tilde{q}_1, \\ S_6 - S_9 &: \tilde{q}(0.25j) = \tilde{q}_2, \\ S_{10} - S_{16} &: \tilde{q}(0.25j, 0.5j) = (\tilde{q}_3, \tilde{q}4). \end{aligned} \tag{6.39}$$

We make a 3-PAM constellation on $\tilde{q}_i \in \{0.5, 1, 1.5\}$. This creates a signal set with 16 elements. Here pulses are extended to $3T_1$ time duration. The resulting constellation has the average power $1.06P_0$ and average time duration $2.236T_1$, where P_0 and T_1 are power and time duration of the benchmark on-off keying system. Therefore the new signal set provides about $\frac{\log 16}{2.236T_1W_0} = 1.79 \times \rho_0$ bits/sec/Hz and operates at $R = 1.79 \times R_0$ for about the same average power. If we fix symbol durations to be the maximum $3T_1$, then the improvement is $\rho = 2.2\rho_0 = 0.73$ bits/s/Hz, at 80% of the average power.

Again, since real part of the eigenvalues is not modulated, signals do not suffer from major temporal or spectral broadening, and there would be no performance loss at the end of the fiber.

Remark 13. Note that modulating the eigenvalues include only the amplitude information and to excite the other half of the degrees of freedom representing the phase, discrete spectral amplitudes should be considered too. While $|\tilde{q}(\lambda_j)|$ may be noisy, the phase $\angle\tilde{q}(\lambda_j)$ or a function of $\{\tilde{q}(\lambda_j)\}_{j=1}^{j=N}$ can be investigated for this purpose. Note however that the asymptotic behavior of the spectral efficiency can be obtained by considering the eigenvalues alone.

6.6.3 Spectral Efficiency of N-Soliton Systems, $N \geq 3$

To achieve high spectral efficiencies, a dense constellation in the upper-half complex plane needs to be considered. A spectral constellation with n eigenvalues in C^+ and m levels for spectral amplitudes provides

$$\log\left(\sum_{k=0}^{n}\binom{n}{k}m^k\right) = n\log\left(m+1\right),$$

bits. One can continue the argument presented in the previous examples by increasing n and m. The receiver architecture presented in this thesis is fairly simple and is able to decode NFT signals rather efficiently. At the transmitter side, one should make sure that all $(m+1)^n$ signals look good in time and frequency. Some pulses may have a large peak to average power, bandwidth or (99%) width. We have not found rules for modulating the spectrum such that the pulses have "good" properties in time too. While for small examples given here we can check pulse properties directly, in general we require appropriate ways for selecting the spectral data (specially the discrete spectral amplitudes).

In this simulation, we assume a constellation with 30 points uniformly chosen in the interval $0 \leq \lambda \leq 2$ on the imaginary axis and create all N-solitons, $1 \leq N \leq 6$. We then prune signals with undesirable bandwidth or width from this large signal set. The remaining multi-solitons are used as carriers of data in the typical fiber system considered earlier. Here a spectral efficiency of 1.5 bits/s/Hz is achieved. For this calculation, we take the maximum pulse width (containing 99% of the signal energy) and the maximum bandwidth of the signal set. Since pulse widths are large, the shift of the signal energy due to the Gordon-Haus effect is insignificant here. By increasing n and m, the Gordon-Haus effect is as important as it is for the sinc function transmission and backpropagation.

6.7 Multiuser Communications Using the NFT

As mentioned in Chapter 3, a major gain potentially can potentially be obtained by using methods which do not suffer from inter-channel interference, such as NFDM. In fact, interference-free communications is the most promising advantage of the NFT approach.

Recall that the real and imaginary axes of the complex plane in the NFT method represent, respectively, the signal frequency and amplitude. In a multiuser optical communication system, we partition the complex plane into vertical bins. Each bin contains one or more degrees of freedom and is assigned to a user. The function of add-drop mul-

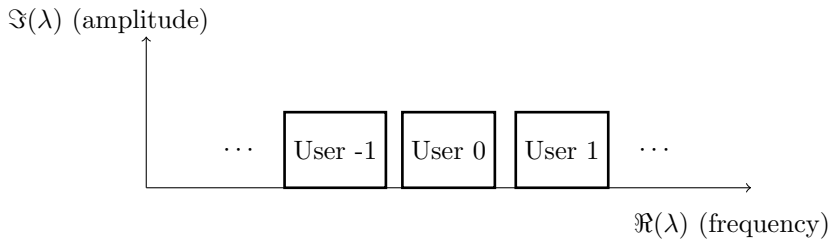

Figure 6.5: Partitioning $\mathbb{C}^+$ for multiuser communication using the NFT.

tiplexers is now modified to multiplex and demultiplex signals in a nonlinear way. Each nonlinear multiplexer/demultiplexer in principle calculates the spectrum of its input signal, filters signals which need to be dropped in the complex plane, and specifies the free bands in the nonlinear spectrum. It then calculates the spectrum of the signals entering the fiber and puts them in unoccupied bands. Finally, the inverse NFT is taken to output a time domain signal. This way each user gets a subspace in the complex plane during its trip in the fiber, operates in that subspace and deterministically does not interfere with other users. For small peak powers on the imaginary axis, the nonlinear multiplexing is equivalent to the regular Fourier transform multiplexing and as per-channel powers are increased, the deviations from the capacity of the linear channels associated with the prior work is best accounted for.

6.7.1 The Need for a Nonlinear Multiplexer/Demultiplexer

It is a conclusion of this thesis that one needs to multiplex and demultiplex signals in nonlinear fashion so as to avoid the interference associated with the WDM method and reach significantly higher spectral efficiencies. The nonlinear frequency-division multiplexer described above is complex in the given form and may not be the best description of a such device (without further simplification). Any multiplexer inducing independent signal propagation for different users is enough to get to the most of the advantages of the NFT method. This is true even if the resulting per user channel models are nonlinear. To find such multiplexer, a *deterministic model*, as noted in Chapter 3 and advocated in this thesis, can be considered.

6.8 Spectral Efficiencies Achievable by Modulating the Continuous Spectrum

In addition to the discrete spectrum, the continuous spectrum can be modulated too. The spectrum of an isolated sinc function is purely continuous in low powers, resembling a sinc function. The continuous spectrum is modulated just like the ordinary Fourier transform and at the receiver can be estimated with great accuracy. The received spectrum is then compared with the spectrum of the possible waveforms at the transmitter in the log-Euclidean norm

$$d(\hat{q}_2(\lambda), \hat{q}_1(\lambda)) = \frac{1}{\pi} \int_{-\infty}^{\infty} \log\left(1 + |\hat{q}_2(\lambda) - \hat{q}_1(\lambda)|^2\right) \mathrm{d}\lambda.$$

Fig. 6.6(a) shows the capacity of a typical single channel fiber-optic system using the backpropagation and the nonlinear Fourier transform. The NFT is calculated on a 1024 and 64 point grid on the real axis. The 1024-point NFT can be compared with the 1024-point FFT implementation of the Split-Step Fourier Method in the backpropagation scheme. As it can be seen, the NFT and backpropagation methods give about the same capacities. The slight improvement in the NFT method can be attributed to the stability of the spectral data compared to the time data (though numerical errors should be considered too).

Simulation is repeated for 5 WDM channels with the system architecture of Fig. 2.8. Here, low-pass filters and ROADMs are placed at the end of each fiber segment. The spectral efficiency in this case is obviously lower due to the inter-channel interference. Here too, NFT and FFT-based backpropagation produce approximately the same results.

From Fig. 6.6 it follows that at low SNRs NFT and backpropagation give about the same capacities. As the SNR is increased, the spectral efficiency of the backpropagation degrades due to ISI (if memory is not accounted for) or inter-channel interference (inevitably). The spectral efficiency of the NFT is expected to grow further due to the immunity to the cross talk. We have not yet simulated the spectral efficiency at SNRs beyond that of Fig. 6.6 due to a large number of simulation variables at high spectral efficiencies, the introduction of the discrete mass points, and the complexity of the NFT multiplexer. The major advantage of the NFDM is yet remained to be illustrated.

Note that often the mutual information is rather flat at the location of the capacity-achieving input distribution. That is to say, the capacity is usually not very sensitive to the details of the channel. Thus although the stability of the spectral data translates to

a small improvement in the capacity in low SNRs, the improvements in the probability of error, as another performance measure, are more substantial in the NFT method.

6.9 Some Remarks

We briefly reiterate few remarks about the NFT method made throughout the thesis to highlight and recapitulate some of its properties.

Noise in the spectral coordinates The NLS equation with additive noise has no known integrability structure, in the sense of possessing a set of non-interacting degrees of freedom, as in the linear or the nonlinear Fourier transform (unless for special cases of noise). As a result, an additive noise in the time domain gets coordinates in the spectral domain which are not independent or orthogonal. Since the noise description is signal-dependent, one gets two kinds of interference in a multiuser nonlinear channel: a large deterministic interference and a smaller stochastic interference. The NFT method does not suffer from the large deterministic interference ("strong interference"). However the smaller stochastic interference is expected to be left over ("weak interference").

Spectral efficiency of the NFDM method asymptotically As stated above, while deterministic channels are parallel and independent in the nonlinear Fourier domain, the presence of the noise correlates degrees of freedom and introduces interference. Thus NFDM is subject to a weak interference (whose strength depends on the noise level and SNR).

Note however that the decline of the capacity in the prior work is mostly due to the (strong) deterministic interference. The stochastic interference is an order of magnitude smaller and its effects are expected to appear at larger SNRs (of order of the inverse of the noise power ϵ^{-1}). As a result, although the spectral efficiency of the NFDM is expected to be higher and may not peak down at the usual SNRs ($\sim$ 25 dB) where the spectral efficiency of the WDM transmission and backpropagation declines [7], it too may ultimately peak down, albeit at much higher SNRs ($>$ 30 dB). We have not yet simulated the capacity at such high SNRs to see that at what SNR this may potentially happen. Such spectral efficiency achievable by the NFDM may be the best achievable rate, since the channel in the presence of the noise is not known to posses any set of non-interacting degrees of freedom and thus is fundamentally interference-limited. The improvements in the spectral efficiency using the NFDM method, compared to the WDM scheme, can still be significant, due to the immunity to the deterministic interference.

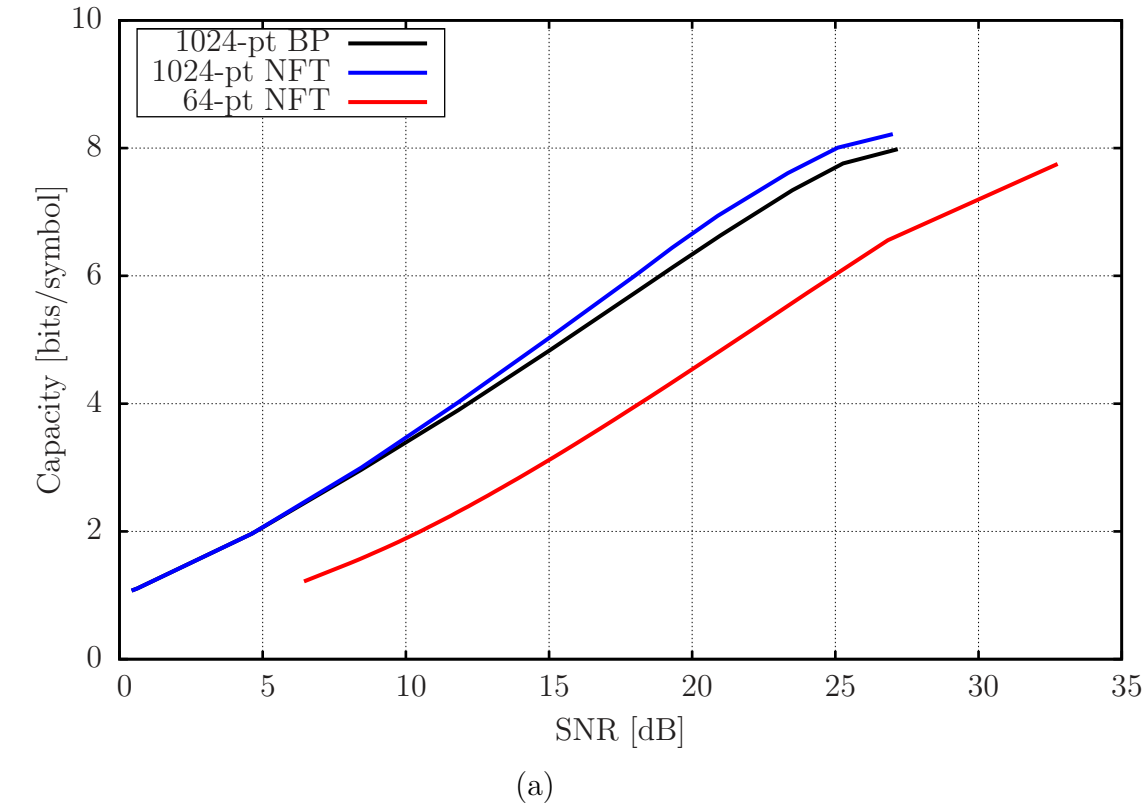

(a)

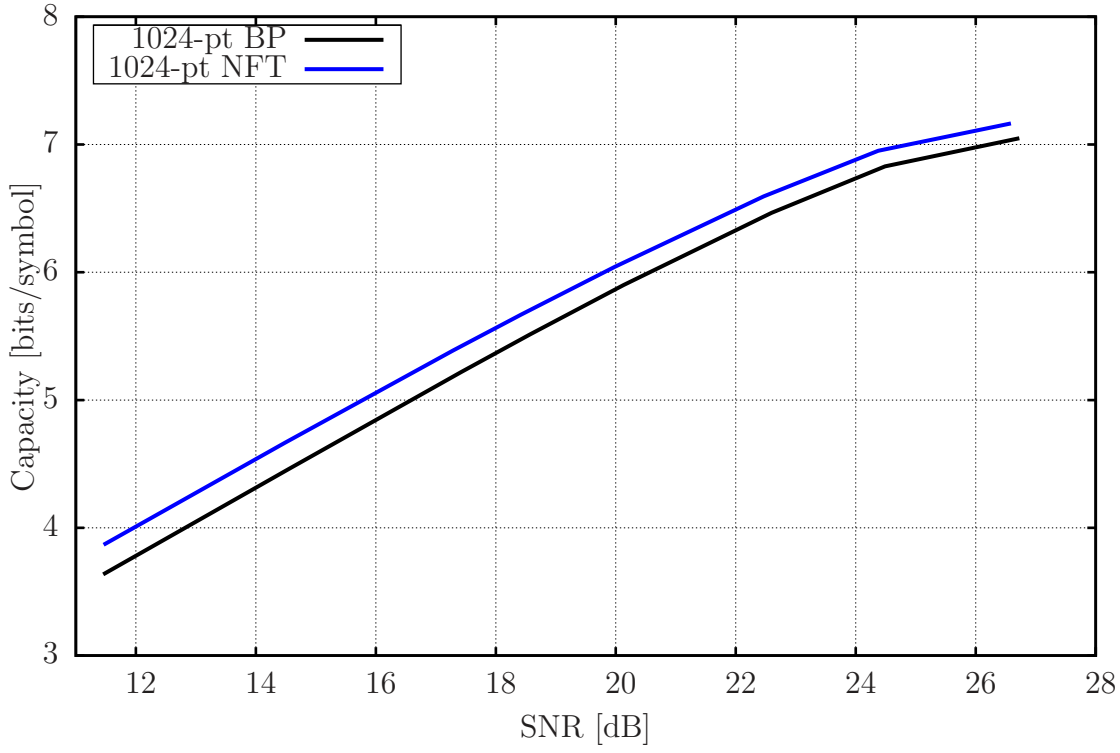

(b)

Figure 6.6: Capacity of (a) single channel, and (b) WDM optical fiber system using the nonlinear Fourier transform and backpropagation. The SNR is calculated at the system bandwidth and can be adjusted to represent the optical signal-to-noise ratio (OSNR).

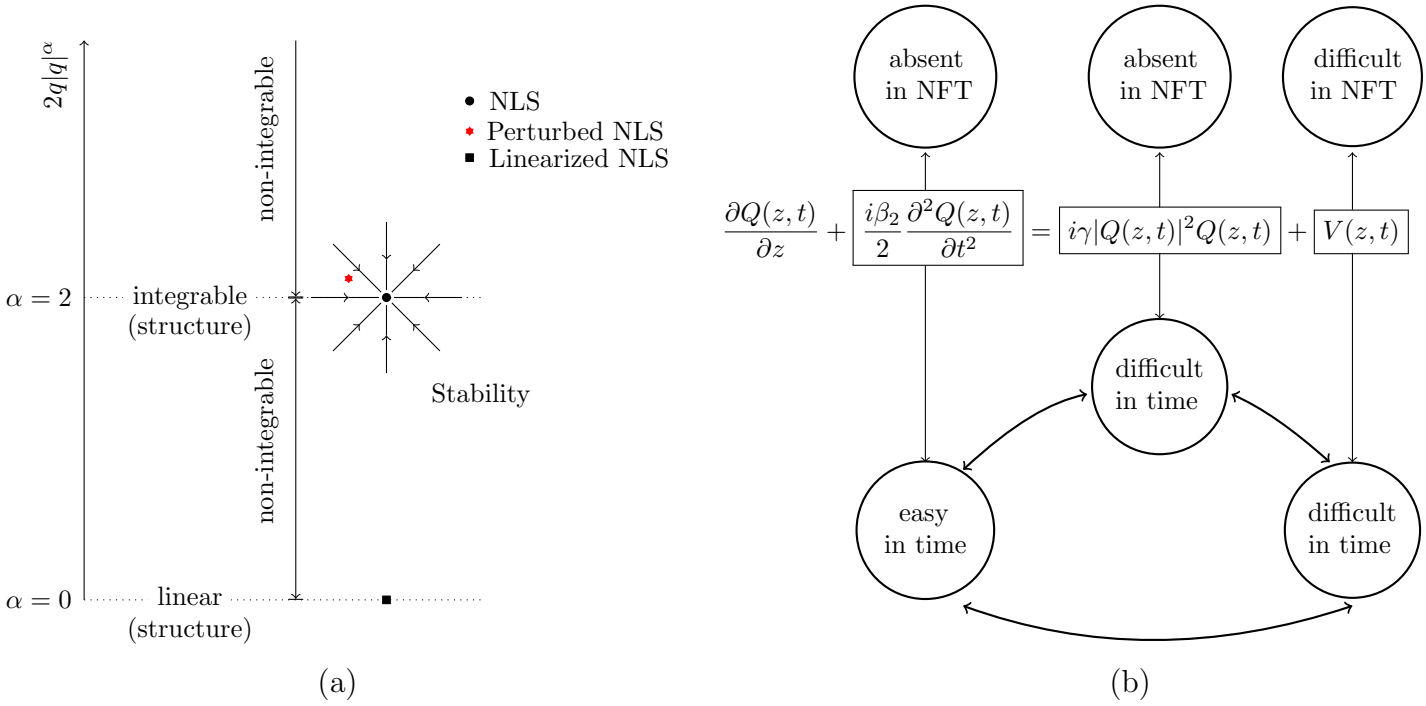

Figure 6.7: (a) As the power of the nonlinearity is increased from $\alpha = 0$ in $jq_z = q_{tt} + 2q|q|^\alpha$, the equation changes from a linear one with structure to a non-integrable equation with no structure, until $\alpha = 2$ where it becomes integrable and again possesses a (self-organizing) structure. For the purpose of the communications, a channel with structure is preferred. Thus the near integrable channel in practice (shown by a star) is equalized to an integrable channel (shown by a circle) as in this thesis, or to a linear channel (shown by a square) as in the prior work. (b) Three terms of the NLS equation in the time and spectral domains.

This can be seen, for instance, from the capacity simulations performed in [7] which illustrate that the spectral efficiency of the WDM method vanishes at high SNRs even if noise is set to zero. This is not the case for the NFDM whose spectral efficiency is unbounded when the noise is zero. This example shows what gains are expected to be achievable using the NFDM. It also shows the importance of considering deterministic models in multi-user optical channels.

Similarities and Differences of NFDM and OFDM

Similarities

1. The degrees of freedom are parallel and independent *when noise is zero.*
2. As in OFDM, one should consider the NFT under periodic boundary conditions and obtain a discrete NFT. The development of the discrete NFT already exists in the mathematics literature [58, 78]. A cyclic prefix may be needed at this stage.

Differences

1. Unlike OFDM, the noise in the NFDM method is correlated across spectral components and is signal-dependent.
2. Frequencies in the NFDM method are complex numbers. Since discrete frequencies in $\mathbb{C}^+$ come in the form of isolated points as a part of the degrees of freedom, they can be chosen from a constellation in $\mathbb{C}^+$ (e.g., QAM) and are subject to noise jitter. Thus eigenvalue communication is modulating the (discrete) support of the nonlinear Fourier transform of the signal (similar to frequency-shift keying). Modulating the remaining degrees of freedom, *i.e.*, the discrete and continuous spectral amplitudes, is in analogy with the OFDM.

Some of the Advantages and Disadvantages of the NFT

Advantages Some of the advantages of using the NFDM were mentioned at the beginning of this chapter (page 122). In short, in this method all deterministic distortions are zero for all users of a multiple user network (*i.e.*, no SPM, XPM, FWM, ISI or interference).

Disadvantages

1. NFDM critically relies on the integrability of the channel. Loss, higher order dispersion, and other perturbations caused by filters and communication equipments

not taken into account here contribute to deviations from integrability. There are however several reasons to believe that the back to back channel from transmitter to the receiver can still be close to an integrable channel:

(a) NFT is applicable as long as one can see solitons in the fiber. Solitons have been implemented in practice in the presence of the communication equipments (filters, multiplexers, analog-to-digital (A/D) converters, etc). This is an indicator that the back to back channel is still nearly integrable.

(b) With employing Raman amplification the effects of the loss are minimal (indeed traded with noise perturbation).

(c) Mathematically one has stability results for solitons. A soliton passing through a filter might be distorted a little, but it re-organizes its shape so as to revert back to its original shape (or form a soliton living nearby in the complex plane). For instance as an application of this property, filters were traditionally used to keep solitons in shape and reduce the Gordon-Haus timing jitter [69].

(d) In the view that the performance of the WDM method is asymptotically severed with SNR, the potential gains of using the NFT can be significant. It may be worthwhile to identify and minimize the perturbations of the integrability.

(e) The current practice of compensating and equalizing a nearly integrable channel to make it as linear as possible might be a more significant effort than making it integrable (see Fig. 6.7 (a)).

2. The nonlinear Fourier coefficients at the receiver are calculated in $\mathcal{O}(n)$ operations per nonlinear frequency, where n is the number of signal samples in time. To compare with FFT, the complexity of an n-point NFT is $\mathcal{O}(n^2)$ (fixed number of Newton steps is assumed in case of discrete frequencies). The complexity of the transmitter can be even more. As a result, NFT is computationally difficult to implement or sometimes to simulate.
3. Optical or electrical signal processing of N-solitons and the required hardware for their nonlinear multiplexing may not be as simple as those in the linear systems. A signal modulated to have desirable properties in the spectrum may translate to a signal in the time domain which is not processed easily with the current technology (*e.g.*, requiring high resolution A/Ds). Note that the NFT decoder typically requires signal samples at increments smaller than the Nyquist rate. An interpolation step may be needed to find all the necessary data.
4. Noise in the NFT domain can be difficult to analyze. However given that this

is the total accumulated noise, and the more important deterministic distortions are not present in the NFDM, nonlinear spectrum is still a more natural domain for information-theoretic analysis (see Fig. 6.7 (b)). In the time domain, all three terms, including the accumulated noise, are difficult to analyze, mainly due to their interactions.

Chapter 7

Conclusion

A man's errors are his portals of discovery.

James Joyce

Motivated by the recent studies showing that the spectral efficiency of optical fiber networks is severely limited by the impacts of the nonlinearity, we revisited information transmission in such nonlinear systems. Among numerous distortions, we identified the inter-channel interference in the multiuser WDM optical networks as the implacable factor limiting the spectral efficiency at high powers. However this distortion and similar ones arising from the nonlinearity, are largely due to the use of methods suited for linear systems, such as pulse train transmission and WDM, for the nonlinear optical channel. Exploiting the integrability of the NLS equation, we presented a nonlinear frequency-division multiplexing method which is fundamentally compatible with the structure of the channel. The distinction with the previous methods is that NFDM is now able to handle the nonlinearity as well, and thus as the the signal power or transmission distance is increased, the new method does not suffer from the cross talk between signal components, which has severed the performance of the prior work. The scheme has numerous other advantages desired in a communication network. We took the first steps towards a communication system implementing the nonlinear Fourier transform. We simplified the task of the transmitter and receiver and provided examples illustrating how to use the NFT for data transmission. Although these small examples clearly demonstrate improvements over their benchmark systems, a high spectral efficiency simulation illustrating the promise of the NFDM that the spectral efficiency does not degrade at moderate SNRs as in the prior work has not yet been performed. Due to the importance of the nonlinearity in optical networks, NFT or a similar idea should ultimately be used in the future to conceive schemes which do not suffer from cross talk or cancel such effects in the existing systems.

Appendices

Appendix A

Spectrum of Bounded Linear Operators

When moving from finite-dimensional spaces (of e.g., matrices) to infinite-dimensional spaces (of e.g., functions and operators), some results do not carry over necessarily. Here we recall a few useful results in functional analysis [46].

Let $\mathcal{H}$ be a Hilbert space, let $\mathcal{D}$ be a dense subset of $\mathcal{H}$, and let $L : \mathcal{D} \to \mathcal{H}$ be an operator.

Definition 8. The *adjoint* of L is the operator L^* whose domain $\mathcal{D}^*$ consists of all $\psi \in \mathcal{H}$ for which there exists an element $L^*\psi \in \mathcal{H}$ such that

$$\langle L^*\psi, \phi \rangle = \langle \psi, L\phi \rangle, \quad \forall \phi \in \mathcal{D}.$$

The operator L is said to be *self-adjoint* if $\mathcal{D} = \mathcal{D}^*$ and $L^* = L$. Ignoring domain subtleties (as is the case for bounded operators), self-adjoint operators are the analogue of Hermitian matrices.

Definition 9. Given an operator L on a Hilbert space, an operator M is said to be the inverse of L if the domain of M is the range of L, the range of M is the domain of L, and $ML = I$ and $LM = I$.

We will restrict ourselves now to operators whose $\mathcal{D}$ is the entire space $\mathcal{H}$.

An operator $L : \mathcal{H} \to \mathcal{H}$ is invertible if it 1) is one-to-one 2) is onto 3) has bounded inverse. In finite-dimensional spaces, only the first condition is required.

An operator is bounded if it maps bounded inputs to bounded outputs. A bounded operator is invertible if it is one-to-one and onto.

Definition 10. The *spectrum* of an operator L on $\mathcal{H}$ is defined as

$$\sigma(L) = \{\lambda \in \mathbb{C} | L - \lambda I \text{ is not invertible } \}.$$

The spectrum of a bounded operator can be partitioned into two classes, depending on the reason that $L - \lambda I$ fails to be invertible.

A complex number λ is considered part of the *discrete spectrum* if $L-\lambda I$ is not one-to-one, i.e., $L\psi = \lambda\psi$ has a non-zero solution $\psi \in H$. In this case, λ is called an *eigenvalue*, and each ψ satisfying this equation for the given λ is an associated *eigenvector*. The set of all eigenvalues is called the *point spectrum* or *discrete spectrum* of L, $\sigma_{\text{disc}}(L)$.

It can also happen that $L - \lambda I$ fails to be surjective, i.e., the range of $L - \lambda I$ is a proper subset of $\mathcal{H}$. We call the set of λ for which this happens the *continuous spectrum* $\sigma_{\text{cont}}(L)$ [46].

In finite-dimensional Hilbert spaces the spectrum is entirely discrete. This may no longer be true in infinite-dimensional spaces, where the eigenvalues (if they exist) may only be one part of the spectrum. The spectrum of a self-adjoint operator is real. In general, $\sigma(L) = \sigma(L^*)$.

The following examples illustrate some these possibilities.

Example 14. The operator $L(x(t)) = tx(t)$, $x(t) \in L^2[0,1]$, has no eigenvalues and its spectrum is purely continuous $\sigma(L) = [0,1]$. □

Example 15. The Fourier transform operator $\mathcal{F}(q)(\omega) = \int_{-\infty}^{\infty} q(t)e^{j\omega t}\mathrm{d}t$, regarded as on operator on $L^2(\mathbb{R})$ has the property $\mathcal{F}^4 = I$. The eigenvalues are therefore the discrete values $\{\pm 1, \pm j\}$. If $p(t)$ is an arbitrary polynomial, then $p(t)\exp(-t^2/2)$ is an eigenfunction. □

Example 16. Let ∇^2 be the Laplace operator and let r denote the radial distance in the three-dimensional space. The operator $L = -\nabla^2 - \frac{1}{r}$ is self-adjoint, and therefore it has a real spectrum. The continuous spectrum is [0,∞) and the discrete spectrum is given by $\lambda_n = -\frac{1}{4n^2}$, $n = 1, 2, \ldots$. □

Example 17. It is possible that the discrete spectrum of an operator is uncountable. For example, for a sequence $(x_0, x_1, \ldots) \in \ell^2 = \{x : \sum_i |x_i|^2 < \infty\}$, let the left-shift operator L be defined as $L\,(x_0, x_1, x_2, \ldots) = (x_1, x_2, \ldots)$. The spectrum consists of the unit disk $|\lambda| \leq 1$. The portion $|\lambda| < 1$ is the discrete spectrum while $|\lambda| = 1$ is the continuous spectrum. The adjoint of L is the right-shift operator $R\,(x_0, x_1, x_2, \ldots) = (0, x_0, x_1, \ldots)$. This operator has the same total spectrum, but it is entirely continuous. □

Example 18. Consider the Zakharov-Shabat system (4.18), in the form $(DI - P)v = 0$, $v \in L^2(\mathbb{R})$. One can see that for $\lambda \in \mathbb{R}$, the eigenvectors $v(t, \lambda)$ contain oscillatory terms $\exp(\pm j\lambda t)$, and thus are not in $L^2(\mathbb{R})$ (unbounded in norm). As a result, the operator $(DI - P)^{-1}$ is unbounded and the inverse $(DI - P)^{-1}$ does not exist on the Hilbert space $L^2(\mathbb{R})$. Thus $\lambda \in \mathbb{R}$ forms the continuous spectrum. This is generally the case where for an operator L on $\mathcal{H}$ for which the eigenproblem $Lv = \lambda v$ has a solution with infinite norm. □

Note that some authors subdivide what we refer to as the continuous spectrum into further classes (e.g., residual spectrum, essential spectrum, etc.) [46]; however, for the purposes of this thesis, classification into discrete and continuous spectra will suffice.

Hermitian matrices are always diagonalizable, have real eigenvalues, and possess a complete set of orthonormal eigenvectors, which provide a basis for the input space. There is a perfect generalization of this result to *compact* self-adjoint operators [46].

Theorem 12 (Hilbert-Schmidt spectral theorem)**.** *Let L be a compact self-adjoint operator in $\mathcal{H}$. Then it is always possible to find eigenfunctions $\{\psi_n\}$ of L forming an orthonormal basis for $\mathcal{H}$.*

The spectral theory of operators that are not compact and self-adjoint is more involved; see [46].

An important class of operators are the multiplication operators, which are analogous to diagonal matrices.

Definition 11 (Multiplication operator)**.** Let $f(t)$ be an arbitrary function. The operator L defined by $(L\psi)(t) = f(t)\psi(t)$, which performs sample-wise multiplication, is called the *multiplication operator* or *diagonal operator* induced by $f(t)$.

Theorem 13. *Every bounded self-adjoint operator in a separable Hilbert space $\mathcal{H}$ is unitarily equivalent to a multiplication operator Γ, i.e., $L = U\Gamma U^{-1}$ where U is unitary.*

It follows that the essence of a bounded self-adjoint operator is just a multiplication operator.

Appendix B

Riemann-Hilbert Factorization Problem

B.1 Preliminary

Recall that a complex function $f(z) = u(x, y) + jv(x, y)$ in the complex plane $z = (x, y)$ is differentiable at a point (x_0, y_0) if and only if the partial derivatives u_x, u_y, v_x and v_y are continuous and

$$u_x = v_y, \quad u_y = -v_x. \tag{B.1}$$

The compatibility conditions (B.1) are called the Cauchy-Riemann conditions and are obtained by equating the limit $\delta z \to 0$ along the real and imaginary axes. This means that, unlike real functions, differentiability of a complex function imposes a constraint between the real and imaginary parts of the function.

A function $f(z)$ is said to be analytic at (x_0, y_0) if it is differentiable in a neighborhood of that point. If $f(z)$ is analytic in an open region Ω of the complex plane, then a power series representation of $f(z)$ is convergent in Ω. Existence of a power series representation has a number of interesting consequences. For instance, the zeros of a non-zero function analytic in an open region Ω of $\mathbb{C}$ are isolated points in Ω [50].

Lemma 14 (Plemelj formulae)**.** *Let C be any smooth, closed, counter-clockwise, contour in the complex plane and let $f(x)$ be any function satisfying a Hölder condition on C defined by*

$$|f(t) - f(\tau)| \leq k|t - \tau|^{\alpha},\ k > 0,\ \forall t, \tau \in C,$$

for some $0 < \alpha \leq 1$. *Then the projection integral*

$$F(\zeta) = \frac{1}{2\pi j} \oint_C \frac{f(z)}{z-\zeta} \mathrm{d}z, \tag{B.2}$$

is analytic everywhere in $\mathbb{C}$ *except possibly at points* ζ *on the contour* C *(where* $F(\zeta)$ *is not defined). If* ζ *approaches* C *along a path entirely inside the contour* C*, then*

$$F^+(\zeta) \triangleq \lim_{z\to\zeta} F(\zeta) = \frac{f(\zeta)}{2} + \frac{1}{2\pi j} \text{ p.v. } \int_C \frac{f(z)}{z-\zeta} \mathrm{d}z. \tag{B.3}$$

If ζ *approaches* C *along a path entirely outside the contour* C*, then*

$$F^-(\zeta) \triangleq \lim_{z\to\zeta} F(\zeta) = -\frac{f(\zeta)}{2} + \frac{1}{2\pi j} \text{ p.v. } \int_C \frac{f(z)}{z-\zeta} \mathrm{d}z. \tag{B.4}$$

Here p.v. *denotes the principal value integral defined by*

$$\text{p.v. } \int_C \frac{f(z)}{z-\zeta} \mathrm{d}z = \lim_{\epsilon\to 0} \oint_{C-C_\epsilon} \frac{f(z)}{z-\zeta} \mathrm{d}z,$$

in which C_ϵ *is an infinitesimal part of* C *centered at* $z = \zeta$ *and with length* 2ϵ.

Proof. See [52]. □

The projected function $F(\zeta)$ is a *sectionally analytic* function of ζ with respect to C, *i.e.*, it is analytic in sections C^+ (the interior of C) and C^- (the exterior of C), and the limits $F^\pm(\zeta)$ exist (as given by (B.3) and (B.4)).

A consequence of Lemma 14 is that $F^\pm(\zeta)$ satisfies the following *jump condition* on the boundary C

$$F^+(t) - F^-(t) = f(t).$$

The projection operator therefore produces functions which are analytic almost everywhere, except on a contour where it experiences a jump in its limits.

B.2 The Scalar Riemann-Hilbert Problem

In the scalar Riemann-Hilbert problem, the task is to find functions $f^+(z)$ and $f^-(z)$, analytic, respectively, inside and outside a given smooth closed contour C, such that on

C

$$f^+(t) = g(t)f^-(t) + h(t) \quad t \in C, \tag{B.5}$$

where $h(t)$ and $g(t)$ (with $g(t) \neq 0$ for all $t \in C$), are given functions satisfying a Hölder condition on C.

Both unknowns $f^+(z)$ and $f^-(z)$ can be determined from the single boundary equation (B.5), using the projection operator (B.2). To see this, first consider the homogeneous case where $h(t) = 0$. One can rewrite (B.5) as a jump condition

$$\log f^+(z) - \log f^-(z) = \log g(z) \quad z \in C.$$

Functions $\log f^+(z)$ and $\log f^-(z)$ can be viewed as portions of a single sectionally analytic function $\log f(z)$ which is analytic in C^+ and C^- and on boundary C its limits jump as $\log g(t)$. In view of the projection operator P (B.2), consider

$$\log f(z) = \frac{1}{2\pi j} \oint_C \frac{\log g(\lambda)}{\lambda - z} \mathrm{d}\lambda.$$

If $\log g(t)$ satisfies a Hölder condition on C, then $\log f(z)$ is analytic strictly inside and outside C. On C, we can define $\log f^+(z)$ and $\log f^-(z)$, respectively, as equal to the limits (B.3) and (B.4). The function obtained in this way satisfies (B.5) and has the desired analyticity properties.

Note however that, unlike $g(t)$, $\log g(t)$ in the integrand may not satisfy a Hölder condition. To resolve this issue, we can multiply $g(t)$ by a decaying factor t^{-k}, for a suitable k, to make $t^{-k}g(t)$ Hölder, and obtain $f^+(t) = \left(t^{-k}g(t)\right)\left(t^k f^-(z)\right)$. Therefore, defining

$$F(z) = \exp\left(\frac{1}{2\pi j} \oint_C \frac{\log \lambda^{-k} g(\lambda)}{\lambda - z} \mathrm{d}\lambda\right),$$

we have the following solution for the homogeneous RH problem:

$$f^+(z) = \begin{cases} F(z) & z \in C^+, \\ F^+(z) & z \in C, \end{cases}$$

and

$$f^-(z) = \begin{cases} z^{-k}F(z) & z \in C^-, \\ z^{-k}F^-(z) & z \in C. \end{cases}$$

Here k can be chosen so that $t^{-k}g(t)$ is continuous and the total phase change of $\log t^{-k}g(t)$ is zero along the closed path C.

The solution $f^{\pm}(z)$ is called the fundamental solution to the scalar RH problem. From the homogeneity of (B.5), one can obtain other solutions by multiplying $f^{\pm}(z)$ by any entire function in C.

We can generalize the above procedure to solve the non-homogeneous Riemann-Hilbert problem (B.5). In this case, we can find a factorization $g(t) = \frac{g^+(t)}{g^-(t)}$ by solving a homogeneous Riemann-Hilbert problem with boundary conditions $g^+(t) = g(t)g^-(t)$. Then (B.5) is reduced to

$$\frac{f^+(t)}{g^+(t)} - \frac{f^-(t)}{g^-(t)} = \frac{h(t)}{g^+(t)},$$

which, as before, can be solved in closed form using the Plemelj formulae.

B.3 The Matrix Riemann-Hilbert Problem

When formulating the inverse nonlinear Fourier transform, we face a matrix Riemann-Hilbert problem (4.36). Matrix RH problems are generally more involved and may not allow closed-form solutions [52]. As we will see in the Appendix C.4, for the particular matrix RH problem (4.36), the projection operator (B.2) is sufficient to solve the problem.

Appendix C

Proofs of Some Results from Chapter 4

C.1 Proof of Elementary Properties of the NFT

In this section, we sketch the proofs of the properties of the NFT stated in Section 4.3.4.

1. If $||q(t)||_{L_1} \ll 1$, then $y^2(t,\lambda)$ and $q^2(t)$ terms can be ignored in (4.30) and (4.31). From the resulting equations, it follows that there is no discrete spectrum and $\hat{q}(\lambda) \to Q(\lambda)$. The quadratic terms are introduced by the NFT to account for the nonlinearity.
2. This follows from 1) in above, and that when $|a| \ll 1$, the squared terms representing the nonlinearity can be ignored.
3. This follows from replacing $q(t)$ with $e^{j\phi}q(t)$ in (4.30) and (4.31).
4. Scaling the Zakharov-Shabat system (4.18) as $t' = t/a$, we obtain the desired result. Note that if $\mathrm{sgn}(a) < 0$, boundary conditions at $\pm\infty$ are interchanged.
5. Property 5) and 6) follow by replacing $q(t)$ with $q(t-t_0)$ and $e^{2j\omega t}q(t)$ in (4.30) and (4.31), and accordingly changing variables.
6. This is the statement of (4.33).
7. The following identity, known as the trace formula, can be easily proved for the nonlinear Fourier transform [10]

$$c_n = \frac{4}{n}\sum_{i=1}^{N} \Im(\lambda_i^n) + \frac{1}{\pi}\int_{-\infty}^{\infty} \zeta^{n-1} \log\left(1+|\rho(\zeta)|^2\right) \mathrm{d}\zeta.$$

   Here c_n are the secondary constants of motion, i.e., quantities, directly in terms of the time domain data, which are preserved during the flow of the NLS equation.

The first few ones are the energy

$$c_1 = \int_{-\infty}^{\infty} |q(t)|^2 \mathrm{d}t,$$

momentum

$$c_2 = \frac{1}{2j} \int_{-\infty}^{\infty} q(t) q_t^*(t) \mathrm{d}t,$$

and the Hamiltonian

$$c_3 = -\int_{-\infty}^{\infty} \left(|q(t)|^4 - |q_t(t)|^2 \right) \mathrm{d}t.$$

Parseval's Identity is the trace formula evaluated at $n = 1$.

8. Let $q(t)$ be supported in the interval $[t_1, t_2]$ and let $K(q(t), t_1, t_2)$ denote a propagator (linear transformation) which maps $v(t, \lambda)$ in (4.18) from $v(t_1, \lambda)$ to $v(t_2, \lambda)$. The propagator is structured as

$$K = \begin{pmatrix} a(\lambda) e^{j\lambda(t_2 - t_1)} & -b^*(\lambda^*) e^{j\lambda(t_2 + t_1)} \\ b(\lambda) e^{-j\lambda(t_2 + t_1)} & a^*(\lambda^*) e^{-j\lambda(t_2 - t_1)} \end{pmatrix}.$$

Let $q_1(t)$ and $q_2(t)$, supported, respectively, in the intervals $[t_1, t_2]$ and $[t_2, t_3]$, $t_1 < t_2 < t_3$, correspond to the propagators $K_1(q_1(t), t_1, t_2)$ and $K_2(q_2(t), t_2, t_3)$. Then $q(t) = q_1(t) + q_2(t)$ is supported in $[t_1, t_3]$, and from linearity corresponds to the propagator $K = K_2 K_1$

$$\begin{aligned} K = & \begin{pmatrix} a_2(\lambda) e^{j\lambda(t_3 - t_2)} & -b_2^*(\lambda^*) e^{j\lambda(t_3 + t_2)} \\ b_2(\lambda) e^{-j\lambda(t_3 + t_2)} & a_2^*(\lambda^*) e^{-j\lambda(t_3 - t_2)} \end{pmatrix} \\ & \times \begin{pmatrix} a_1(\lambda) e^{j\lambda(t_2 - t_1)} & -b_1^*(\lambda^*) e^{j\lambda(t_2 + t_1)} \\ b_1(\lambda) e^{-j\lambda(t_2 + t_1)} & a_1^*(\lambda^*) e^{-j\lambda(t_2 - t_1)} \end{pmatrix}. \end{aligned}$$

The 1×1 and 2×1 elements are

$$\begin{aligned} K_{11} &= e^{j\lambda(t_3 - t_1)} \left(a_1(\lambda) a_2(\lambda) - b_1(\lambda) b_2^*(\lambda^*) \right), \\ K_{21} &= e^{-j\lambda(t_3 + t_1)} \left(a_1(\lambda) b_2(\lambda) + b_1(\lambda) a_2^*(\lambda^*) \right). \end{aligned}$$

Comparing with $K_{11} = a(\lambda) e^{j\lambda(t_3 - t_1)}$ and $K_{21} = b(\lambda) e^{-j\lambda(t_3 + t_1)}$, we get the desired

result.

C.2 Proof of Lemma 10

Analyticity of the canonical eigenvectors is directly a property of the Zakharov-Shabat system (4.18). Let us scale canonical eigenvectors as $V^2 = v^2 e^{j\lambda t}$, $\tilde{V}^2 = \tilde{v}^2 e^{-j\lambda t}$,$V^1 = v^1 e^{-j\lambda t}$ and $\tilde{V}^1 = \tilde{v}^1 e^{j\lambda t}$. Transforming the Zakharov-Shabat system (4.18), the scaled eigenvectors satisfy

$$\begin{aligned} V^2_t &= \begin{pmatrix} 0 & q \\ -q^* & 2j\lambda \end{pmatrix} V^2, \quad V^2(-\infty) = \begin{pmatrix} 1 \\ 0 \end{pmatrix}, \\ \tilde{V^2}_t &= \begin{pmatrix} -2j\lambda & q \\ -q^* & 0 \end{pmatrix} \tilde{V^2}, \quad \tilde{V^2}(-\infty) = \begin{pmatrix} 0 \\ 1 \end{pmatrix}, \\ \tilde{V^1}_t &= \begin{pmatrix} 0 & q \\ -q^* & 2j\lambda \end{pmatrix} \tilde{V^1}, \quad \tilde{V^1}(\infty) = \begin{pmatrix} 1 \\ 0 \end{pmatrix}, \\ V^1_t &= \begin{pmatrix} -2j\lambda & q \\ -q^* & 0 \end{pmatrix} V^1, \quad V^1(\infty) = \begin{pmatrix} 0 \\ 1 \end{pmatrix}. \end{aligned} \tag{C.1}$$

Let us, for instance, solve for the canonical eigenvector V^2 in (C.1). Considering the q terms as an external force and using the Duhamel formula [79], (C.1) can be transformed into its integral representation

$$\begin{aligned} V^2(t,\lambda) &= \begin{pmatrix} 1 \\ 0 \end{pmatrix} \\ &+ \int_{-\infty}^{\infty} h(t-t',\lambda) \begin{pmatrix} 0 & q(t') \\ -q^*(t') & 0 \end{pmatrix} V^2(t',\lambda) \mathrm{d}t', \end{aligned} \tag{C.2}$$

where the system impulse response $h(t,\lambda)$ is

$$h(t,\lambda) = \begin{pmatrix} u(t) & 0 \\ 0 & e^{2j\lambda t} u(t) \end{pmatrix}, \tag{C.3}$$

and we have ignored transient terms since the boundary condition starts at $t = -\infty$.

The analyticity of eigenvectors can be seen intuitively at at this stage. The impulse response (C.3) involves the term $e^{2j\lambda t}u(t)$ and hence (C.1) is well defined in $\mathbb{C}^+$ if $q \in L^1(\mathbb{R})$. The impulse response for the V^1 equation involves $-e^{-2j\lambda t}u(-t)$ and hence it is bounded in the same region. The impulse response for $\tilde{V}^2$ and $\tilde{V}^1$ have terms proportional

to $e^{-2j\lambda t}u(t)$ and $-e^{2j\lambda t}u(-t)$, respectively, and therefore these eigenvectors are analytic in $\mathbb{C}^-$ for $q \in L^1(\mathbb{R})$.

A more precise argument proceeds by solving (C.2) explicitly. Duhamel's integral (C.2) is of the form of a fixed-point map

$$V^2 = \begin{pmatrix} 1 \\ 0 \end{pmatrix} + T(V^2),$$

where T is the linear operator underlying (C.2). A candidate for the solution is the sum

$$V^2 = \sum_{k=0}^{\infty} U^k \tag{C.4}$$

where U^k satisfy the iteration

$$U^{k+1} = T(U^k) + \begin{pmatrix} 1 \\ 0 \end{pmatrix}, \quad U_0 = \begin{pmatrix} 0 \\ 0 \end{pmatrix}.$$

The first few terms are

$$U^1 = \begin{pmatrix} 1 \\ 0 \end{pmatrix}, \quad U^2 = \begin{pmatrix} 0 \\ -\int\limits_{t_1=-\infty}^{t} q^*(t_1)e^{2j\lambda(t-t_1)}\mathrm{d}t_1 \end{pmatrix}, \tag{C.5}$$

$$U^3 = \begin{pmatrix} -\int\limits_{t_2=-\infty}^{t}\int\limits_{t_1=-\infty}^{t_2} q(t_2)q^*(t_1)e^{2j\lambda(t_2-t_1)}\mathrm{d}t_1\mathrm{d}t_2 \\ 0 \end{pmatrix}, \tag{C.6}$$

and the k^{th} term is recursively defined by

$$U^{k+1} = \begin{pmatrix} 1 \\ 0 \end{pmatrix} + \int\limits_{-\infty}^{t} \begin{pmatrix} q(t')U_2^k(t',\lambda) \\ -q^*(t')U_1^k(t',z)e^{2j\lambda(t-t')} \end{pmatrix} \mathrm{d}t'. \tag{C.7}$$

By induction on k, as (C.7) suggests, if U^k is analytic and $q(t) \in L^1(\mathbb{R})$, then U^{k+1} is analytic. In addition, the series (C.4) is uniformly convergent on t and thus V^2 is analytic in $\mathbb{C}^+$.

Similarly one proves the analyticity of the other canonical eigenvectors in their corresponding region.

C.3 Asymptotics of Canonical Eigenvectors and Nonlinear Fourier Coefficients when $|\lambda| \gg 1$

If $\lambda \in C^+$ and $|\lambda| \gg 1$, then $\frac{1}{j(\omega-2\lambda)} = \frac{-1}{2j\lambda} + O(\lambda^{-2})$ and, taking the inverse Fourier transform, we can approximate $e^{2j\lambda t}u(t) = -\frac{1}{2j\lambda}\delta(t) + O(\lambda^{-2})$. Substituting into (C.4), (C.5), (C.6), for $|\lambda| \gg 1$ we obtain

$$V^2(t,\lambda) = \begin{pmatrix} 1 + \frac{1}{2j\lambda}\int_{-\infty}^{\infty} |q(t)|^2 \mathrm{d}t \\ \frac{1}{2j\lambda} q^*(t) \end{pmatrix} + O(\lambda^{-2}). \tag{C.8}$$

A similar asymptotic expression can be derived for V^1 ($\lambda \gg 1$)

$$V^1(t,\lambda) = \begin{pmatrix} \frac{1}{2j\lambda} q(t) \\ 1 + \frac{1}{2j\lambda}\int_{-\infty}^{\infty} |q(t)|^2 \mathrm{d}t \end{pmatrix} + O(\lambda^{-2}).$$

If $|\lambda| \to \infty$, q can be assumed zero in (4.18) compared to $j\lambda$. Thus $v(t,\lambda)$ approaches the boundary conditions at $t = \pm\infty$. Therefore

$$\begin{aligned} a(\lambda) &= \langle v^2(t,\lambda), v^1(t,\lambda)\rangle_s = \langle v^2(+\infty,\lambda), v^1(+\infty,\lambda)\rangle_s \\ &\to \langle v^2(-\infty,\lambda), v^1(+\infty,\lambda)\rangle_s = 1. \end{aligned} \tag{C.9}$$

Similarly, it is shown that $b(\lambda) \to 0$ as $|\lambda| \to \infty$.

C.4 Solution of the Riemann-Hilbert Problem in the NFT

In Section 4.6, the inverse nonlinear Fourier transform was formulated as an instance of the Riemann-Hilbert factorization problem. Using hints given in the Appendix B, the resulting factorization problem can be solved in a simplified manner via an appropriate contour integration.

Dividing both sides of the projection equations (4.24)-(4.25) by $a(\lambda)(\lambda - \zeta)$, for parameter $\zeta \in C^-$, and integrating on the real axis $-\infty < \lambda < \infty$, we obtain

$$\frac{1}{2\pi j}\int_{\lambda=-\infty}^{\infty} \frac{V^2(t,\lambda)}{a(\lambda)(\lambda-\zeta)}\mathrm{d}\lambda = \frac{1}{2\pi j}\int_{\lambda=-\infty}^{\infty} \frac{\tilde{V}^1(t,\lambda^*)}{\lambda-\zeta}\mathrm{d}\lambda + \frac{1}{2\pi j}\int_{\lambda=-\infty}^{\infty} \frac{\hat{q}(\lambda)e^{2j\lambda t}V^1(t,\lambda)}{\lambda-\zeta}\mathrm{d}\lambda, \tag{C.10}$$

in which the integration is performed on the *open path* $z = \lambda, -\infty < \lambda < \infty$. The integration path thus passes the singularity $\lambda = \zeta$ from above in all the integrals.

Cauchy integrals in (C.10) are computed from the residue theorem. The integration path $-\infty < \lambda < \infty$ can be closed in the upper or lower half-planes. To compute the first integral, we close the path in the upper half-plane and denote the resulting closed contour by $C^+_{-\zeta}$, i.e., the upper half plane and excluding the singularity $z = \zeta$

$$\begin{aligned}\frac{1}{2\pi j}\int\limits_{\lambda=-\infty}^{\infty}\frac{V^2(t,\lambda)}{a(\lambda)(\lambda-\zeta)}\mathrm{d}\lambda &= \frac{1}{2\pi j}\oint_{C^+_{-\zeta}}\frac{V^2(t,z)}{a(z)(z-\zeta)}\mathrm{d}z - \lim_{R\to\infty}\frac{1}{2\pi j}\int\limits_{Re^{j0}}^{Re^{j\pi}}\frac{\begin{pmatrix}1\\0\end{pmatrix}}{a(z)(z-\zeta)}\mathrm{d}z\\ &= \sum_{i=1}^{N}\frac{V^2(t,\lambda_j)}{a'(\lambda_j)(\lambda_j-\zeta)} - \frac{1}{2}\begin{pmatrix}1\\0\end{pmatrix}\\ &= \sum_{i=1}^{N}\frac{b(\lambda_i)e^{2j\lambda_i t}V^1(t,\lambda_i)}{a'(\lambda_i)(\lambda_i-\zeta)} - \frac{1}{2}\begin{pmatrix}1\\0\end{pmatrix}\\ &= \sum_{i=1}^{N}\frac{\tilde{q}(\lambda_i)e^{2j\lambda_i t}V^1(t,\lambda_i)}{\lambda_i-\zeta} - \frac{1}{2}\begin{pmatrix}1\\0\end{pmatrix},\end{aligned} \tag{C.11}$$

where, in the second line, when $R \to \infty$, we have used the asymptotic values (C.8) and (C.9) in Appendix C.3. Note that we assumed that eigenvalues λ_j are all *simple* zeros of $a(\lambda)$, *i.e.*, no multiplicity.

To compute the second integral in (C.10), we close the integration path in the lower half-plane and denote the resulting closed contour by $C^-_{+\zeta}$, i.e., the lower half-plane and including the singularity $z = \zeta$

$$\begin{aligned}\frac{1}{2\pi j}\int\limits_{\lambda=-\infty}^{\infty}\frac{\tilde{V^1}(t,\lambda^*)}{\lambda-\zeta}\mathrm{d}\lambda &= \frac{1}{2\pi j}\oint_{C^-_{+\zeta}}\frac{\tilde{V^1}(t,z^*)}{z-\zeta}\mathrm{d}z - \lim_{R\to\infty}\frac{1}{2\pi j}\int\limits_{Re^{j2\pi}}^{Re^{j\pi}}\frac{\begin{pmatrix}1\\0\end{pmatrix}}{z-\zeta}\mathrm{d}z\\ &= -\tilde{V^1}(t,\zeta) + \frac{1}{2}\begin{pmatrix}1\\0\end{pmatrix}.\end{aligned} \tag{C.12}$$

The last integral in (C.10) is left uncomputed, because the boundedness of $e^{2j\lambda t}$ depends on the sign of t. For $t > 0$, we can consider $C^+_{-\zeta}$ which leads to the expression (C.11) multiplied by $u(t)$. For $t < 0$, we should inevitably consider $C^-_{+\zeta}$, where poles of $V^1(x,\lambda)$ are unknown. As a result, this integral is left untreated.

Using (C.11) and (C.12) in (C.10), we obtain an integral equation relating canonical

eigenvectors V^1 and $\tilde{V^1}$ to $\hat{q}(\lambda)$ and $\tilde{q}(\lambda_j)$

$$\tilde{V^1}(t,\zeta^*) = \begin{pmatrix} 1 \\ 0 \end{pmatrix} + \sum_{i=1}^{N} \frac{\tilde{q}(\lambda_i) e^{2j\lambda_i t} V^1(t,\lambda_i)}{\zeta - \lambda_i} + \frac{1}{2\pi j} \int_{\lambda=-\infty}^{\infty} \frac{\hat{q}(\lambda) e^{2j\lambda t} V^1(t,\lambda)}{\lambda - (\zeta - j\epsilon)} \mathrm{d}\lambda. \tag{C.13}$$

This is the first equation in the Riemann-Hilbert system (4.37) when ζ approaches the real line from below. Since (C.13) holds for any $\zeta \in C^-$, evaluating (C.13) at $\zeta = \lambda_j^*$, $j = 1, \ldots, N$, produces the third equation in (4.37). The remaining equations are obtained by taking the $\sim$ operation from these two equations and subsequently replacing λ and λ_m with, respectively, λ^* and λ_m^*.

Appendix D

Proof of the Darboux Theorem

The proof of a more general theorem can be found in [72]. We prove it here too to save the reader delving in [72].

Let $\phi(t, \lambda; q)$ be a known eigenvector associated with λ and q, i.e., satisfying $\phi_t = P(q, \lambda)\phi$. Its adjoint $\tilde{\phi}(t, \lambda) = [\phi_2^*, -\phi_1^*]$ satisfies $\tilde{\phi}_t(t, \lambda) = P(q, \lambda^*)\tilde{\phi}(t, \lambda)$. Denote this known solution as $S = [\phi, \tilde{\phi}]$, $\Gamma = \text{diag}(\lambda, \lambda^*)$, and $\Sigma = S\Gamma S^{-1}$.

We can verify that $S_t = JS\Gamma + QS$, where $J = \text{diag}(j, -j)$ and $Q = \text{offdiag}(q, -q^*)$. In addition we have $\Sigma_t = [J\Sigma + Q, \Sigma]$.

Given that $\phi(t, \lambda; q)$ is known, the Darboux transformation maps $\{v(t, \mu; q), \tilde{v}(t, \mu; q)\}$ to $\{u(t, \mu; \tilde{q}), \tilde{u}(t, \mu; \tilde{q})\}$ according to

$$U = V\Lambda - \Sigma V,$$

where $V = [v, \tilde{v}]$, $U = [u, \tilde{u}]$, $\Lambda = \text{diag}(\mu, \mu^*)$.

We have $V_t = JV\Lambda + QV$ and

$$\begin{aligned}
U_t &= V_t\Lambda - (\Sigma_t V + \Sigma V_t) \\
&= (JV\Lambda + QV)\Lambda - ([J\Sigma + Q, \Sigma]V + \Sigma(JV\Lambda + QV)) \\
&= (JV\Lambda + QV)\Lambda - \Sigma JV\Lambda - \{[J\Sigma + Q, \Sigma] + \Sigma Q\} V \\
&= J(V\Lambda - \Sigma V)\Lambda + J\Sigma V\Lambda - \Sigma JV\Lambda \\
&\quad +QV\Lambda - ([J\Sigma + Q, \Sigma] + \Sigma Q) V \\
&= JU\Lambda + [J, \Sigma]V\Lambda - ([J\Sigma + Q, \Sigma] + \Sigma Q) V + QV\Lambda \\
&= JU\Lambda + [J, \Sigma]V\Lambda - \left(J\Sigma^2 + Q\Sigma - \Sigma J\Sigma\right) V + QV\Lambda \\
&= JU\Lambda + [J, \Sigma]V\Lambda - [J, \Sigma]\Sigma V - Q\Sigma V + QV\Lambda \\
&= JU\Lambda + [J, \Sigma](V\Lambda - \Sigma V) - Q\Sigma V + QV\Lambda \\
&= JU\Lambda + [J, \Sigma]U + Q(V\Lambda - \Sigma V) \\
&= JU\Lambda + (Q + [J, \Sigma]) U \\
&= JU\Lambda + \tilde{Q}U,
\end{aligned}$$

where

$$\tilde{Q} = Q + [J, \Sigma]. \tag{D.1}$$

In the same manner we can show that u and $\tilde{u}$ satisfy the M-equation $v_z = M(\lambda, \tilde{q})$ and $\tilde{v}_t = M(\lambda^*, \tilde{q})$.

Bibliography

[1] I. P. Kaminov, T. Li, and A. E. Willner, *Fiber Optic Telecommunications, Vol. 5, Part A: Components and Subsystems.* Academic Press, 2008.

[2] E. Desurvire, "Capacity demand and technology challenges for light-wave systems in the next two decades," *IEEE J. Lightwave Techn.*, vol. 24, no. 12, pp. 4697–4710, 2006.

[3] R. W. Tkach, "Scaling optical communications for the next decade and beyond," *IEEE J. Lightwave Techn.*, vol. 14, no. 4, pp. 3–9, 2010.

[4] J. Tang, "The Shannon channel capacity of dispersion-free nonlinear optical fiber transmission," *IEEE J. Lightwave Techn.*, vol. 19, no. 8, pp. 1104–1109, 2001.

[5] E. E. Narimanov and P. Mitra, "The channel capacity of a fiber optics communication system: perturbation theory," *IEEE J. Lightwave Techn.*, vol. 20, no. 3, pp. 530–537, 2002.

[6] P. P. Mitra and J. B. Stark, "Nonlinear limits to the information capacity of optical fiber communications," *Letters to Nature*, vol. 411, pp. 1027–1030, 2000.

[7] R. J. Essiambre, G. Kramer, P. J. Winzer, G. J. Foschini, and B. Goebel, "Capacity limits of optical fiber networks," *IEEE J. Lightwave Techn.*, vol. 28, no. 4, pp. 662–701, Feb. 2010.

[8] R. J. Essiambre, G. J. Foschini, P. J. Winzer, and E. C. Burrows, "The capacity of fiber-optic communication systems," *Optical Fiber Communication Conference*, pp. 1–3, 2008.

[9] M. J. Ablowitz and H. Segur, *Solitons and the Inverse Scattering Transform*, 1st ed. Society for Industrial and Applied Mathematics (SIAM), 2000.

[10] L. D. Faddeev and L. A. Takhtajan, *Hamiltonian Methods in the Theory of Solitons.* Springer Verlag, 2007.

[11] C. E. Shannon, "A mathematical theory of communications, I and II," *Bell Syst. Tech. J*, vol. 27, pp. 379–423, 623–656, July, October 1948.

[12] J. Gleick, *The Information: A History, a Theory, a Flood*. Pantheon, 2011.

[13] T. M. Cover and J. A. Thomas, *Elements of Information Theory*. John Wiley & Sons, Inc., 2006.

[14] I. Csiszar, *Information Theory: Coding Theorems for Discrete Memoryless Systems*. Academic Press, 1981.

[15] M. Ledoux, *The Concentration of Measure Phenomenon*. American Mathematical Society, 2001, vol. 89.

[16] J. Bucklew, *Introduction to Rare Event Simulation*. Springer Verlag, 2004.

[17] M. S. Pinsker, *Information and Information Stability of Random Variables and Processes*. Holden-Day, 1964.

[18] K. C. Kao and G. A. Hockham, "Dielectric-fiber surface waveguides for optical frequencies," *Proceedings of the Institution of Electrical Engineers*, vol. 113, pp. 1151–1158, 1966.

[19] R. J. Mears, L. Reekie, I. M. Jauncey, and D. N. Payne, "Low-threshold erbium-doped fiber amplifier operating at 1.54 m," *Electron Letters*, vol. 23, pp. 1026–1027, 1987.

[20] E. Desurvire, J. R. Simpson, and P. C. Becker, "High-gain erbium-doped traveling-wave fiber amplifier," *Opt. Lett.*, vol. 12, no. 11, pp. 888–890, 1987.

[21] G. P. Agrawal, *Nonlinear Fiber Optics*. Springer, 2006.

[22] J. P. Gordon, W. H. Louisell, and L. R. Walker, "Quantum fluctuations and noise in parametric processes II," *Phys. Rev.*, vol. 129, no. 1, pp. 481–485, 1963.

[23] V. E. Zakharov and A. B. Shabat, "Exact theory of two-dimensional self-focusing and one-dimensional self-modulation of waves in nonlinear media," *Soviet Physics-JETP*, vol. 34, pp. 62–69, 1972.

[24] C. W. Gardiner, *Handbook of Stochastic Methods for Physics, Chemistry, and the Natural Sciences*. Springer-Verlag, 1985.

[25] A. E. Gamal and Y. H. Kim, *Network Information Theory*. Cambridge University Press, 2011.

[26] B. W. Göbel, "Information-theoretic aspects of fiber-optic communication channels," Ph.D. dissertation, Technische Universität München, 2010.

[27] A. Mecozzi and R. J. Essiambre, "Nonlinear Shannon limit in pseudolinear coherent systems," *IEEE J. Lightwave Techn.*, vol. 30, no. 12, pp. 2011–2024, 2012.

[28] E. Agrell, "The channel capacity increases with power," *CoRR*, vol. abs/1108.0391, 2011.

[29] M. I. Yousefi and F. R. Kschischang, "On the per-sample capacity of nondispersive optical fibers," *IEEE Trans. Inf. Theory*, vol. 57, no. 11, pp. 7522–7541, Nov. 2011.

[30] G. Kramer, A. Ashikhmin, A. J. Wijngaarden, and X. Wei, "Spectral efficiency of coded phase-shift keying for fiber-optic communication," *IEEE J. Lightwave Techn.*, vol. 21, no. 10, p. 2438, 2003.

[31] S. M. Moser, "Duality-based bounds on channel capacity," Ph.D. dissertation, ETH Zurich, Switzerland, 2004.

[32] E. Ip and J. M. Kahn, "Compensation of dispersion and nonlinear impairments using digital backpropagation," *IEEE J. Lightwave Techn.*, vol. 26, no. 20, pp. 3416–3425, 2008.

[33] K. Roberts, C. Li, L. Strawczynski, M. O'Sullivan, and I. Hardcastle, "Electronic precompensation of optical nonlinearity," *IEEE Photon. Technol. Lett.*, vol. 18, no. 2, pp. 403–405, 2006.

[34] Y. Cai, J. X. Cai, A. Pilipetskii, G. Mohs, and N. Bergano, "Spectral efficiency limits of pre-filtered modulation formats," *Opt. Exp.*, vol. 18, no. 19, pp. 20 273–20 281, 2010.

[35] A. Tarighat, R. C. J. Hsu, A. Shah, A. H. Sayed, and B. Jalali, "Fundamentals and challenges of optical multiple-input multiple-output multimode fiber links," *Communications Magazine, IEEE*, vol. 45, no. 5, pp. 57–63, 2007.

[36] L. Beygi, E. Agrell, M. Karlsson, and P. Johannisson, "Signal statistics in fiber-optical channels with polarization multiplexing and self-phase modulation," *IEEE J. of Lightwave Techn.*, vol. 29, pp. 2379–2386, 2011.

[37] T. Tao and C. Thiele, "Nonlinear Fourier analysis," UCLA Department of Mathematics, http://www.math.ucla.edu/∼thiele/lecturenotes/nlft.pdf, Tech. Rep., 2006.

[38] A. Hasegawa and T. Nyu, "Eigenvalue communication," *IEEE J. Lightwave Techn.*, vol. 11, no. 3, pp. 395–399, 1993.

[39] R. J. Essiambre, G. J. Foschini, G. Kramer, and P. J. Winzer, "Capacity limits of information transport in fiber-optic networks," *Phys. Rev. Lett.*, vol. 101, no. 16, p. 163901, 2008.

[40] E. Fermi, J. Pasta, and S. Ulam, "Studies of nonlinear problems," *Los Alamos document LA 1940*, 1955.

[41] N. J. Zabusky and M. D. Kruskal, "Interaction of "solitons" in a collisionless plasma and the recurrence of initial states," *Phys. Rev. Lett.*, vol. 15, no. 6, pp. 240–243, 1965.

[42] C. S. Gardner, J. M. Greene, M. D. Kruskal, and R. M. Miura, "Method for solving the Korteweg-de Vries equation," *Phys. Rev. Lett.*, vol. 19, no. 19, pp. 1095–1097, 1967.

[43] P. D. Lax, "Integrals of nonlinear equations of evolution and solitary waves," *Comm. Pure Appl. Math*, vol. 21, no. 5, pp. 467–490, 1968.

[44] V. E. Zakharov and F. Calogero, *What is Integrability?* Springer-Verlag, 1991.

[45] A. C. Singer, "Signal processing and communication with solitons," Ph.D. dissertation, Massachusetts Institute of Technology, 1996.

[46] M. Reed and B. Simon, *Methods of Modern Mathematical Physics: Vol 1, Functional Analysis*. Academic Press, 1980.

[47] L. C. Evans, *Partial Differential Equations*. American Mathematical Society, 2010.

[48] M. J. Ablowitz, D. J. Kaup, A. C. Newell, and H. Segur, "The inverse scattering transform—Fourier analysis for nonlinear problems," *Stud. Appl. Math.*, vol. 53, pp. 249–315, 1974.

[49] A. S. Fokas, "A unified transform method for solving linear and certain nonlinear PDEs," *Proc. Royal Society London A*, vol. 453, pp. 1411–1443, 1997.

[50] E. M. Stein and R. Shakarchi, *Complex Analysis*. Princeton University Press, 2003.

[51] M. Klaus and J. K. Shaw, "On the eigenvalues of Zakharov-Shabat systems," *SIAM J. Math. Analys.*, vol. 34, no. 4, pp. 759–773, 2003.

[52] N. I. Muskhelishvili and J. R. M. Radok, *Singular Integral Equations*, 2nd ed. Dover Publications, 2008.

[53] J. Stoer and R. Bulirsch, *Introduction to Numerical Analysis*, 2nd ed. Springer-Verlag, 1993.

[54] D. W. McLaughlin and C. M. Schober, "Chaotic and homoclinic behavior for numerical discretizations of the nonlinear Schrödinger equation," *Physica D*, vol. 57, pp. 447–465, 1992.

[55] C. P. Olivier, "A numerical study of the spectrum of the nonlinear Schrödinger equation," Master's thesis, University of Stellenbosch, Dept. of Mathematics, Dec. 2008.

[56] R. C. S. Burtsev and I. Timofeyev, "Numerical algorithms for the direct spectral transform with applications to nonlinear Schrödinger type systems," *Journal of Computational Physics*, vol. 147, no. 1, pp. 166–186, 1998.

[57] M. I. Yousefi and F. R. Kschischang, "Information transmission using the nonlinear Fourier transform, Part I: Mathematical tools," submitted to *IEEE Trans. Inf. Theory*, Feb. 2012.

[58] A. R. Osborne, *Nonlinear Ocean Waves and the Inverse Scattering Transform*. Burlington, MA: Academic Press, 2010.

[59] G. Boffetta and A. Osborne, "Computation of the direct scattering transform for the nonlinear Schrödinger equation," *Journal of Computational Physics*, vol. 102, no. 2, pp. 252–264, 1992.

[60] J. Skaar and O. H. Waagaard, "Design and characterization of finite-length fiber gratings," *IEEE J. Quantum Electron.*, vol. 39, no. 10, pp. 1238–1245, 2003.

[61] M. J. Ablowitz and J. F. Ladik, "Nonlinear differential–difference equations and Fourier analysis," *J. of Math. Phys.*, vol. 17, p. 1011, Jun. 1976.

[62] T. R. Taha and M. J. Ablowitz, "Analytical and numerical aspects of certain nonlinear evolution equations. II. Numerical, nonlinear Schrödinger equation," *Journal of Computational Physics*, vol. 55, no. 2, pp. 203–230, 1984.

[63] J. Weideman and B. Herbst, "Finite difference methods for an AKNS eigenproblem," *Mathematics and computers in simulation*, vol. 43, no. 1, pp. 77–88, 1997.

[64] J. H. Wilkinson, *The Algebraic Eigenvalue Problem*. Oxford University Press, 1988.

[65] J. H. Wilkinson, C. Reinsch, and F. L. Bauer, *Handbook for Automatic Computation, Vol. 2: Linear Algebra*. Springer Verlag, 1986.

[66] A. R. Bishop, D. W. McLaughlin, M. G. Forest, and E. A. Overman II, "Quasi-periodic route to chaos in a near-integrable PDE: Homoclinic crossings," *Phys. Rev. Lett.*, vol. 127 A, 1988.

[67] M. J. Ablowitz and B. M. Herbst, "On homoclinic structure and numerically induced chaos for the nonlinear Schrödinger equation," *SIAM J. on Appl. Math.*, vol. 50, no. 2, pp. 339–351, Apr. 1990.

[68] J. Satsuma and N. Yajima, "Initial value problems of one-dimensional self-modulation of nonlinear waves in dispersive media," *Prog. Theoret. Phys. Suppl.*, vol. 55, pp. 284–306, 1974.

[69] L. F. Mollenauer and J. P. Gordon, *Solitons in Optical Fibers: Fundamentals and Applications*. Academic Press, 2006.

[70] E. Meron, M. Feder, and M. Shtaif, "On the achievable communication rates of generalized soliton transmission systems," *CoRR*, vol. abs/1207.0297, 2012.

[71] R. Hirota, *The Direct Method in Soliton Theory*. Cambridge University Press, 2004.

[72] V. B. Matveev and M. A. Salle, *Darboux Transformations and Solitons*. Springer-Verlag Berlin, 1991.

[73] V. I. Karpman and V. V. Solov'ev, "A perturbational approach to the two-soliton systems," *Physica D: Nonlinear Phenomena*, vol. 3, no. 3, pp. 487–502, 1981.

[74] V. I. Karpman and E. M. Maslov, "A perturbation theory for the Korteweg-de Vries equation," *Physics Letters A*, vol. 60, no. 4, pp. 307–308, 1977.

[75] D. J. Kaup, "A perturbation expansion for the Zakharov-Shabat inverse scattering transform," *SIAM J. on Appl. Math.*, vol. 31, no. 1, pp. 121–133, 1976.

[76] V. Konotop and L. Vázquez, *Nonlinear Random Waves*. World Scientific Publishing Company Inc., 1994.

[77] P. Kazakopoulos and A. L. Moustakas, "Nonlinear Schrödinger equation with random Gaussian input: Distribution of inverse scattering data and eigenvalues," *Phys. Rev. E*, vol. 78, no. 1, p. 016603, 2008.

[78] Y. C. Ma and M. J. Ablowitz, "The periodic cubic Schrödinger equation," *Studies in Applied Mathematics*, vol. 65, pp. 113–158, 1981.

[79] T. Tao, *Nonlinear Dispersive Equations: Local and Global Analysis*. American Mathematical Society, 2006.